2011-04-29

Engineering an Optimal Bioartificial Pancreas for Islet Transplantation Using Bioactive Scaffolds

Eileen Pedraza
University of Miami, rumplestilsken_99@yahoo.com

UNIVERSITY OF MIAMI

ENGINEERING AN OPTIMAL BIOARTIFICIAL PANCREAS FOR ISLET TRANSPLANTATION USING BIOACTIVE SCAFFOLDS

By

Eileen Pedraza

A DISSERTATION

Submitted to the Faculty
of the University of Miami
in partial fulfillment of the requirements for
the degree of Doctor of Philosophy

Coral Gables, Florida

May 2011

UNIVERSITY OF MIAMI

A dissertation submitted in partial fulfillment of
the requirements for the degree of
Doctor of Philosophy

ENGINEERING AN OPTIMAL BIOARTIFICIAL PANCREAS FOR ISLET TRANSPLANTATION USING BIOACTIVE SCAFFOLDS

Eileen Pedraza

Approved:

Cherie L. Stabler, Ph.D. Assistant Professor of Biomedical Engineering	Terri A. Scandura, Ph.D. Dean of the Graduate School
Antonello Pileggi, M.D., Ph.D. Associate Professor of Surgery	Herman Cheung, Ph.D. Knight Professor of Biomedical Engineering
Weiyong Gu, Ph.D. Professor of Biomedical Engineering	Fotios Andreopoulos, Ph.D. Associate Professor of Biomedical Engineering

UNIVERSITY OF MIAMI

PEDRAZA, EILEEN (Ph.D., Biomedical Engineering)

Engineering an Optimal Bioartificial Pancreas for Islet Transplantation using Bioactive Scaffolds (May 2011)

Abstract of a dissertation at the University of Miami.

Dissertation supervised by Professor Cherie L. Stabler
No. of pages in text. (215)

Clinical islet transplantation is a promising treatment for type 1 diabetes. It involves the transplantation of pancreatic islets, isolated from a donor, into the portal vein of a recipient in order to replace his/her dysfunctional islets. Though promising, islet implantation into the liver is greatly hindered by numerous problems, including mechanical stresses, inflammatory responses, exposure to high drug and toxin loads, as well as irretrievability. In order to address these concerns, investigation into alternative implant sites, such as the subcutaneous site, has intensified. Transplantation of islets within these extrahepatic sites is commonly met with three primary obstacles: 1) inadequate spatial distribution of the cells; 2) oxygen deficiency in the local environment; and 3) insufficient vascularization within and around the implant. Thus, the objective of this proposal is to engineer a superior bioartificial pancreas, a device combining novel biomaterials and insulin-secreting cells, by focusing on these *critical issues*, specifically how to best reduce islet aggregation, as well as increase oxygen delivery, both in the short term and long term. A highly macroporous silicone scaffold will be engineered to distribute the islets three-dimensionally, while not imparting diffusion resistances commonly encountered in microporous materials. Macroporous scaffolds will also permit

vascular in-growth. In order to sustain oxygen levels at the moment of device implantation, a novel, oxygen generating disk, which relies on the decomposition of calcium peroxide, will be developed and incorporated alongside the scaffold to deliver short-term supplemental oxygen. Therefore, it is postulated that these bioactive scaffolds, which interact with islets on a spatial, chemical, and biological level, will improve the viability as well as the function of islets, both in vitro and in vivo, as compared to naked islets under extrahepatic conditions.

ACKNOWLEDGMENTS

I would like to acknowledge all of the people who contributed invaluably towards the work presented in this dissertation. My committee members graciously offered their time to guide and assist me. Everyone at the University of Miami, College of Engineering, and the Diabetes Research Institute has been kind and considerate. Everyone whom I have worked with at the labs of Dr. Stabler, Dr. Kenyon and Dr. Mendez has been very supportive. I would especially like to thank those who partnered with me during so many experiments: Leslie Goldberg, Ann-Christina Brady, and María Coronel. Thank you, Christopher A. Fraker, for always putting up with all of my questions, helping me out and teaching me, whether it is about cell culture techniques or the history of music. I could not imagine having had anyone else as mentor than Dr. Cherie L. Stabler. Thank you for supporting me every step of the way and preparing me for my academic future.

TABLE OF CONTENTS

LIST OF FIGURES

LIST OF TABLES

CHAPTER 1. SPECIFIC AIMS

1.1 INTRODUCTORY REMARKS

While the current cell transplantation protocol for treating T1DM, clinical islet transplantation, has demonstrated the superiority of islet transplantation over standard insulin therapy in providing optimal blood glucose control, it is now recognized that the current transplantation site of the liver microvasculature is not ideal. For several years, numerous investigators have studied the feasibility of using a device for housing transplanted pancreatic islets within an alternative site. All of these designs, however, have been plagued with problems such as poor engraftment, requirement for a high number of islet cells for loading, instability, and the inability to scale-up the dimensions of the device from rodent to human requirements. All of these problems are in major part caused by poor nutrient delivery, primarily of oxygen, to all of the transplanted islets, which is inherent in the design of these devices. The issue of nutrient delivery is critical to our field of diabetes, because islets have remarkably high metabolic demands. In this dissertation, however, we seek to advance the field of islet transplantation by utilizing biomaterials as a means to enhance nutrient delivery and islet engraftment. Therefore, we are shifting the biomaterial paradigm from using an inert biomaterial to developing an "active" material capable of promoting islet viability and function through active interactions with the host and the transplanted cells.

The central hypothesis of this dissertation is that a ***highly porous scaffold, fabricated from biocompatible and biostable materials, will enhance islet engraftment and function within an alternative transplant site, by providing mechanical protection, spatial distribution, and intra-device vascularization***. In addition, by utilizing the

biomaterial as a means to supplement oxygen short-term, as well as a platform for the introduction of cells that accelerate vascularization for the long term, a superior bioartificial pancreas device, requiring only a reasonable number of islets and scalable to humans, can be produced. Initial studies were focused on the development of a biomaterial scaffold that is capable of mechanically protecting the islets and spatially distributing them, while also allowing for intra-device vascularization. Next, the oxygen generating potential of novel encapsulated solid peroxide was evaluated. Then, the scaffolds and oxygen generator were evaluated for their effect in promoting islet survival and function.

1.2 SPECIFIC AIMS

The **long-term goal** of this research is to treat type 1 diabetes mellitus (T1DM) by developing a biocompatible, cell-based, tissue engineered device, for transplantation into extrahepatic sites. In order to address these goals, the following specific aims will be pursued:

Specific Aim #1: To design and fabricate a highly porous scaffold capable of providing three-dimensional spatial distribution to the islets, while permitting intra-device vascularization, thereby improving implant efficacy in-vivo compared to free islet controls. Macroporous PDMS scaffolds will be fabricated using solvent casting particulate leaching technique, assessed for porosity and particle retention, and surface modified for cell culture. Islets will be cultured on the scaffold for short-term and assessed for retention, viability, and insulin secretion function. The applicability of the scaffolds as a platform for drug delivery and for co-culture of "helper" cells, such as

mesenchymal stem cells, will be explored. Finally, the efficacy of islet-loaded scaffolds transplanted into the omentum of syngeneic rats for reversing chemically induced diabetes will be determined.

Specific Aim #2: To design and incorporate oxygen enhancing materials into the device as a complementary approach designed to increase islet viability and short-term islet survival. The kinetics of oxygen release from calcium peroxide powder will be determined. Encapsulation of calcium peroxide in a hydrophilic versus a hydrophobic polymer will be compared. Oxygen releasing disks, consisting of calcium peroxide encapsulated in PDMS, will be assessed for harmful byproduct release and modeled for oxygen release. The effects on cell viability and insulin secretion function will be determined for cells and islets cultured with the disk. Finally, PDMS encapsulated calcium peroxide will be incorporated into three dimensional constructs and assessed for oxygen release as well as cell and islet culture.

1.3 CONTENTS OF THIS DISSERTATION

The overall objective of this dissertation is to develop an oxygen generating, macroporous scaffold for extrahepatic islet transplantation in order to treat type 1 diabetes mellitus (T1DM). A background of the causes and treatments for type 1 diabetes are presented in Chapter 2. Also included in this chapter is a literature review of previous approaches to developing devices for islet transplantation and to developing oxygen generating materials. Finite element analysis is used to model the design of the scaffold and oxygen generators.

Chapter 3 is based on the design and development of macroporous scaffolds fabricated from PDMS and sodium chloride using the solvent casting and particulate leaching technique. The degree of porosity and pore size of the scaffold is optimized to achieve high mechanical stability (assessed via porosity measurements and scanning electron microscopy) and high retention of loaded islets (assessed via retention of spherical particles substituting for islets). The scaffold surface is modified by physical adsorption of proteins for cell adherence. The suitability of the scaffolds for in-vivo implantation is determined by assessment of endotoxin levels and in-vivo biocompatibility studies.

In Chapter 4, the applicability of PDMS scaffolds for cell culture is explored by assessing the viability and proliferation of MIN6 cells and human mesenchymal stem cells cultured on PDMS scaffolds. Moreover, the retention, viability, and insulin secretion function of rat, nonhuman primate, and human islets cultured on the scaffolds is assessed. Finally, the efficacy of scaffolds for reversing diabetes is investigated by transplanting islet loaded scaffolds into alternative sites within diabetic syngeneic rats.

In Chapter 5, a novel oxygen generating material in the form of a PDMS encapsulated calcium peroxide disk is designed and developed. The kinetics of oxygen release from the raw material, calcium peroxide is derived, and the rate constants of its decomposition reaction are determined. Oxygen release from the PDMS encapsulated calcium peroxide disk is then modeled by combining the reaction kinetics with solute transport by diffusion. Through this analysis, we are able to characterize the design parameters necessary to design the optimal oxygen generating material for cell-based studies.

In Chapter 6, the suitability of encapsulated calcium peroxide disks for cell culture is determined. Harmful release of hydrogen peroxide and hydroxyl radical from the disks is assessed. In-vitro studies incubating MIN6 cells and islets with encapsulated calcium peroxide is carried out to evaluate the capacity of these optimally designed materials to prevent death due to hypoxia.

In Chapter 7, the feasibility of incorporating PDMS encapsulated calcium peroxide into three dimensional constructs is investigated. Given that the ultimate goal is to develop an implant capable of supplementing oxygen within a tissue engineered implant in-vivo, two designs for importation of these oxygen generating materials in a three-dimensional scaffolds were compared and contrasted. Oxygen release from oxygen generating scaffolds was theoretically predicted and experimentally evaluated. In-vitro studies are performed incubating MIN6 cells and islets with scaffolds containing encapsulated calcium peroxide.

Chapter 8 concludes this dissertation by presenting a summary of the major findings. Recommendations for future directions to address the main goals of this work are also presented.

CHAPTER 2. BACKGROUND AND SIGNIFICANCE

2.1 FUNCTION OF ISLETS OF LANGHERHANS FROM PANCREAS

The pancreas is the organ in the body of vertebrates that functions both as an exocrine gland, by secreting pancreatic juice, and as an endocrine gland, by producing various important hormones. The exocrine tissue is composed of acinar cells that produce digestive enzymes, which help break down carbohydrates, proteins, and lipids in the digestive track. The endocrine tissue is comprised of large, spherical clusters called islets of Langerhans, each containing thousands of cells that are classified into four types on the basis of the hormone they secrete: α-cells (secrete glucagon when glucose is low), β-cells (secrete insulin when glucose is elevated), δ-cells (secrete somatostatin to regulate α and β cells), and PP cells (secrete pancreatic polypeptide). Pancreatic β-cells are continuously sensing blood glucose levels. They produce and store the hormone insulin, which they release in direct proportion to the sensed blood glucose levels. The released insulin decreases elevated blood glucose and allows cells to uptake circulating glucose. The different cells are tightly clustered together within the islet and are infiltrated by a dense network of capillaries, resulting in most cells being in direct contact with blood vessels. As a consequence of this complex configuration, it is difficult to isolate individual cells from each other without destroying the surrounding cells and vasculature (R. N. Wang & L Rosenberg 1999). It is critically important to keep the cluster of islets uncompromised in order to retain adequate functionality. Due to the importance of the pancreas in regulating and balancing hormone levels in the body, damage or disease to the organ leads to severe metabolic imbalances, as in the case of diabetes.

2.2 DIABETES MELLITUS

Type 2 diabetes mellitus (T2DM) is characterized by insulin resistance or relative insulin deficiency. Type 1 diabetes mellitus (T1DM) is the autoimmune destruction of pancreatic β-cells, cells which are absolutely necessary for the regulation of blood glucose levels in the body. Therefore, since patients with type 1 diabetes lack these vital cells, they are unable to generate insulin and consequently glucose utilization is substantially impaired. Glucose is the vital currency of energy in the body, and when its accessibility is jeopardized, the body is severely compromised. Tragically, the incidence of diabetes is constantly on the rise, especially in recent years with the ongoing decline in people's diet and exercise. In the span of just six years, from 1997 to 2005, the number of new cases of diabetes that were detected increased by 77% (CDC's Division of Diabetes Translation Division of Health Interview Statistics 2006). Diabetes mellitus is a chronic medical condition, meaning that although there is treatment for it, there is currently no cure.

2.3 CURRENT ISLET TRANSPLANTATION TREATMENTS

Currently, the most widespread treatment for diabetes is exogenous insulin treatments, either by manual injections or an insulin pump, both of which are unable to provide tight, physiological control of blood glucose levels, leading to complications such as diabetic retinopathy, nephropathy, and neuropathy (A. Silva & M Mateus 2009). The 1993 Diabetes Control and Complications Trial (DCCT) highlighted the need for the development of a treatment that provides for a more physiological regulation of blood glucose levels to reduce common long-term diabetic complications (Anon 1993). This need for a more physiological treatment is fulfilled by a cell-based treatment, which

provides optimal regulation, long-term treatment, and significant reduction in detrimental side effects.

Clinical islet transplantation offers a solution to restoring β-cell function through the transplantation of allogeneic pancreatic islets. Currently this procedure is performed by transplanting into an intrahepatic site. Current clinical trials have resulted in improved patients who, when compared to themselves before treatment, exhibit superior control in blood glucose levels, high C-peptide levels, and insulin independence for several years (A. M. Shapiro et al. 2006). These promising results are dampened, however, by some of the limitations of this treatment, such as the high islet demand per patient and moderate long term function. Several studies suggest that the high rate of dysfunction and early islet destruction observed after intraportal islet infusion, both in animal models and in clinical trials, is primarily due to mechanical stress, inflammatory response, and immune attack. Islets in direct contact with blood initiate an acute inflammatory injury (IBMIR) leading to functional stunning and/or destruction of a large portion of the transplanted islets, which subsequently amplifies immune reactions (Mattsson et al. 2004; Moberg et al. 2002; U. Johansson et al. 2003; H. Johansson et al. 2005; Z. Yang et al. 2004; van der Windt et al. 2007; Bennet et al. 2000). Islets lodged within the liver microcirculation may also be exposed to undesirable conditions, such as high drug and toxin loads. If the islets are embolized within the bloodstream and subsequently trapped within the liver microvasculature, they will endure mechanical stress, a strong trigger of islet apoptosis (R Paul Robertson 2002; E. Kuntz & H.-D. Kuntz 2005; Paraskevas et al. 2000).

Moving islets to other sites, however, is fraught with challenges, as the transplantation of islets, in the absence of biomaterial support, at alternative sites such as

the subcutaneous space has performed poorly due to the lack of adequate mechanical protection, spatial distribution, and vascular bed. The design of an alternative site and device for islet cell transplantation that minimizes these factors would provide a superior environment for the islets, leading to reduced islet loss and improved function. Therefore, there is a strong need to develop alternative sites and devices for islet cell transplantation that would provide mechanical protection to the islets, while providing a minimally invasive implantation and the safety of retrievability.

2.4 DESIGN OF A BIOARTIFICIAL PANCREAS

2.4.1 PHYSICAL STRESSES

Alternative transplantation sites that will prevent direct exposure to allogeneic blood and its resulting inflammatory response require a structure that will provide mechanical protection (Bennet et al. 1999). When high numbers of islets transplanted in a small volume, the dense packing increases the stress on the islets and reduces the ability of nutrients and waste to diffuse into or out of the pelleted islet mass. When islets aggregate, the diffusion of nutrients and oxygen to the core is limited, resulting in necrosis and malfunction of transplanted islets (Q. P. Hou & Bae 1999). The number of islets required for transplantation may be significantly reduced, if the islets are maintained homogenously dispersed three-dimensionally. Moreover, a method of trapping islets at the transplant site, preventing loss of islets to surrounding tissue, is important for implant efficacy (Dufour et al. 2005). Therefore, for transplantation of islets into alternative sites, islets should address physical concerns of: mechanical protection; spatially distribution; and retention. A macroporous scaffold could be designed to meet these requirements and would be ideal for this purpose.

2.4.2 NUTRIENT CONCERNS

A cell-based tissue engineered device, i.e. the incorporation of biomaterials and cells within a device, could provide cell-based treatment within an alternative site that would provide optimal mechanical protection and limited direct contact with blood. It would also allow for ease in implantation, biopsy, and retrieval. Over the past decades, several researchers have designed and tested numerous devices of this type for treatment of T1DM in multiple different forms such as beads, sheets, rods, disks, and intravascular devices (Storrs et al. 2001; A. M. Sun 1988; H. Yang et al. 1994; Ohgawara et al. 1998; Calafiore et al. 1992; Calafiore et al. 2006). Previously, the majority of these devices focused on the development of immunoisolation devices, which also prevents vasculature migration to the islet site. The major problem with this approach, however, is the significant depletion of nutrients due to high metabolic demand of the islets. With the oxygen consumption rate for human islets up to 10^6 fold higher than for chondrocytes and 10^4 fold higher than for endothelial cells (W. Wang et al. 2005; Motterlini et al. 1998; Heywood et al. 2006), avascular devices containing islets are constantly plagued with nutrient delivery problems, leading to cell death in the inner portions of the device. Efficient nutrient delivery within a cell-based device is critical to sustaining the total islet implant. In order to compensate for this problem, researchers have designed devices with shorter diffusion distances and reduced cell loading densities, but this leads to challenges when attempting to scale up these devices to humans (Storrs et al. 2001). So, it becomes evident that there is a critical need for the design of a cell-based tissue engineered device that simultaneously allows for adequate nutrient delivery, low cell loading density requirements, and is adaptable for scaling from rat to human dimensions.

2.4.3 VASCULARIZATION CONCERNS

In stark contrast to the portal vein, the subcutaneous site has poor nutrient and waste flow. Diffusion of nutrients and waste to cells is only effective at distances shorter than 200 μm. Pancreatic tissue is densely populated with many blood vessels throughout. In contrast, implantable biomedical devices do not have an interconnecting vascular network at the implant site. Since the formation of a vascular network within the scaffold is of critical importance for the transport of nutrients to the transplanted islets, it is imperative to develop methods for stimulating angiogenesis at the implant site.

Nutrient delivery to the transplanted islets is highly dependent on the extent of vascularization at the implantation site and on the physical, diffusion limitations inherent to the device design. Recent studies have looked into various methods for inducing angiogenesis at the transplant site prior to islet implantation, thereby avoiding the exposure of sensitive islets to significant nutritional gradients. While immunoisolation is not provided, these devices have the capacity to avoid the detrimental conditions present during intraportal liver transplantation. One such example of transplantation of pancreatic islets into neovascularized devices was published by Pileggi et al, see Figure 2-1. In this study, pancreatic islets were transplanted into a subcutaneous, neovascularized biohybrid device in diabetic rats (Antonello Pileggi et al. 2006). By implanting a stable, porous device 40 days prior to islet transplantation, they improved the incorporation of connective tissue and neovascularization to the device, thereby improving upon earlier, non-vascularized methods. Furthermore, the use of the pre-vascularized biohybrid chamber at the subcutaneous site allowed for the successful reversal of the diabetic state following islet loading, by providing mechanical protection and adequate vasculature. This is in stark comparison to the loading of naked islets, which quickly underwent

apoptosis and exhibited minimal, transient efficacy in restoring normoglycemia (Pileggi, not published). The islets within the device controlled blood glucose levels comparable to liver sites, while the device design allowed for retrievability and ease of transplantation.

This study demonstrates the critical importance of adequate vascularization to the survival of islets and consequently to the efficacy of transplants. Constructs for extrahepatic transplantation should also allow for easy retrieval at later time points (Dufour et al. 2005). Moreover, they should allow for minimally invasive reseeding of islets at later time points in order to reduce scar formation (Q. P. Hou & Bae 1999). Therefore, the ideal scaffold should be biocompatible and have large pores to encourage vascularization, as well as be biostable to allow retrievability and reseeding.

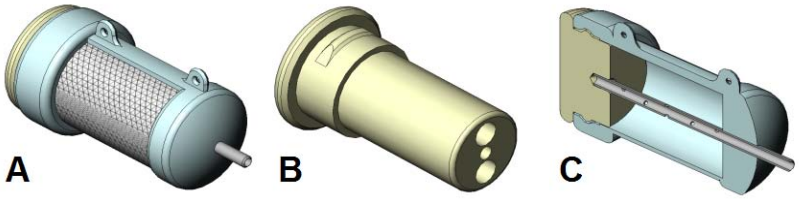

Figure 2-1: Schematic representation of biohybrid device chamber. A) Outer chamber of mesh cylinder with 500 μm pores; B) Plunger placed within device during prevascularization stage. Plunger is removed prior to islet transplantation; C) Inner chamber of device, illustrating inner lumen.

2.5 BIOACTIVE SCAFFOLD AS A BIOARTIFICIAL PANCREAS

To address the issues with nutrient delivery, we have formulated a two-pronged plan that applies biomaterial science and tissue engineering to increase the access, availability, and delivery of oxygen. In order to maximize the accessibility of the transplanted islets to the oxygen already present in the device, a very promising solution is to minimize the agglomeration of the islets by spatially distributing them on a porous scaffold designed and fabricated from biomaterials. Secondly, in order to increase the

short-term availability of oxygen, we will supply additional oxygen by designing an oxygen generating biomaterial and incorporating it into the scaffold.

2.6 SCAFFOLDS FOR TISSUE ENGINEERING

Given the high metabolic demand of the islets, it is critical to design a device that allows for both intra-device vascularization and a means to spatially distribute the cells within the device. When islets are simply loaded as a cell suspension within a fluid, they will quickly settle, sediment, and clump together. This configuration is undesirable, because it increases the mechanical stresses caused from the weight of islets on top of each other and results in increased void space within the device. This superfluous void space contributes to the problem of making the devices too large when scaled up for human application. More importantly, the clustering of islets leads to significant nutritional gradients within the islet pellet, with the islets on the outer edges of the pellet receiving the bulk of the nutrients, and the inner sections receiving inadequate nutritional support. The use of a biomaterial to spatially distribute the cells would allow for a more desirable three-dimensional arrangement of the cells and result in a more efficient delivery of nutrients.

2.6.1 SCAFFOLDS FOR EXTRAHEPATIC TRANSPLANTATION OF ISLETS

The selection of an appropriate biocompatible biomaterial that allows for spatial distribution, mechanical protection, and intra-device vascularization is a complicated task. The ideal matrix would be one that is highly porous, with deep, inter-connected pores to trap the islets throughout the device, while also allowing for vascular infiltration. In a recent publication, Blomeier et al demonstrated that a highly porous Poly(D,L-

lactide-co-glycolide) (PLG) scaffold seeded with islets and transplanted into the intraperitoneal fat of a mouse, could be highly efficacious in treating diabetic rats (Blomeier et al. 2006). They found significant improvements in efficacy for islets loaded within a 5 mm × 5 mm PLG cylinder over islets implanted without the scaffold. Vascular infiltration was also evident in histological sections. While the degradation of the scaffold over time limits the ability to remove the implant at a later date, this study illustrates the importance of scaffolding in mechanically protecting and spatially distributing the transplanted islets.

2.6.2 SCAFFOLD MATERIAL SELECTION

Scaffold material selection is tissue-specific and requires balancing the desired mechanical properties, pore structure, immunogenicity, biostability, biorecognition, etc of the scaffold. Several biomaterials have been used, both for in-vitro and in-vivo studies, to generate macroporous scaffolds, including collagen, chitosan, hydroxyapatite, poly(α-hydroxy esters) like poly(glycolic acid) (PGA), poly(lactic acid) (PLA), and poly(lactic-*co*-glycolic acid) (PLGA). In general, natural materials have the benefit of high cellular recognition and tissue compatibility, but are costly, variable, biodegradable, and require high levels of purification (Vacík et al. 2008). Synthetic materials, on the other hand, can be fabricated with uniformity between batches, precise control over rates of degradation, and modified chemical properties (Ratner et al. 2004). Hydroxyapatite scaffolds, a bio-derived material commonly used in the fabrication of bone graft substitutes, have the desirable properties of established cell biocompatibility, promotion of vascular infiltration, and high pore interconnectivity (Low et al. 2006; Dong et al. 2001; H. W. Kim et al. 2005; Gao et al. 2006; Mastrogiacomo et al. 2005). PLG, a synthetic,

biocompatible, and biodegradable polymer, has ease in variation of degradation rates and growth factor release kinetics, through the manipulation of molecular weight and composition. Moreover, the characteristics of the scaffold can be specifically tailored (Blomeier et al. 2006; Hsiong & D J Mooney 2006; Harris et al. 1998; Oh et al. 2006; Ellis & Chaudhuri 2006).

In this dissertation, we sought to find a stable, biocompatible, highly porous biomaterial, which could also serve as a platform capable of incorporating bioactive agents, particularly oxygen generating agents. Based on extensive literature searches, we identified a material that has been demonstrated suitable to our needs: poly(dimethyl)siloxane (PDMS). This material exhibits superior biocompatibility and biostability following clinical implantation, making it an excellent candidate for this application (Hodgins et al. 2007; Khorasani & Mirzadeh 2004; Aucoin et al. 2002; Teixeira et al. 2007; Heise et al. 1990; Bucholz et al. 1987; Nunes et al. 1997). Non-toxic, macroporous PDMS sponges can be fabricated with a large surface to volume ratio and controllable porosity. Due to its hydrophobicity, in its natural state, PDMS is not an optimal surface for cell adhesion. However, it can be modified using any one of a multitude of methods to encourage cell adhesion. For example, the surface can be rendered hydrophilic via plasma oxygenation (Norman & Desai 2005; Murakami 1998; Roth et al. 2008; Armani et al. 1999; Nishikawa et al. 2008). Also, various protein coatings can be achieved via nonspecific physical adsorption (G. Toworfe et al. 2006). Alternatively, arginine-glycine-aspartic acid (RGD) peptides can be conjugated to the surface (B. Li et al. 2006). Furthermore, the degradation products of silicone are efficiently removed by the kidneys (Low et al. 2006). In addition, the oxygen solubility

of PDMS is high, with diffusivity values of approximately 6×10^{-9} m^2s^{-1} (Vollmer et al. 2005; Cox 1986; Merkel et al. 2000). This property ensures that PDMS introduces only a minimal diffusion barrier, so that oxygen transfer will occur readily through it. Furthermore, the capacity of PDMS to serve as platform for the slow delivery of agents has long been demonstrated. PDMS platforms have been used for numerous drug delivery applications, from dexamethasone to matrix metalloproteinases (MMPs), as outlined in Section 1.8. Therefore, the first objective of this dissertation was to design and fabricate a highly porous PDMS scaffold capable of providing mechanical support and spatial distribution to the islets, while permitting intra-device vascularization, thereby improving implant efficacy in-vivo.

2.7 OXYGEN RELEASING COMPOUNDS

The oxygen concentration of the islets' environment is a critical component to the islets' survival. Cell death by necrosis is common under anoxic culture conditions (~0 mmHg O_2) since metabolic pathways are restricted and plasma membrane integrity is jeopardized (Herman et al. 1988). Hypoxia conditions (5-15 mmHg O_2) usually cause cells to shift towards anaerobic metabolic activities and to express factors that favor oxygen delivery (Semenza 1999). Normoxic conditions (30-90 mmHg O_2) are optimal for achieving baseline metabolism and function (Jungermann & Kietzmann 2000). Islets are particularly sensitive to changes in oxygen conditions, with insulin production levels being reduced by 50% at the threshold between normoxia and hypoxia (Dionne et al. 1993). Fully vascularized devices may exhibit normoxic conditions prior to cell implantation; however, the effective oxygen available to the islets once inside of a device is significantly lower due to high cell loading densities and transport limitations

introduced by the poor spatial distribution of the islets inside of the device. In the initial days following islet implantation, in the absence of intra-vascular infiltration, the maximal oxygen concentration occurs at the outer boundaries of the device and progressively decreases in the inward radial direction. In mathematical terms, this trend in the reduction in oxygen can be described as the concentration of oxygen is inversely proportional to the path length squared. The sharp discrepancy in how maximal oxygen concentration occurs at the outer boundaries of the device and decreases to a minimal value at the center of the device is due to diffusion and oxygen consumption by cells. Therefore, during the design phase of the device, its dimensions must be carefully considered in order to minimize the diffusion path length. Another factor to consider is that greater islet loading densities increase the percent volume oxygen consumption rate. When the oxygen consumption rate of the islets exceeds the rate of diffusion of oxygen from the surrounding area, an oxygen deficit is created. Software computational models can be used to gain realistic insight on the effects of the geometric design of the device on islet viability. These computational models demonstrate that for many current bioartificial device models, only a thin outer ring of islets are exposed to suitable non-hypoxic conditions. The viability of the islets dramatically increases with small increments in oxygen concentration.

Prevascularization of the implant could serve to provide a means to minimize the exposure of islets to hypoxic conditions. Several studies have illustrated the benefits of utilizing a two-step method for islet transplantation, i.e. where the device is prevascularized prior to the implantation of the islets. Implantation of devices secreting vascular endothelial growth factor or fibroblast growth factor 2 resulted in superior

vascularization of the site and improved initial cell survival in rats (Sakurai et al. 2004; Trivedi et al. 2000). Islets implanted into prevascularized chambers (implanted 3 weeks earlier) in the epigastric pedicle in the groin of diabetic mice had lowered blood glucose levels compared to islets implanted into nonvascularized chambers (Hussey et al. 2009). Similarly, transplant engraftment and islet survival was improved by prevascularizing alginate scaffolds in the intramuscular site of rats 2 weeks prior to islet loading (P. Witkowski et al. 2009). While these methods substantially improve islet viability, hence enhancing the potential of islet transplantation within alternative sites, the need for two surgeries does make the transplant scheme less desirable.

In this dissertation, we sought to identify and develop methods to increase oxygen availability to islets immediately, to serve as a bridge between implantation and the development of an adequate intra-islet vascular network. Wound healing studies have found this vascularization period to be on the order of 5 to 14 days, although this network development is highly dependent on the implantation site and angiogenic cues provided in the implant milieu (van der Veen et al. 2010; B.S. Harrison et al. 2007; Marques et al. 2005; Metcalfe & Ferguson 2007).

2.7.1 OXYGEN GENERATORS IN TISSUE ENGINEERING

Currently, various agents are being investigated for their oxygen generating potential, including electrochemical degradation, photosynthesis, oxygen tanks, and peroxide reactivity. In situ oxygen was successfully generated by employing the electrolytic decomposition of water into oxygen and hydrogen. In-vitro culture experiments with βTC3 islets found that the presence of the electrochemical generator caused an increase in cell layer thickness and cell viability (H Wu et al. 1999). Bloch et al

has exploited the natural process of photosynthesis in microalgae to produce oxygen, which showed promising preliminary results (Bloch et al. 2006). Previously, a one-compartment system was introduced, but close proximity of unicellular algae to the islets led to undesirable side-effects such as algal overgrowth, a switch from photosynthetic to heterotrophic nutrition of the algae, the accumulation of toxic metabolites, and competition for nutrients between plant and mammalian cells. A two-compartment system was created to address these issues, but resulted in decreased overall performance and efficiency of the strategy (Bloch et al. 2006).

2.7.2 ENCAPSULATED SOLID PEROXIDES

Research in our laboratory has investigated the effects of enhanced oxygen delivery on islet viability and function. Specifically, we have focused our efforts on introducing oxygen generating agents and enhancing oxygen transport to the islet's immediate environment through the combination of biomaterials and agents capable of enhancing or generating oxygen. One potent source of oxygen that is particularly attractive to us is oxygen generation through the decomposition of solid peroxides. As is commonly known, hydrogen peroxide spontaneously decomposes exothermically into water and oxygen gas via the reaction shown in Equation (2-1). In a similar, but slower manner, peroxide hydrates, such as sodium percabonate, release oxygen via the reaction shown in Equation (2-2). Even slower rates of oxygen are released by solid peroxides, such as calcium peroxide and magnesium peroxide, by the reaction shown in Equation (2-3).

$$2H_2O_2 \rightarrow 2H_2O + O_2 \quad (2\text{-}1)$$

$$4Na_2CO_3{*}1.5H_2O_2 \rightarrow 8Na^- + 4CO_3^- + 6H_2O_2 \quad (2\text{-}2)$$

$$2CaO_2 + 2H_2O \rightarrow 2Ca(OH)_2 + O_2 \quad (2\text{-}3)$$

Since extremes in oxygen tension, both hypoxia and hyperoxia, may be detrimental to islets, our goal of slow, sustained oxygen release would be best met by solid peroxides. Calcium peroxide, in particular, was selected because of its extensive history of application in the bioremediation and aquaculture fields, as well as its low cost. The oxygen release from solid peroxide powders in solution, however, is still too rapid to last for the duration of time until adequate vasculature is formed. Moreover, when directly added to aqueous solutions, solid peroxide powder immediately releases hydroxide ions, turning the pH highly basic (pH ~11) (Northup & D. Cassidy 2008), and generating toxic by-products. For these reasons, we sought to modulating oxygen release as well as inhibiting formation of harmful byproducts through the encapsulation of calcium peroxide within a biomaterial.

Our work in demonstrating the oxygen generation of encapsulated solid peroxide was in collaboration with the research team of Anthony Atala and Ben Harrison at Wake Forest University, who are focused on using oxygen generating materials for wound healing. They implemented this approach using films of poly(D,L-lactide-*co*-glycolide) (PLGA) to encapsulate either sodium percarbonate or solid calcium peroxide. PLGA and sodium percarbonate films significantly reduced necrosis compared to control films, when implanted into the skin flap model in nude mice. Unfortunately, since the conversion of the sodium percarbonate was completed after only 24-70 h, the benefits of the POG films in-vivo were only observed at early time points (before 7 days). This is

because sodium percarbonate is not a true peroxide, but rather an adduct of sodium bicarbonate with hydrogen peroxide. They sought to extend the oxygen release by replacing sodium percarbonate with calcium peroxide, but still, the measured release of oxygen was low (approximately 1 mmHg per day) (B.S. Harrison et al. 2007; Oh et al. 2009). While Harrison's initial studies examined the improvement in healing skin grafts, our focus is on the effects of encapsulated peroxide in improving islet function in-vivo. Although this demonstrates the possibilities of exploiting peroxides for improved in-vitro and in-vivo performance of cells, neither material provides sufficient amounts of oxygen for an extended period of time (at least 2 weeks) to meet the high demands of islets. Of additional concern is the exposure of islets, and specifically beta cells, to the by-products of solid peroxide degradation, namely hydrogen peroxide and free radicals. While Dr. Harrison's group sought to mitigate these factors through the incorporation of catalase, we sought to design a material that would minimize exposure of cells to these detrimental by-products.

These experiments were performed with PLGA, a polymer that degrades hydrolytically; we hypothesize that by encapsulating solid peroxide in a hydrophobic polymer, such as PDMS, the barrier will induce a delay in oxygen generation, resulting in greater temporal modulation of oxygen release providing a gradual, sustained release of oxygen (B.S. Harrison et al. 2007). Furthermore, by selecting a highly oxygen permeable material, the release of oxygen from the PDMS material following degradation of the peroxide should be highly efficient. Finally, by modulating the reaction of the solid peroxide, the release of by-products may also be modulated. The end goal of this research is to incorporate solid peroxide within a stable, macroporous scaffold, in order to

significantly improve the oxygenation of all of the islets. We postulate that by minimizing cell death during the fragile initial engraftment periods by minimizing hypoxia, improved engraftment and efficacy of the transplant will be observed.

2.8 SCAFFOLDS AS A MULTI-FUNCTIONAL PLATFORM

We anticipate that the macroporous, PDMS scaffold will serve a dual purpose as not only a carrier for islets, protecting them from mechanical stresses and maintaining them spatially distributed, but also as a future platform for delivery of molecules or co-culture of cells. Thus, the scaffold provides a micro niche environment for localized activity.

2.8.1 DELIVERY OF MOLECULES

PDMS scaffolds may function as a platform for delivery of molecules, such as drugs or growth factors. A large class of drugs is hydrophobic, and by encapsulating them within the hydrophobic PDMS scaffold, you could attain a slow release into the surrounding tissue. By delivering the drugs via the scaffold, instead of intravenously, you would not only achieve a slower release, but a targeted release. For example, slow, targeted release of dexamethasone, an immunosuppressive drug of interest in diabetes, from PDMS has been demonstrated (Simmons et al. 2008). Model intraocular lenses of silicone rubber have demonstrated continuous release of matrix metalloproteinase inhibitors (MMPI) over 5 months (Morarescu et al. 2010). Also, PDMS can be formulated into PDMS droplets for release of lipophilic drugs, modeled as di-butyl-phthalate (DBP) (Simovic & Prestidge 2007). Commercially, implantable PDMS devices have demonstrated 5 yr release of levonorgestrel for contraceptive use and 200-400 day

release of 17 β-estradiol for cattle growth promotion (Di Colo 1992). Therefore, if drugs were implemented into the scaffold, the effects of the drug could be localized. Alternatively, vascular formation could be encouraged by delivering various angiogenic factors, such as vascular endothelial growth factor (VEGF), basic fibroblast growth factor (b-FGF), and granulocyte-colony stimulating factor (G-CSF) through the scaffold.

2.8.2 CO-CULTURE WITH CELLS

Potentially, scaffolds can serve as a co-culture system by having adherent cell lines proliferate on the scaffold surface prior to islet loading. For example, co-culture of mesenchymal stem cells may have a positive effect on islet viability and function, stimulating angiogenesis, or immunomodulating the environment.

There is a lot of promising research in a wide range of fields investigating the potential of mesenchymal stem cells (MSCs) for inducing angiogenesis. According to Caplan et al, MSCs secrete bioactive molecules that limit the field of injury, inhibit scarring at the site of injury, bring in a new blood supply by stimulating angiogenesis, and stimulate the mitosis of progenitors like cardiac and neural stem cells (Caplan 2009). In-vitro studies demonstrate that MSCs play an active role in the cellular process involved in the formation, stabilization, and maturation of newly formed vessels. In a rat model of stroke, human umbilical multipotent mesenchymal stromal cells were shown to increase vascular density and vascular endothelial growth factor and basic fibroblast growth factor expression (W. Liao et al., 2009). MSCs were found to accelerate angiogenesis by increasing expression of VEGF and increasing the number of adventitial vessels when impregnated into artificial dermis used to treat diabetic wounds in rats (H. Inoue et al. 2008). MSCs also contributed to vascularization in a mouse bone model

(Moioli et al. 2008). However, the angiogenic potential of MSCs may be time and dose dependent (Otsu et al. 2009).

In addition to having angiogenic potential, MSCs also exhibit immunomodulatory behavior. Strong evidence suggests that human MSCs do not possess antigens on the cell surface and therefore are not recognized as foreign to the host's immune response (Krampera et al. 2003; Tse et al. 2003). Studies have shown MSCs to be capable of suppressing T-cell proliferation and inhibiting the proliferation and IgG secretion of B-cells. They may also render T-cells anergic by inhibiting dendritic cell maturation (Abdi et al. 2008). The finding that MSCs are able to inhibit an in-vitro mixed lymphocyte assay and that they do not display any MHC class II cell surface markers, suggests that MSCs have promising potential as therapeutic allogeneic cells (Caplan 2009; Maitra et al. 2004).

The niche of the macroporous scaffold is highly conducive to the MSCs exerting their angiogenic and immunomodulatory behavior effectively, because it maintains them in close proximity to the islets at the implantation site. In other words, the scaffold would allow the MSCs and islets to be co-localized, possibly maximizing the effectiveness of MSCs as a therapeutic strategy.

2.9 FINITE ELEMENT ANALYSIS (FEM)

The designs of the scaffold and oxygen generator require careful consideration of how the design parameters will affect nutrient delivery. To facilitate the process and predict outcomes for in-vitro translation, finite element analysis was implemented. COMSOL, formerly known as FEMLAB, is multi-physics simulation software that utilizes a finite element analysis to derive quantitative solutions for various multi-physics

applications. This software is used to quantitatively predict the nutrient delivery potential of our tissue engineered construct, based on theoretical mass-balance equations that describe nutrient consumption and nutrient transport. The software performs a series of iterative computations to predict transient and steady state values. The user can translate all of the parameters of the system into input that can be understood by the software.

For example, the device geometry can be defined, material properties of the islets and surrounding environment (oxygen consumption rate (OCR), Michaelis-Menten constant (K_m), and diffusion coefficient) can be specified, and boundary conditions can be selected. Moreover, the results can be post-processed to highlight specific areas of interest, such as showing percent volume of anoxic islets. This software platform has been shown to be highly useful in evaluating the oxygen environment in culture platforms (Peter Buchwald 2009), as well as numerous other biomedical applications, such as transport through porous tissue engineering constructs (Lawrence et al. 2009; Devarapalli et al. 2009; Pierre & Oddou 2007), drug delivery (Bocca et al. 2008), and electrical stimulation of nerve cells (Martinek et al. 2008).This will be used to model diffusion and consumption of oxygen by islets in scaffolds of varying geometries. In addition, models will be generated to illustrate the diffusion and reaction kinetics that characterize the oxygen release from PDMS-encapsulated calcium peroxide.

CHAPTER 3. DESIGN AND CHARACTERIZATION OF MACROPOROUS PDMS SCAFFOLDS FOR ISLET TRANSPLANTATION

3.1 INTRODUCTORY REMARKS

Clinical islet transplantation (CIT), the intraportal infusion of allogeneic islets into patients with Type I diabetes, has shown tremendous promise. Following the intraportal infusion of islets, however, early islet destruction has been observed, which is postulated to be due to the liver site. The intraportal site subjects islets to mechanical stress, high drug and toxin loads, inflammatory responses, and immune attack (Mattsson et al. 2004; Moberg et al. 2002; U. Johansson et al. 2003; H. Johansson et al. 2005; Z. Yang et al. 2004; van der Windt et al. 2007; Bennet et al. 2000; R Paul Robertson 2002; E. Kuntz & H.-D. Kuntz 2005; Paraskevas et al. 2000). The design of an alternative site for islet cell transplantation that minimizes these factors would provide a superior environment for the islets, leading to reduced islet loss and improved function. Simply loading islets freely within alternative sites such as the subcutaneous space, however, has been ineffective. This is likely due to the lack of adequate mechanical protection, spatial distribution, and vascular bed, whereby islets are subjected to mechanical stress and compete with each other for nutrients (Dufour et al. 2005; Blomeier et al. 2006; Salvay et al. 2008). Therefore, there is a strong need to develop alternative devices for islet cell transplantation that would provide mechanical protection and three-dimensional distribution to the islets, while also providing a minimally invasive implantation and the safety of retrievability.

Over the past decades, several researchers have designed and tested numerous devices of this type for the treatment of T1DM, in multiple different forms such as beads sheets, rods, disks, and intravascular devices (Storrs et al. 2001; A. M. Sun 1988; H. Yang et al. 1994; Ohgawara et al. 1998; Calafiore et al. 1992; Calafiore et al. 2006). Previously, the majority of these devices focused on the development of immunoisolation devices, which prevent vasculature migration to the islet site (N. Kobayashi 2008; Q. P. Hou & Bae 1999; Calafiore 1998; A. I. Silva et al. 2006; A. Silva & M Mateus 2009; De Vos et al. 2002; Chaikof 1999; Zeng et al. 2005). The major problem with this approach, however, is the significant depletion of nutrients due to high metabolic demand of the islets. With the oxygen consumption rate for human islets up to 10^6 fold higher than for chondrocytes and 10^4 fold higher than for endothelial cells (W. Wang et al. 2005; Motterlini et al. 1998; Heywood et al. 2006), avascular devices containing islets are constantly plagued with nutrient delivery problems, leading to cell death in the inner portions of the device (A. I. Silva et al. 2006; De Vos et al. 2002; A. Silva & M Mateus 2009). In order to compensate for this problem, researchers have designed devices with shorter diffusion distances and reduced cell loading densities; however, this leads to challenges when attempting to scale up these devices to humans (Storrs et al. 2001). Therefore, it becomes evident that there is a critical need for the design of a cell-based tissue engineered device that simultaneously allows for adequate nutrient delivery, low cell loading density requirements, and is adaptable for scaling from rat to human dimensions.

Given the high metabolic demand of the islets, it is critical to design a device that allows for both intra-device vascularization and a means to spatially distribute the cells

within the device. When islets are simply loaded as a cell suspension within a fluid, they will quickly settle, sediment, and clump together. This configuration is undesirable in that it leads to significant nutritional gradients within the islet pellet, with the islets on the outer edges of the pellet receiving the bulk of the nutrients, and the inner sections receiving inadequate nutritional support. The use of a biomaterial to spatially distribute the cells would allow for a more desirable three-dimensional arrangement of the cells and result in a more efficient delivery of nutrients. Furthermore, it has been shown that islets have improved viability when they are sustained in a matrix similar to their native architecture by encouraging normal inter-cell regulatory interactions (Beattie et al. 2002; Amory et al. 1988; Lucas-Clerc et al. 1993; Montesano et al. 1983; Falorni et al. 1996; Ohgawara et al. 1991; M D Brendel et al. n.d.).

Biomaterials can be implemented to maintain cells spatially distributed in three dimensions in many forms: encapsulation in polymer spheres, immobilization within gels, or adhesion or entrapment within scaffolds. Encapsulation of islets for this particular purpose is not applicable, because each capsule is limited to housing only a few islets in order to prevent severe oxygen gradients throughout the capsule. Hydrophilic gels of gelatin or agarose are effective for maintaining a homogeneous distribution of cells, but slow down the transport of nutrients and waste due to the lower rate of diffusion of molecules through the gel compared to fluid. Porous scaffolds may be the best option for islets, since they distribute cells while minimizing the interference of the biomaterial to nutrient transport. Scaffolds can be microporous (pores smaller than 2 nm), mesoporous (2 to 50 nm), or macroporous (greater than 50 nm). Microporous and mesoporous scaffolds are ideal for facilitating diffusive transport of solutes, whereas macroporous

scaffolds are intended for cell and tissue penetration (Woerly 2000). The scaffold needs to be macroporous in order to allow infiltration of blood vessels and to accommodate islets, which are at least 50 μm in diameter.

The selection of an appropriate biocompatible biomaterial and method of fabrication that allows for spatial distribution, mechanical protection, and intra-device vascularization is a complicated task. Material selection is tissue-specific and requires balancing the desired mechanical properties, pore structure, immunogenicity, biostability, biorecognition, etc of the scaffold. Materials commonly used for scaffolds in tissue engineering may be synthetic or natural and degradable or nondegradable. Common natural materials are fibrin, chitosan, collagen, and bone (T. Hayashi 1994). Fibrin glues have been used as gels and as coatings to promote cell colonization on the surface of synthetic polymers (Khor et al. 2003). Collagen and chitosan are heavily used in wound healing due to their high biocompatibility, and are often incorporated into other polymers to have their structural stability increased (Kellouche et al. 2007; H. Liu et al. 2004). Gelatin, while being a collagen derivative, has limited application due to its low mechanical strength (Deng et al. 2007; T.-W. Wang et al. 2006; S. B. Lee et al. 2005). Generally, natural materials are costly, variable, biodegradable, and require high levels of purification. Synthetic materials, on the other hand, have limited cellular recognition and tissue compatibility (Vacík et al. 2008). While not natural to the body, they can have the advantages of controllability, uniformity, and limited biodegradation. Also, many polymers can be functionalized by converting end groups or adding side chains. Thus, they can be cross-linked with themselves, other polymers, proteins, or bioactive molecules (Behravesh et al. 1999). Synthetic materials commonly used for tissue

engineering scaffolds include poly(ε-caprolactone (PCL), poly(ethylene glycol) (PEG), poly(α-hydroxy esters) like poly(glycolic acid) (PGA), poly(lactic acid) (PLA), and poly(lactic-*co*-glycolic acid) (PLGA) (Sachlos et al. 2003; Ratner et al. 2004). PEG is nondegradable and is frequently used in copolymer blends to contribute hydrophilicity, biocompatibility, and softness. Oligo [poly(ethylene glycol) fumarate] (OPF) is an oligomer containing PEG that forms biodegradable hydrogels with a high degree of swelling (Jo et al. 2001; Temenoff et al. 2003). PGA and PLGA have been particularly prevalent in the design of scaffolds for transplantation into extrahepatic sites (A. I. Silva et al. 2006; Dufour et al. 2005; Blomeier et al. 2006). Also, knitted meshes of PLGA have been used successfully to treat full-thickness diabetic foot ulcers due to their high mechanical strength, capable of withstanding cell contractile forces. Issues with surface hydrophobicity and limited cell adhesion may be ameliorated by combining these synthetic polymers with natural polymers (Guoping Chen et al. 2005). Degradable polymers are desirable when you want the tissue to replace the scaffold without having to retrieve it; however, degradation of a material typically invokes a cellular response and some degradation byproducts are toxic (Sachlos et al. 2003; T. Hayashi 1994).

Some common fabrication methods include: fiber bonding, gas foaming, solvent casting particulate leaching, critical freeze drying, and electrospinning. Fiber bonding can create porosities as high as 81% and interconnected pores up to 500 μm in diameter, but uses toxic solvents (A G Mikos, Sarakinos, et al. 1993; A G Mikos, Bao, et al. 1993). Gas foaming produces highly porous structures (up to 93%), but limits pore size to 100 μm that tend to be unconnected (D J Mooney et al. 1996). Similarly, emulsification/freeze drying and liquid-liquid phase separation also produce high porosities (95%), but small

pore sizes (13-35 μm) (Whang et al. 1995; Lo et al. 1995; Lo et al. 1996). Electrospinning is capable of controlling porosity and pore sizes to a certain degree, but is more useful for creating scaffolds of smaller pore sizes or for growing cells that would benefit from the surface interactions with the rod structure. Moreover, the process requires specialized equipment and has many variables that must be adjusted to achieve the desired parameters.

The solvent casting and particulate leaching technique (SCPL) does not involve any hazardous solvents and is very straightforward: the degree of porosity can be controlled by varying the percent of particulate to solvent, and the pore size is dictated by the diameter of the porogen. Employing compression to the scaffolds during curing improves uniformity of the structure by removing random void spaces of undefined dimensions. Also, the interconnectedness of the pores can be improved by fusing the salt before curing (Murphy et al. 2002) or by using two porogens (Ghosh et al. 2007). In SPCL technique, however, the resulting pores will be square and residual particulate may remain trapped in the scaffold. In addition, the process of particulate leaching is time consuming.

We sought to develop a novel scaffold for housing islets that would serve as a multi-functional platform by which the local microenvironment may be modulated. With this long term goal in mind, we selected the polymer poly(dimethylsiloxane) (PDMS). PDMS is an excellent candidate for long term implantation, due to its demonstrated biocompatibility and biostability following clinical implantation (Hodgins et al. 2007; Khorasani & Mirzadeh 2004; Aucoin et al. 2002; Teixeira et al. 2007; Heise et al. 1990; Bucholz et al. 1987; Nunes et al. 1997). This makes it ideal for evaluating the interactions

and efficacy of the scaffold at different potential implant sites, since the scaffolds can be easily explanted for histological examination. In addition, given the high oxygen demand of islets, the high solubility of oxygen in PDMS renders it an ideal material for housing islets (Vollmer et al. 2005; Cox 1986; Merkel et al. 2000). Furthermore, PDMS can be easily surface modified, via adsorption of proteins, plasma oxygenation, or conjugation of RGD peptides, to create surfaces that promote cellular adhesion, making it an adaptable platform for the co-delivery of islets with "helper" cells, such as mesenchymal stem cells (Shiku et al. 2006; Brown et al. 2005; B. Li et al. 2006; G. K. Toworfe et al. 2004; Hillborg et al. 2000; Mata et al. 2005; Nishikawa et al. 2008). Additionally, the hydrophobic nature of PDMS permits the encapsulation of compounds for slow release into the scaffold microenvironment. In this manner, the scaffold can be used as a platform for drug delivery, if doped with immunosuppressant compounds.

In this study, we demonstrate that macroporous PDMS scaffolds can be fabricated with a large surface to volume ratio and controllable porosity. Parameters of pore size, degree of porosity, and tortuosity of the resulting scaffold were assessed. Given that retention of islets within the porous scaffold is of critical importance, we evaluated the capacity of these scaffolds to retain particles of equivalent sizes of islets. The ability to modify the hydrophobic surface of the scaffold was also evaluated, through coating with proteins. The implications of this platform for the housing of islets within extrahepatic sites are also discussed.

3.2 MATERIALS AND METHODS

3.2.1 MATERIALS

The silicone polymer components were purchased from GE Silicone (RTV 615). Sodium chloride crystals were purchased from Mallinckrodt Baker (NJ). ChromoSphere Polymer Microspheres (Part # BK050, RD100, BK150, RD200) of diameters 50 µm, 100 µm, 150 µm, and 200 µm were obtained from Thermo Fisher Scientific. Sieves with openings of 53 µm, 106 µm, 150 µm, 250 µm, 300 µm, 355 µm, 425 µm, and 600 µm were purchased from W.S. Tyler through VWR. Bovine serum albumin (BSA) and human plasma fibronectin (FN) were purchased from VWR and Gibco, respectively. Biotin conjugated antifibronectin was purchased from Rockland Immunochemicals (PA) and Streptavidin-FITC was purchased from Sigma-Aldrich (MO). All culture media was purchased from Mediatech. MTT kit was purchased from Promega (Madison, WI). LIVE/DEAD Viability/Cytotoxicity Assay Kit and CAS blocker were purchased from Invitrogen. Insulin ELISA was purchased from Mercodia (Winston Salem, NC). Chromogenic kinetic limulus amebocyte lysate (LAL) assay was purchased from Lonza.

3.2.2 SCAFFOLD FABRICATION

Macroporous PDMS scaffolds were fabricated using the solvent casting and particulate leaching technique (SCPL) where the particulate is sodium chloride (NaCl) crystals and poly(dimethyl)siloxane (PDMS) is the solvent. Pore size and degree of porosity were individually optimized by varying the particle size and polymer to particle ratio, respectively. The salt was dried for at least 24 hrs and stored at 40 °C in a drying oven to remove residual air moisture. It was sifted through sieves of varying mesh sizes in order to obtain a specific range of salt diameters: 53 to 106 µm, 150 to 250 µm, 250 to

425 µm, 355 to 425 µm, and 425 to 600 µm. The density of the silicone polymer components and the salt for each size range was determined by weight and volume measurements. Scaffolds were fabricated with varying expected porosities: 85%, 90%, 95% and 97%, based on the volumetric percentage of salt to total volume of scaffold. First in scaffold fabrication, the silicone polymer was prepared by mixing PDMS monomer with platinum catalyst, 4:1 v/v. Then, the desired volume of salt was weighed out (based on density calculations) and thoroughly mixed into the PDMS. The salt/silicone mixture was loaded into prefabricated, PDMS based molds (10 mm diameter, 2 mm height) and incubated at 37 °C for 48 hours in order to completely crosslink the silicone. The salt was leached out from the scaffolds by soaking them in deionized water for 72 hours, with water changes every 24 hours. To demonstrate complete dissolution of salt, scaffold was sectioned 24, 48, and 72 hrs after salt leaching and imaged by SEM for absence of salt crystals. Afterwards, the scaffolds were dried in an oven at 40 °C for 24 hours and steam sterilized in an autoclave.

Scaffold design parameters were optimized by assessing scaffolds of varying pore sizes and intended porosities for differences in structural stability, porosity, and particle retention. First, degree of porosity was optimized by fabricating scaffolds of same pore size (250 to 425 µm) and varying intended porosities (85%, 90%, 95% and 97%). They were examined for structural stability by visual inspection, SEM imaging, and porosity measurements. Second, pore size was optimized by fabricating scaffolds with the same porosity (based on the preceding study's results) and varying pore sizes (53 to 106 µm, 150 to 250 µm, 250 to 425 µm, 355 to 425 µm, and 425 to 600 µm). They were examined

for porous structure by SEM imaging and porosity measurements, followed by quantitative and qualitative assessment of particle retention.

3.2.3 MORPHOLOGICAL CHARACTERIZATION OF SCAFFOLDS

Scanning electron microscopy (SEM) (JEOL, JSM-5600LV, 29 Pa, 20 kV) was employed to visualize surface roughness, pore size, degree of porosity, and tortuosity of the scaffold for varying porosities and pore sizes. Gold sputter coating prevents melting of the scaffold, but alters the scaffold surface. Therefore, sputter coating was circumvented by acquiring images using back-scatter. Total porosity (interconnected and non-connected pores) of the scaffold was quantified by gross measurements and weights. The dry weight ($m_{silicone}$) and wet weight (m_w+$m_{silicone}$), following soaking in ddH_2O, of scaffolds was recorded. Porosity was calculated using known densities of water and silicone (ρ_w and $\rho_{silicone}$), by applying it to Equation (3-1).

$$porosity = \frac{m_w / \rho_w}{m_w / \rho_w + m_{silicone} / \rho_{silicone}} \tag{3-1}$$

3.2.4 RETENTION STUDIES

Retention studies were performed for scaffolds of varying pore size using chromosphere beads as mock islets. Typical size distributions of islets were obtained from the last rat (n=9) and nonhuman primate (n=3) isolations at the Diabetes Research Institute, where islets were counted according to their range of diameters: 50 to 100 µm, 100 to 150 µm, 150 to 200 µm, and 200 to 300 µm. The volumetric contribution of each size range to the total volume of the islet preparation was calculated as the average of the

minimum and maximum volume for that size range. Thus for the size range d_{min} to d_{max}, the volumetric contribution, V_c, can be calculated using Equation (3-2).

$$V_c = \frac{1}{2} \times \frac{4}{3} \pi \left(\left(\frac{d_{\min}}{2} \right)^3 + \left(\frac{d_{\max}}{2} \right)^3 \right) \tag{3-2}$$

Chromospheres of different diameters: 50 µm, 100 µm, 150 µm, and 200 µm, were mixed together in ratios representative of typical isolations. The distribution of spheres was determined by calculating the number of spheres of a given diameter necessary to occupy the same volume as the similarly sized islets. Since the spheres are prone to static interactions, they were kept in a solution containing 10% FBS, 3 mg/mL BSA, and .2% sodium azide in dPBS. Scaffolds used were 2 mm thick, 90% porous, 10 mm in diameter, coated in 3 mg/mL BSA, and had a pore size of: 150 to 250 µm, 250 to 425 µm, or 425 to 600 µm. For loading, they were placed on top of Millicell inserts and each received 1500 IEQ per 300 µL. They were "pulled" through the scaffold by applying a negative pressure gradient and received 3 washes. The number of spheres lost during the initial loading was determined by collecting the remaining spheres in 300 µL and performing manual counts of three 20 µL aliquots with the assistance of a microscope. This loss was labeled "loss after loading". Half of the loaded scaffolds were then immersed in solution, gently shaken for 2 mins at 200 rpm, and the chromospheres lost in solution were counted. The other half of the loaded scaffolds were sectioned and imaged through a stereo microscope to visualize the distribution of the spheres in all planes.

3.2.5 ENDOTOXIN EVALUATION

Following fabrication and sterilization, endotoxin levels within noncoated and fibronectin coated scaffolds were quantified by chromogenic kinetic limulus amebocyte lysate (LAL) assay (Lonza, MD). The assay was performed on both the eluent from the scaffold and on the scaffold itself in order to detect any persistently adherent endotoxins. Eluent was obtained following incubation of 3 scaffolds in 1 mL deionized water for 24 hr. Endotoxin presence on the scaffold surface was evaluated via incubation with the enzyme and monitoring changes in optical density at 405 nm for 1 hour. Results were compared to a calibration curve of endotoxin standards of .005, .05, .25, .5, and 5 EU/mL and dH_2O only controls.

3.2.6 SURFACE MODIFICATION

In selected studies, the scaffold surface was coated with either bovine serum albumin (BSA) or human plasma fibronectin (FN) by incubating the scaffold in a 4 mg/mL BSA or 250 µg/mL FN solution in water for 24 hours. Surface coating of proteins for FN coated scaffolds was visualized via confocal microscopy. First, unbound FN was washed from the coated scaffolds using deionized water (two 1 mL washes, 2 min each), followed by incubation of the scaffolds in CAS blocker for 24 hrs. Scaffolds were incubated with 10 µg/mL of biotin conjugated anti-fibronectin for 1 hr, and subsequently incubated in 10 µg/mL of Streptavidin-FITC for 30 min. Following labeling, scaffolds were washed in PBS. The uniformity of the FN coated scaffold surface was visualized through confocal imaging (Zeiss LSM 510) and compared to controls: 1) uncoated scaffolds treated with both primary and secondary antibodies; and 2) FN coated scaffold treated only with secondary antibody (no primary).

3.2.7 BIOCOMPATIBILITY OF SCAFFOLD

In-vivo biocompatibility of the silicone scaffold was assessed via subcutaneous implantation of 5 mm diameter – 2 mm thick PDMS scaffolds (90% v/v and 250-425 µm pore size) into 1 cm subcutaneous pockets in the back of Lewis rats. All procedures were conducted according to the guidelines of the Committee on Care and Use of Laboratory Animals, Institute of Laboratory Animal Resources (National Research Council, Washington DC). Implants were explanted on days 3, 14, and 30, fixed in formalin, and sliced into 5 µm cross-sections. Histological analysis performed included hematoxylin and eosin (H&E) and Mason's trichrome stain. Silicone scaffold with or without fibronectin coating was compared to absence of material (negative control) and Dacron (positive control).

Scoring of host response to material was performed via a scoring system, which ranked the presence of giant cells and/or macrophages, degree of lymphocytic infiltrate, and degree of fibrosis. Giant cell and/or macrophage presence was graded on a scale from no cells (0) to scattered cells (1), to numerous cells at focal interfaces of the material (2), to numerous cells surrounding the material (3). The degree of lymphocytic infiltrate was graded from no visible infiltrate (0) to minor infiltrate (2), to moderated infiltrate (2), to extensive infiltrate (3). The degree of fibrosis was scaled from none (0), to 1-2 cell layer (1), to 3 to 5 cell layer (2), to greater than 5 cell layer (3). Up to four sections of particular material was assessed independently by three reviewers for each implantation time point. Final scores were then normalized to control implants and averaged. Infiltration of host tissue into the material for uncoated versus FN coated PDMS scaffolds was evaluated via Metamorph analysis, where trichrome stained samples were assessed. The periphery of the scaffold was highlighted as the area of interest (AOI). Positive

staining within the AOI was then quantified and expressed as the percentage of the total AOI area.

3.2.8 STATISTICAL ANALYSIS

The number of replicates is indicated in the figure legends, and results are expressed as mean ± SD. Statistical analysis was performed on all samples using a paired Student's test, where differences were considered significant when $P < 0.05$.

3.3 RESULTS

3.3.1 FABRICATION AND CHARACTERIZATION OF PDMS SCAFFOLDS

Macroporous PDMS scaffolds (10 mm diameter, 2 mm thickness) were fabricated and assessed for optimal porosity and pore size. Optimal porosity was established by examining scaffolds of 250 to 425 μm pore size and varying porosities: 85, 90, 95, and 97% for mechanical stability by visual inspection, SEM (97% porosity excluded), and porosity measurements. A photograph illustrating the macroscopic dimensions of the scaffold can be seen in Figure 3-1. Visually, 85% and 90% porous scaffolds retained their original dimensions (10 mm diameter, 2 mm height) while 95% and 97% porous scaffolds were significantly shrunken (7 mm and 6 mm in diameter, respectively, 1 mm height).

Figure 3-2 contains SEM images of 85%, 90%, and 95% porous scaffolds at low and high magnification. There is a trend of increasing void volume with increasing intended porosity. It can be observed that 85% porous scaffolds have fewer open, interconnected pores than 90% and 95% porous; however, 95% porous scaffolds clearly exhibit collapse and distortion of the pores. Calculations of porosity from gross

measurements and weights (n=3 per group) indicated that for the theoretical porosities of 85%, 90%, 95%, and 97%, the actual porosity was 80%, 85%, 79%, and 73% (± 5 %), respectively. This further indicates a collapse of pore structure when the void space within the scaffold exceeds 90 %. Based on this analysis, 90% porosity was used for subsequent studies.

The effect of salt size on the final pore size of the scaffold was examined for 90% porous scaffolds by varying salt diameters within the following ranges: 53 to 106 µm; 150 to 250 µm; 250 to 425 µm; 355 to 425 µm; and 425 to 600 µm. The structure of silicone scaffolds (90% porous) was evaluated by scanning electron microscopy. SEM images in Figure 3-3 illustrate the highly porous structure of the PDMS scaffolds, with pore sizes representative of the salt crystal diameter. Moreover, the pores appear interconnected and tortuous, with interconnectedness being directly related to pore size, i.e. the greater the pore size, the greater the interconnectivity. The PDMS surface is not as smooth as anticipated; the edges are rough and there is extraneous debris/flack. All scaffolds, with the exception of scaffolds exceeding 90% porosity, were mechanically sound, maintaining their original shape and dimension. Gross measurements and weights (n=3) found that 53 to 106 µm pore size scaffolds had an actual porosity of 73%, while the rest of the scaffolds had an actual porosity of 85% porosity (± 5 %). Therefore, with the exception of the smallest particulate size measured, the porosity of the scaffold did not vary depending on pore size.

Figure 3-1: Representative photograph image of 10 mm diameter, 2 mm thickness PDMS scaffold of 250 to 425 µm pore size.

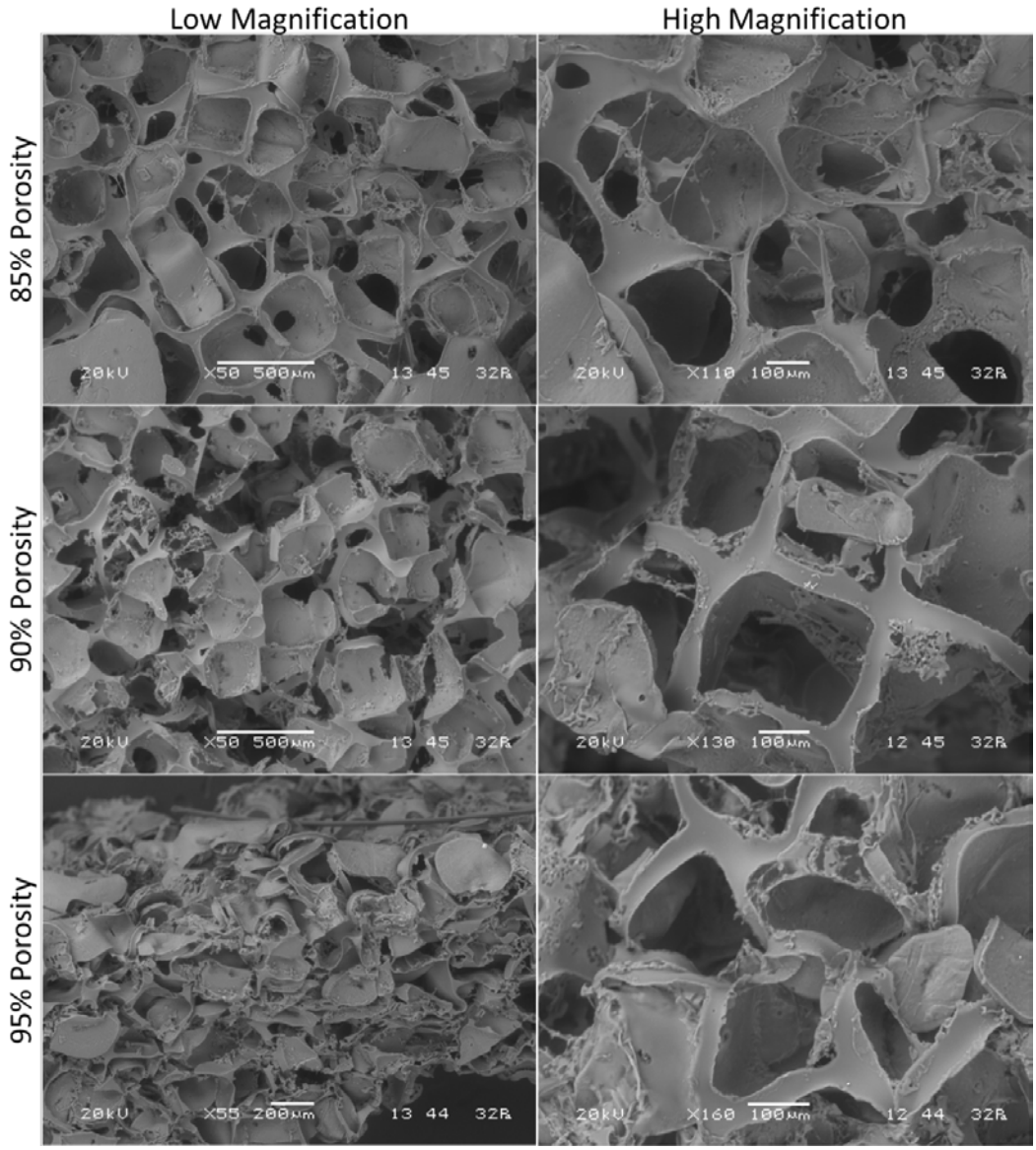

Figure 3-2: Scanning electron microscope images at low (50-55X) and high magnification (110-160X) of 250 to 425 µm pore size scaffolds of 85% porosity, 90% porosity, and 95% porosity.

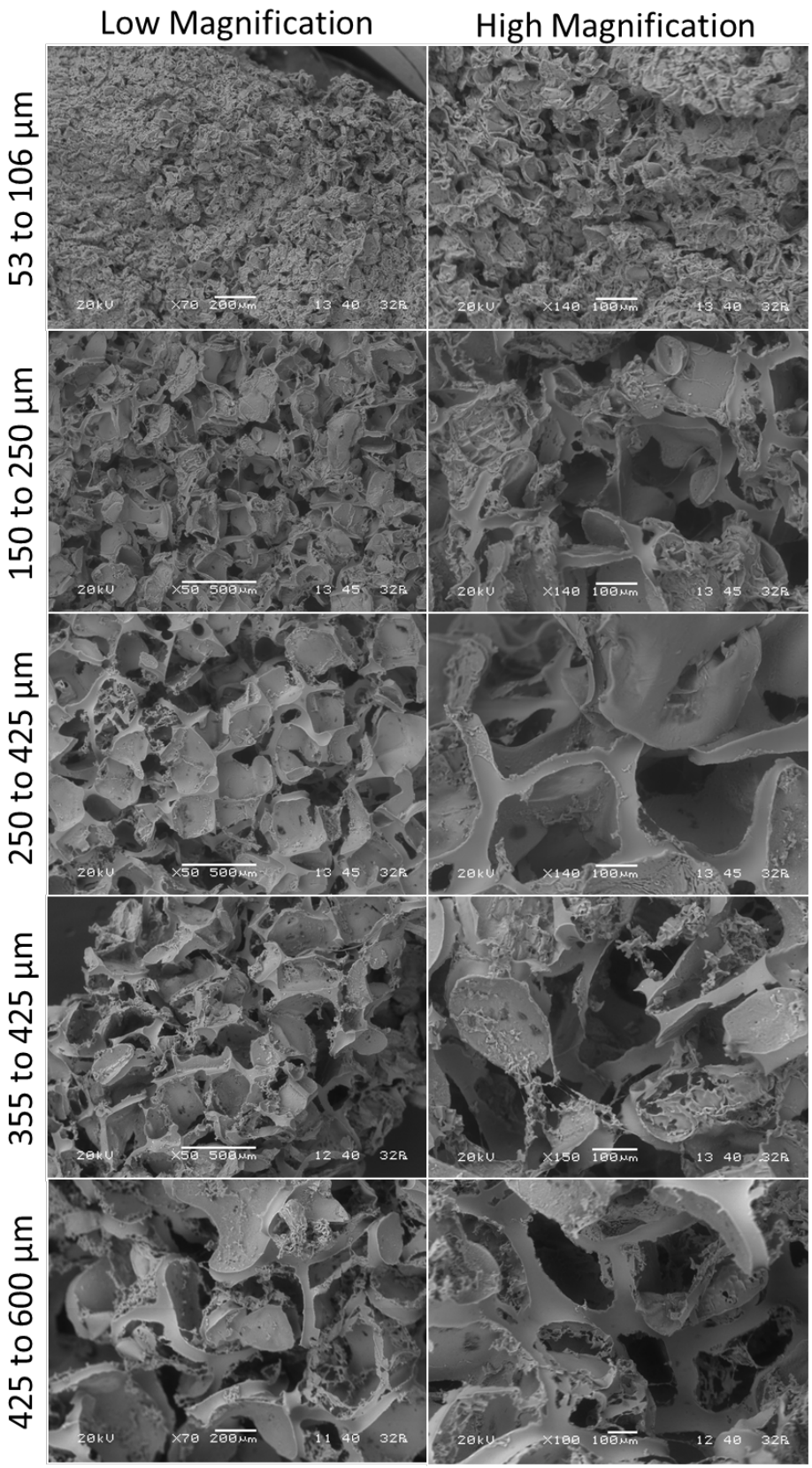

Figure 3-3: SEM at low (50-70X) and high magnification (100-150X) of 90% porous scaffolds of varying pore size diameters.

Optimal pore size for retaining islets was determined by testing retention of ChromoSpheres. Chromospheres served as islet substitutes to permit for the systematic optimization of the scaffolds as a function of pore size range. Scaffold tested were all 90% porosity, but with varying pore size ranges from 150 to 250 µm, 250 to 425 µm, or 425 to 600 µm. Mixtures of Chromospheres were prepared to mimic 1500 IEQ of either rat or nonhuman primate islet distributions (as based on previous isolation size ranges, see Methods) and were loaded onto scaffolds. Distributions by IEQ (percent volume contribution) of typical islet preparations and resulting ChromoSphere mixtures, used for this study, are shown in Table 3-1. Retention was assessed qualitatively by visual inspection of cross-sectional slices and quantitatively by counting. Figure 3-4 and Figure 3-5 show representative cross-sectional sections of these scaffolds, illustrating the distribution of the Chromospheres through the scaffolds of varying pore size ranges. As these figures exhibit, 50 µm are the only ChromoSpheres that can migrate through the scaffolds of 150 to 250 µm pore size range, while particles of larger sizes remain on the top of the scaffold.. In contrast, scaffolds of 250 to 425 µm and 425 to 600 µm pores allowed all of the ChromoSpheres particle sizes tested to pass through, with the greatest distribution of the larger ChromoSpheres (150 and 200 µm) by the 425 to 600 µm scaffold.

Table 3-1: Distribution of islets for islet isolations performed at the Diabetes Research Institute for rat (n=9) and nonhuman primate (n=4).

Islets	50-100 µm	100-150 µm	150-200 µm	200-250 µm	250-300 µm	300-350 µm	350-400 µm
Rat	2%	20%	27%	32%	20%	0%	0%
Nonhuman Primate	34%	34%	16%	14%	2%	0%	0%

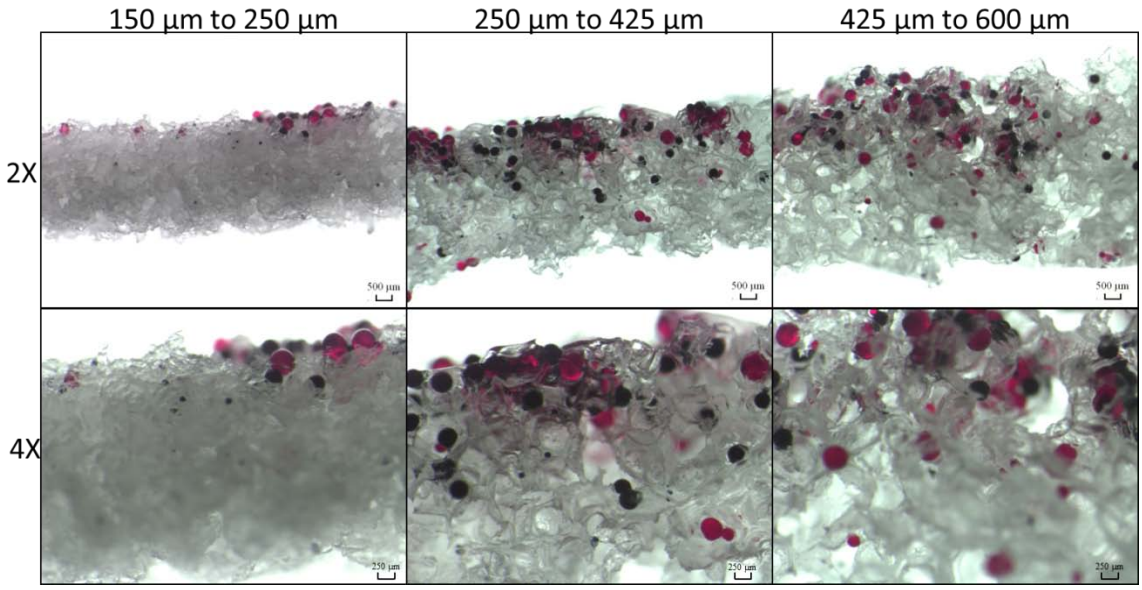

Figure 3-4: Microscope images of cross-sectional slices of 90% porous scaffolds (varying pore sizes) loaded with "1500 IEQ rat solution" of ChromoSpheres. ChromoSpheres were loaded from the top and trickled to the bottom of the scaffold through applied suction.

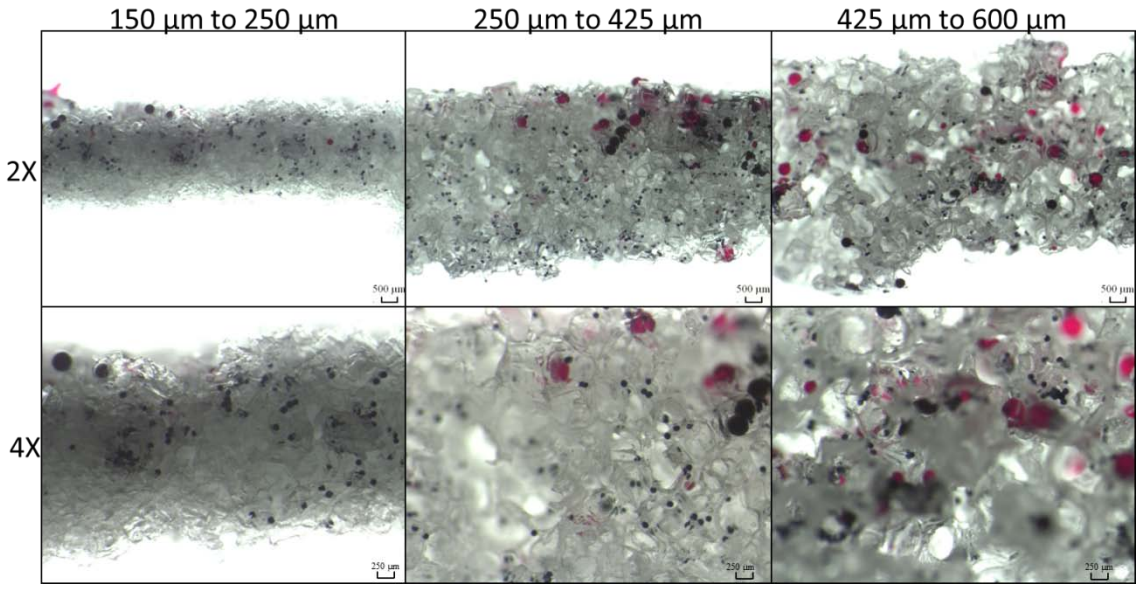

Figure 3-5: Microscope images of cross-sectional slices of 90% porous scaffolds (varying pore sizes) loaded with "1500 IEQ nonhuman primate solution" of ChromoSpheres. ChromoSpheres were loaded from the top and trickled to the bottom of the scaffold through applied suction.

For quantitative assessment of retention during initial loading and following bathing in external fluid, ChromoSpheres loss from the scaffold was counted following initial loading and after washing with dPBS (see Methods section for details). Following initial loading, the trend observed in the microscope images were verified by particle counting, where ChromoSphere counts of particles lost during loading is summarized on the left sides of Figure 3-6 and Figure 3-7, for ChromoSphere particles representing size ranges of both rat and non-human primate islets. As shown in these figures, the greatest loss of particles was in the largest pore size range, 425 to 600 μm. For the smallest particle size, 50 μm, a trend of increased retention with decreasing pore size range was observed. For the larger particle sizes, a negligible loss of particles is observed for all pore sizes (< 2%). Once submerged, however, a greater loss of the particles was observed, as illustrated in the right side of Figure 3-6 and Figure 3-7. Following these washes, the larger spheres resting on top of the scaffolds were typically washed into the solution. This loss was greatest for the scaffold of the smallest pore size range, given that the vast majority of the larger particle sizes accumulated in the top portion of the scaffold (see Figure 3-4). Loss of the 100 μm particles was insignificant for all scaffolds. Loss of particles larger than 150 μm was substantial for all scaffold size ranges tested. Comparing retention between the "rat ChromoSpheres" and the "nonhuman primate ChromoSpheres", there is a greater loss of the smaller particles for the nonhuman primate model beads, but this is expected given their greater presence in the model particles. Based on the results from the SEM and particle retention studies, the 90% porous PDMS scaffold made using 250 to 425 μm salt crystals was used for all subsequent studies.

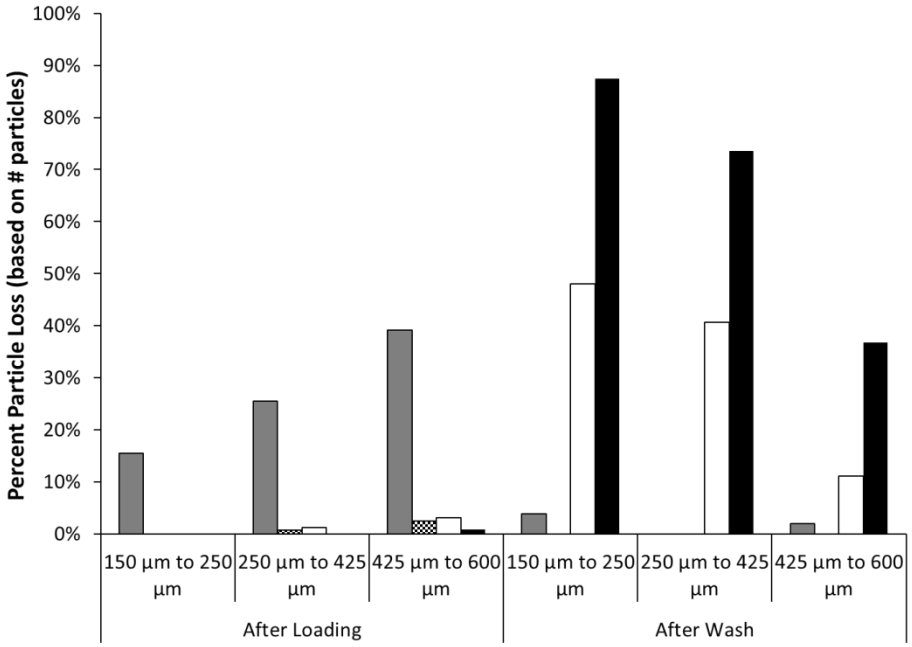

Figure 3-6: Percent particle loss of "1500 IEQ rat solution" of ChromoSpheres, after loading onto scaffold and after washing in dPBS solution, for varying particle diameters: 50 µm (grey bar), 100 µm (checkered bar), 150 µm (white bar), and 200 µm (black bar).

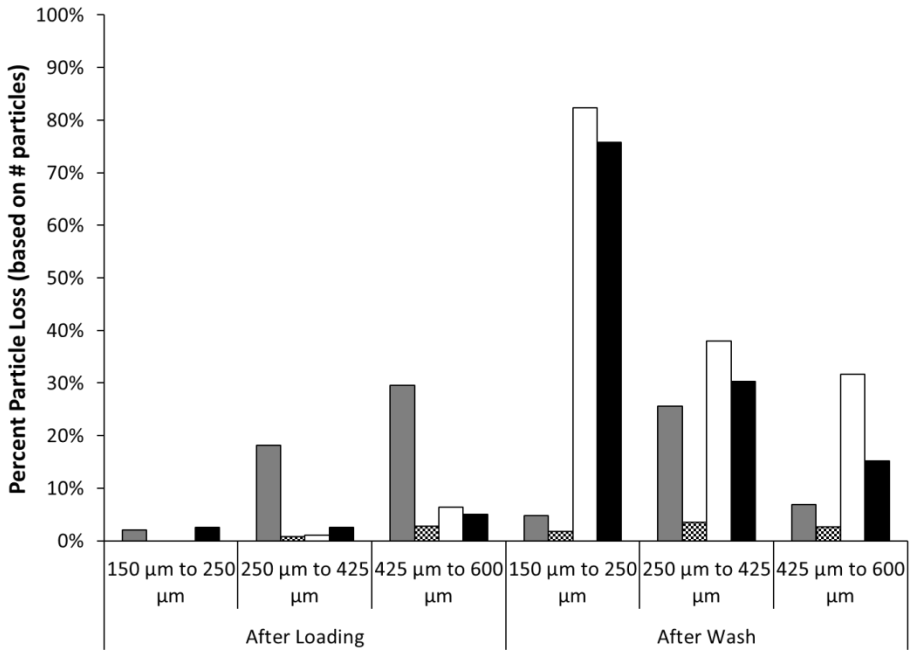

Figure 3-7: Percent particle loss of "1500 IEQ nonhuman primate solution" of ChromoSpheres, after loading onto scaffold and after washing in dPBS solution, for varying particle diameters: 50 µm (grey bar), 100 µm (checkered bar), 150 µm (white bar), and 200 µm (black bar).

The endotoxin level of the scaffold was assessed to minimize the potential to induce a pyrogenic response to the PDMS scaffold when implanted. Endotoxin levels were below 0.05 EU/mL for both noncoated and fibronectin coated scaffolds (values fell within the range of 0.005 EU/mL to 0.05 EU/mL for the n = 3 scaffolds tested for each group).

Surface modification of the PDMS scaffolds with BSA or fibronectin was achieved via overnight incubation with 250 µg/mL fibronectin solution. Following incubation and washing, the surface characteristics of the hydrophobic material was observationally different, with ease in hydration of inner scaffold region following protein coating. The presence of the FN coating on scaffolds was evaluated through confocal imaging of fluorescent antibody stains. Figure 3-8 illustrates a uniform fluorescence throughout the surface and within the inner pore surfaces of PDMS scaffolds incubated with fibronectin, indicating a uniform coating of the fibronectin on the scaffold surface. Positive fluorescent staining was absent for uncoated scaffolds.

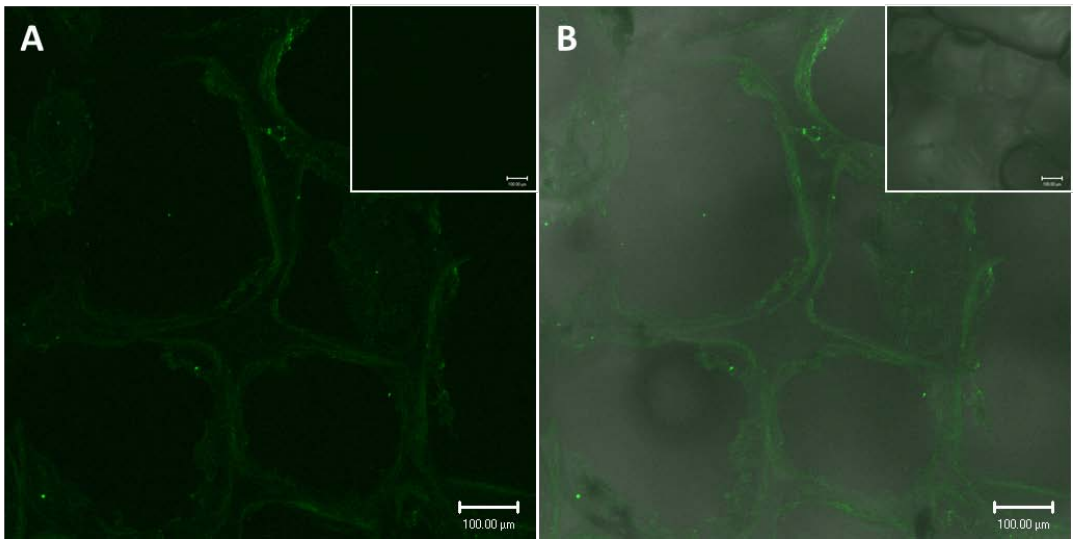

Figure 3-8: Confocal imaging (fluorescent (A) and fluorescent/light (B)) of fibronectin coated PDMS scaffold (main) and noncoated scaffold (inset) stained with anti-fibronectin-biotin primary and streptavidin-FITC secondary antibodies.

3.3.2 BIOCOMPATIBILITY OF SCAFFOLD

PDMS scaffolds, with or without BSA or fibronectin coating, were implanted in the subcutaneous space in rats and explanted on Days 7, 14, and 30. PDMS scaffolds were compared to Dacron (positive control) and absence of material (negative control) by hematoxylin and Masson's trichrome stain. H&E permits visualization of cellular presence, whereas trichrome identifies collagen deposition (blue) and elastin or fibrous deposition (red). Histological assessment found strong biocompatibility, host integration, and biostability of the PDMS scaffolds. As shown in Figure 3-9 and Figure 3-10, histological cross-sections of explanted implants found silicone to be superior to Dacron material, with positive remodeling and matrix deposition within pores, as well as the absence of significant fibrotic tissue. After 30 days, no significant degradation or infiltration within the PDMS material itself, indicating high biostability of the PDMS scaffolds. Biostability measurements via potassium hydroxide washing to remove tissue was prevented for this study, given that PDMS will also dissolve in this media. As Figure 3-11 shows, multiple blood vessels were observed infiltrating into all scaffolds on days 14 and 30. Cellular and vascular infiltration into scaffold was also observed, indicating that the macro-porosity of the implants permits ease in the infiltration of host cells and vasculature. Furthermore, when comparing uncoated to FN coated PDMS scaffolds, it was found that the fibronectin coating encouraged a substantially higher degree of cellular infiltration and ECM deposition compared to the uncoated scaffold. Metamorph analysis, shown in Figure 3-12 and Figure 3-13, quantitatively determined that there was both greater collagen deposition and total cellular infiltration in fibronectin coated scaffolds than noncoated scaffolds. Of further note is the shift in the deposition of matrix from fibrin-based (red on Trichrome staining) to collagen-based (blue on

Trichrome staining) between Day 7 and Day 14, indicating positive remodeling within the scaffold environment, which was observed qualitatively via trichrome images and measured quantitatively with enhanced positive collagen staining, Figure 3-13. Scoring of the biocompatibility of these scaffolds resulted in the observations that infiltration by lymphocytes, while moderate on Day 7, was resolved by Day 14. In addition, minimum fibrosis was observed in the scaffolds, even on Day 30. The only concern for these implants was the presence of macrophages and giant cells after 14 days in-vivo. This presence was still observed on Day 30. These results illustrate the compatibility of the PDMS macroporous scaffold in-vivo, as well as the ability to modulate the surface of the scaffold from low cellular infiltration to high. Overall, the results of these biocompatibility studies indicate that the PDMS scaffold is biostable and encourages positive remodeling in the form of collagen deposition and cellular infiltration, without any visible formation of a fibrotic capsule.

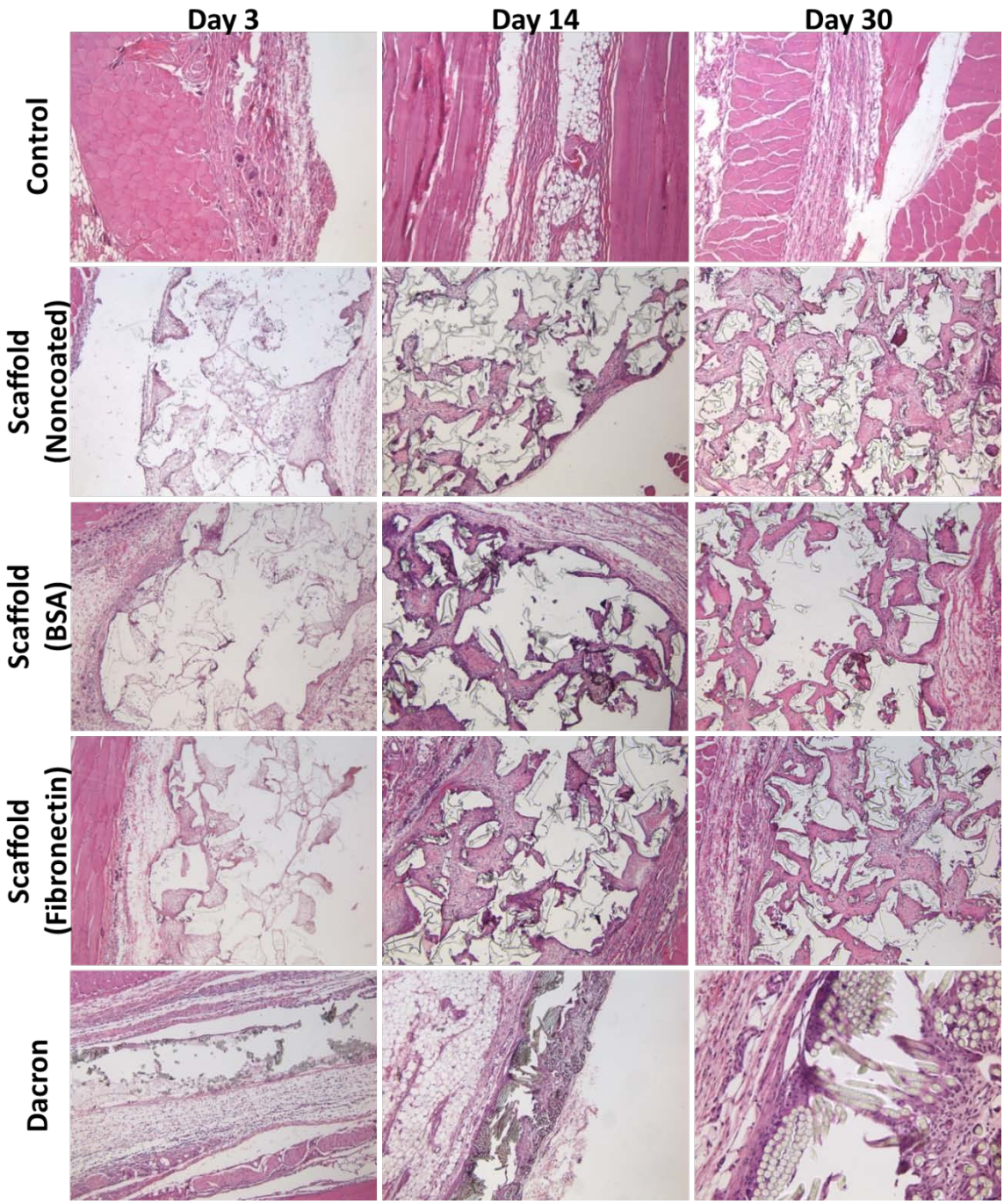

Figure 3-9: 10X magnification of histological cross-sections (using hematoxylin/eosin stains) illustrating degree of biocompatibility and potential for vascular infiltration of various biomaterials implanted into rodents.

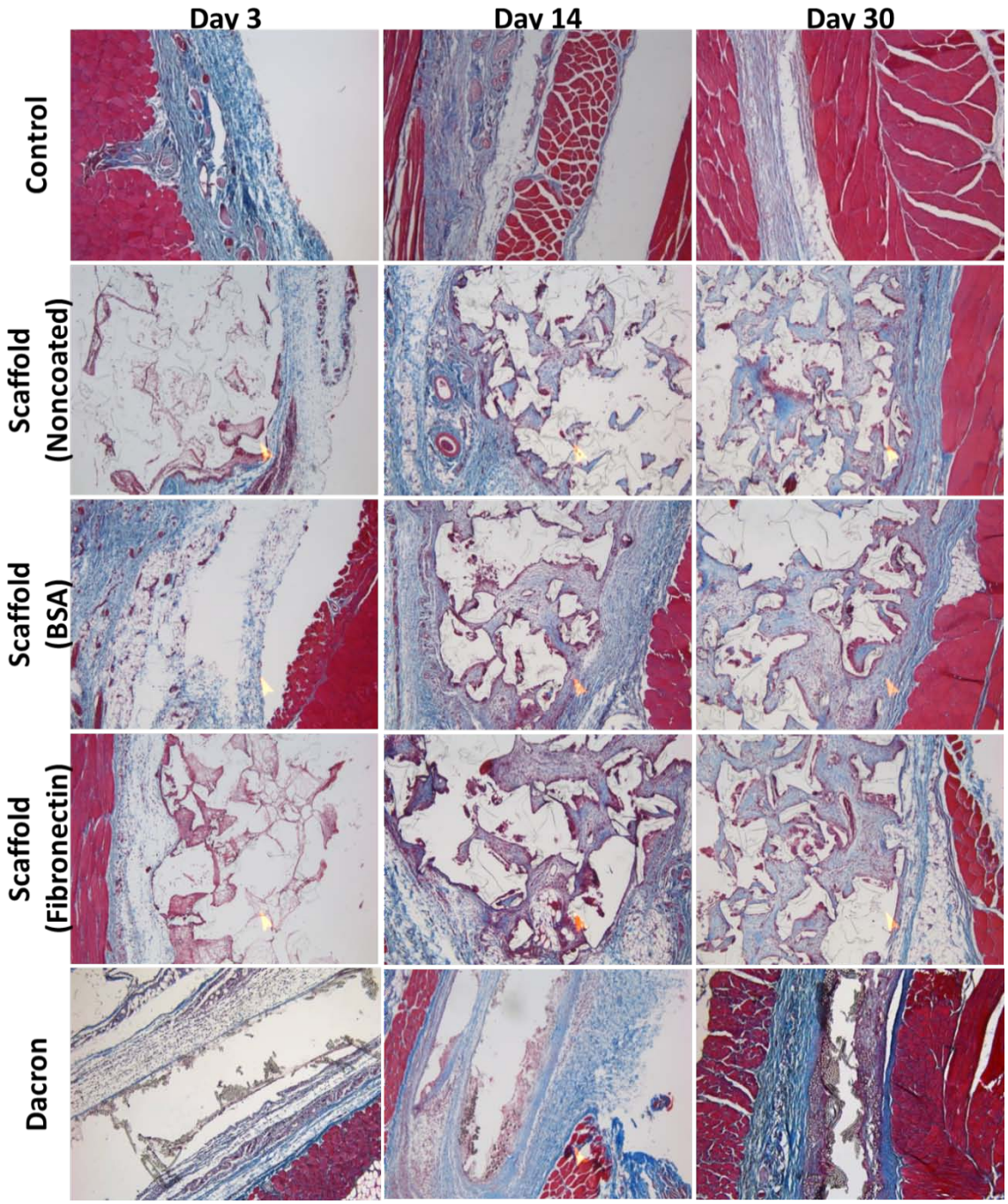

Figure 3-10: 10X magnification of histological cross-sections (using Masson's trichrome stain) illustrating degree of biocompatibility and potential for vascular infiltration of various biomaterials implanted into rodents.

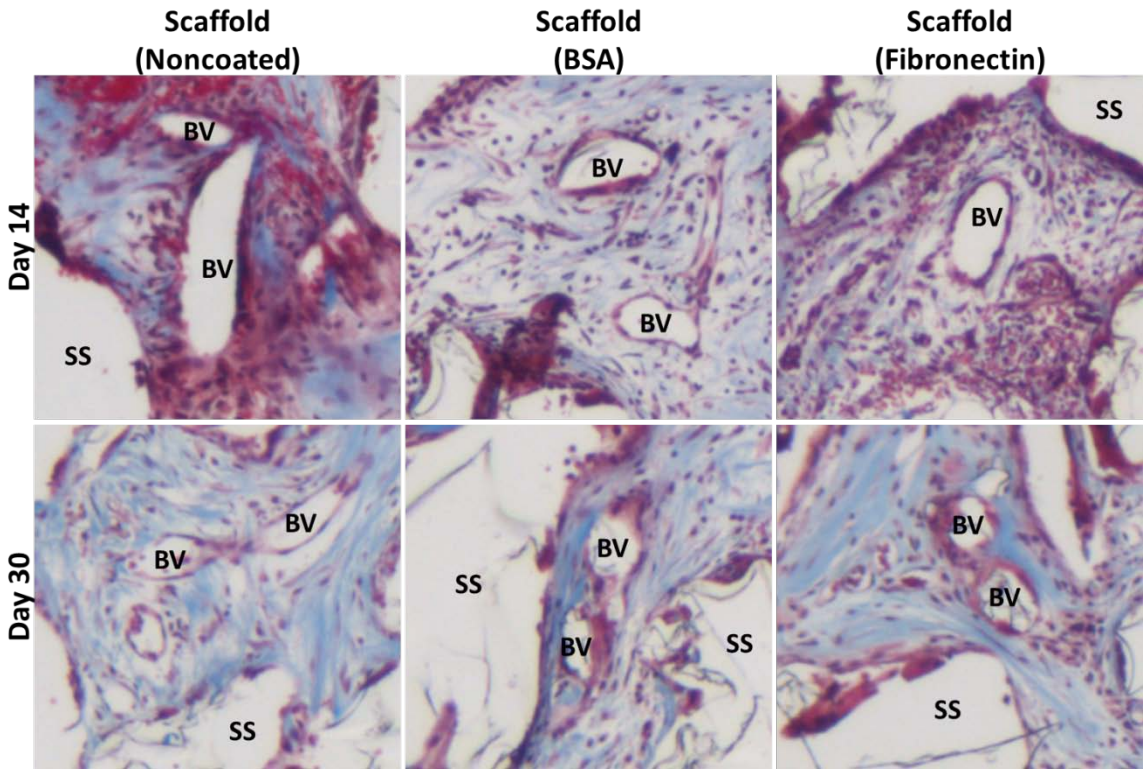

Figure 3-11: Identification of blood vessel (BV) infiltration into scaffolds (SS) on histological cross-sections (using Masson's trichrome stain).

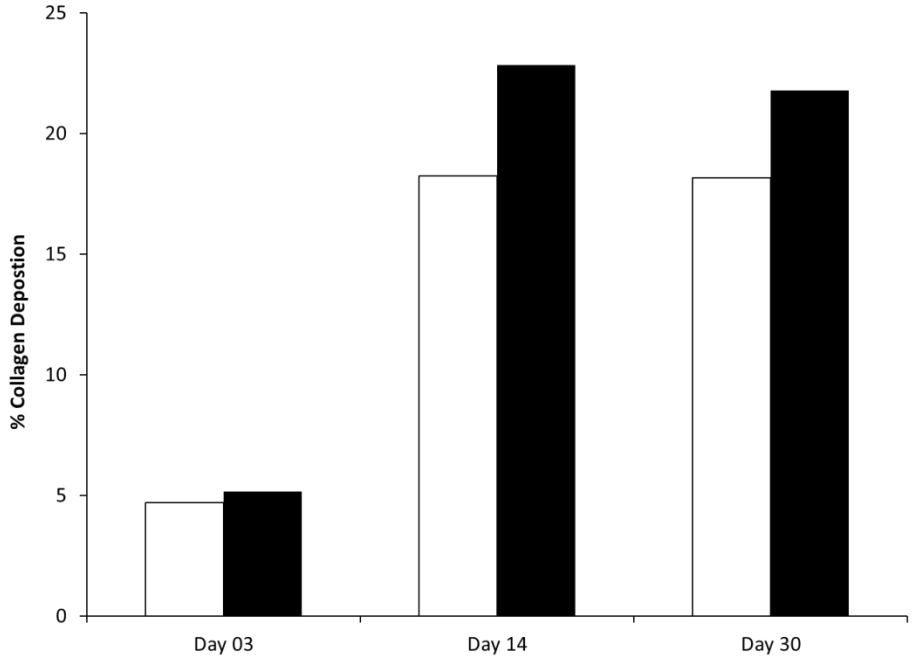

Figure 3-12: Deposition of collagen into noncoated (white bars) and fibronectin coated (black bars) scaffolds over time as determined by Metamorph Analysis of blue areas in Masson's trichrome stain.

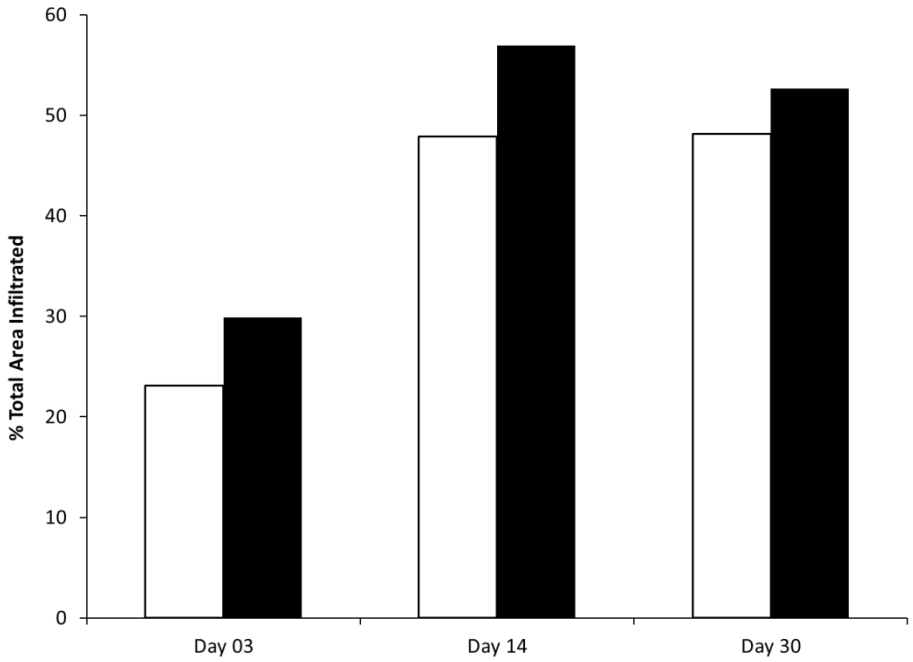

Figure 3-13: Total infiltration into noncoated (white bars) and fibronectin coated (black bars) scaffolds over time as determined by Metamorph Analysis of total area not occupied by the scaffold material itself in Masson's trichrome stain.

3.4 DISCUSSION

In this study, we sought to fabricate a highly porous scaffold capable of spatially distributing islets and providing mechanical support for them. PDMS material was selected for its biocompatibility, biostability, and high diffusivity for oxygen, while the SCPL technique was selected for its controllable pore size and porosity. The porosity of the scaffold must be optimized, so that a low volume of bulk material can be balanced with high mechanical stability. SEM and porosity measurements found scaffolds fabricated with porosity greater than 90 %, to be mechanically unstable. This is likely due to the high void volume, which weakens the scaffold structure causing it to collapse on itself. Scaffolds with 90 % porosity achieved the best compromise between low bulk material volume and high mechanical stability and were used for all subsequent studies.

The high void volume combined with the high diffusivity of oxygen through silicone ensures that the scaffold will have favorable transport of oxygen to the islets.

The pore size of a scaffold is of critical importance, because adequate vascularization of the scaffold and high retention of islets is vital for transplant efficacy. The pore size should be large enough to accommodate large islets and incoming blood vessels, but also small enough to entrap smaller islets within the scaffold. SEM analysis and porosity measurements showed that salt crystal size directly affected final pore size, but not degree of porosity. For the various salt crystal diameters tested, most scaffolds had a similar structure (but of varying size), with the exception of the 53 to 106 μm, which was found to have a significantly lower final porosity. This suggests that these salt particles create smaller pores within the walls of the pore itself, causing the pore to lose its structural integrity. Another possible explanation is that the 53 to 106 μm salt crystals have a different geometry (not as cuboidal) than the larger sized crystals. In general, the large pore sizes of the scaffold, as evidenced by SEM, indicate that the scaffold is conducive to accommodating islets, as well as incoming blood vessels.

Results of ChromoSphere retention studies demonstrated that particle retention within the scaffold is highly dependent on size of the particle, as well as the size of the scaffold pore range. Scaffolds with smaller pore sizes, such as 150 to 250 μm, had higher retention of 50 μm ChromoSpheres, but substantially decreased distribution of the particles throughout the scaffold. The converse was true for scaffolds of larger pore sizes, with a greater loss of the smaller particles, but optimal distribution throughout the scaffold. Based on imaging, the smaller scaffold pore size range tested, the 150 to 250 μm size range is non-ideal, as it does not result in the actual distribution of the particles.

This leaves the size ranges of 250 to 425 µm or 425 to 600 µm. For these scaffold ranges, the optimal pore size of the scaffold would depend on the typical size of the islets. Compared to the other scaffolds, the 425 to 600 µm scaffold had significantly higher retention of "rat chromospheres", because those islets tend to be large. The difference was not as pronounced when comparing "nonhuman primate chromospheres", since the typically smaller non-human primate islets were adequately retained by the smaller pore sizes. However, it is important to note that smaller islets do not contribute significantly to the total IEQ (volume). Nonetheless, it is important to consider their retention, since some islet preparations may be predominantly comprised of small islets (~50 µm). Therefore, the pore size of 250 to 425 µm gives the best compromise for retaining islets from different species and consequently different sizes. While the use of ChromoSphere permitted for the detailed characterization of particle distribution and retention within these macroporous scaffolds, it should be noted that the translation of these results to islets may not be as direct. The ChromoSpheres tend to aggregate, as well as express static interference and non-adhesion to surfaces. In this manner, the loss of particles out of these scaffolds, particularly following washing with solutions, may be over-exaggerated. In light of this, methods that would enhance the adhesive capacity of the PDMS scaffold should be beneficial to increasing islet retention long term.

Since the native PDMS surface is hydrophobic, it is important to be able to modify it for cell adherence. Surface modification of the PDMS was easily performed via nonspecific adsorption of BSA or fibronectin, where antibody labeling of the coating illustrated a homogenous coating throughout the scaffold. This indicates that the silicone scaffold surface can be readily modified with various protein coatings to encourage

cellular attachment. More elegant methods for surface medication are feasible; with published methods illustrating the use of plasma oxygenation for simple surface conjugation to create surfaces that promote cellular adhesion (Shiku et al. 2006; Brown et al. 2005; B. Li et al. 2006; G. K. Toworfe et al. 2004; Hillborg et al. 2000; Mata et al. 2005; Nishikawa et al. 2008). Future studies could explore these methods to further enhance surface modification.

Silicone is known for its high biocompatibility and biostability (Darren J Martin et al. 2000; Simmons et al. 2004; Karunakaran & Kennedy 2007; Shiku et al. 2006). Our biocompatibility studies reinforced this by finding that these scaffolds (noncoated, BSA coated, and fibronectin coated) did not exhibit signs of degradation during the 30 days tested. The inflammatory reactions between the scaffold and the host are minimal, with resolution of infiltrate within 2 weeks and the absence of significant fibrosis. Surface modification of the scaffold via coating of fibronectin enhanced positive remodeling, as evidenced by increased collagen deposition and vascularization over time (Q. P. Hou & Bae 1999). The favorable results of the biocompatibility and endotoxin tests demonstrate that PDMS scaffolds are suitable for application in-vivo. Furthermore, the biostability of silicone permits retrievability following implantation, if desired.

PDMS is a material with a long history in medical implantation and has been incarnated in multiple forms for various tissue engineering applications. However, it has not, to our knowledge, been previously developed into a macroporous scaffold. For example, in the development of a bioartificial pancreas, PDMS has been blended with polyurethane into tubular membranes, demonstrating high rates of diffusion for glucose and oxygen (C K Colton & Avgoustiniatos 1991). Also, Norman et al microfabricated

PDMS scaffolds with molded collagen matrix for fibroblast growth (Norman & Desai 2005). These scaffolds were not porous, but rather consisted of an array of 40 μm wide channels separated by 25 μm walls. Brown et al grew smooth muscle cells on a PDMS "scaffold" consisting of a sheet of PDMS surface modified by a layer-by-layer self-assembly (LBL) method (Brown et al. 2005). Similarly, PDMS films with adsorbed fibronectin were used for culturing osteoblast-like cells (G. K. Toworfe et al. 2004). Therefore, we believe this represents a novel scaffold for housing cellular transplants in-vivo.

Most devices for transplantation of islets have been focused on immunoisolation. They entail "blocking" islets from the immune system by sequestering them within a semi-permeable membrane, inadvertently aggregating islets and hindering nutrient transport (H. Iwata et al. 1994; N. Kobayashi 2008; A. I. Silva et al. 2006). Others scaffolds for islet transplantation seek natural, degradable materials that mimic the extracellular matrix and aim to restore islet-matrix interactions originally present in the pancreas. In contrast, the purpose of our device is not to immunoisolate or to directly mimic the pancreas, but rather to maximize the spatial distribution of the islets and mechanically protect them from surrounding tissue, when implanted into extrahepatic sites, while also promoting acceptance of the implant through the migration of healthy host tissue into the void space. Therefore, this work has a strong design component where the parameters of material selection, fabrication method, pore size, and porosity were varied to achieve optimal porous structures, retention, and biocompatibility. Others examine only the effects of the scaffold on islet viability and function and success of the

graft (Blomeier et al. 2006; Perez-Basterrechea et al. 2008), which we ourselves will investigate in the next chapter.

Moreover, the scaffold has the potential to serve as a platform for further modulating the local environment. The nature of PDMS is one where materials may be incorporated within the matrix for slow release. Of particular interest is the incorporation of hydrophobic drugs, which may then release in a controllable manner over time. Many popular scaffolds for drug release in tissue engineering have been biodegradable, releasing degradation products along with the drug (Howard et al. 2008; Ratner & Bryant 2004). These degradation products may be toxic or may induce inflammatory responses that would be detrimental to islets. Alternatively, slow release of drugs from hydrophobic polymers has demonstrated success (D. L. Ely et al. 1991; Simmons et al. 2008; Jewrajka et al. 2007). By applying this technique to the scaffold, a new material can be created that provides a microniche for islets. Future studies are evaluating the potential of this PDMS-based macroporous platform to deliver beneficial agents, including anti-inflammatory and/or immunomodulatory agents, to the localized islet transplant environment.

3.5 CONCLUSION

Biocompatible, PDMS scaffolds were successfully fabricated with intended porosities and a controllable pore size range. Optimization of scaffold design found these platforms to be suitable for retaining particles of size ranges from 50 to 200 μm. The biocompatibility of these PDMS scaffolds makes them appropriate for in-vivo implantation. They can function as platforms that are conducive to tailoring to various particulate sizes, via variations in salt crystals, as well as surface properties, via protein coatings, to permit ease in application to a wide range of tissue engineered implants.

CHAPTER 4. MACROPOROUS PDMS SCAFFOLDS FOR ISLET TRANSPLANTATION: SHORT-TERM CELL CULTURE AND IN-VIVO EFFICACY

4.1 INTRODUCTORY REMARKS

Treatment of type I diabetes via intraportal infusion of islets has demonstrated success in current clinical trials resulting in patients with superior control in blood glucose levels, high C-peptide levels, and insulin independence for several years after treatment (A. M. Shapiro et al. 2006). However, the high rate of dysfunction and early islet destruction observed in both the clinical transplants and in animal models has been primarily associated with the location of the transplant – the intraportal vein of the liver, which subjects islets to mechanical stress, high drug and toxin loads, inflammatory responses, and immune attack (Mattsson et al. 2004; Moberg et al. 2002; U. Johansson et al. 2003; H. Johansson et al. 2005; Z. Yang et al. 2004; van der Windt et al. 2007; Bennet et al. 2000; R Paul Robertson 2002; E. Kuntz & H.-D. Kuntz 2005; Paraskevas et al. 2000). The design of an alternative site for islet cell transplantation that minimizes these factors would provide a superior environment for the islets, leading to reduced islet loss and improved function. However, transplantation of islets into alternative sites, such as the subcutaneous space, necessitates a device that would provide adequate mechanical protection, spatial distribution, and vascular infiltration (Dufour et al. 2005; Blomeier et al. 2006; Salvay et al. 2008). Therefore, there is a strong need to develop alternative devices for islet cell transplantation that would provide mechanical protection and three-dimensional distribution to the islets, while also providing a minimally invasive implantation and the safety of retrievability. Over the past decades, several researchers

have designed and tested numerous devices of this type for the treatment of T1DM, in multiple different forms such as beads, sheets, rods, disks, and intravascular devices (Storrs et al. 2001; A. M. Sun 1988; H. Yang et al. 1994; Ohgawara et al. 1998; Calafiore et al. 1992; Calafiore et al. 2006). Previously, the majority of these devices focused on the development of immunoisolation devices, which prevent vasculature migration to the islet site (N. Kobayashi 2008; Q. P. Hou & Bae 1999; Calafiore 1998; A. I. Silva et al. 2006; De Vos et al. 2002; Chaikof 1999; Zeng et al. 2005). The major problem with this approach, however, is the significant depletion of nutrients due to high metabolic demand of the islets. With the oxygen consumption rate for human islets up to 10^6 fold higher than for chondrocytes and 10^4 fold higher than for endothelial cells (W. Wang et al. 2005; Motterlini et al. 1998; Heywood et al. 2006), avascular devices containing islets are constantly plagued with nutrient delivery problems, leading to cell death in the inner portions of the device (A. I. Silva et al. 2006; De Vos et al. 2002; A. Silva & M Mateus 2009). In order to compensate for this problem, researchers have designed devices with shorter diffusion distances and reduced cell loading densities. However, this leads to challenges when attempting to scale up these devices to humans (Storrs et al. 2001). Therefore, it becomes evident that there is a critical need for the design of a cell-based tissue engineered device that simultaneously allows for adequate nutrient delivery, low cell loading density requirements, and is adaptable for scaling from rat to human dimensions.

Given the high metabolic demand of the islets, it is critical to design a device that allows for both intra-device vascularization and a means to spatially distribute the cells within the device. When islets are simply loaded as a cell suspension within a fluid, they

will quickly settle, sediment, and clump together. This configuration is undesirable in that it leads to significant nutritional gradients within the islet pellet, with the islets on the outer edges of the pellet receiving the bulk of the nutrients, and the inner sections receiving inadequate nutritional support. The use of a biomaterial to spatially distribute the cells would allow for a more desirable three-dimensional arrangement of the cells and result in a more efficient delivery of nutrients.

The selection of an appropriate biocompatible biomaterial that allows for spatial distribution, mechanical protection, and intra-device vascularization is a complicated task. The ideal matrix would be one that is highly porous, with deep, interconnected pores to trap the islets throughout the device, while also allowing for vascular infiltration. Previously, Blomeier et al demonstrated that a highly porous Poly(D,L-lactide-co-glycolide) (PLG) scaffold seeded with islets and transplanted into the intraperitoneal fat of a mouse could be highly efficacious in a diabetic syngeneic mouse model (Blomeier et al. 2006). They found significant improvements in efficacy for islets loaded within a 5 mm × 5 mm PLG cylinder over islets implanted without the scaffold. Vascular infiltration was also evident in histological sections. While the degradation of the scaffold over time restricts the ability to remove the implant at a later date, this study illustrates the importance of scaffolding in mechanically protecting and spatially distributing the transplanted islets.

Another important factor to consider for extrahepatic transplantation is selection of the transplant site, which should optimize islets survival and function. Implantation sites that have been studied include: epiploic chambers in the great omentum, area around the splenic vein, external wall of the stomach, intramuscular, peritoneal cavity, renal

cavity, kidney capsule, and subcutaneous sites (Dufour et al. 2005; A. I. Silva et al. 2006; Kin et al. 2003; Aoki et al. 2005; X. Chen et al. 2007; Weber et al. 1978; Rafael et al. 2008; Speier et al. 2008). The subcutaneous site in particular has been extensively used, especially when it has been pre-vascularized in order to mimic the islets' native environment and minimize diffusion limitations (Juang et al. 1995; De Vos et al. 1997; Antonello Pileggi et al. 2006). For small animal models, islets are often transplanted under the kidney capsule or spleen with demonstrated success (Hesse et al. 1986; Warnock et al. 1990; Kaufman et al. 1990; Warnock & R V Rajotte 1992; S. A. White et al. 2001; S. A. White et al. 2000). For mice in particular, the epididymal fat pad is a promising site with preliminary success, because of its reasonable size, good vascularization, and accessibility. However, the kidney capsule and fat pad sites have reduced clinical relevance, since they do not translate well to human anatomy (Dufour et al. 2005; Blomeier et al. 2006). Moreover, for transplantation in large animal models and humans, the scaffold size must be scaled up to account for the larger islet mass required, necessitating a site that can accommodate a larger tissue volume. The omental pouch meets these requirements and has been used to cure diabetes in rats and dogs (Kin et al. 2003; Juang et al. 1995; R Paul Robertson 2004; Ao et al. 1993; Yasunami et al. 1983; Guan et al. 1998). It has portal drainage of secreted hormones without direct exposure to high concentrations of immunosuppressive drugs, host platelets, and complement. Studies demonstrate that portal drainage results in improved physiological function of islets compared to systemic drainage (Cuthbertson & Mandel 1986). Moreover, it is easily accessible, allowing for retrieval of implants, if necessary (Dufour et al. 2005).

Therefore, we have focused our in-vivo experiments on transplantation of the scaffold into the omental pouch.

In earlier studies, we sought to develop a novel scaffold for housing islets that would serve as a multi-functional platform by which the local microenvironment may be modulated. As such, we fabricated macroporous PDMS scaffolds via the solvent casting and particulate leaching technique (SCPL). PDMS was selected as the biomaterial, based on its biostability, demonstrated biocompatibility in-vivo, oxygen solubility, and ease in surface modification. Resulting scaffolds demonstrated high mechanical stability, even with 90 % void space, and the volume ratio and porosity could be controlled.

Herein, we investigated the suitability of these PDMS macroporous scaffolds for housing pancreatic islets, through assessment of islet viability and function following loading. The ability of this PDMS platform to serve as a means to co-deliver both islets and "helper" cells was also evaluated by characterizing the attachment and proliferation of mesenchymal stem cells. Finally, we evaluated the capacity of these islet-loaded scaffolds to restore normoglycemia within an alternative transplant site in syngeneic, streptozotocin -induced diabetic Lewis rats. We selected the omentum as the transplant site, given the clinical relevance of this site. The use of this novel PDMS-based platform to house islets within alternative sites is discussed.

4.2 MATERIALS AND METHODS

4.2.1 MATERIALS

The silicone polymer components were purchased from GE Silicone (RTV 615). Sodium chloride crystals were purchased from (Mallinckrodt Baker (NJ). Sieves with openings of 250 μm and 425 μm were purchased from W.S. Tyler through VWR. Bovine

serum albumin (BSA) and human plasma fibronectin (FN) were purchased from VWR and Gibco, respectively. Agarose powder type VII was purchased from Sigma-Aldrich. All culture media was purchased from Mediatech. MTT kit was purchased from Promega (Madison, WI). LIVE/DEAD Viability/Cytotoxicity Assay Kit was purchased from Invitrogen. Insulin ELISA was purchased from Mercodia (Winston Salem, NC).

4.2.2 SCAFFOLD FABRICATION

Macroporous PDMS scaffolds were fabricated using the solvent casting and particulate leaching technique (SCPL). Pore size and degree of porosity were individually controlled by varying the particle size and polymer to particle ratio, respectively. Scaffolds were composed of 90% v/v sodium chloride salt crystals, 250 μm to 425 μm in diameter, mixed with silicone polymer. The silicone polymer was prepared by mixing PDMS monomer with platinum catalyst, 4:1 v/v. The salt/silicone mixture was loaded into prefabricated, stainless steel molds (10 mm diameter, 2 mm height), pressurized to 1500 psi, and incubated at 37 °C for 48 hours in order to completely crosslink the silicone. The salt was leached out from the scaffolds by soaking them in deionized water for 72 hours, with water changes every 24 hours. Afterwards, the scaffolds were dried in an oven at 40 °C for 24 hours and steam sterilized in an autoclave.

The scaffold surface was coated with either human plasma fibronectin (FN) by incubating the scaffold in a 4 mg/mL BSA or 250 μg/mL FN solution in water for 24 hours.

4.2.3 CELL ISOLATION AND CULTURE

Mesenchymal stem cells (MSC), isolated from human umbilical cord blood, were kindly donated by Dr. Luca Inverardi at passage 3. Prior to seeding on scaffolds, MSCs were cultured at monolayers in α-minimum essential medium (α-MEM; Gibco) supplemented with fetal bovine serum (FBS; Gibco) in a humidified 37°C, 5% CO_2 / 95% air incubator. All MSC experiments were conducted between passages 4-6.

MIN6 cells (passages 30-40) were cultured as monolayers in T-flasks and fed every 2-3 days with fresh medium comprised of Dulbecco's modified Eagle's medium (DMEM) supplemented with 10% FBS, 1% penicillin-streptomycin (P/S), and 0.001 % (v/v) β-mercaptoethanol.

Rat pancreatic islets were isolated from male Lewis rats, obtained from Harlan Laboratory (Indianapolis, IN) and weighing between 250 and 280 g, using methods described elsewhere (Antonello Pileggi et al. 2006). Nonhuman primate baboon (NHP) islets were isolated using methods described elsewhere (Berman et al. 2010). All procedures were conducted according to the guidelines of the Committee on Care and Use of Laboratory Animals, Institute of Laboratory Animal Resources (National Research Council, Washington DC). Human pancreatic islets of Langerhans were obtained from the NIH/JDRF ICR Consortium or from the Diabetes Research Institute at the University of Miami. For rat and NHP islets, islets were cultured in CMRL 1066 (Mediatech) for 24 hrs prior to seeding into scaffolds. Human islets were cultured in MM1 (Mediatech) for 24 hrs following arrival prior to loading into scaffolds. CMRL 1066 and MM1 media was supplemented with 10% fetal bovine serum (FBS; Sigma), 1% penicillin-streptomycin (Sigma), and 1% L-glutamine (Sigma).

4.2.4 CELL LOADING ON SCAFFOLDS

For MSCs, cells were harvested from monolayers via 0.25% (w/v) trypsin–EDTA (Gibco) and counted via trypan blue. MSCs were seeded onto either uncoated, BSA coated, or FN coated PDMS scaffolds at a loading density of $3x10^5$ cells per scaffold in 50 µL of media and incubated for 30 min prior to the addition of 4 mL of media for long term culture.

Islets used were either of rat, nonhuman primate, or human origin. Scaffolds were prepared for islet loading via washing with respective islet culture media. Islets were visually counted using methods described previously to calculate islet equivalent (IEQ) (Peter Buchwald et al. 2009). Islets were loaded at the desired islet equivalent (IEQ) density into the fabricated scaffolds, concentrating the desired IEQ into 50 µL of media and pipetting them onto the scaffolds, where they filtered through the micro-sized pores. For a subset of scaffolds, fibrin glue was added to the islet loaded scaffolds by pipetting 30 µL onto the top of the PDMS scaffold. Islet loaded scaffolds were then incubated at 37 °C for 15 min. Scaffolds were then transferred to 35 mm culture dishes, 4 mL of media was added, and they were cultured at either 5% or 20% oxygen.

We sought to compare the viability of islets cultured on PDMS scaffolds to islets cultured on a typical three-dimensional construct, such as agarose. Cylindrical agarose constructs (10 mm in diameter, 2 mm final thickness) were fabricated by carefully suspending rat islets in 2% agarose at 37 °C at a density of 1000 IEQ (for rat islets) or 1500 IEQ (for nonhuman primate islets) per construct, and allowing to gel for 3 mins at room temperature. Islets were loaded on scaffolds as previously described; agarose and PDMS scaffolds were cultured in 35 mm culture dishes with 4 mL of culture media for 2

days at 5% oxygen. The agarose-cell constructs were assessed for cell viability via MTT metabolic assay (Promega, WS) and live/dead staining (Invitrogen, CA).

4.2.5 ISLET RETENTION AND METABOLIC VIABILITY IN SCAFFOLDS

MTT assay (Promega, WI) was used to evaluate the metabolic activity of islets. Samples were washed once, suspended in 250 µL of media within a 48-well non-tissue culture treated plate, and placed in a humidified incubator for 1 hr to recover from manipulation. Following 1 hr incubation, 28 µL of MTT dye was added to each well and samples were incubated for an additional 1 hr. Afterwards, 185 µL of stop/solubilization solution was added to each well to quench the reaction and the plate was wrapped in parafilm protected from light, and stored for 24 hr to solubilize the formazan crystals. The next day, 120 µL samples from each well were dispensed into a 96-well plate and the absorption at 570 nm was measured using a plate reader. Changes in optical density due to culture media used were compensated for by subtracting media blanks from all wells.

For islet retention studies, islet loss from the scaffold was evaluated 4 hr after loading within the scaffold. Following the addition of 0.5 mL of media to the well containing the scaffolds, scaffold were then moved into a separate well. Assessment of both the scaffold and the islets remaining in the well following scaffold removal was conducted via MTT assay. Retention % is expressed as the percentage of islets retained within the scaffold, via division of absorbance of islets in scaffold by total absorbance (islets in scaffold + islets in well). For metabolic assessment of islets within scaffolds, islet loaded scaffolds were cultured for 2 days under normal (140 mmHg) oxygen

tensions in a humidified 37°C, 5% CO_2 / 95% air incubator prior to viability measurements via MTT.

4.2.6 LIVE/DEAD VIABILITY

Cell viability was visualized by the LIVE/DEAD Viability/Cytotoxicity Assay Kit (Invitrogen) and imaged through a confocal microscope (Zeiss LSM) using methods outlined previously (Hall et al. 2011). Briefly, cells were rinsed in HBSS and incubated for 45 min in 4 µM calcein AM and 8 µM ethidium homodimer-1 (EthD-1) solution diluted in PBS. Following a second rinse in HBSS, scaffolds were imaged via a fluorescent scanning confocal microscope (LSM 510, Zeiss, Germany). Live cells (green) were detected by excitation with light at 494 nm and emission at 517 nm while dead cells (dead) were detected by excitation at 528 nm and emission at 617 nm. Multi-slice images were collected and merged using the projection function on LSM image browser (Zeiss, Germany) software.

4.2.7 INSULIN SECRETION FUNCTION

The functional insulin secretion rate of islets was determined via static glucose-stimulated insulin release (GSIR) assay. Groups were sequentially incubated for one hour intervals in glucose solutions: low glucose (40 mg/dL) high glucose (300 mg/dL), and low glucose again; using a column method, as described elsewhere (Chris Fraker et al. n.d.; Embury et al. 2001). Briefly, 10mL Poly-Prep columns (Bio-Rad) were placed in Poly-column rack (Bio-Rad), filled with 400 µL of a slurry of Sepharose G-10 (GE Healthcare)/dPBS (10% w/v) and washed with low glucose (2.2 mM) KREB's buffer (26mM sodium bicarbonate, 25mM HEPES, and 0.2% w/v BSA). Free islets or islet

containing scaffolds (150 IEQ total) were then placed within the columns and an additional 600 µL of bead slurry was added to each column. Columns were then flushed with 4mL of low glucose KREB's solution. Flow in the columns ceased when the liquid level reached the surface of the beads keeping the fluid volume in each column constant. Columns were then incubated for 1 hr for pre-incubation, followed by a 4mL wash with low glucose KREB's, at which the first step of the glucose challenge (Low1) was initiated. After 1 hr, low glucose KREBs was exchanged with high glucose (16.7 mM) KREBs to begin step two of the challenge (High1). After this hr, high glucose was exchanged with low glucose KREB to begin step three of the challenge (Low2). During each exchange, 1 mL of the respective KREBs solution was added and the 1 mL eluate was collected in tubes and stored at – 80 °C for later analysis. Insulin was quantified using the Mercodia Rat or Human Insulin ELISA (Winston Salem, NC), depending on the islet type.

4.2.8 ISLET TRANSPLANTATION AND GRAFT ASSESSMENT

All animal studies were reviewed and approved by the University of Miami Institutional Animal Care and Use Committee. Female Lewis rats, obtained from Harlan Laboratory (Indianapolis, IN) and weighing between 175 and 185 g, were used as transplant recipients. The Preclinical Translational Core at the Diabetes Research Institute assisted with diabetes induction and maintenance of the animals. Rats were rendered diabetic by intravenous administration of the beta cell toxin streptozotocin (two intravenous injections of 60 mg/kg 2-3 days apart; Sigma-Aldrich, St. Louis, MO) and were used as recipients of syngeneic islets only if overtly diabetic (three consecutive readings of non-fasting blood glucose levels > 350 mg/dL).

Under general anesthesia (isoflurane USP; Baxter, Deerfield, IL), a mid line incision was made and the omentum was mobilized, exposed, and spread out using saline. A single 10 mm diameter, 2 mm thick PDMS scaffold was placed on the exposed omentum. 1800 IEQ islets were concentrated into 50 µL of saline and loaded onto the scaffold using a pipette. Subsequently, 30 µL of fibrin was added to the islet loaded scaffold. After 30 sec, the omentum was then wrapped around the scaffold by folding each side inward. The edges were subsequently sealed with fibrin glue. Following 1 min, the scaffold loaded omental pouch was then loaded back into the peritoneal cavity and the incision was sutured and stapled.

Graft function was defined as non-fasting glycemic levels < 200 mg/dL, assessed from tail bleeds using a portable blood glucose meter (Bayer). A glucose tolerance test was performed 130 days after transplantation for metabolic assessment of the grafted islets. After overnight fasting, rats received an intravenous glucose bolus (2 g/kg in saline) and blood glucose was monitored until it read below 200 mg/dL. Glucose clearance was evaluated by calculating the area under the curve (AUC) from the first reading until one reading < 200 mg/dL. To ensure that the function observed for graft-bearing normoglycemic animals was due to the islet transplant, the omentum, and hence the islet loaded scaffold, was explanted in a survival surgery and the blood glucose levels of the rats were monitored to ensure the prompt return to the diabetic state.

Explanted grafts were evaluated via histological analysis. Following fixation in 10% formalin buffer, grafts were paraffin embedded and sectioned into 10 µm sections. Tissue sections were stained with hematoxylin and eosin, as well as Masson trichrome staining (Richard Allan Scientific). Immunofluorescence was used to stain the islets via

the primary guinea pig anti-insulin antibody (Dako) and a secondary goat anti-guinea pig Alexa-568 conjugated antibody (Molecular Probes).

4.2.9 STATISTICAL ANALYSIS

The number of replicates is indicated in the figure legends, and results are expressed as mean ± SD. Statistical analysis was performed on all samples using a paired Student's test, where differences were considered significant when $p < 0.05$.

4.3 RESULTS

4.3.1 PROLIFERATION OF CELLS ON SCAFFOLD

The effects of surface modification on the attachment and proliferation of adherent cells was investigated through the use of mesenchymal stem cells. Scaffolds evaluated included: untreated, bovine serum albumin (BSA) coated, or fibronectin coated. Proliferation and viability of cells was evaluated 2 and 7 days after loading using LIVE/DEAD assay and confocal microscopy. As Figure 4-1 illustrates, cellular adhesion on the uncoated and BSA coated scaffolds was minimal, with rounded, non-adherent cells observed on Day 2 and 7, and no observable increase in cell number. Conversely, for fibronectin coated scaffolds, adherent cells adopted a stretched, adherent morphology. An increase in MSC cell presence was observed between Day 2 and 7, indicating proliferation of the MSCs on the scaffold. Additional measurements of MSC proliferation was performed via MTT, which found significant increases in cell number over the seven day culture period (data not shown). For all subsequent studies using cells, the scaffolds were always coated with fibronectin.

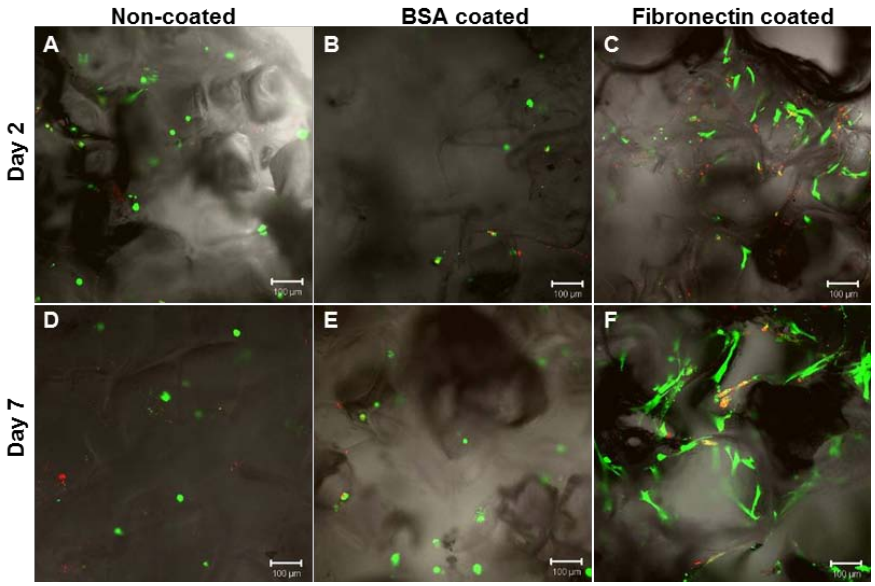

Figure 4-1: Analysis of the effects of scaffold coating on cellular adhesion by visualizing live/dead human MSCs growing on scaffolds. Evaluated scaffolds on days 2 (top row) and 7 (bottom row), respectively: untreated surface (A, D), BSA coated (B, E), and fibronectin coated (C, F).

Cell growth of scaffolds in comparison to standard culture conditions was also evaluated to assess the capacity of the three-dimensional, macroporous environment to permit cellular growth. MIN6 cells, an adherent beta cell line, were seeded onto plates or scaffolds at different cell densities (2×10^5, 1.2×10^6, and 1.4×10^6 cells per well or scaffold) (n=3 per group) and assessed via MTT viability assay after 48 hours at standard 20% oxygen culture conditions. As demonstrated in Figure 4-2, cell viability was greater on the scaffold than on culture plates for all loading densities tested. Moreover, the difference in cell viability between controls and scaffolds increased with initial cell loading density, where over a 5-fold increase in cell viability was observed at the highest cell loading tested.

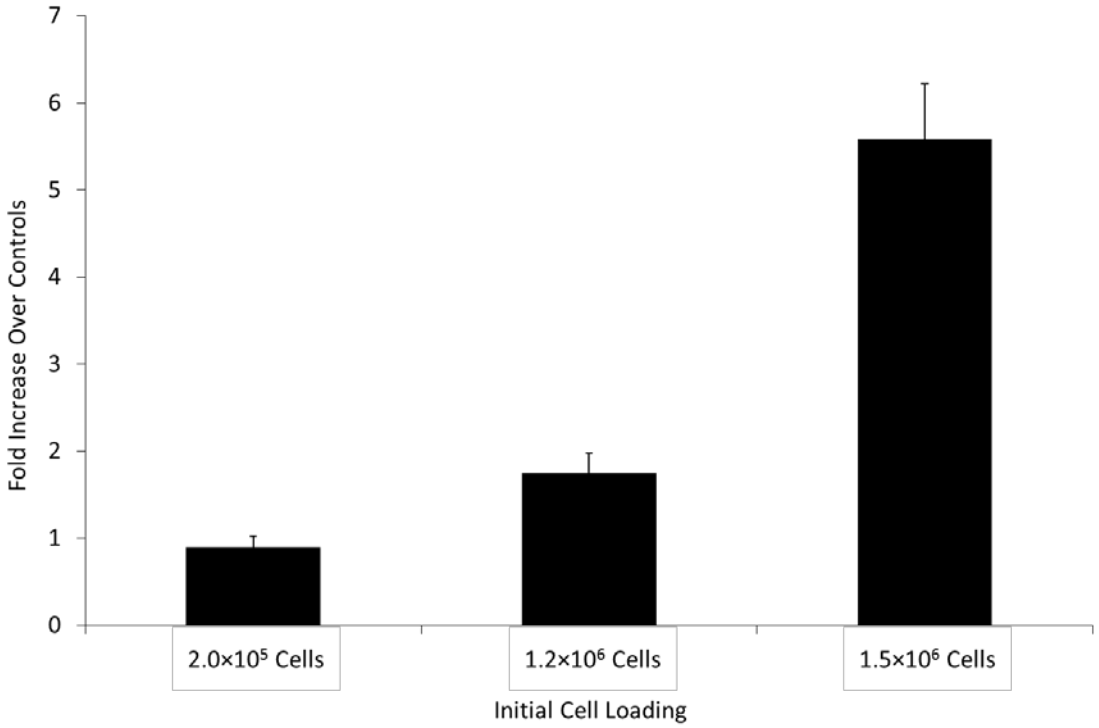

Figure 4-2: Fold increase of MTT optical density of adherent cells on scaffold for different initial cell loading densities following 48 hrs of culture. Values expressed as fold increase over controls, which is standard two-dimensional culture of the same loading density.

4.3.2 RETENTION OF ISLETS ON SCAFFOLD

The retention of islets on the PDMS scaffold, with or without the addition of fibrin glue, was characterized for two different islet sources: nonhuman primate and rat. To accomplish this, scaffolds were seeded with 1,500 IEQ islets, with a subset of scaffolds receiving the addition of fibrin glue. By quantifying the amount of islets leaving the scaffold following submersion in media, the percent loss of islets from the scaffold was determined. Figure 4-3 shows that scaffolds loaded with rat islets retained approximately 80% of the islets, regardless of the presence of fibrin gel. On the other hand, only 30% of nonhuman primate islets were retained on scaffolds without fibrin gel. The incorporation of fibrin gel increased islet retention to 80%. In evaluating the

disparity between the two islet sources, it was noted that the size distribution, as evaluated via IEQ counts (based on percent volume contribution), between the rat and nonhuman primate islets was significantly different. Nonhuman primate islets had 34% of the islets smaller than 100 μm, while 98% of the rat islets were larger than 100 μm. Thereby, there is a correlation between islet retention and islet size.

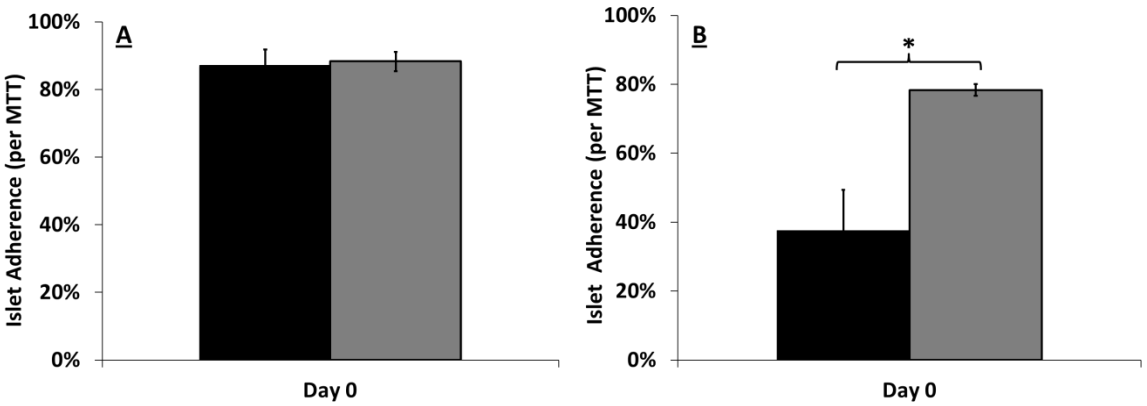

Figure 4-3: Retention of islets within scaffold alone (black bar) and scaffold with fibrin (grey bar) as measured by MTT for rat islets (A) and nonhuman primate islets (B). Asterisk indicates statistical significance ($p<0.05$).

4.3.3 VIABILITY AND FUNCTION OF ISLETS ON PDMS MACROPOROUS SCAFFOLDS UNDER STANDARD CULTURE CONDITIONS

The introduction of PDMS scaffolds and fibrin glue might affect diffusion to the islets. Since islets are very sensitive to their surrounding environment, it was important to determine what effect the scaffold would have on islet viability. The viability of human, nonhuman primate, and rat islets in standard Petri dishes was compared to that of islets on fibronectin coated silicone scaffolds. Nonhuman primate and rat islets were also evaluated with the addition of the fibrin glue. Scaffolds were seeded with 1,500 IEQ of islets and subsequently cultured at 20% oxygen for 24 hours. MTT and LIVE/DEAD viability were performed after 0 and 24 hours in culture. As Figure 4-4 and Figure 4-5

illustrate, the viability of the islets at 20% oxygen was not significantly affected by culturing on scaffolds. In addition, confocal microscopy images of scaffolds illustrate a uniform distribution of islets throughout the PDMS scaffold.

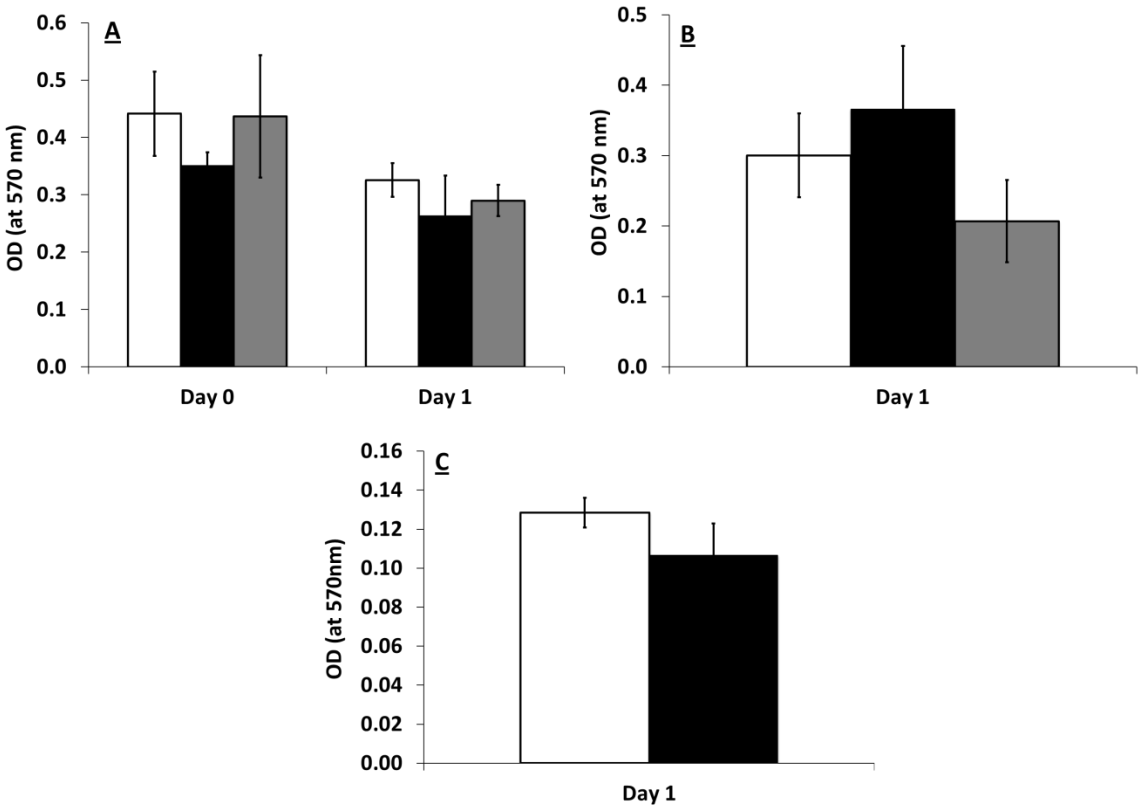

Figure 4-4: MTT viability of 1500 IEQ islets in two-dimensional standard culture dish controls (white bars), within scaffold without fibrin (black bars), or within scaffold with fibrin (grey bars) for rat islets (A), nonhuman primate islets (B), and human islets (C). Islets were cultured for 0 and 24 hr for rat islets and 24 hr for non-human primate and human islets.

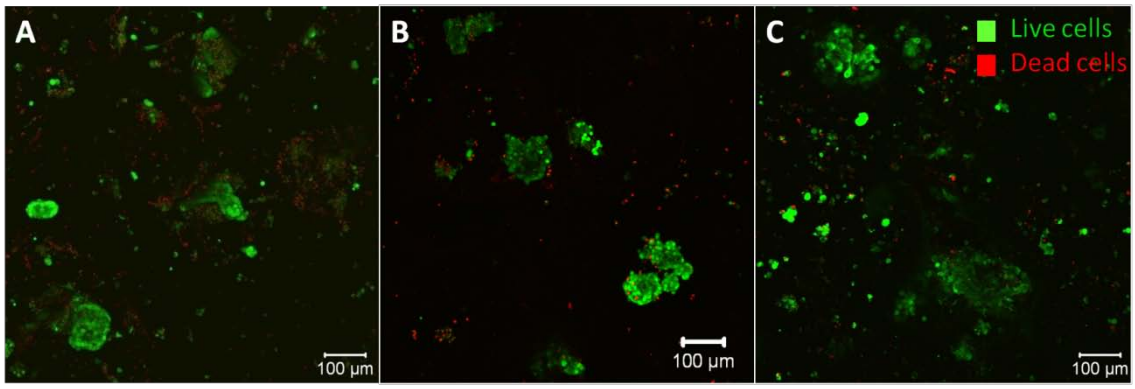

Figure 4-5: Confocal imaging of LIVE/DEAD (green: viable; red: dead) staining of (A) rat islets, (B) nonhuman primate islets, or (C) human islets within PDMS macroporous scaffolds following 24 hrs in culture.

The insulin secretion of islets loaded into fibronectin coated PDMS macroporous scaffolds, with and without fibrin glue, was performed to evaluate the effects of confinement within these macroporous scaffold on islet function. Scaffolds were seeded with islets and subsequently cultured at 20% oxygen for 24 hours. Insulin secretion was evaluated via a static glucose stimulated insulin secretion assay after this time period. Results are expressed in Figure 4-6 as stimulation index (insulin release during high glucose over release during low glucose). For all cases, insulin stimulation was higher during the high glucose period than for both low periods (low 1 and low 2, see Methods for details). For all cases, low 2 values were close to or equal to low 1 values, indicating normal insulin profiles. The insulin secretion index of islets cultured on silicone scaffolds was typical of healthy islets: approximately 2.5 for rat islets, 3 for nonhuman primate islets, and 3 for human islets (see Figure 4-6). The fibrin glue did not significantly alter the insulin secretion of either rat or nonhuman primate islets on scaffolds ($p>0.05$).

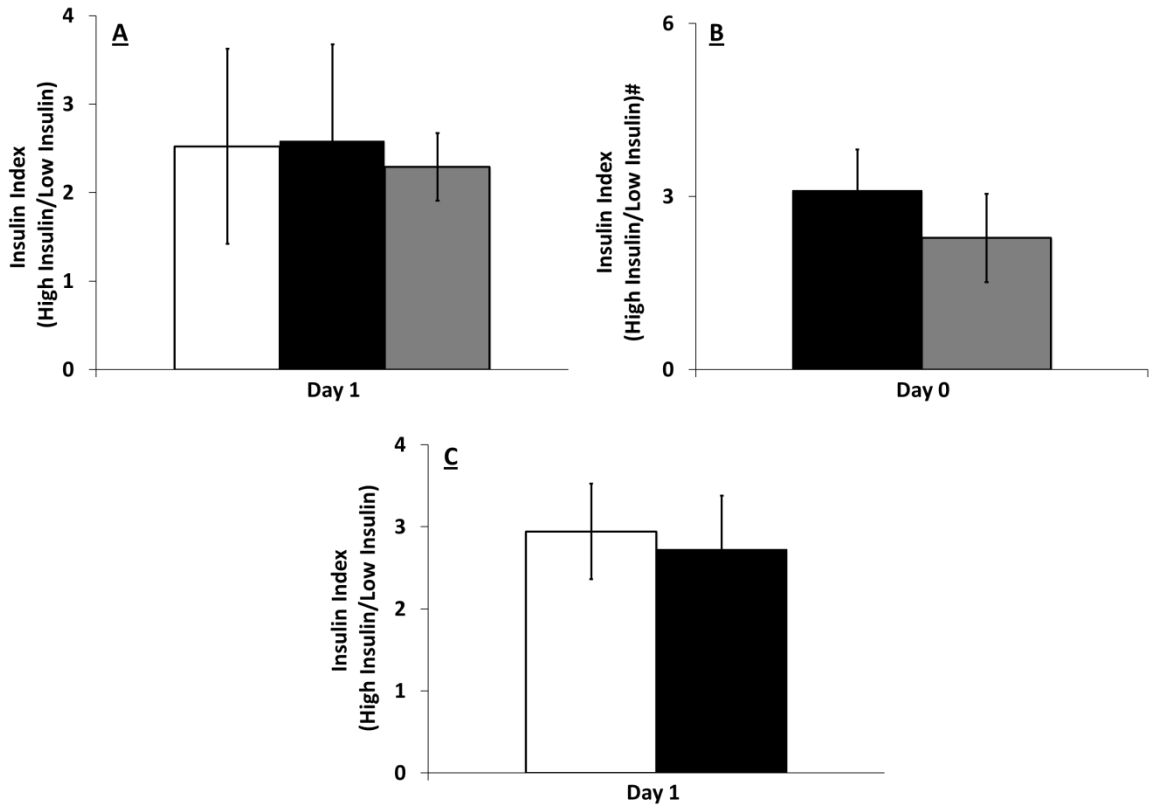

Figure 4-6: Insulin secretion of 150 IEQ islets cultured as 2D controls (white bar), within scaffold without fibrin (black bar), or within scaffolds with fibrin (grey bar) for rat islets (A), nonhuman primate islets (B), and human islets (C). Insulin index calculated as high insulin divided by low insulin 1, except as noted by #.

4.3.4 EVALUATION OF PDMS SCAFFOLD UNDER HYPOXIC CULTURE CONDITIONS

Comparison of the benefits of the PDMS macroporous scaffold for the culture of islets to islets cultured in a standard Petri dish at 20 % oxygen likely does not highlight the benefits of a three-dimensional culture system. As such, islets loaded within our PDMS macroporous scaffolds were cultured at 5% oxygen to simulate in-vivo conditions and the ability of this scaffold to provide an enhanced oxygen environment compared to 2-D controls was evaluated. As Figure 4-7 shows, 3000 IEQ rat islets on the scaffold had higher viability, per MTT assessment, than controls at 5% oxygen after 72 hrs. In

addition, the insulin stimulation index was slightly higher, although both values were dysfunctional, as they were below 1.0.

Similarly, 1500 IEQ human islets were cultured on the PDMS macroporous scaffold for up to 96 hrs at 5% oxygen and compared to standard 2-D controls. Figure 4-8 shows the changes in islet viability, per MTT, expressed as fold changes over 2-D culture controls. For the first 72 hrs, scaffold had viability was comparable to controls after 24 and 72 hrs at 5% oxygen, with no statistical variation from 1.0. After 96 hrs, however, islet cultured on PDMS macroporous scaffolds exhibited higher cell viability, when compared to 2-D controls, at both 5% and 20% oxygen at 1.24 And 1.84, respectively.

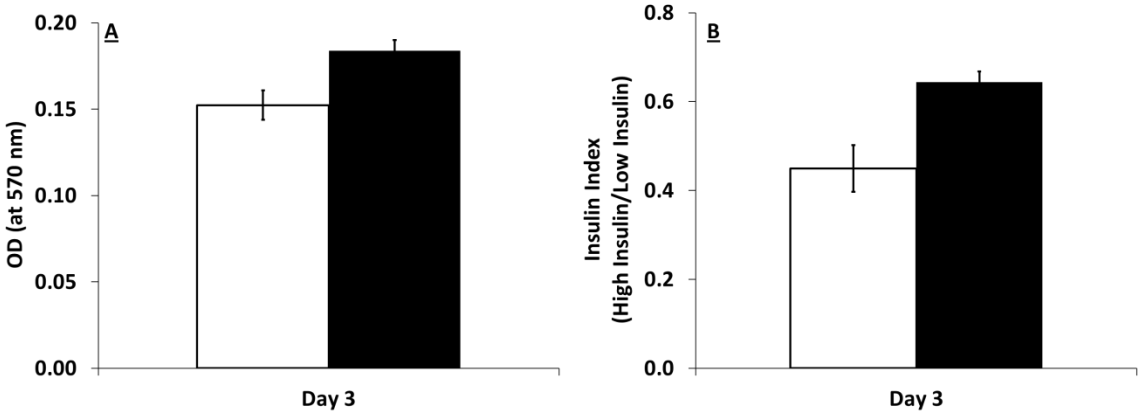

Figure 4-7: (A) MTT viability, represented by optimal density (OD), and insulin stimulation index, ratio of insulin secretion under high glucose to that under low glucose, following a (B) static glucose insulin secretion assay of 3000 IEQ rat islets cultured within standard two-dimensional Petri dishes (white bar) or within PDMS macroporous scaffolds (black bar) for 72 hrs at 5% oxygen.

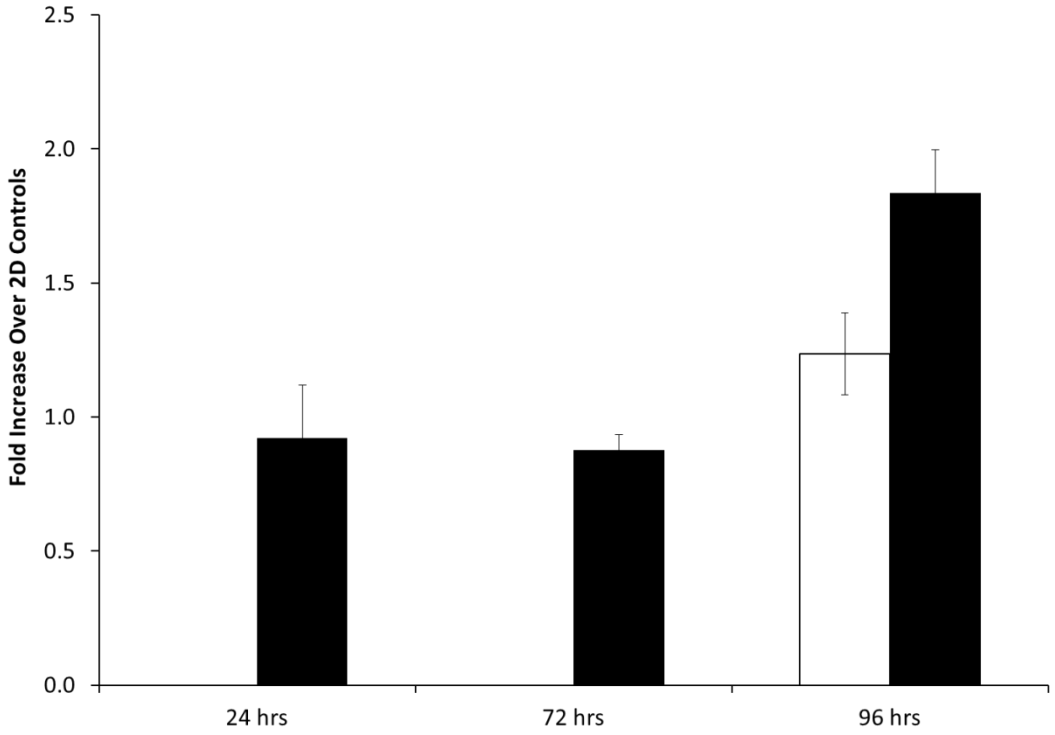

Figure 4-8: Fold increase in MTT viability results, compared to standard two-dimensional controls, of 1500 IEQ human islets cultured on PDMS macroporous scaffolds at 5% oxygen (black bars) and 20% oxygen (white bar) after 24, 72, and 96 hrs of culture.

4.3.5 COMPARISON OF MACROPOROUS SCAFFOLDS TO HYDROGELS

To evaluate the benefits of the use of a macroporous scaffold to standard hydrogel encapsulation of islets within macro-scale scaffolds, the viability and function of rat and non-human primate islets was evaluated within PDMS macroporous scaffolds and within 2 % agarose gels at 5 % oxygen. As illustrated in Figure 4-9, the viability, per MTT, of islets within PDMS macroporous scaffolds is substantially higher than that within 2 % agarose gels after 48 hrs of culture, with almost a two-fold increase in optical density when islets were loaded within the PDMS macroporous scaffolds. Evaluation of non-human islets within these two scaffold systems were even more pronounced, with a substantial decrease in cell viability, per MTT, for islets loaded into agarose gels, as

shown in Figure 4-10. Furthermore, insulin function is also effected when islets are encapsulated within agarose gels, where the stimulation index is dysfunctional at ~ 0.6. This is in stark comparison to islets within PDMS macroporous scaffolds, which exhibit a response of 1.1. While this is still quite low, this is likely a result of culturing at 5 % oxygen.

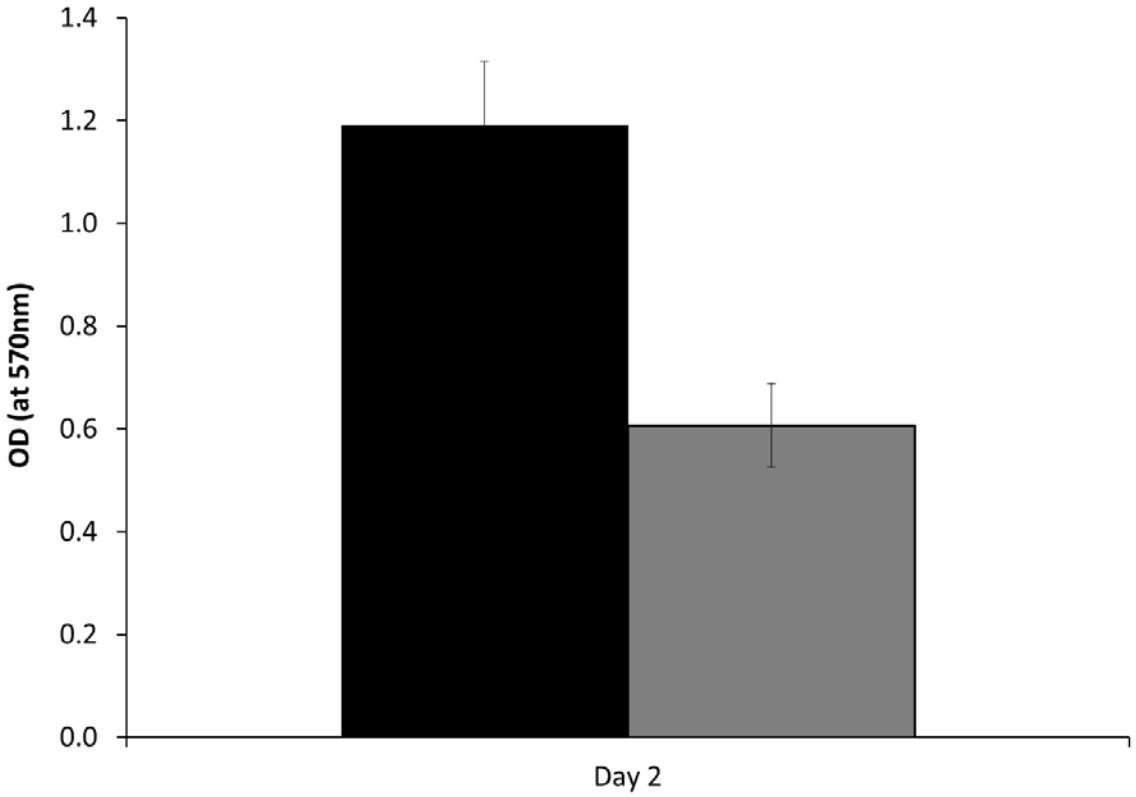

Figure 4-9: MTT viability, expressed as optical density (OD), of 1000 IEQ rat islets loaded within a PDMS macroporous scaffold (black bar) or a 0.2% agarose gel (grey bar) and cultured for 48 hrs at 5% oxygen.

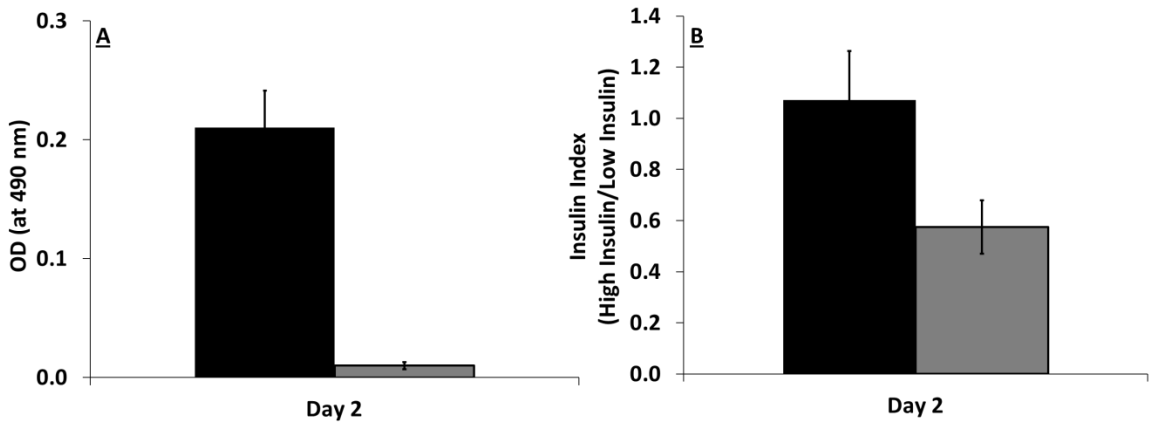

Figure 4-10: (A) MTT viability, expressed as optical density (OD), of 1500 IEQ nonhuman primate islets loaded within PDMS macroporous scaffolds (black bar) or in a 2% agarose gel (grey bar) and cultured for 48 hrs at 5% oxygen. (B) Insulin stimulation index, ratio of insulin secretion under high glucose to that under low glucose, following a static glucose insulin secretion assay of 1500 IEQ nonhuman primate islets loaded within a PDMS macroporous scaffold (black bar) or in a 2 % agarose gel (grey bar) and cultured for 48 hrs at 5% oxygen.

4.3.6 SYNGENEIC ISLET TRANSPLANTATION INTO SCAFFOLDS

PDMS macroporous scaffolds were evaluated in-vivo using a syngeneic chemically induced diabetic rat transplant model. The omentum was selected as the transplant site. Following placement of the scaffold on the omentum, 1800 IEQ islets were loaded into the scaffold. The scaffold was subsequently wrapped in the omentum and sealed with fibrin glue. For comparison, two control groups were used: free islets in an omental pouch; and free islets in the kidney capsule. For all transplants performed, no major adverse events were recorded and all animals survived the surgery.

Nonfasting blood glucose results illustrate prompt reversal to normoglycemia for all transplants (Figure 4-11). The transplant of islets in PDMS scaffolds in the omentum resulted in reversal of the diabetic state in 5 of the 6 animals (83.3%) transplanted with a mean reversal time of 1.4 ± 0.55 days (1 - 2 days, n = 6). For islets freely loaded into an omental pouch, 2 of the 3 animals (66.6%) reverted to normoglycemia, with a reversal

time on day 2. Islets in the kidney capsules resulted in reversal from diabetic state in 2 of the 2 animals (100%) on days 1 and 6. Following reversal, nonfasting blood glucose values for all groups were steady throughout the course of the transplant. Body weight of the recipients increased over the time course of the experiment. Following removal of the omentum, all animals reverted to the diabetic state, confirming that the transplanted grafts were responsible for diabetes reversal.

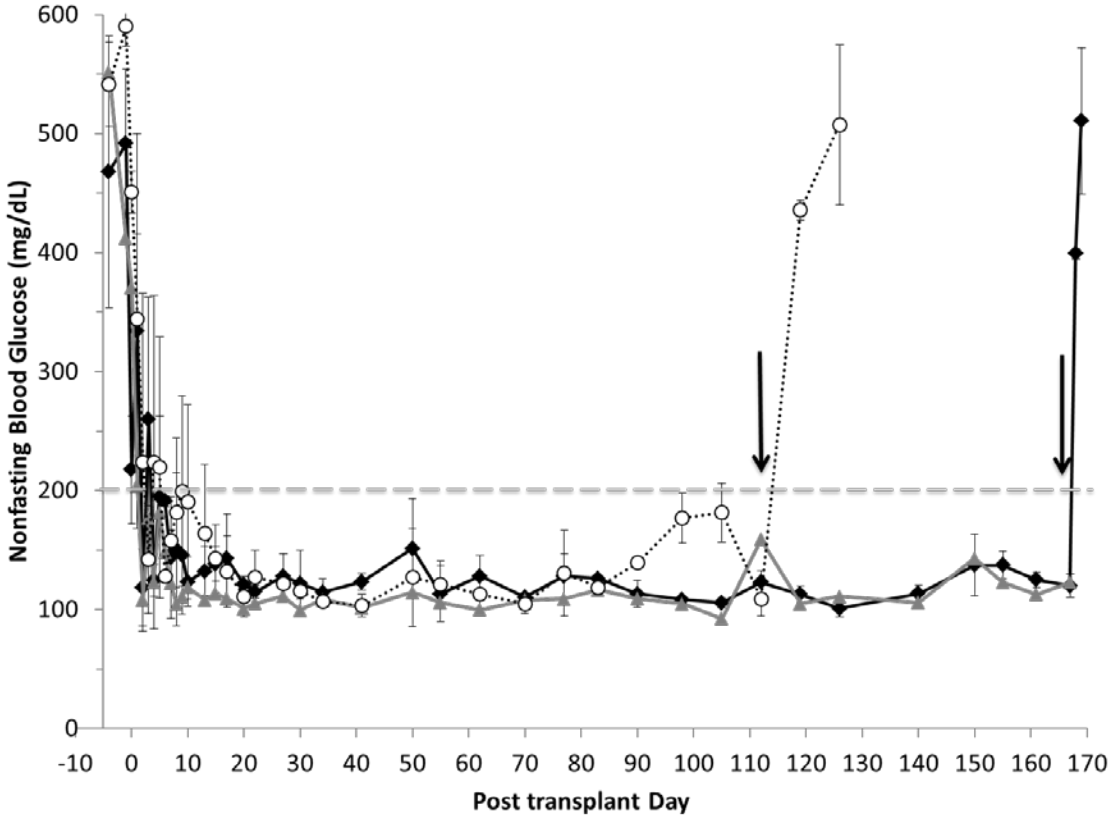

Figure 4-11: Nonfasting blood glucose levels following transplantation of islets into: PDMS macroporous scaffolds in the omentum (n=6) (black diamond, solid line); freely loaded into the omentum (n=3) (open circle, dotted line); or freely loaded into the kidney capsule (n=2) (grey triangle, solid line). Grafts were removed on day 112 for free islets in the omentum and day 168 for islets in PDMS scaffolds, where prompt reversal to diabetic state was observed for all animals.

Evaluation of metabolic control through a glucose challenge found good control for all effective transplants. Glucose tolerance tests on fasted rats (performed > 100 days) were found to result in prompt clearance of glucose, with restoration to normoglycemic levels (< 200 mg/dL) by 60 mins for all groups, as shown in Figure 4-12. Clearance of bolus glucose was slightly higher for omental transplants, with AUC values at 25,552 and 22,376 for islets in the scaffold and free islets, respectively, while kidney capsule AUC values were 18,300.

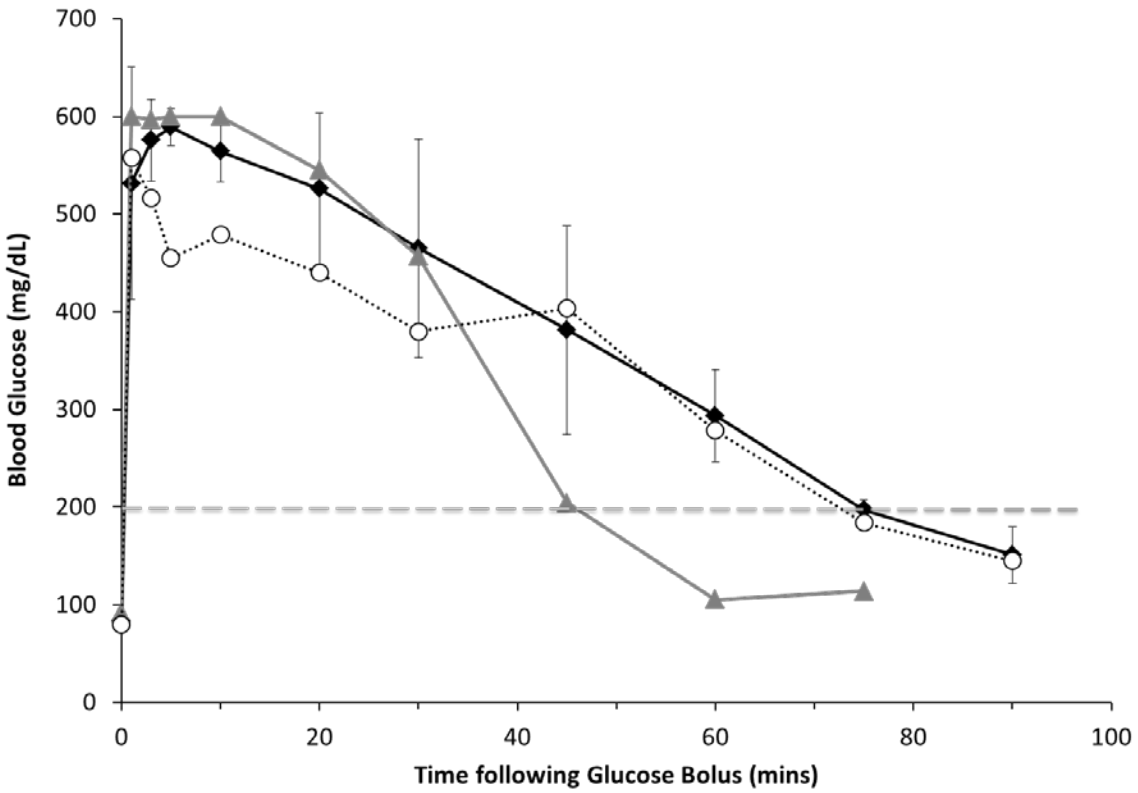

Figure 4-12: Intravenous glucose tolerance test performed on functional graft recipients > 100 days post transplant. Blood glucose measurements were collected at time points indicated, following injection of bolus glucose, for islets in silicone scaffold in omentum (n=3) (black diamond, solid line); islets freely loaded in omentum (n=2) (open circle, dashed line); and islets freely loaded into the kidney capsule (n=2) (grey triangle, solid line).

Histological assessment of islets within PDMS scaffolds found robust islets expressing high levels of insulin, as shown in Figure 4-13 and Figure 4-14. H/E staining of explanted grafts also found host infiltration into the graft, with positive remodeling of the void space within the scaffold and complete integration of scaffold into surrounding tissue. No observable infiltrate or fibrotic response was detected on sections. Blood vessels were observed both surrounding the scaffold, within the pores of the scaffold, and within and around islets, indicating a high degree of vascularization of both the scaffold and the islets.

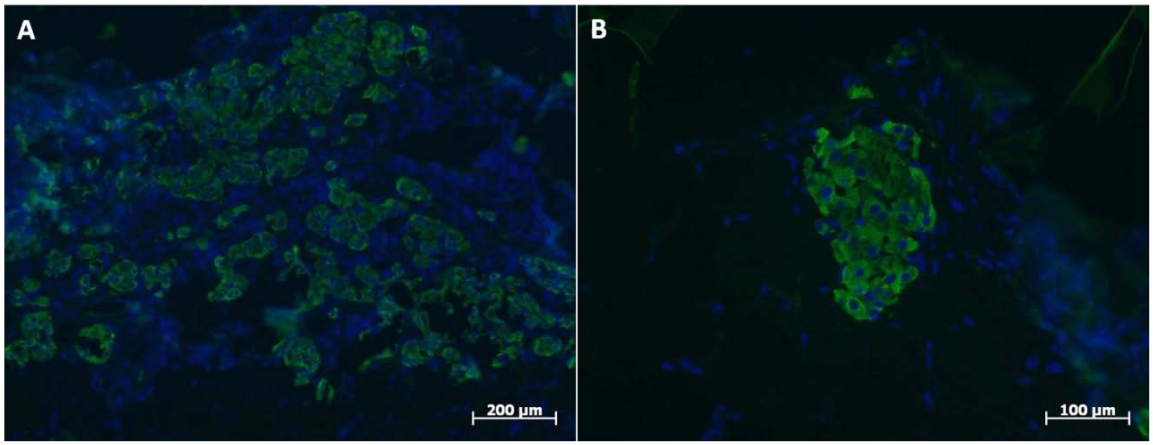

Figure 4-13: 10X (A) and 20X (B) magnifications of immunofluorescence staining of explanted grafts for nuclei (blue) (via DAPI) and islets (green) (via a primary guinea pig anti-insulin antibody and a secondary goat anti-guinea pig Alexa-568 conjugated antibody).

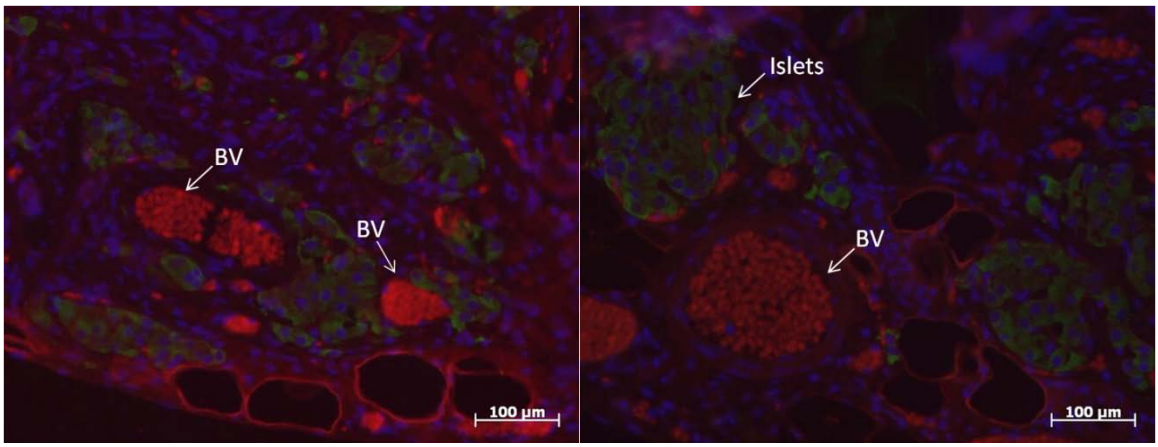

Figure 4-14: 20X magnification of immunofluorescence staining of explanted grafts for nuclei (blue), islets (green), and red blood cells (red, labeled "BV") (via auto fluorescence of red blood cells at excitation/emission 590/617 nm). Nuclei were stained via DAPI and insulin was stained via a primary guinea pig anti-insulin antibody and a secondary goat anti-guinea pig Alexa-568 conjugated antibody.

4.4 DISCUSSION

In this study, we sought to evaluate the capacity of a macroporous scaffold to serve as a platform for housing islets within an alternative transplant site. PDMS macroprous scaffolds, designed in earlier studies, were evaluated for their capacity to retain islet viability and function, both in-vitro and in-vivo.

As illustrated in the results, the pore size of a scaffold is of critical importance, because the pore size should be large enough to accommodate large islets and incoming blood vessels, but also small enough to entrap smaller islets within the scaffold. Islets, regardless of species origin, consistently distribute evenly throughout the scaffold. Retention studies demonstrated that islet retention within the scaffold is highly dependent on islet size. Nonhuman primate islets, which tend to be smaller islets, had much lower retention than rat islets. Since islet size is highly variant and species-dependent, the scaffold pore size can be optimized for improved retention of islets. Nonetheless, the

addition of fibrin glue was instrumental in improving the retention of small islets by trapping them within the scaffold.

Not only is the scaffold conducive to housing large cell clusters like islets simply by physical entrapment, but the positive results of MIN6 and human MSC studies demonstrate that the scaffold is also effective for growing adherent cell lines. Both cell types successfully attached to the scaffold surface and proliferated gradually over time. Comparisons of MSC growth on scaffolds with different surface protein coatings illustrate the need for surface modification of the hydrophobic PDMS surface and that careful selection of the adhesion proteins may be needed for different cell types. Moreover, enhanced cell viability of MIN6 was observed on the scaffolds at higher cell loading densities, suggesting that three-dimensional cultures are most beneficial when there are two-dimensional area constraints.

For islet experiments, islets were loaded at relatively low loading densities: 1500 IEQ per scaffold or 12 % v/v. The viability and functionality of islets at 20% oxygen was not adversely affected by loading within silicone scaffold and was similar to controls. Since these experiments were conducted under normal oxygen tension, they are not reflective of the low oxygen tension of in-vivo conditions. Therefore, the results of those studies understate the potential of the scaffold at enhancing islet viability. However, the studies at 5% oxygen demonstrate that the distribution of islets throughout a three-dimensional scaffold results in higher cellular viability and insulin secretion indices, when compared to two dimensional cell cultures. In addition, comparisons with agarose gels demonstrate that the scaffold maintains higher cell viability and insulin secretion than alternative three-dimensional constructs. This can be explained by the high degree of

porosity of the scaffold and the high diffusivity of oxygen in PDMS. Others have entrapped islets within gel matrices in order to prevent aggregation of islets, which encourages loss of islet function or impairment through hypoxia or central necrosis (Lacy et al. 1991). From their studies, only agarose and sodium alginate gels (not collagen or hyaluronic acid) maintained islets intact and evenly dispersed (Aung et al. 1995).

Moreover, the scaffold has the potential to serve as a platform for promoting islets engraftment. As illustrated above, fibronectin coated PDMS scaffolds can serve as scaffolds for MSC culture, with evidence of strong cellular adhesion and proliferation on these scaffolds in culture. Given recent publications on the benefits of MSCs in the presence of islets, a platform that provides the means to deliver both islets and MSCs in a three dimensional environment could be highly beneficial in promoting neovascularization, as well as immunomodulation. Future studies are focused on evaluating the potential of these scaffolds as co-culture systems for islets and complimentary cells, as well as the manipulation of this platform for the slow release of additional factors to promote islet engraftment and protection. Similar approaches to co-immobilization of other cells with islets within three-dimensional constructs have been successfully attempted, such as the co-encapsulation of chondrocytes within polyglycolic acid (PGA) polymer (Pollok et al. 1997).

Islet loaded scaffolds transplanted into the omental pouch of diabetic syngeneic rats successfully reverted diabetes in slightly shorter time than islets transplanted there without the scaffold. While this does not indicate that the scaffold improves graft function, it does demonstrate that can be implanted without instigating a negative host foreign body response. Due to the material selection, we did not encounter breakage of

the implant as seen in implantation of flat sheet devices in the peritoneal cavity (Storrs et al. 2001). This is significant because it serves as further evidence for transplantation of islets within a three-dimensional biomaterial into a clinically relevant site. By transplanting islets into a site that is easily accessible and using a scaffold that is biostable, the site could be easily pre-vascularized for seeding islets at later time points. Explants stained for insulin showed that transplanted islets remained within the scaffold, which is important for maintaining islets localized to one area. Moreover, histological analysis showed strong engraftment of the scaffold and infiltration of vasculature into the scaffold. Given the fast metabolism of islets, formation of an integral, well-developed vascular network is a critical component to graft responsiveness.

It is hypothesized that the scaffold improves islet function in-vivo by minimizing loss of islets to surrounding tissue and maximizing islet survival. By seeding islets into the scaffold and subsequently trapping them with fibrin glue, islets are retained localized within the implant site. It has been shown that grafts of islets similarly trapped in Matrigel had improved function over controls due to higher islet retention as evidenced by higher levels of mean cellular insulin (Dufour et al. 2005). The scaffold also serves as a support structure providing mechanical protection and minimizing damage from immediate contact of the islets with the surroundings. An additional aspect to consider is that the fibrin glue may have stimulated vascularization into the scaffold, as seen in mice studies with PGA implanted subcutaneously (Juang et al. 1995).

Finally, this study illustrates that the use of a macroporous structure can provide a means to competently house islets in an alternative site. This study lays the foundation for future work focused on using this PDMS platform to further modulate the local

environment. Given the material selected, this platform serves as an ideal means for the local and slow delivery of anti-inflammatory drugs and possibility immunomodulatory agents. Furthermore, we are evaluating the potential of this scaffold to serve as an oxygen generating platform, through the incorporation of oxygen generating agents (see subsequent chapters). Hence, future studies are focused on translating this platform to a bioactive material, capable of actively modulating the surrounding milieu.

4.5 CONCLUSIONS

Given the deficiencies of the intraportal vein for clinical islet transplantation, finding alternative sites is important. Housing of islets within a three-dimensional structure like our PDMS scaffold is essential for offering: spatial distribution, mechanical protection, and intradevice vascularization. Biocompatible, PDMS scaffolds were successfully fabricated with intended porosities and a controllable pore size range (250-425 μm), which is conducive to housing islets of average sizes. We have demonstrated that macroporous PDMS scaffolds can be used for high retention of islets while maintaining islet viability and function, as well as for proliferation of adherent cell lines. Their biocompatibility makes them appropriate for in-vivo implantation.

By transplanting them into the omental pouch we have shown feasibility of both the biocompatible scaffold and anatomically relevant omental site for clinical transplantation. The PDMS scaffold represents a self-contained vehicle for not only transplanting islets, but also for co-culture of "helper cells" like MSCs, and delivery of drugs within the microniche of the transplant site. We designed and developed these PDMS scaffolds specifically for islet transplantation, but they can be easily tailored to other applications by modifying its: geometry, porosity, pore size, protein surface

coating, and preculture of cells. These results are promising in that they indicate the potential for transplanting islets into alternative sites by addressing the issues of spatial distribution of islets, mechanical protection, and intra-device vascularization.

CHAPTER 5. OXYGEN RELEASE KINETICS AND MODELING OF SOLID CALCIUM PEROXIDE (CaO_2) ENCAPSULATED IN PDMS

5.1 INTRODUCTORY REMARKS

The implantation of cellular-based devices is commonly hampered by inadequate oxygen delivery. This is a particular challenge in islet transplantation, where islets are highly susceptible to functional impairment with insulin production levels being reduced by 50% at the threshold between normoxia and hypoxia (Dionne et al. 1993). When the oxygen consumption rate of the cells exceeds the rate of diffusion of oxygen from the surrounding area, an oxygen deficit is created. Software computational models can be used to gain realistic insight on the effects of the geometric design of the device on islet viability. Computational models by our lab demonstrate that for devices with the dimensions required for cell loading demands, only a thin outer ring of islets are exposed to suitable non-hypoxic conditions. The viability of the islets, however, can be dramatically increased with small incremental increases in oxygen concentration. Therefore, it is critical to identify and develop methods to increase oxygen availability to cells. Other laboratories have investigated various agents for their oxygen generating potential, such as the electrolytic decomposition of water into oxygen and hydrogen (H Wu et al. 1999) and photosynthetic microalgae (Bloch et al. 2006). In this study, we sought to design and develop an oxygen generating biomaterial in the form of solid peroxide encapsulated in silicone, for sustained and continuous delivery of oxygen. By encapsulating solid peroxide, the barrier induces a delay in oxygen generation, resulting in temporal modulation of oxygen release providing a gradual, sustained release of oxygen (B.S. Harrison et al. 2007).

PDMS encapsulated in solid peroxide is appealing as a potential source of oxygen generation for tissue engineering, particularly for pancreatic islets. To investigate this, we measured the release of oxygen from various concentrations of calcium peroxide powder in solution. The release pattern was curve fitted to an equation describing first order, reversible chemical reaction kinetics, in order to obtain a function that would predict oxygen release for any given concentration of reactants. In addition, calcium peroxide was encapsulated within hydrophilic agarose and hydrophobic PDMS polymer and the release of oxygen from these disks was measured and compared. Finally, finite element analysis models were created to predict the combined effects of chemical reaction kinetics and diffusion on the release of oxygen from PDMS encapsulated calcium peroxide. Due to variability in cell types, cell loading densities, and device geometry, the oxygen requirements for different cellular-based devices will vary. These models will provide a means to design the optimal configuration, density, and geometry of the encapsulated PDMS-CaO_2 that should be used to supplement oxygen for a given device.

5.2 BACKGROUND

5.2.1 OXYGEN RELEASING COMPOUNDS

Oxygen releasing compounds exist in the form of peroxides or peroxyhydrates and release oxygen upon contact with water in a manner similar to the decomposition of hydrogen peroxide (see Equation (5-1)). Peroxyhydrates have hydrogen peroxide adducts associated within their structure that escapes and reacts with water, quickly releasing oxygen (see Equation (5-2)). Oxygen is released more slowly from divalent alkali earth metal peroxides, such as calcium peroxide and magnesium peroxide, which are "true peroxides" containing the "O-O" bond (Schumb et al. 1955).

$$2H_2O_2 \rightarrow 2H_2O + O_2 \quad (5\text{-}1)$$

$$4Na_2CO_3{*}1.5H_2O_2 \rightarrow 8Na^- + 4CO_3^- + 6H_2O_2 \quad (5\text{-}2)$$

For our studies, we selected calcium peroxide (CaO_2) because it is cost effective and has been extensively used in bioremediation research and out in the field (D. P. Cassidy & Irvine 1999; Chevalier & Mccann 2008). Multiple companies manufacture their particular formulation for the agriculture industry (Hanh et al. 2005; A. M. Baker & Hatton 1987). Calcium peroxide is a pale yellow powder and is typically prepared as having water adducts and varying concentrations of calcium hydroxide ($Ca(OH)_2$). As long as it is kept in a sealed container away from moisture and extreme temperatures (it will combust above 400 °C), the concentration of calcium peroxide remains relatively stable (Schumb et al. 1955).

5.2.2 DECOMPOSITION OF SOLID PEROXIDES

The process of oxygen generation from divalent metal (M) peroxides may occur in two sequential steps by the reaction in Equation (5-3) ($\Delta G° = -20.7$ kJ/mol) followed by the reaction in Equation (5-1) ($\Delta G° = -119.2$ kJ/mol). Therefore, the decomposition of hydrogen peroxide into oxygen and water (Equation (5-1)) could be a rate-controlling step (Schmidtke et al. 1999). However, at neutral and basic pH, Equation (5-1) is favored, causing hydrogen peroxide to quickly disproportionate, rendering it impossible to identify as a reaction intermediate (Watts et al. 1999; Northup & D. Cassidy 2008; Waite et al. 1999). This reaction can be catalyzed by various agents: microbial enzyme catalase, iron (Fe^{2+}), manganese (Mn^{2+}), nickel, copper, zinc, and lead (R. E. Hinchee & Olfenbuttel 1991; Schmidtke et al. 1999). The presence of phosphate in solution with

acidic pH, may inhibit hydrogen peroxide disproportionation, by lowering dissolved metal concentrations through precipitation or converting them to more stable complexes with hydrogen peroxide, but this is ineffective at neutral pH (R. Hinchee 1991; Watts et al. 1999). Therefore, assuming the reaction in Equation (5-1) is instantaneous, the conversion of calcium peroxide to oxygen may be simply expressed as the reaction in Equation (5-4), which is the sum of the reactions in Equations (5-1) and (5-3) (Watts et al. 1999; Schumb et al. 1955; Waite et al. 1999; Schmidtke et al. 1999).

$$CaO_2 + 2H_2O \rightarrow Ca(OH)_2 + H_2O_2 \quad (5\text{-}3)$$

$$2CaO_2 + 2H_2O \rightarrow 2Ca(OH)_2 + O_2 \quad (5\text{-}4)$$

5.2.3 KINETICS AND STOICHIOMETRY

Calcium peroxide and calcium hydroxide both have low solubilities in water (9.8×10^{-9} and 9.8×10^{-9}, respectively) (Waite et al. 1999). Calcium peroxide dissolves very slowly, especially at high pH (greater than 9), suggesting that oxygen release is controlled by chemical reaction kinetics of dissolution, which has both chemical and thermodynamic limitations (Waite et al. 1999; Greenberg 1995; Atlas 1977). We will derive a mathematical equation describing this kinetics in order to predict oxygen release as a function of starting concentrations of calcium peroxide and oxygen.

The release of oxygen from calcium peroxide can be described as a one step, reversible reaction as shown in the reaction in Equation (5-5), where A = CaO_2, B = H_2O, C = $Ca(OH)_2$, D = O_2, k_1 is the forward rate constant, and k_2 is the reverse rate constant. The rate of oxygen generation ($d[O_2]/dt = d[D]/dt$) can be described by Equation (5-6), where a, b, c, and d denote the rate order for reactant and product. Note

that the rate order (e.g. a, b, c, d) with respect to a substance is not necessarily equivalent to its stoichiometric coefficient. In this paper, we will use experimentally collected oxygen release data from calcium peroxide in solution to determine the rate order of this reaction and derive an expression for the rate of oxygen generation.

$$2A + 2B \underset{k_2}{\overset{k_1}{\rightleftarrows}} 2C + D \tag{5-5}$$

$$\frac{d[D]}{dt} = k_1[A]^a[B]^b - k_2[C]^c[D]^d \tag{5-6}$$

5.2.4 ENCAPSULATION OF SOLID PEROXIDES

Since the release of oxygen from peroxide is dependent upon the interaction with water, we hypothesize that reactivity could be dampened and controlled by encapsulating the peroxide in a material that hinders diffusion of water to the peroxide. For example, some companies have incorporated phosphate ions into mixtures of solid peroxides to achieve this effect (Oxygen Release Compound Advanced by Regensis (San Clemente, CA)), and IXPER Calcium Peroxide by Solvay Chemicals (Houston, TX)). Others have encapsulated solid peroxide in poly(D,L-lactide-*co*-glycolide) (PLGA) (Oh et al. 2009). Encapsulation in a hydrophilic material such as a hydrogel, e.g. agarose, would only be slightly effective, due to its high water content and diffusivity . A hydrophobic material like poly(dimethyl) siloxane (PDMS) should be more effective at modulating peroxide reactivity with water, since water diffusion into the material is significantly inhibited. PDMS also has a low chemical reactivity, thereby reducing the potential for reactivity with peroxide itself. Finally, PDMS has a high diffusivity for oxygen, thereby permitting

for the prompt diffusion of oxygen out of the system (J. C. McDonald et al. 2000; Peterson et al. 2004).

A critical factor that will determine the release of oxygen from the disks will be the diffusion of water in and the diffusion of oxygen out of the disks. Therefore, it is important to have an understanding of the behavior of water around PDMS surfaces. Values for the diffusion coefficient and partition coefficient of oxygen and water in PDMS and water are needed. Unfortunately, there is scarce quantitative analysis of the mass transfer of oxygen at the interface between water and PDMS (J. C. McDonald et al. 2000; Peterson et al. 2004).

The diffusion coefficient of oxygen in PDMS is reported as 5.2×10^{-6} to 3.4×10^{-5} cm^2s^{-1} (Merkel et al. 2000; Zanzotto et al. 2004). Similarly, the diffusion coefficient of oxygen in PBS (equivalent to water) is reported as 2.1×10^{-5} cm^2s^{-1} (Shiku et al. 2006). The partition coefficient, K_p, of oxygen between water and PDMS is given by the ratio of the concentration of oxygen in PDMS to the concentration of oxygen in water at equilibrium and is found to be K_p = 2 mM/.204 mM = 10 (Kamiya et al. 1990).

The diffusion coefficient of water in PDMS is reported as $\sim\times10^{-11}$ m^2s^{-1} (Zhan et al. 2009), 8.5×10^{-10} m^2s^{-1} (Randall & Doyle 2005), 1.2×10^{-9} m^2s^{-1} (Watson & Payne 1990), 2.49×10^{-9} m^2s^{-1} (Watson 1996), and $\sim10^{-9}$ m^2s^{-1} (Leng et al. 2006; Watson 1996). The PDMS/aqueous partition coefficient, K_p, for water is reported to be 0.02580. For comparison, the partition coefficient for ethanol is 0.04624, illustrating a much higher solubility than water in PDMS (Zhan et al. 2009).

Values for diffusion coefficient of water reported in the literature were given at differing temperatures. In order to determine the diffusion coefficient, D, at the

temperature of interest, 37 °C, we calculated it according to an Arrhenius behavior (George 2001), where D_0 is a pre-exponential factor, E_A is the activation of energy of diffusion (14 kJ/mol) (Ranjitprakash et al. 2006), and R is the universal gas constant (8.314 $mol \cdot kJ^{-1} \cdot K^{-1}$):

$$D = D_0 e^{\frac{-E_A}{RT}} \tag{5-7}$$

Encapsulation in PDMS polymer also introduces transport limitations, which will be considered separately in our finite element analysis models.

5.2.5 FINITE ELEMENT ANALYSIS

Finite element analysis in COMSOL software provides a theoretical basis for useful predictions on reaction kinetics and transport by diffusion. COMSOL is multi-physics simulation software that utilizes a finite element analysis to derive quantitative solutions for various multi-physics applications. This software is used to quantitatively predict the nutrient delivery potential of our device, based on theoretical mass-balance equations that describe nutrient consumption and nutrient transport. The software performs a series of iterative computations to predict transient and steady state values. The user can then translate all of the parameters of the system into input that can be understood by the software.

For example, the device geometry can be defined, material properties of the islets and surrounding environment (oxygen consumption rate (OCR), Michaelis-Menten constant (K_m), and diffusion coefficient) can be specified, and boundary conditions can be selected. Moreover, the results can be post-processed to highlight specific areas of

interest, such as showing percent volume of anoxic islets. This can be used to predict percent viable cell mass.

5.3 METHODS AND MATERIALS

5.3.1 MATERIALS

Calcium peroxide powder was purchased from Sigma-Aldrich (Cat. No. 466271). It has a particle size of -200 mesh and is 75% calcium peroxide with the remainder as calcium hydroxide. Polydimethyl siloxane (PDMS) was purchased from GE Silicones. dPBS was purchased from Mediatech and pH balanced to 7.4 using NaOH and HCl.

5.3.2 PREPARATION OF CALCIUM PEROXIDE SOLUTIONS

Solutions of calcium peroxide powder in dPBS were prepared at various concentrations: 0.25, 0.5, 1.0, 2.5, 5.0, and 10.0 mg/mL. The dPBS was preheated to 37 °C and the calcium peroxide was only added immediately before the oxygen measurements.

5.3.3 FABRICATION OF AGAROSE ENCAPSULATED CALCIUM PEROXIDE (AGAROSE-CaO_2) DISKS

Oxygen generating disks (*Agarose-CaO_2* disks) were fabricated by mixing varying concentrations (w/w %) of solid calcium peroxide powder (Sigma Aldrich) with 2% w/w agarose. The calcium peroxide/agarose solution was loaded into cylindrical molds of 1 mm height and 3 mm diameter and allowed to gel at 4 °C for 5 minutes. The disks were deemed not suitable for storage and were used immediately for oxygen measurements.

5.3.4 FABRICATION OF PDMS ENCAPSULATED CALCIUM PEROXIDE (PDMS-CaO_2) DISKS

Oxygen generating disks (PDMS-CaO_2 disks) were fabricated by mixing varying concentrations (w/w %) of solid calcium peroxide powder (Sigma Aldrich) with polydimethyl siloxane (PDMS) silicone polymer (GE Silicones). The calcium peroxide/silicone mixture was loaded into cylindrical molds of 1 mm height and varying diameters (3 to 10 mm). Subsequently, air bubbles were removed by placing in a vacuum for one hour, and the disks were cured at 40 °C for 24 hrs. Preceding oxygen measurements, the disks were placed in ethanol for 30 mins to sterilize them and remove the initial burst of oxygen.

5.3.5 MEASUREMENT OF OXYGEN PRODUCTION

Constructs were assessed for release of oxygen in dPBS at 37 °C. A closed system consisting of a sealed, titanium chamber in fluorescence amplitude micro oxygen monitoring systems (Instech Laboratories, PA) was used for determining release kinetics. Oxygen concentration was measured using PreSens (Germany) non-invasive oxygen sensors, which consist of a ruthenium-based spot sensor transmitting fluorescence signals to the computer through optical fiber cables. Blue LED excites the sensor to emit fluorescence, but the fluorescence is quenched when it collides with oxygen molecules. Therefore, the changes in fluorescence can be correlated to oxygen concentration in the solution. These sensors possess a high sensitivity and high signal to noise ratio, and can measure oxygen levels non-invasively without disturbing the culture environment. Oxygen concentrations were recorded by the software in units of mmHg (torr). For our

analysis, these values were converted to mol/m^3 by multiplying by the conversion factor 0.21 mol·m^3/158.8 mmHg.

5.3.6 STOICHIOMETRY AND ANALYSIS OF KINETICS

Calculations were made to predict the theoretical maxima of oxygen, hydrogen peroxide, and hydroxyl radical that could be produced from calcium peroxide. This is based on the stoichiometry of the different possible reactions.

In order to devise an expression for the rate of oxygen release, the rate order of the reaction had to be determined first. Within the early stages of the reaction (initial 5 mins), it can be assumed that the concentration of the products is sufficiently low that is does not influence the reaction. Thus, the rate order with respect to calcium peroxide was determined by comparing the initial reaction rate for varying concentrations of calcium peroxide. A log/log plot of initial oxygen production versus calcium peroxide concentration exhibited a linear relationship with a slope of one, indicating first order (a=1). Based on a review of the literature and analysis of the reaction mechanism, first order was expected for the other reactants and products as well (b=c=d=1). This was confirmed by trial-and-error curve fitting of the reaction rate for various rate orders. Moreover, since the reaction takes place in a fixed volume of solution where the concentration of water does not change appreciably, the concentration of water ([B]) was assumed to be a constant and was factored into the forward rate constant of the reaction. Therefore, Equation (5-6) becomes Equation (5-8) to give the rate of oxygen production, d[D]/dt.

$$\frac{d[D]}{dt} = k_1[A] - k_2[C][D] \tag{5-8}$$

Recall that A = CaO_2, B = H_2O, C = $Ca(OH)_2$, D = O_2. We will define the variable "Q(t)" as the extent of the forward reaction at any time, so that based on stoichiometry we have Equation (5-9). The concentration of each reactant and product can be expressed in terms of its initial concentration and "Q(t)" (its accumulation or consumption) as shown in Equation (5-10) (Lavabre et al. 1993; Meagher & Rorabacher 1994; Levine 2009). Thus, we will modify Equation (5-8) by substituting in Equation (5-10) to arrive at Equation (5-11). Note that all of the following steps are based off of established principles for deriving reaction kinetics (Yeargers et al. 1996; Jordan 2007; Hogg 1999; Koopman & H. H. Lee 1992; Brezonik 1994).

$$Q(t) = [A]_0 - [A](t) = -[C]_0 + [C](t) = 2 \times (-[D]_0 + [\mathrm{D}](t)) \tag{5-9}$$

$$A(t) = A_0 - Q(t);\ C(t) = C_0 + Q(t);\ D(t) = D_0 + \frac{1}{2}Q(t) \tag{5-10}$$

$$\frac{dQ(t)}{dt} = k_1([A]_0 - \mathrm{Q}(t)) - k_2([C]_0 + \mathrm{Q}(t))([D]_0 + \frac{1}{2}Q(t)) \tag{5-11}$$

Expanding and collecting Q(t):

$$\frac{dQ(t)}{dt} = -\frac{1}{2}k_2Q(t)^2 + \left(-k_1 - \frac{k_2}{2}[C]_0 - k_2[D]_0\right)Q(t) + k_1[A]_0 - k_2[C]_0[D]_0 \tag{5-12}$$

At equilibrium state, the rates of the reaction in the forward and reverse order are equivalent, so that that the rate of change (d/dt) of products (Q(t)) formed is zero:

$$\frac{dQ(t)}{dt} = 0;\ Q(t) = constant = Q_{eq} \tag{5-13}$$

Therefore, similarly to Equations (5-11) and Equation (5-12), after expanding and collecting Q_{eq}:

$$\frac{dQ(t)}{dt} = k_1([A]_0 - Q_{eq}) - k_2([C]_0 + Q_{eq})([D]_0 + \frac{1}{2}Q_{eq}) = 0 \tag{5-14}$$

$$-\frac{1}{2}k_2Q_{eq}^2 + \left(-k_1 - \frac{k_2}{2}[C]_0 - k_2[D]_0\right)Q_{eq} + k_1[A]_0 - k_2[C]_0[D]_0 = 0 \tag{5-15}$$

Subtracting Equation (5-15) from Equation (5-12):

$$\frac{dQ(t)}{dt} - \frac{dQ_{eq}}{dt} = -\frac{1}{2}k_2\left(Q(t)^2 - Q_{eq}^2\right) - \left(k_1 + \frac{k_2}{2}[C]_0 + k_2[D]_0\right)(Q(t) - Q_{eq}) \tag{5-16}$$

We clean up the equation by defining the variable β (see Equation (5-17)) and substituting it into Equation (5-16):

$$\beta = k_1 + \frac{1}{2}k_2[C]_0 + k_2[D]_0 \tag{5-17}$$

$$\frac{dQ(t)}{dt} = -\frac{1}{2}k_2\left(Q(t)^2 - Q_{eq}^2\right) - \beta(Q(t) - Q_{eq}) \tag{5-18}$$

Thus, the integral form of the equation becomes:

$$\int_0^Q \frac{1}{-\frac{1}{2}k_2\left(Q^2 - Q_{eq}^2\right) - \beta(Q - Q_{eq})}dQ = \int_0^t 1\,dt \tag{5-19}$$

Which when solved, by looking up in a table for the solution of a rational integral of this general form (Ryzhik et al. 2007) results in:

$$\frac{-(\ln(Q-Q_{eq})-\ln(\frac{k_2}{2}Q+\beta+\frac{k_2}{2}Q_{eq}))}{\beta+k_2Q_{eq}}+\frac{\ln(-Q_{eq})-\ln(\beta+\frac{k_2}{2}Q_{eq})}{\beta+k_2Q_{eq}}=t \quad (5\text{-}20)$$

Solving this equation in terms Q(t) results in:

$$Q(t)=Q_{eq}\frac{\beta e^{(t\beta+2tk_2Q_{eq})}+k_2Q_{eq}e^{(t\beta+2tk_2Q_{eq})}-\beta-k_2Q_{eq}}{\beta e^{(t\beta+2tk_2Q_{eq})}+k_2Q_{eq}e^{(t\beta+2tk_2Q_{eq})}+k_2Q_{eq}} \quad (5\text{-}21)$$

Since Q_{eq} is unknown to us, we can determine its value by finding the roots of Equation (5-15):

$$-\frac{1}{2}k_2Q_{eq}^2-\beta Q_{eq}+k_1[A]_0-k_2[C]_0[D]_0=0 \quad (5\text{-}22)$$

If we clean up by introducing Q_c:

$$Q_c=k_1[A]_0-k_2[C]_0[D]_0 \quad (5\text{-}23)$$

Thus, by substitution of Equation (5-23) into Equation (5-22), we find the roots:

$$0=Q_{eq}^2+\frac{2\beta}{k_2}Q_{eq}-\frac{2}{k_2}Q_c \quad (5\text{-}24)$$

$$Q_{eq}=-\frac{2\beta}{k_2}\pm\sqrt{\left(\frac{2\beta}{k_2}\right)^2+\frac{8Q_c}{k_2}} \quad (5\text{-}25)$$

This can be substituted into the equation for Q(t) (Equation (5-21)). Further, to find an expression for K_{eq}, we need to solve for k_1 using Equation (5-22).

$$k_1 = \frac{k_2([C]_0 + Q_{eq})([D]_0 + \frac{1}{2}Q_{eq})}{([A]_0 - Q_{eq})} \tag{5-26}$$

$$K_{eq} = \frac{k_1}{k_2} \tag{5-27}$$

Therefore, the concentration of oxygen generated as a function of time is expressed by the following equation where $[D]_0$ is the initial concentration of oxygen and Q(t) is given by Equation (5-21):

$$[\text{Oxygen}](t) = [D](t) = [D]_0 + \frac{1}{2}Q(t) \tag{5-28}$$

The oxygen release profiles for varying concentrations of calcium peroxide powder in dPBS solution were fitted to the equation for reversible kinetics. Values for k_1 and k_2 were obtained by non-linear least squares fitting of data using Solver in Excel and were averaged.

5.3.7 FINITE ELEMENT MODELING

Oxygen release from PDMS encapsulated CaO_2 is dependent on chemical kinetics and on the diffusion of water and oxygen into and out of the PDMS material. Due to the complexity of the problem, oxygen release from the disks was modeled using COMSOL software, Chemical Engineering Reaction module for fine element analysis (COMSOL 2010b; COMSOL 2010a). The general process was modeled for two-

dimensional systems by Equation (5-29) where the first term on the left side of the equation is the change in oxygen concentration over time. It is equal to the diffusion of oxygen (first term on right) and the rate of oxygen production (R_{oxy}). The diffusion of oxygen is given by the product of the diffusion coefficient of oxygen in the material (PDMS or water) and the concentration gradient (spatial derivative) for two-dimensions.

$$\frac{\partial C_{oxy}}{\partial t} = D\nabla^2 C_{oxy} + R_{oxy} \tag{5-29}$$

5.3.7.1 SUB-DOMAIN CONDITIONS

The model consisted of two sub-domains: (1) the surrounding dPBS solution, and (2) the PDMS disk. In sub-domain 2 there is the chemical reaction for the production of oxygen (R), which as demonstrated earlier, will depend on the concentrations of calcium peroxide, calcium hydroxide, oxygen, and water. There will also be diffusion of the oxygen, and water (we assume that because the calcium peroxide and calcium hydroxide are cured within the PDMS they will be immobilized within sub-domain 2). This gives rise to the following partial differential equations, where $D_{solute,domain}$ is the diffusion coefficient of that solute in the material for that domain and the solutes are oxygen (oxy), calcium peroxide (CaO_2), calcium hydroxide ($Ca(OH)_2$), and water:

$$\frac{\partial C_{oxy,2}}{\partial t} = \nabla.(D_{oxy,2}\nabla C_{oxy,2}) + R_{oxy} \quad (5\text{-}30)$$

$$\frac{\partial C_{CaO2,2}}{\partial t} = -2R_{oxy} \quad (5\text{-}31)$$

$$\frac{\partial C_{CaOH2,2}}{\partial t} = 2R_{oxy} \quad (5\text{-}32)$$

$$\frac{\partial C_{water,2}}{\partial t} = \nabla.\left(D_{water,2}\nabla C_{water,2}\right) - 2R_{oxy} \quad (5\text{-}33)$$

In sub-domain 1, no chemical reactions take place. Also, the concentration of water is assumed to be negligibly affected. This gives rise to the following partial differential equations:

$$\frac{\partial C_{oxy,1}}{\partial t} = \nabla.(D_{oxy,1}\nabla C_{oxy,1}) \quad (5\text{-}34)$$

$$\frac{\partial C_{CaO2,1}}{\partial t} = 0 \quad (5\text{-}35)$$

$$\frac{\partial C_{CaOH2,1}}{\partial t} = 0 \quad (5\text{-}36)$$

$$\frac{\partial C_{water,1}}{\partial t} = 0 \quad (5\text{-}37)$$

5.3.7.2 INTERFACE CONDITIONS

Since the solutes must dissolve into the hydrophobic PDMS sub-domain, interface conditions are needed to account for the transport of the solutes at the water-PDMS interface. The conservation of mass indicates that the flux must be continuous between the different sub-domains. To account for the discontinuities in the concentration profile at the boundaries between the liquid and membrane phase, two separate variables are needed for each solute to describe the concentration in the respective phases. The

interface conditions for the concentration between the aqueous and membrane phases can be described by the dimensionless partition coefficient, K_p. Then, the interface conditions are (Chaudhry et al. 2009), where n_i denotes the outward normal vector of the ith sub-domain:

$$C_{oxy,2} = K_{p,oxy} C_{oxy,1} \tag{5-38}$$

$$D_{oxy,1} \frac{\partial C_{oxy,1}}{\partial \boldsymbol{n}_1} + D_{oxy,2} \frac{\partial C_{oxy,2}}{\partial \boldsymbol{n}_2} \tag{5-39}$$

$$C_{water,2} = K_{p,water} C_{water,1} \tag{5-40}$$

$$D_{water,1} \frac{\partial C_{water,1}}{\partial \boldsymbol{n}_1} + D_{water,2} \frac{\partial C_{water,2}}{\partial \boldsymbol{n}_2} \tag{5-41}$$

Continuous flux over the boundaries is enforced in COMSOL by applying the stiff-spring method [COMSOL Chemical Engineering Dialysis Model]. It is achieved by introducing a constant, M that is large enough to force concentration differences to approach zero:

$$D_{oxy,2} \frac{\partial C_{oxy,2}}{\partial \boldsymbol{n}_2} = M(C_{oxy,1} - K_{p,oxy} C_{oxy,2}) \tag{5-42}$$

$$D_{water,2} \frac{\partial C_{water,2}}{\partial \boldsymbol{n}_2} = M(C_{water,1} - K_{p,water} C_{water,2}) \tag{5-43}$$

5.3.7.3 BOUNDARY CONDITIONS

The outer boundaries of the fluid (sub-domain 1) are assumed to be closed. Also, calcium peroxide is limited to sub-domain 2. So, Neumann Boundary Conditions are needed for all solutes at the outer boundary of sub-domain 1, and for calcium peroxide at the outer boundary of sub-domain 2:

$$\frac{\partial C_{all\ solutes,1}}{\partial \boldsymbol{n}_1} = 0 \tag{5-44}$$

$$\frac{\partial C_{CaO2,2}}{\partial \boldsymbol{n}_2} = 0 \tag{5-45}$$

5.3.7.4 INITIAL CONDITIONS

We assume that at the initial time zero, everything is equilibrated with room air (20% oxygen), which sets the initial condition of $[Oxygen]_0$=0.2 mol/m^3. Also, initial concentrations for calcium peroxide and calcium hydroxide were set according to the concentrations incorporated into the disk.

5.3.7.5 CHEMICAL REACTION

The reaction rate for oxygen release (R_{oxygen}) from calcium peroxide in solution was developed based on the assumption that the water concentration was constant. This was an acceptable assumption for powder in solution, but cannot be applied to the PDMS-CaO_2 disks, where contact with the water is diffusion limited. Therefore, taking into account the concentration of water as a variable, Equation (5-5) does not become Equation (5-8), but rather becomes Equation (5-46):

$$\frac{d[D]}{dt} = k'_1[A][B] - k_2[C][D] \tag{5-46}$$

Using similar manipulations as before,

$$\frac{dQ(t)}{dt} = \alpha\left(Q(t)^2 - Q_{eq}^2\right) - \beta(Q(t) - Q_{eq}) \tag{5-47}$$

Where,

$$\alpha = k'_1 - \frac{1}{2}k_2 \tag{5-48}$$

$$\beta = k'_1 + \frac{1}{2}k_2[C]_0 + k_2[D]_0 \tag{5-49}$$

Integral forms of the equation:

$$\int_0^Q \frac{1}{\alpha\left(Q^2 - Q_{eq}^2\right) - \beta(Q - Q_{eq})} dQ = \int_0^t 1\, dt \tag{5-50}$$

This gives:

$$\frac{-(-\ln(Q - Q_{eq}) + \ln(\alpha Q - \beta + \alpha Q_{eq}))}{-\beta + 2\alpha Q_{eq}} + \frac{\ln(-Q_{eq}) - \ln(-\beta + \alpha x Q_{eq})}{-\beta + 2\alpha Q_{eq}} = t \tag{5-51}$$

Solving for x gives:

$$Q(t) = Q_{eq}\frac{\beta e^{(-t\beta - 2t\alpha Q_{eq})} + \alpha Q_{eq} e^{(-t\beta - 2t\alpha Q_{eq})} - \beta - \alpha Q_{eq}}{\beta e^{(-t\beta - 2t\alpha Q_{eq})} + \alpha Q_{eq} e^{(-t\beta - 2t\alpha Q_{eq})} + \alpha Q_{eq}} \tag{5-52}$$

This expression allows us to determine the concentration of any of the reactants or products at any given time by plotting in graphical software. For application in COMSOL, however, this complicated expression is not necessary. Instead, since COMSOL solves in incremental time steps (Δt), it allows you to directly input the reaction as a function of the instantaneous concentration of the reactants and products, specifically:

$$\frac{d[D]}{dt} = k'_1[A][B] - k_2[C][D] \quad (5\text{-}53)$$

Note that the value for the forward rate constant, k'_1, (units = $m^3/mol \cdot s$) here is not equivalent to the one presented earlier, k_1, (units = 1/s) where the concentration of water was assumed constant. They are related by Equation (5-54), where $[B]=5.56\times10^4$ mol/m^3, considering the density (1 kg/L) and molecular weight (18 g/mol) of water under standard conditions.

$$k'_1 = \frac{k_1}{[B]} \quad (5\text{-}54)$$

5.4 RESULTS

5.4.1 CALCIUM PEROXIDE IN SOLUTION

Solutions of varying concentrations (mg/mL) of calcium peroxide in dPBS were prepared and assessed for oxygen release. dPBS was pre-warmed to 37 °C; as soon as calcium peroxide was added to the dPBS, the solution was placed in the oxygen measuring chamber and monitored for 4-24 hours. Due to the slow rate of dissolution of calcium peroxide in water, the mixture had to be vigorously mixed while adding to the chamber in order to prevent it from sedimenting and creating a nonuniform mixture. It was observed that for the duration of the studies the calcium peroxide did not fully dissolve. Figure 5-1 shows the release of oxygen for varying concentrations of calcium peroxide in dPBS (as averaged from three separate runs). As expected, the initial rate of oxygen production increased with increasing concentration of initial calcium peroxide. Similarly, the saturation value of oxygen increased with increasing concentration of initial calcium peroxide. It should be noted that these saturation oxygen values are only a

fraction of the theoretical maximum of oxygen that can be produced for a given amount of calcium peroxide as shown in Table 5-1 .

Due to the extended length of time necessary to reach equilibrium, the experiment was terminated before the reactions reached complete equilibrium, with the exception of the 0.25 mg/mL concentration. Higher concentrations of calcium peroxide, > 2.5 mg/mL, produced oxygen concentrations that were too high for the sensors to measure, thereby leading the inability to accurate measure oxygen. The pH of the dPBS was initially balanced to 7.4, but was not readjusted after rising. For each case, the pH rose to approximately 13 following the addition of the calcium peroxide powder.

Table 5-1: Theoretical maximum (based on 100% conversion through the reaction in Equation (5-4)) of oxygen that can be released from the varying concentrations of calcium peroxide powder tested.

Starting Reactants			**Theoretical Maximum of Final Products**
CaO_2 Concentration (mg/mL)	**CaO_2 Concentration (mol/m^3 or mM)**	**$Ca(OH)_2$ Concentration (mol/m^3 or mM)**	**O_2 Concentration (mol/m^3 or mM)**
0.25	2.60	0.84	1.30
0.50	5.20	1.69	2.60
1.00	10.41	3.37	5.20
2.50	26.01	8.44	13.01
5.00	52.03	16.87	26.01
10.00	104.06	33.74	52.03

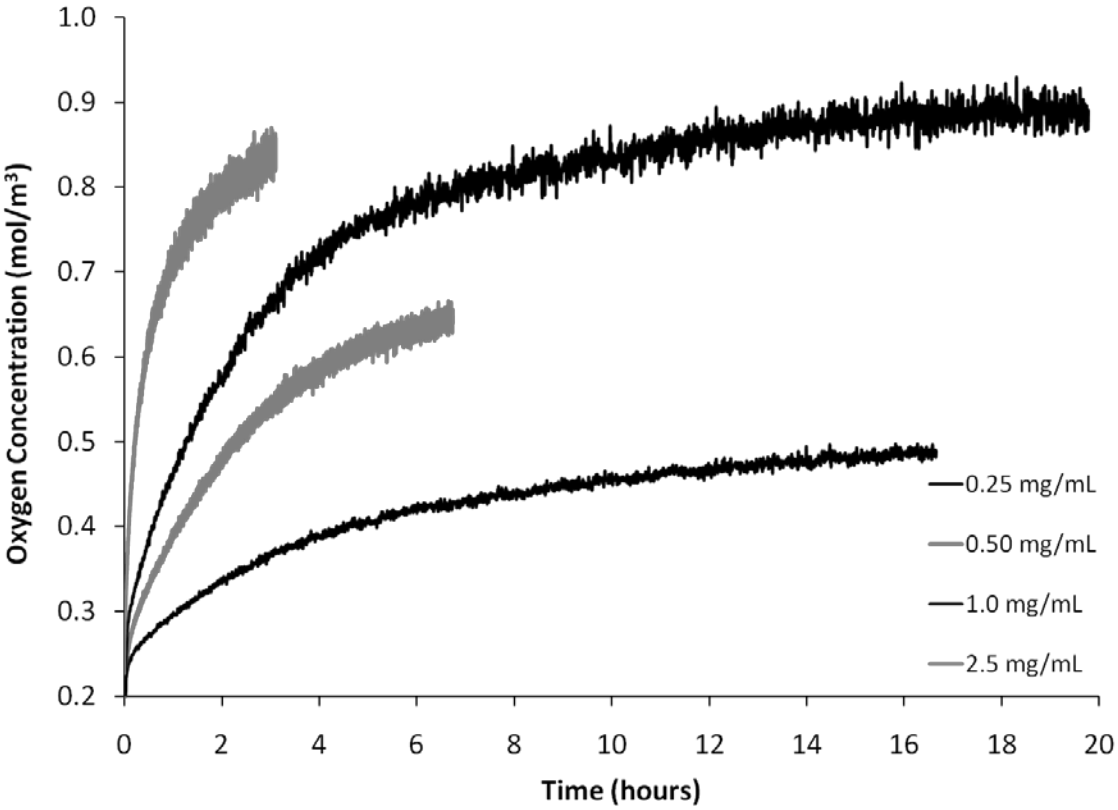

Figure 5-1: Observed release of oxygen from varying concentration of calcium peroxide in dPBS solutions: 0.25, 0.5, 1.0, 2.5, 5.0, and 10.0 mg/mL, as measured via noninvasive sensors in sealed chamber.

5.4.2 KINETICS OF OXYGEN RELEASE

Curves were fitted to the equation for a reversible reaction first order in all reactants and products to determine the values of the forward and reverse rate constants, k_1 and k_{-1}, respectively. Curve fitting was done by using Excel solver to find the least sum of squares. The forward reaction rate was determined to be 6.12×10^{-7} $m^3mol^{-1}s^{-1}$ and the reverse reaction rate was 0.090 $m^3mol^{-1}s^{-1}$. The equilibrium constant, K_{eq}, of the reaction can be expressed as the quotient between k_1 and k_2. For our studies, we calculated an equilibrium constant of 6.80×10^{-6}. This indicates that the reverse reaction is favored over the forward reaction. The initial rate of oxygen release is primarily dependent on the concentration of oxygen; however, as the reaction progresses and the

concentration of the products, oxygen and calcium hydroxide, rises, the release of oxygen is inhibited and the reaction reaches equilibrium. As shown in Figure 5-2, in general, the fit was in fair agreement even for highly variable concentrations of calcium peroxide. Residual sum of squares values were 3-5 for low calcium peroxide concentrations (0.25-0.50 mg/mL) and 10-15 for high calcium peroxide concentrations (1.0-2.5 mg/mL).

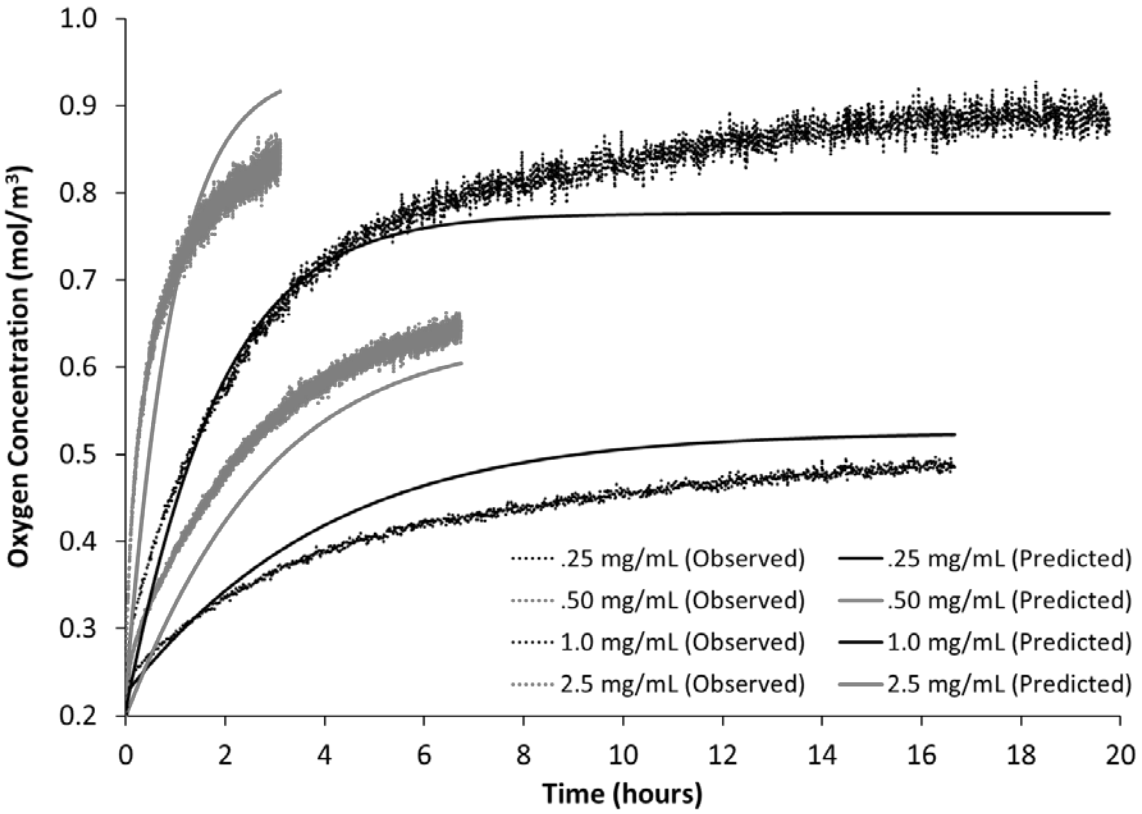

Figure 5-2: Predicted and observed values for oxygen release from calcium peroxide in dPBS solutions: 0.25, 0.5, 1.0, 2.5, 5.0, and 10.0 mg/mL, as measured via noninvasive sensors in sealed chamber.

5.4.3 CALCIUM PEROXIDE ENCAPSULATED IN AGAROSE

The effect of agarose encapsulation on oxygen release from calcium peroxide was investigated and compared to PDMS encapsulation. Calcium peroxide was encapsulated into cylindrical 3 mm disks (1 mm thick) of either agarose or PDMS at varying

concentrations: 0, 5, 10, and 15 %w/w. Figure 5-3 shows the measured oxygen release, where oxygen generation increases substantially with corresponding increases in the concentration of calcium peroxide. Also, for each concentration, the release of oxygen from agarose disks was found to be significantly faster than from PDMS disks. The theoretical maximum of oxygen that can be produced for each disk diameter and concentration is shown in Table 5-2.

Table 5-2: Theoretical maximum (based on 100% conversion through reaction in Equation (5-4)) of oxygen that can be released from the PDMS-CaO_2 disks of varying concentrations and disk diameters. Concentration of calcium peroxide and oxygen is expressed as total moles in disk divided by 1 mL (volume of chamber, not disk).

Starting Reactants			**Theoretical Maximum of Final Products**
CaO_2 Concentration (w/w %)	**Diameter (mm)**	**CaO_2 Concentration (mol/m^3 or mM)**	**Concentration O_2 (mol/m^3 or mM)**
2.5	3	1.93	0.96
2.5	6.5	9.05	4.52
2.5	10	21.41	10.71
5	3	3.92	1.96
5	6.5	18.40	9.20
5	10	43.54	21.77
10	3	8.11	4.05
10	6.5	38.06	19.03
10	10	90.09	45.04
15	3	12.60	6.30
15	6.5	59.13	29.57
15	10	139.96	69.98
25	3	22.61	11.31
25	6.5	106.14	53.07
25	10	251.23	125.61
50	3	56.00	28.00
50	6.5	262.89	131.44
50	10	622.22	311.11

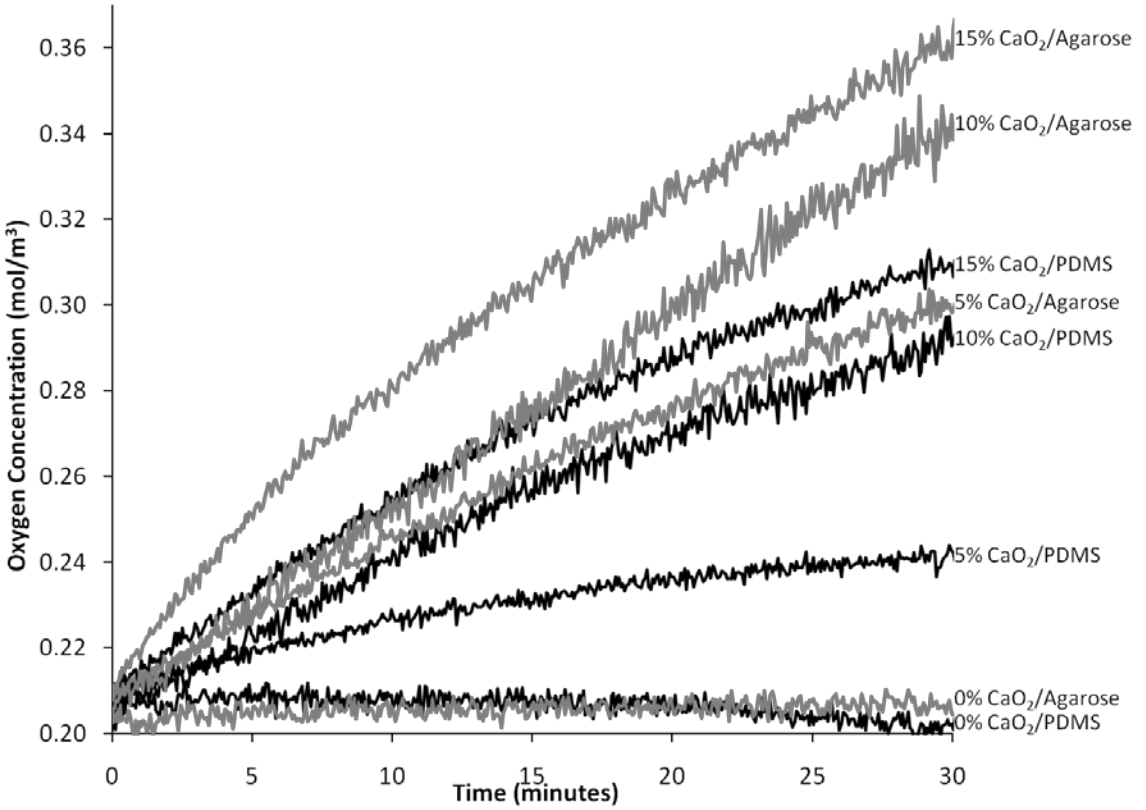

Figure 5-3: Effect of either agarose or PDMS encapsulation on the release of oxygen from varying concentrations of calcium peroxide: 0, 5, 10, and 15 % w/w, as measured via noninvasive sensors in sealed chamber.

5.4.4 CALCIUM PEROXIDE ENCAPSULATED IN PDMS

After having demonstrated effective attenuation of oxygen release from calcium peroxide by encapsulating in PDMS instead of agarose, we sought to investigate the effect of PDMS encapsulation on oxygen release from calcium peroxide in more detail. Varying amounts of calcium peroxide (50, 25, 15, 10, 5.0, and 2.5 w/w %) were encapsulated into cylindrical PDMS disks (1 mm thick) of 10 mm in diameter. In addition, the effect of diameter was evaluated by incorporating 15 w/w % calcium peroxide within PDMS disks (1 mm thick) of varying diameters, 3, 6.5, and 10 mm. Due to the pale yellow color of calcium peroxide powder, disks with different concentrations of calcium peroxide were visibly distinguishable from each other in terms of color and

opacity. Figure 5-4 summarizes the oxygen release profiles for 10 mm diameter disks of varying CaO_2 concentrations. Figure 5-5 shows the oxygen release profiles for 15% w/w PDMS-CaO_2 disks of varying diameters. The measured oxygen release increased greatly with concentration of calcium peroxide and the diameter of the disks. At higher concentrations of oxygen, the noise of the sensor measurements increased, reducing accuracy. The pH of the surrounding dPBS solution did not fluctuate from the original value of 7.4. At the conclusion of the measurements, a white precipitate was noted on the rough surface of the disk (the side originally in contact with the fabrication mold).

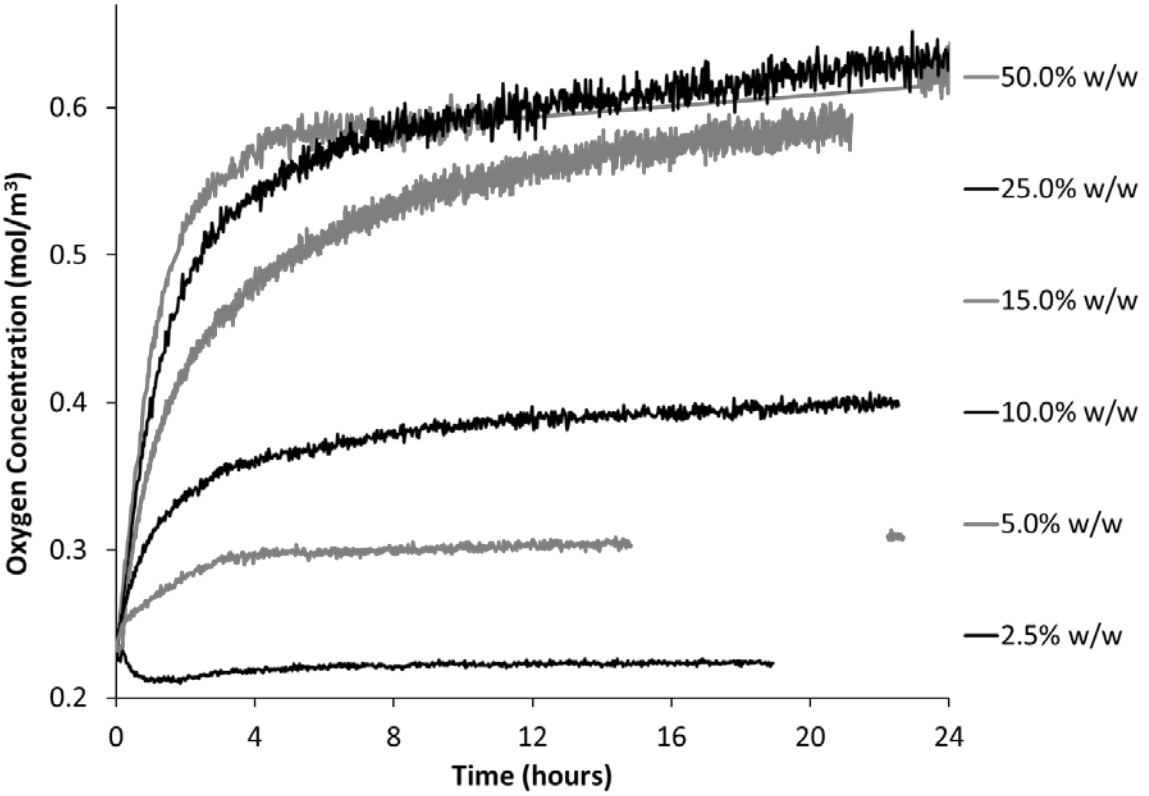

Figure 5-4: Oxygen release from calcium peroxide PDMS disks of varying concentrations: 0, 2.5, 5, 10, 15, 25, 50 % w/w, as measured via noninvasive sensors in sealed chamber.

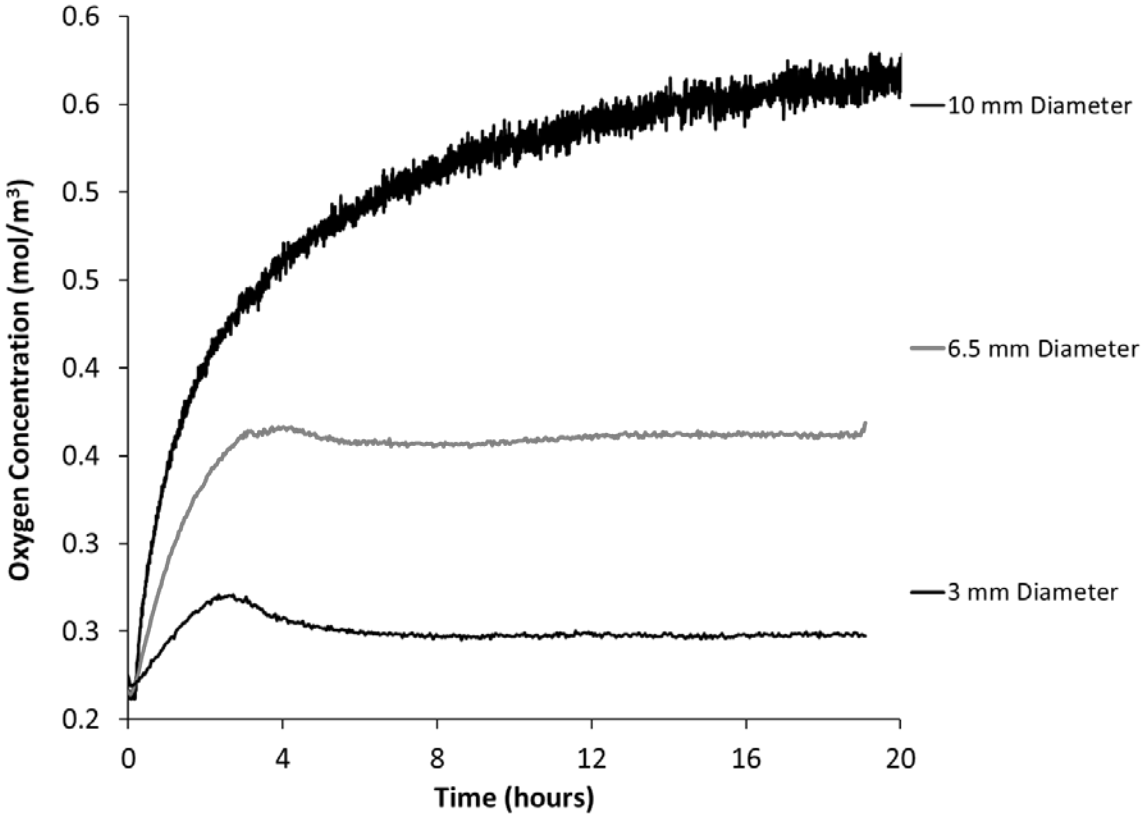

Figure 5-5: Oxygen release from 15% w/w calcium peroxide PDMS disks of varying diameters: 3, 6.5, 5, and 10 mm, as measured via noninvasive sensors in sealed chamber.

We compared the effects of initial w/w % calcium peroxide loading and disk diameter on the final oxygen concentration after saturation. As Figure 5-6 shows, for medium sized disks (6 mm diameter) there is an almost linear relationship between w/w % calcium peroxide and oxygen saturation. For small disks (3 mm diameter), the saturation oxygen concentration increases only slightly within the low range of initial w/w% calcium peroxide, but increases greatly within the high range. The larger disks (10 mm diameter) exhibit the inverse correlation.

As shown, PDMS-CaO_2 disks released oxygen up to a saturation oxygen value. We sought to demonstrate that this oxygen saturation was due to inhibition of the forward reaction by the high concentration of products relative to reactants (reversible kinetics)

and not depletion of the calcium peroxide. The solution of 10 mm diameter 25 % w/w PDMS-CaO_2 disks was refreshed after the oxygen plateaued and was repeatedly observed to rise (see Figure 5-7).

It was not clear to what extent water infiltrates into the disk, if at all. However, this was investigated by finely cutting up 3 mm diameter 25% w/w PDMS-CaO_2 disks that were no longer releasing oxygen (even upon refreshing the solution), thus exposing previously unexposed inner surfaces. When placed inside the chambers again, no additional oxygen was released (data not shown).

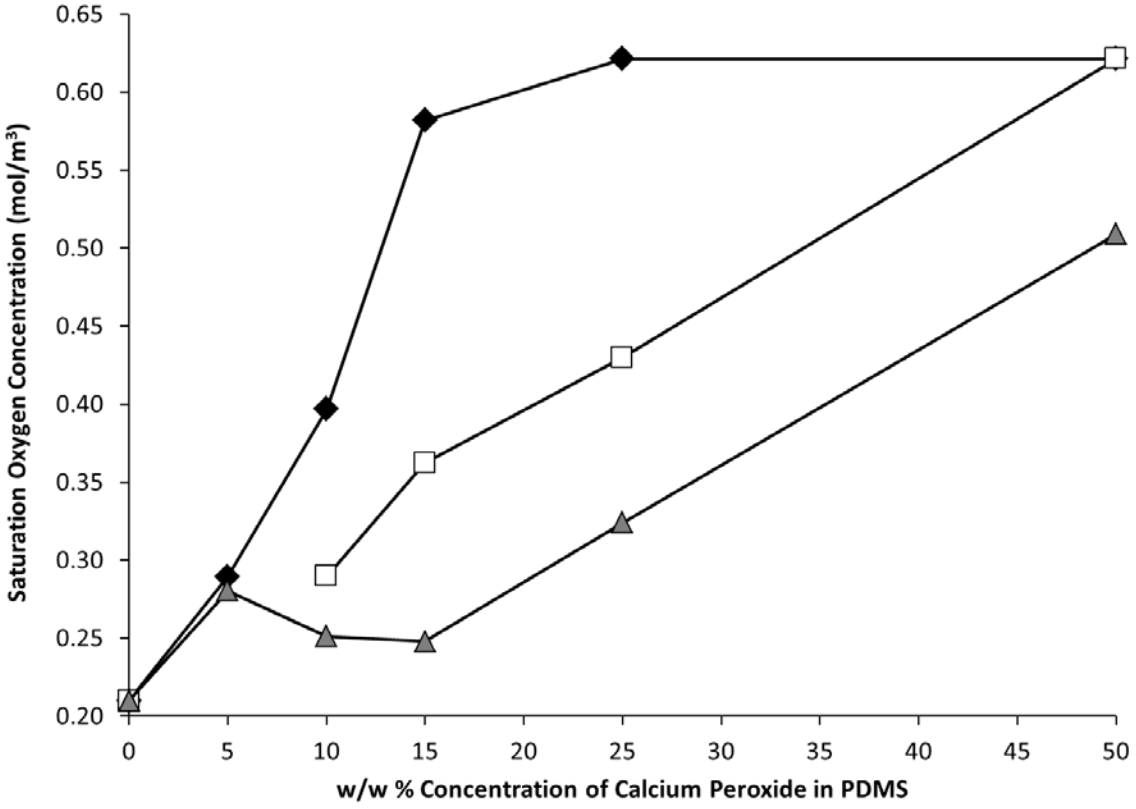

Figure 5-6: Effects of w/w% calcium peroxide in PDMS and disk diameters: 3 mm (grey triangles), 6 mm (white squares), and 10 mm (black diamonds) on the saturation oxygen concentration.

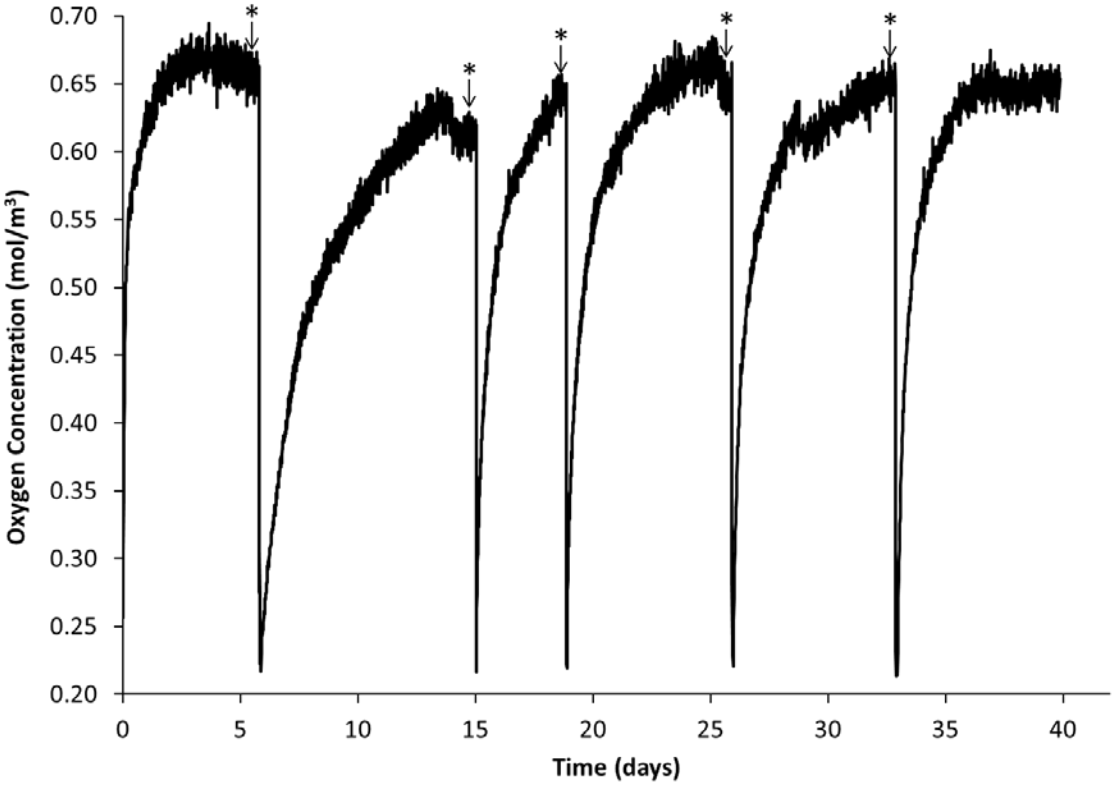

Figure 5-7: Oxygen release from 25% w/w calcium peroxide PDMS disks (10 mm diameter) after multiple refreshes of solution (as indicated by the asterisk).

5.4.5 FINITE ELEMENT ANALYSIS

PDMS-CaO_2 disks of varying concentrations and diameters were modeled in COMSOL. First, the model was validated by simulating the reaction of calcium peroxide in solution without PDMS encapsulation. The reaction rate constants that had been previously derived using Excel were input into the models and the chemical reaction was modeled neglecting diffusion (since the solution in the chamber is thoroughly mixed). The results obtained in COMSOL were nearly identical to those obtained in Excel (results not shown). Next, PDMS encapsulated calcium peroxide models coupled the diffusion of water and oxygen into the disks with the decomposition kinetics of calcium peroxide. Calcium peroxide was only considered reactive (dissolvable) when the water

had diffused to the location of the peroxide. Figure 5-8 summarizes the values for oxygen release as observed experimentally and as predicted by COMSOL models for 25% w/w PDMS-CaO_2 disks of varying diameters. In general, there is fair agreement between the actual and theoretical releases. In particular, the model consistently predicts the saturation concentration of oxygen at equilibrium for all concentrations of calcium peroxide and all disk diameters with high accuracy (residual sum of squares was approximately 5 for 10 mm diameter disks). For small diameters, the model tended to overestimate the amount of time necessary to achieve equilibrium (sum of squares was approximately 15-20 for 3 and 6.5 mm diameter disks).

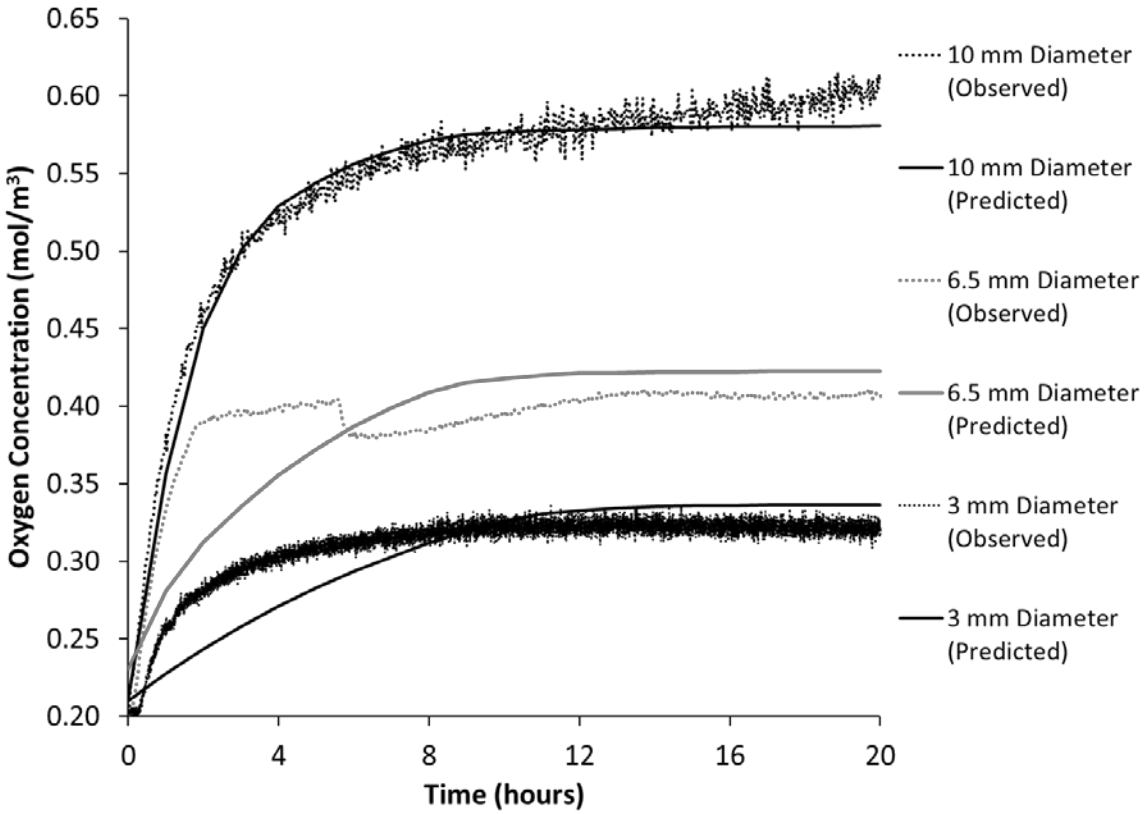

Figure 5-8: Comparison of observed and predicted values for oxygen release from 25%w/w calcium peroxide PDMS disks of varying diameters: 0, 3, and 6.5 mm.

5.5 DISCUSSION

As expected, upon coming in contact with water, calcium peroxide began to dissolve and release oxygen into the surrounding solution. The oxygen release from calcium peroxide in solution was found to increase with the initial concentration of calcium peroxide and to follow the kinetics of a reversible reaction that is first order forward and second order overall in the reverse. High concentrations of calcium peroxide maxed out the signal within a few minutes or produced significant noise. Therefore, low to mid concentrations of calcium peroxide provided data that was more reliable for estimating reaction kinetics. Despite this, the higher concentration of calcium peroxide that we tested fit the theoretical values well. The amount of oxygen measured by the system was only approximately 20% of the theoretical maximum, which is similar to values reported commercially (Chemicals n.d.). This may be explained by the elevated pH of calcium peroxide in solution, which inhibits CaO_2 dissolution. Furthermore, calcium hydroxide produced by the decomposition reaction may precipitate and thereby coat the reactant particle and block its pore structures, leading to transport-limited kinetics (Waite et al. 1999). Alternatively, the calcium peroxide may undergo other chemical reactions (Romero et al. 2009).

Oxygen release from calcium peroxide was successfully modulated by encapsulation in agarose, which introduced a diffusion barrier to water reacting with the calcium peroxide. In comparison with free calcium peroxide, agarose encapsulated calcium peroxide reactivity was dampened by approximately 10%. It cannot be discerned in these figures, but the initial oxygen release rate (first 5 mins) from calcium peroxide in solution is much steeper than for the agarose encapsulated calcium peroxide. It then bends to a lower release rate that is still faster than for the encapsulated disks. This early,

heightened release rate may be due to the fact that the water and all of the calcium peroxide come into contact with each other immediately. The encapsulated calcium peroxide, on the other hand, only has the calcium peroxide on the surface immediately in contact with the water. Oxygen release was further modulated by encapsulation in PDMS, we believe due to the fact that the hydrophobicity of PDMS inhibits water from entering, as indicated by the low partition coefficient of water in PDMS. Oxygen measurements of equivalent concentrations of calcium peroxide in solution were attempted, but produced oxygen too quickly to be measured by our system. The concentration of oxygen increased linearly with the concentration of calcium peroxide. Since the calcium peroxide is immobilized within the PDMS disks, the water will initially react with calcium peroxide on the surface of the disks before diffusing inside to react with the core. A white substance detected on the surface of the CaO_2-PDMS disks was presumed to be precipitate of calcium hydroxide. This further supports the possibility of calcium hydroxide forming and blocking the reactivity of water with calcium peroxide. The saturation value of oxygen concentration was found to depend on disk dimensions and calcium peroxide loading. The plot of oxygen saturation values versus w/w % calcium peroxide in PDMS showed different relationships depending on diameter: linearity for medium disks, exponential for small disks, and logarithmic for large disks.

Additional release of oxygen was observed when the solution of plateaued CaO_2-PDMS disks was refreshed. This shows that the reaction had not completed, but rather had reached a state of equilibrium. This finding reinforces that the reaction is reversible. In contrast, no additional oxygen was observed by finely cutting up 3 mm diameter 25%

w/w CaO_2-PDMS disks, thus exposing previously unexposed inner surfaces. Therefore, it does not appear to be that the lack of diffusion of water into the core is an issue.

Finite element analysis permitted for the coupling of our chemical reaction kinetics to diffusion of solutes in order to model oxygen release from PDMS encapsulated calcium peroxide. The fact that simulations of calcium peroxide solution in the chamber reproduced experimentally observed results demonstrates verifies the validity of our chemical reaction kinetics model in COMSOL. While the COMSOL results were not identical, this could be due to the fact that the precision of the calculated values is dependent on the time steps taken by the solver. COMSOL models were able to accurately predict the equilibrium concentration of oxygen for PDMS-CaO_2 disks. Thus, the models can be very useful for predicting the necessary calcium peroxide loading and disk geometries in order to achieve a targeted concentration of oxygen at equilibrium. However, in this study, the models did not always accurately predict the time to reach equilibrium. Flaws in the model can be caused by a multitude of factors, due to the complexity of the system and the various assumptions made. First, the fundamental reaction rate kinetics implemented here may not be sufficiently accurate or applicable to the system. For example, the calcium peroxide solutions we assessed in order to derive the reaction rate constants were of highly dilute concentrations. Their preparation required measuring of minute masses and consistent mixing in order to minimize sedimentation. Due to the kinetics of the reaction, small differences in the concentration of the reactants have a strong effect on the rate, leading to reduced accuracy in calculating the rate. Therefore, errors in the measurement of the initial reactant concentrations would be amplified in the error of the products (Hogg 1999). Moreover,

our experimental results suggested that the reaction was first-order with respect to each reactant and product. However, rate orders are not limited to whole integers, but may also take fractional form, further complicating calculations (Jordan 2007; Yeargers et al. 1996). A second concern is how PDMS encapsulation may directly affect the reactivity of the calcium peroxide. In this study, we assumed that calcium peroxide and calcium hydroxide would not diffuse out of the disks because they were embedded in the PDMS. Hence, the reaction was initiated upon contact with water, since it is a decomposition reaction that depends directly on calcium peroxide dissolution. A stronger model might be created by incorporating the transport of the calcium peroxide and calcium hydroxide through the PDMS.

The behavior of water at the surface of PDMS is complex and poorly understood (Shiku et al. 2006). The diffusion of water into PDMS is so slow that it is sometimes neglected in microfluidics. However, it does occur and can produce significant effects (Randall & Doyle 2005; Verneuil et al. 2004). The behavior of water in PDMS is subject to debate and has been described by statistical-mechanical water clustering and polycondensation theories that explain equilibrium sorption data and steady state diffusion data (Barrie & Machin 1969; Favre et al. 1994; Watson 1996). There is a high variability in the values reported for the diffusion of water into and through PDMS. Such differences for such commonplace molecules as water and PDMS are a testament to the difficulty of measuring diffusion of water accurately (Watson 1996). Using erroneous values for the diffusivity of water in the COMSOL models could lead to incorrect predictions for the oxygen release. Moreover, the oxygen permeability of PDMS may change depending on the PDMS surface condition (Shiku et al. 2006). Therefore, these

models are limited by our understanding of the fundamental principles behind the reaction mechanisms and the behavior of molecules around PDMS.

5.6 CONCLUSION

Calcium peroxide has an established role in bioremediation and aquaculture as an oxygen releasing material; however, little is known about the precise mechanism or kinetics behind its generation of oxygen. In this study, we proposed that the process can be described by a one-step reversible reaction. The data collected and shown here on the release of oxygen for varying concentrations of calcium peroxide in solution supported this, demonstrating that the reaction is first order in reactants and products. Furthermore, others have modified oxygen release by incorporating materials that hinder the diffusion of water through methods that are either patented or still in development, with a primary focus on soil remediation. However, by encapsulating in hydrophobic PDMS, we have successfully modulated oxygen release by using a material that is biocompatible and approved for medical applications. Therefore, this oxygen generator has the potential for use in cell biology applications, where biocompatibility and maintaining a neutral pH are important. By applying these release kinetics and finite element analysis models, the release of oxygen can be optimized to meet cellular demands by varying the concentration of calcium peroxide and geometry of the oxygen generator system.

CHAPTER 6. INVESITGATION OF PDMS ENCAPSULATED CALCIUM PEROXIDE FOR IN-VITRO CULTURE WITH CELLS AND ISLETS

6.1 INTRODUCTORY REMARKS

The implantation of cellular-based devices is commonly hampered by inadequate oxygen delivery (A. I. Silva et al. 2006; De Vos et al. 2002; A. Silva & M Mateus 2009). The inevitable delay in angiogenesis following implantation can result in the significant loss of transplant viability due to inadequate oxygenation of transplanted cells. Cell death by necrosis is common under anoxic culture conditions (~0 mmHg O_2), since metabolic pathways are restricted and plasma membrane integrity is jeopardized (Herman et al. 1988). Hypoxia conditions (5-15 mmHg O_2) usually cause cells to shift towards anaerobic metabolic activities and to express factors that favor oxygen delivery (Semenza 1999). Normoxic conditions (30-90 mmHg O_2) are optimal for achieving baseline metabolism and function (Jungermann & Kietzmann 2000). Therefore, in order to prevent massive cell loss following implantation, ensuring the appropriate oxygen tension in the transplant environment should be a critical component in designing an optimal implant.

In the development of an islet-based transplant for the treatment of diabetes, ensuring adequate oxygenation is a substantial challenge. Islet oxygen consumption rates are up to 10^6 fold higher for human islets than for chondrocytes and 10^4 fold higher than for endothelial cells (W. Wang et al. 2005; Motterlini et al. 1998; Heywood et al. 2006). In addition, islets are highly susceptible to functional impairment at moderate oxygen tensions (De Vos et al. 2002; Papas et al. 2007). Therefore, while cell viability may be unaffected, insulin production levels can be reduced by as much as 50% at the

threshold between normoxia and hypoxia (Dionne et al. 1993). Combining islets within a macro-scale device for implantation at alternative sites further compounds this challenge. In the initial days following islet implantation, in the absence of intra-vascular infiltration, the maximal oxygen concentration occurs at the outer boundaries of the device and progressively decreases in the inward radial direction. In mathematical terms, this trend in the reduction in oxygen can be described as the concentration of oxygen is inversely proportional to the path length squared. The sharp discrepancy in how maximal oxygen concentration occurs at the outer boundaries of the device and decreases to a minimal value at the center of the device is due to diffusion. Another factor to consider is that greater islet loading densities increase the percent volume oxygen consumption rate. Even fully vascularized devices may exhibit hypoxic gradients, when presented with high cell loading densities and transport limitations introduced by the poor spatial distribution of the islets inside of the device.

Software computational models can be used to gain realistic insight into the effects of the geometric design of the device on islet viability. These computational models can provide guidelines for the design of devices to prevent hypoxic conditions once fully vascularized. For example, modeling can predict the appropriate islet loading density and overall dimensions of the device to ensure adequate oxygen diffusion to all the transplanted cells. For avascular implants, however, designing the appropriate device dimensions to limit hypoxia is an arduous task. When the oxygen consumption rate of the islets exceeds the rate of diffusion of oxygen from the surrounding area, an oxygen deficit is created. In order to minimize islet death due to oxygen deficiency, islet loading densities must be low within the implant. However, to achieve such low cell loading

densities, the size of the device must be increased to dimensions that are impractical for clinical implantation (Folkman & Hochberg 1973). Therefore, in order to ensure adequate oxygenation during the engraftment period, it is critical to identify and develop methods to increase oxygen availability to islets. These methods should serve as a bridge between implantation and the development of an adequate intra-islet vascular network, which, based on wound healing studies, is on the order of 5 to 14 days (Metcalfe & Ferguson 2007; Marques et al. 2005; B.S. Harrison et al. 2007; Calafiore 1998).

Currently, various agents are being investigated for their oxygen generating potential. Wu et al successfully generated oxygen in situ by electrolytically decomposing water into oxygen and hydrogen. Control over the rate of oxygen generation was achieved by changing the electrical current. In-vitro culture experiments with βTC3 islets found that the presence of the electrochemical generator caused an increase in cell layer thickness and cell viability (H Wu et al. 1999). Bloch et al has exploited the natural process of photosynthesis in microalgae to produce oxygen, which showed promising preliminary results (Bloch et al. 2006). At first, they utilized a one-compartment system where islets were in close proximity to the unicellular algae. However, this configuration led to undesirable side-effects: algal overgrowth, a switch from photosynthetic to heterotrophic nutrition of the algae, accumulation of toxic metabolites, and competition for nutrients between plant and mammalian cells. A two-compartment system was created to address these issues, but resulted in decreased overall performance and efficiency of the strategy (Bloch et al. 2006).

Research in our laboratory has been focused on introducing oxygen generating agents and enhancing oxygen transport to the islet's immediate environment through the

combination of biomaterials and agents capable of enhancing or generating oxygen. Of particular interest to us is the incorporation and subsequent encapsulation of solid peroxide within biomaterials. As is commonly known, hydrogen peroxide spontaneously decomposes exothermically into water and oxygen gas via the reaction shown in Equation (6-1). Similarly, solid peroxide produces oxygen by the reactions shown in Equation (6-2) for high pH and Equation (6-3) for low pH. By encapsulating solid peroxide, the barrier induces a delay in oxygen generation, resulting in temporal modulation of oxygen release, thereby providing a gradual, sustained release of oxygen (B.S. Harrison et al. 2007).

$$2H_2O_2 \rightarrow 2H_2O + O_2 \quad (6\text{-}1)$$

$$2CaO_2 + 2H_2O \rightarrow 2Ca(OH)_2 + O_2 \text{ (at high pH)} \quad (6\text{-}2)$$

$$CaO_2 + 2H_2O \rightarrow Ca(OH)_2 + H_2O_2 \text{ (at low pH)} \quad (6\text{-}3)$$

Dr. Harrison's group has utilized this platform using films of poly(D,L-lactide-*co*-glycolide) (PLGA) to encapsulate either sodium percarbonate or solid calcium peroxide, with a focus on improving the efficacy of healing for skin grafts (B.S. Harrison et al. 2007; Oh et al. 2009). Earlier, polymeric oxygen generating (POG) films were fabricated from PLGA and sodium percarbonate using a solvent casting process. When implanted into a critically/marginal perfused tissue in-vivo, such as the skin flap model in nude mice, the POF films significantly reduced necrosis compared to control films. Unfortunately, since the conversion of the sodium percarbonate was completed after only 24-70 h, the benefits of the POG films in-vivo were only observed at early time points (before 7 days). This is because sodium percarbonate is not a true peroxide, but rather an adduct of sodium bicarbonate with hydrogen peroxide. In their second study, they sought

to extend the oxygen release by replacing sodium percarbonate with calcium peroxide at loadings of 1-10 wt%. These constructs increased the proliferation of fibroblasts as evidenced by MTS and live/dead, but measured release of oxygen was extremely low (approximately 1 mmHg per day). Although this demonstrates the possibilities of exploiting peroxides for improved in-vitro and in-vivo performance of cells, neither material provides sufficient amounts of oxygen for an extended period of time (at least 2 weeks) to meet the high demands of islets.

We have sought to translate this oxygen generating platform to improve the viability and function of islets. However, there are concerns about oxidative stress caused by peroxide reaction byproducts. As the reaction in Equation (6-3) suggests, hydrogen peroxide may be generated during calcium peroxide decomposition. Additionally, hydroxyl radicals ($OH^{\cdot}$) may be produced by the reaction shown in Equation (6-4). This modified Fenton reaction requires reduced iron, which may be in the form of naturally occurring iron minerals (Watts & Teel 2005; Ravikumar & Gurol 1994; Miller 1995; Watts et al. 2009). Hydroxyl radicals are strong, relatively indiscriminate oxidants that react with most organic compounds at rate constants of 10^{9}-10^{10} M^{-1} s^{-1}, which is near diffusion-limited rates (Walling 1975; Ge Chen et al. 2001).

$$H_2O_2 + Fe^{2+} \rightarrow Fe^{3+} + OH^{-} + OH^{\cdot} \qquad (6\text{-}4)$$

Of particular concern for utilizing solid peroxide in the presence of islets is the reduced free radical scavenging capacity of these cells. Hydroxyl radicals can damage DNA bases and mediate redox alteration of cell-membrane calcium ion channels (Nagano 2009). Since islets have very limited levels of antioxidant enzymes, they are more susceptible to reactive oxygen species-induced toxicity (Tiedge et al. 1997; Kimoto et al.

2003). This has been further demonstrated in studies where antioxidant supplementation was able to reduce oxidative damage to islets possessing reduced free radical scavenging potential (Meghana et al. 2007; Kaneto et al. 1999). We sought to minimize the exposure of islets to ROS and peroxide, as well as modulate oxygen release, through the use of a hydrophobic material, namely poly(dimethyl siloxane) (PDMS). We postulate that the use of a hydrophobic material will inhibit the exposure of cells to hydroxyl radicals by initially isolating the radicals within the PDMS microenvironment and introducing a diffusion gradient that will allow the free radicals to oxidize before reaching the cells.

In this paper we report the design and fabrication of PDMS encapsulated calcium peroxide (PDMS-CaO_2) disks. The long-term releases of oxygen and hydrogen peroxide, as well as the immediate release of hydroxyl radical, from the PDMS-CaO_2 disks were assessed. The effects of PDMS-CaO_2 disks on the viability and function of MIN6 in long-term culture and rat and human islets in short-term culture were assessed. Implications of this platform for in situ generation of supplemental oxygen in-vivo, as well as its applicability for tissue engineered constructs, is discussed.

6.2 MATERIALS AND METHODS

6.2.1 MATERIALS

Calcium peroxide powder was purchased from Sigma-Aldrich (Cat. No. 466271). It has a particle size of -200 mesh and is 75% calcium peroxide, with the remainder as calcium hydroxide. Poly(dimethyl siloxane) (PDMS) silicone polymer RTV 615 A+B (room temperature vulcanized) was purchased from GE Silicones. Agarose Type VII was purchased from Sigma-Aldrich. dPBS was purchased from Mediatech and pH balanced to 7.4 using NaOH and HCl. 2-[6-(4'-hydroxy)phenoxy-3H-xanthen-3-on-9-yl]benzoic acid

(HPF) was purchased from Calbiochem. Horseradish peroxidase type II (HRP) was purchased from Sigma. Bovine serum albumin (BSA) was purchased from VWR. MTT kit was purchased from Promega (Madison, WI). LIVE/DEAD Viability/Cytotoxicity Assay Kit was purchased from Invitrogen. A 500 mL solution of AT-Extraction buffer was prepared by mixing: 33.3 mL 1N ammonium hydroxide, 1 mL Triton X-100, and 465.7 mL of dH_2O. Quanti-iT PicroGreen dsDNA kit was purchased from Invitrogen. Insulin ELISA was purchased from Mercodia (Winston Salem, NC).

6.2.2 FABRICATION OF AGAROSE-CaO_2 DISKS

Oxygen generating disks (*Agarose-CaO_2* disks) were fabricated by mixing 25% w/w of solid calcium peroxide powder (Sigma Aldrich) with 2% w/w agarose heated to 37 °C. The calcium peroxide/agarose solution was loaded into cylindrical molds of 1 mm height and 10 mm diameter and allowed to gel at 4 °C for 5 minutes. The disks were deemed not suitable for long-term storage and were used immediately for oxygen measurements and hydrogen peroxide assessment.

6.2.3 FABRICATION OF PDMS-CaO_2 DISKS

Oxygen generating disks (PDMS-CaO_2 disks) were fabricated by mixing 25% w/w of calcium peroxide powder (Sigma Aldrich) with poly(dimethylsiloxane) (PDMS) silicone polymer (GE Silicones). Silicone polymer was prepared by mixing 4 parts volume of PDMS monomer with 1 part volume of platinum catalyst. The calcium peroxide/silicone mixture was loaded into cylindrical molds (10 mm diameter, 1 mm height). Air bubbles are subsequently removed by placing in a vacuum for one hour, and the disks are cured at 40 °C for 24 hrs. Preceding oxygen measurements, the disks are

placed in ethanol for 30 mins to sterilize them and remove any peroxide on the material surface.

6.2.4 MEASUREMENT OF OXYGEN RELEASE

Constructs were assessed for long-term release of oxygen in dPBS at 37 °C. Open-air oxygen production was monitored by placing disks in an open, fluid filled container within a 5% oxygen humidified incubator, while closed-system oxygen production was monitored within a sealed, titanium chamber in fluorescence amplitude micro oxygen monitoring systems (Instech Laboratories, Plymouth Meeting, PA). Oxygen concentration was measured using PreSens (Germany) non-invasive oxygen sensors, which consist of a ruthenium-based spot sensor transmitting fluorescence signals to the computer through optical fiber cables. Blue LED excites the sensor to emit fluorescence, but the fluorescence is quenched when it collides with oxygen molecules. Therefore, the changes in fluorescence can be correlated to oxygen concentration in the solution. These sensors possess a high sensitivity and high signal to noise ratio, and can measure oxygen levels non-invasively without disturbing the culture environment (Papas et al. 2007).

6.2.5 MEASUREMENT OF HYDROGEN PEROXIDE PRODUCTION

To assess hydrogen peroxide production, PDMS-CaO_2 disks were incubated in 24-well plates with 1 mL of either dPBS or culture media at 37 °C for 80 days. Samples were taken every day for the first four weeks and then once every 7 days afterwards. When samples were collected, 200 µL of fluid was removed from the wells and replaced with fresh fluid. Hydrogen peroxide concentration was measured using a colorimetric

assay (assay designs). Removal and replacement of solution was accounted for in the final analysis of release and values were expressed as the average total release of hydrogen peroxide per day.

6.2.6 ASSESSMENT OD HYDROXYL RADICAL PRODUCTION

A novel fluorescence probe, 2-[6-(4'-hydroxy)phenoxy-3H-xanthen-3-on-9-yl]benzoic acid (HPF) (Calbiochem), developed by Nagano et al was used to selectively detect the release of hydroxyl radicals ($OH^{\cdot}$) from PDMS-CaO_2 disks (Nagano 2003). To assess hydroxyl radical production, PDMS-CaO_2 disks were incubated in 24-well plates with 1 mL of either dPBS or culture media at 37 °C, and triplicate samples of solution were taken at 24 and 72 hours. Samples were incubated at 37 °C for 30 mins in a 96-well black, florescence plate with the HPF probe (final 10 μM). The relative fluorescence units were measured in a plate reader by excitation at 490 nm and emission at 515 nm. Some literature suggests creating a hydroxyl radical standard curve via modified Fenton chemistry by titrating reduced iron (Fe^{2+}) (5 to 100 μM) to hydrogen peroxide (final 1 mM) (Nagano 2003). However, this method produced inconsistent results since it is difficult to calculate the concentration of hydroxyl radicals produced from a Fenton reaction (Cohn et al. 2008). Instead, the HPF probe was incubated with varying concentrations of hydrogen peroxide (100 to 1000 nM) in the presence of horseradish peroxidase (HRP, Sigma type II) (2.95 units/mL or 0.2 μM). Since the probe is oxidized stoichiometrically, relative fluorescence can be correlated to the concentration of hydrogen peroxide, which in turn is equivalent to the concentration of hydroxyl radical.

6.2.7 CELL ISOLATION AND CULTURE

MIN6 cells (passages 30-40) were cultured as monolayers in T-flasks and fed every 2-3 days with fresh medium comprised of Dulbecco's modified Eagle's medium (DMEM) supplemented with 10% FBS, 1% penicillin-streptomycin (P/S), and 0.001 % (v/v) β-mercaptoethanol. Rat pancreatic islets were isolated from male Sprague-Dawley (SD) rats using methods described elsewhere (Antonello Pileggi et al. 2006). Nonhuman primate baboon islets were isolated using methods described elsewhere (Berman et al. 2010). All procedures were conducted according to the guidelines of the Committee on Care and Use of Laboratory Animals, Institute of Laboratory Animal Resources (National Research Council, Washington DC). Human pancreatic islets of Langerhans were obtained from the NIH/JDRF ICR Consortium. Following isolation, islets were cultured in CMRL 1066 (Mediatech) for 48 hrs (rat islets) or MM1 (Mediatech) for 24 hrs following arrival (human islets) in a humidified 37°C, 5% CO_2 / 95% air incubator. CMRL 1066 and MM1 media was supplemented with 10% fetal bovine serum (FBS; Sigma), 1% penicillin-streptomycin (Sigma), and 1% L-glutamine (Sigma).

6.2.8 OXYGEN CONSUMPTION BY MIN6 CELLS

The ability of PDMS-CaO_2 disks to supply sufficient oxygen to compensate for the consumption of oxygen by cells was assessed by incubating MIN6 cells with the disk within a sealed chamber. MIN6 cells were loaded into the chamber at a density of 2.5×10^6 cells per 1 mL in culture media. A single PDMS disk (with/without CaO_2) was suspended within the chamber via suture. The chamber solution was gently mixed by a

glass stir bar and maintained at 37 °C. After 30 min, the cells were removed from the chamber and assessed for MTT viability.

6.2.9 LONG-TERM CULTURE OF MIN6 WITH PDMS-CaO_2 DISKS

Mouse insulinoma (MIN6) cells were cultured at an initial loading density of 3×10^5 cells on top of a 10 mm Millicell culture insert (Millipore) within a 24-well plate with/without the PDMS-CaO_2 disk placed beneath the insert for 3 weeks, with media changes every 2-3 days. To evaluate the transient effects of PDMS-CaO_2 disks on the cells, subsets of cells had the PDMS-CaO_2 disk removed 3-4 days before viability assessment. Control groups were cells cultured at 5% oxygen or standard 20% oxygen conditions with a plain silicone disk. Every 3-4 days, the cells were assessed for cell viability by MTT metabolic assay (Promega, WS) and live/dead staining (Invitrogen, CA).

6.2.10 CULTURE OF ISLETS WITH PDMS-CaO_2 DISKS

Islets used were either of rat or human origin. Islets were cultured at an islet equivalent (IEQ) density of 1500 IEQ on top of a 10 mm Millicell culture insert (Millipore) within a 6-well plate with/without the PDMS-CaO_2 disk placed beneath the insert for 72 hours. After 48 hours in culture, the insulin secretion function of 150 IEQ islets was determined, as outlined below. The Stimulation Index (SI) of the islets was calculated as insulin secretion during high glucose over the secreted during low glucose. After 48 hrs and 72 hrs, the viability of 1500 IEQ islets was determined by MTT and live/dead.

6.2.11 METABOLIC VIABILITY

Metabolic activity of islets was assessed by MTT assay (Promega). Samples were washed once, suspended in 250 µL of media within a 48-well non-tissue culture treated plate, and placed in a humidified incubator for one hour to recover from manipulation. 28 µL of MTT dye was added to each well and samples were incubated for one more hour. Afterwards, 185 µL of stop/solubilization solution was added to each well and the plate was stored, wrapped in parafilm, for 24 hours in order to stop metabolism of MTT dye and allow the formazan crystal to be solubilized. The next day, 120 µL samples from each well were dispensed into a 96-well plate and the absorption at 570 nm was measured using a plate reader. Changes in optical density due to culture media used were compensated for by subtracting media blanks from all wells.

6.2.12 QUANTIFICATION OF DNA

Total DNA content of MIN6 cells was determined every 3-4 days using Quanti-iT PicoGreen dsDNA kit (Invitrogen). Samples were washed once, pelleted, had fluid aspirated off, and frozen at -80 C. The samples were thawed 24 hrs later, suspended in 300 µL of AT extraction buffer, sonnicated within in a water bath, had an additional 700 µL of AT extraction buffer added, frozen until quantification. Then, samples were thawed again and further diluted in AT buffer (at varying dilutions). DNA concentration was determined by measuring changes in fluorescence due to DNA binding to PicoGreen dsDNA reagent by excitation at 480 nm and emission at 520 nm, and comparison to a DNA standard curve.

6.2.13 LIVE/DEAD VIABILITY

Cell viability was visualized by the LIVE/DEAD Viability/Cytotoxicity Assay Kit (Invitrogen) and imaged through a confocal microscope (Zeiss LSM). Cells were briefly rinsed in HBSS once and then incubated for 45 min in a phosphate buffered saline solution composed of 4 µM calcein AM and 8 µM ethidium homodimer-1 (EthD-1) [reference Kristina Hall]. Afterwards, cells were rinsed a second time in HBSS and placed on a glass slide for visualization via a fluorescence scanning confocal microscope (LSM 510, Zeiss, Germany). Live cells (green) were detected by excitation with light at 494 nm and emission at 517 nm while dead cells (dead) were detected by excitation at 528 nm and emission at 617 nm. Multi-slice images were collected and merged using the projection function on LSM image browser (Zeiss, Germany) software.

6.2.14 INSULIN SECRETION FUNCTION

The functional insulin secretion rate of 150 IEQ islets was determined via static glucose-stimulated insulin release (GSIR) assay. Groups were sequentially incubated for one hour intervals in glucose solutions: low glucose (40 mg/dL) high glucose (300 mg/dL), and low glucose again; using a column method, as described elsewhere (Chris Fraker et al. n.d.; Embury et al. 2001). Briefly, 10mL Poly-Prep columns (Bio-Rad) were placed in Poly-column rack (Bio-Rad), filled with 400 µL of a slurry of Sepharose G-10 (GE Healthcare)/dPBS (10% w/v) and washed with low glucose (2.2 mM) KREB's buffer (26mM sodium bicarbonate, 25mM HEPES, and 0.2% w/v BSA). Islet containing scaffolds were then placed within the columns and an additional 600 µL of bead slurry was added to each column. Columns were then flushed with 4mL of low glucose KREB's solution. Flow in the columns ceased when the liquid level reached the surface

of the beads keeping the fluid volume in each column constant. Columns were then incubated for 1 hr for pre-incubation, followed by a 4mL wash with low glucose KREB's, at which the first step of the glucose challenge (Low1) was initiated. After 1 hr, low glucose KREBs was exchanged with high glucose (16.7 mM) KREBs to begin step two of the challenge (High1). After this hour, high glucose was exchanged with low glucose KREB to begin step three of the challenge (Low2). During each exchange, 1 mL of the respective KREBs solution was added and the 1mL eluate was collected in tubes and stored at – 80 °C for later analysis. Insulin was quantified using the Mercodia Rat or Human Insulin ELISA (Winston Salem, NC), depending on the islet type.

6.2.15 STATISTICAL ANALYSIS

The number of replicates is indicated in the figure legends, and results are expressed as mean ± SD. Statistical analysis was performed on all samples using a paired Student's test, where differences were considered significant when $p < 0.05$.

6.3 RESULTS

6.3.1 OXYGEN GENERATION

To evaluate the effect of biomaterial encapsulation of solid peroxide on oxygen generation, solid peroxide was encapsulated within either hydrophilic material, agarose, or hydrophobic material, PDMS, at 25% w/w and its oxygen generating potential was characterized. The 10 mm diameter disks were incubated in dPBS solution within 24-well plates and placed within a humidified, 5% oxygen incubator. Within this open system, gas exchange between the solution and air occurred at diffusion-limited rates. Oxygen concentration in the dPBS solution was monitored by a fluorescence based spot sensor

placed at the base of the plate. Figure 6-1 shows the average daily oxygen concentration within the solution for agarose-CaO_2 and PDMS-CaO_2 disks as well as a control PDMS-only disk. As shown, over a 2-fold increase in the oxygen tension is observed in the presence of the PDMS-CaO_2 disk, with a sustained and continuous release over the course of at least 10 days. They produced oxygen for over 2 weeks at an average rate of 0.4 mmHg per day. In contrast, agarose, being a hydrogel, exhibits a more dynamic release with a strong burst of oxygen over 5-fold higher than respective controls, albeit more temporary, with the majority of the oxygen generated within the first four days. The PDMS-CaO_2 disks continued to generate oxygen for at least an additional 40 days after the agarose-CaO_2 material had been depleted. As observed, through the encapsulation of solid peroxide within a biomaterial, oxygen generation was modulated. The motility of water within the biomaterial plays as role, as encapsulation within the hydrophobic PDMS polymer resulted in greater attenuation of oxygen release compared to encapsulation within the hydrophilic agarose gel.

In order to obtain more controlled measurements of oxygen release than in the open system (incubator), PDMS-CaO_2 disks were monitored for oxygen release within a closed system (sealed titanium chambers). The incubating solution was maintained at 37 °C and evenly mixed by a magnetic, glass stir bar. As can be seen in Figure 6-2, the concentration of oxygen within the chamber reaches a plateau after approximately 5 days. We demonstrated in the previous chapter that this can be explained by the reversibility of the chemical reaction, which causes increasing oxygen concentrations to inhibit further oxygen release (see Chapter 5). The chamber solution was refreshed whenever a plateau was reached (every 4-7 days, as indicated by the asterisks). As illustrated, a significant

amount of oxygen was produced by the encapsulated oxygen disks after over 40 days. The overall generation of oxygen was below the theoretical maximum of 1,220 mmHg possible, based on the amount of calcium peroxide in disks.

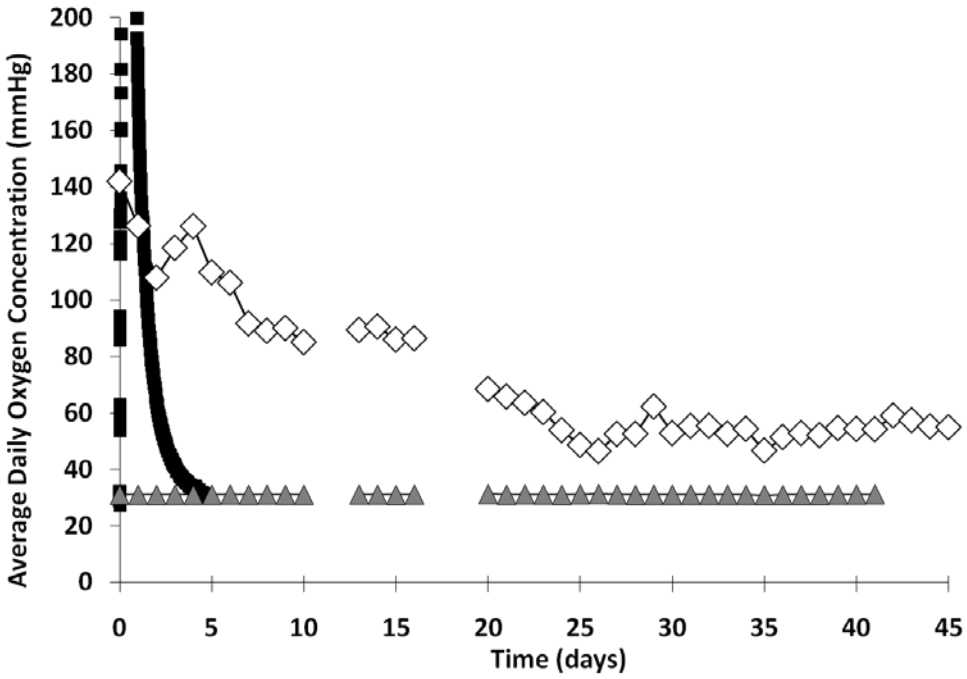

Figure 6-1: Long-term oxygen generation was measured in an open system set at 5% oxygen for 25% w/w calcium peroxide encapsulated in either agarose (white diamonds) or PDMS (black squares), or from control PDMS only disks (grey triangles).

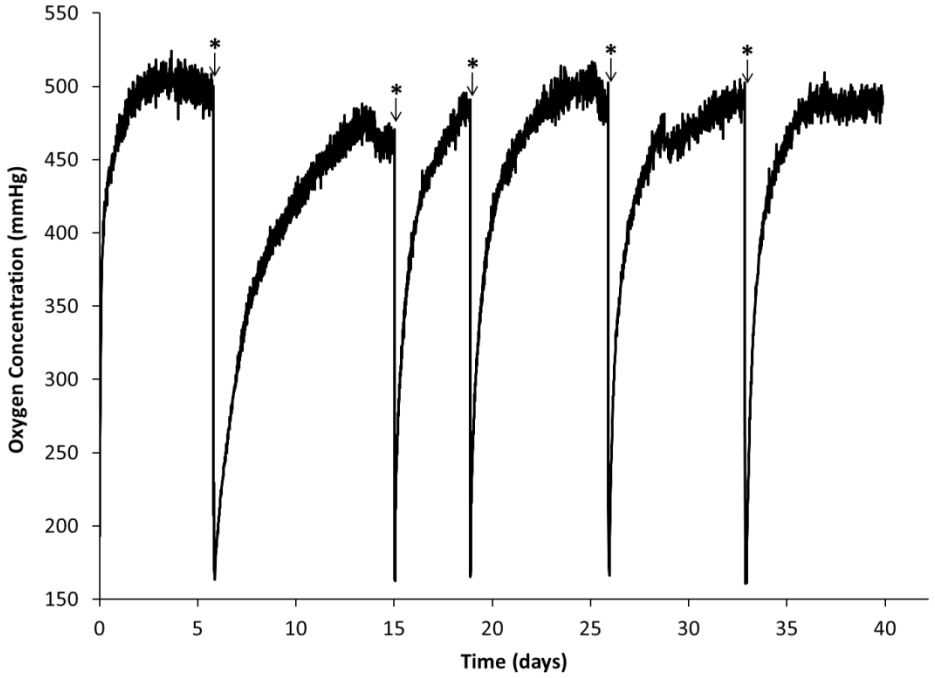

Figure 6-2: Long-term oxygen generation from 25% w/w calcium peroxide encapsulated in PDMS disks was measured in a closed system consisting of a sealed titanium chamber originally equilibrated with 20% oxygen. Buffer replacements, and oxygen re-equilibration, was performed every 4-7 days, as indicated by asterisks.

6.3.2 HYDROGEN PEROXIDE PRODUCTION

Hydrogen peroxide production was assessed from PDMS-CaO_2 and Agarose-CaO_2 disks containing 25% w/w solid calcium peroxide. Agarose-CaO_2 disks were monitored for one week and overall, produced ten times more hydrogen peroxide than PDMS-CaO_2 disks, when evaluated in saline solution (data not shown). Figure 3 summarizes the accumulated hydrogen peroxide release from a single PDMS-CaO_2. Total hydrogen peroxide release into dPBS solution peaked within the first hour to 425 μM, before decreasing to less than 100 μM by 60 hrs (see Figure 6-3). In comparison, when disks were incubated in cell culture media, the production of hydrogen peroxide did not peak, but rather fluctuated around an average concentration of < 10 μM for the first three weeks. As the collection time points became less frequent around day 30 (every 7

days instead of every 1-2 days), the calculated values for average daily hydrogen peroxide rose and fluctuated to < 30 µM. Hydrogen peroxide released in both dPBS and cell culture media was well below the theoretical maximum possible based on the amount of calcium peroxide in disks (281 mM).

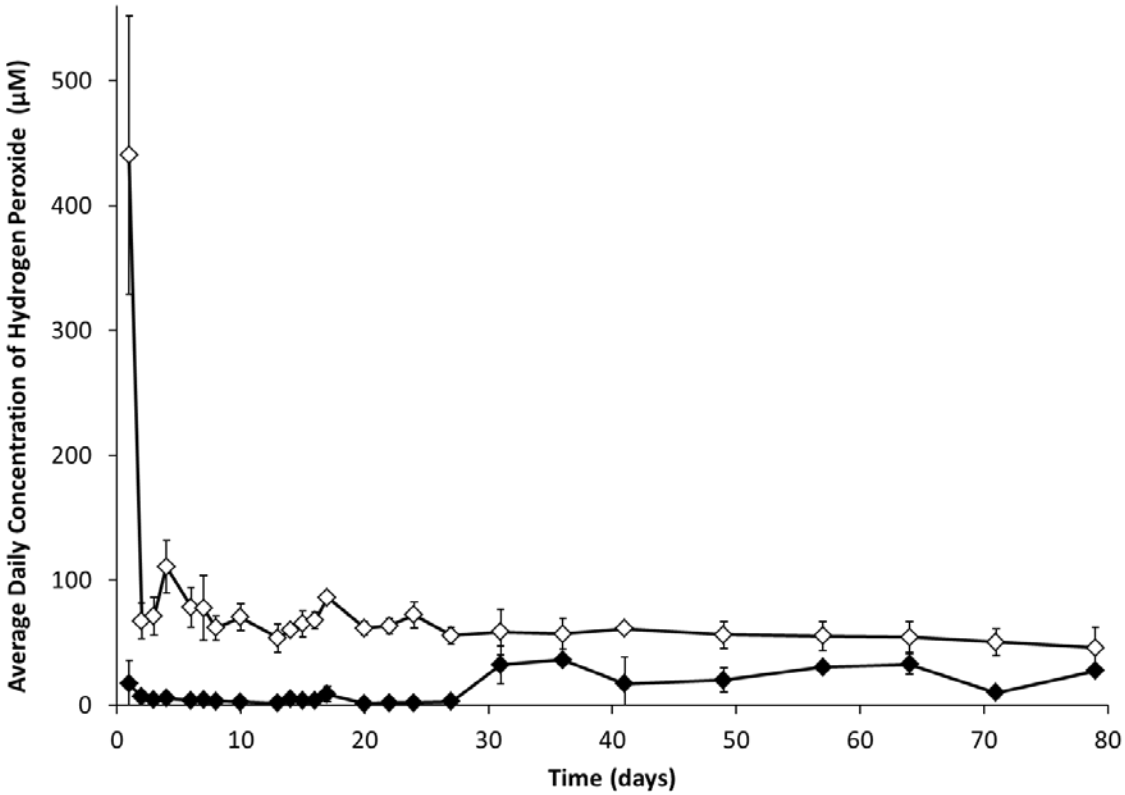

Figure 6-3: The average daily concentration of hydrogen peroxide produced by disks of 25% w/w calcium peroxide encapsulated in PDMS was determined in saline solution (open diamonds) and cell culture media (closed diamonds).

6.3.3 HYDROXYL RADICAL PRODUCTION

Hydroxyl radical release from 25% w/w PDMS-CaO_2 disks was determined after 24 and 72 hrs in dPBS and cell culture media via HPF fluorescent probe. For both dPBS and cell culture media, the relative fluorescence was below the minimum value of the hydroxyl radical (100 nM) standard curve (data not shown). Extrapolation of the curve to

lower values suggests a hydroxyl radical concentration around 5 nM, but the sensitivity of the probe is not reliable in this low range. Hydroxyl radical release is well below the theoretical maximum of 281 nM, based on the amount of calcium peroxide present in the disks.

6.3.4 OXYGEN CONSUMPTION BY MIN6 CELLS

Since the goal of the oxygen generating disks is to provide supplemental oxygen for cells, we sought to determine how the release of oxygen from PDMS-CaO_2 disks compared to consumption of oxygen by cells. As such, oxygen levels were monitored for 2.5×10^6 MIN6 cells (per mL) incubated in a sealed chamber with/without PDMS-CaO_2 disks. PDMS only disks were run as controls to ensure that the PDMS material itself was not a factor. As Figure 6-4 shows, as soon as MIN6 cells were added to the chamber, the oxygen concentration in the control chamber decreased quickly in a linear fashion, due to oxygen consumption by the cells. Their rate of oxygen consumption was approximately 5.22 mmHg per second. Within 30 minutes, the cells had consumed all of the oxygen inside of the chamber. On the other hand, when a PDMS-CaO_2 disk was added together with the cells, there was a severe dampening in the total rate of decline of oxygen in the chamber to 0.29 mm Hg per second. Assuming that the rate of oxygen consumption by the cells is constant, regardless of the presence/absence of the disk, the oxygen release from the PDMS-CaO_2 disks can be deduced by comparing these two different rates for oxygen disappearance in the chamber. Therefore, the oxygen release from PDMS-CaO_2 disks in the presence of a continuous oxygen demand from cells can be approximated as 4.93 mm Hg per second.

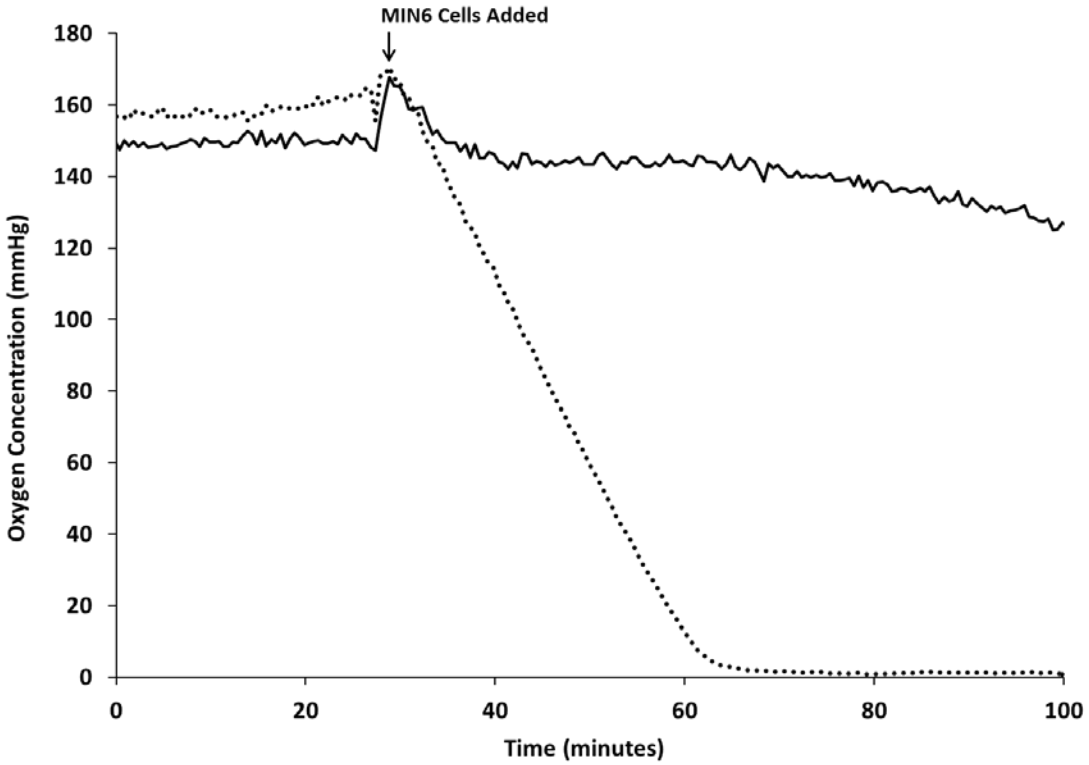

Figure 6-4: Oxygen consumption by 2.5×10^6 MIN6 cells without (dotted) or with (solid) 25% w/w calcium peroxide encapsulated in PDMS disk, as measured in a sealed titanium chamber MIN6 cells were added to the chamber at the time point indicated.

6.3.5 PROLIFERATION OF MIN6 CELLS INCUBATED WITH PDMS-CaO_2

The effects of PDMS-CaO_2 material on the proliferation and viability of cells at low and normal oxygen tensions was investigated by incubating MIN6 cells with a single 10 mm diameter, 1 mm thick PDMS-CaO_2 (25 % w/w CaO_2) for 3 weeks. MTT viability, total DNA content, and live/dead viability of cells was evaluated every 3-4 days. As Figure 6-5 shows, controls cultured at 5% oxygen without a PDMS-CaO_2 disk maintained their cell number without any significant growth and plateaued at 4×10^5 cells/mL, based on MTT results. Conversely, the cells cultured at 5% oxygen with a PDMS-CaO_2 disk quickly increased in metabolic activity within the first 3 days to 7.8×10^5 cells/mL and exhibited metabolic activity equivalent to double the cell numbers

of the 5% oxygen controls throughout the experiment ($p<0.05$). For 20 % oxygen control wells, cells exhibited a similar trend, where cell viability leveled to 12×10^5 cells / mL (data not shown). Introduction of the PDMS-CaO_2 disk to cells at 20% oxygen, however, did not significantly affect cell numbers (data not shown). Moreover, controls of plain PDMS disks without CaO_2 were the same as controls of absence of material. For a select group of cells at 5% oxygen with a PDMS-CaO_2 disk, the PDMS-CaO_2 disk was removed on days 3, 7, and 17 and the cells were assessed 3-4 days later. Upon removal of the PDMS-CaO_2 disks, MTT readings returned to the same value as the 5% oxygen controls.

As Figure 6-6 shows, the DNA content of the cells when cultured with the PDMS-CaO_2 disks was substantially higher than controls. Within the first three days, there was minimal increase in the DNA content, but by day 7 there was a over a 2.5 – fold increase in the total DNA content of the groups with the PDMS-CaO_2 disks, compared to the controls. This large discrepancy in DNA content between the two groups continued for the duration of the experiment.

As the confocal microscopy images of the cells (see Figure 6-7) illustrates, cells cultured at 5% oxygen exhibited greater proliferation when incubated with PDMS-CaO_2 disks. In addition, cells incubated with PDMS-CaO_2 disks tended to form larger cellular spheroids, either due to growth of the cells into these clusters or aggregation.

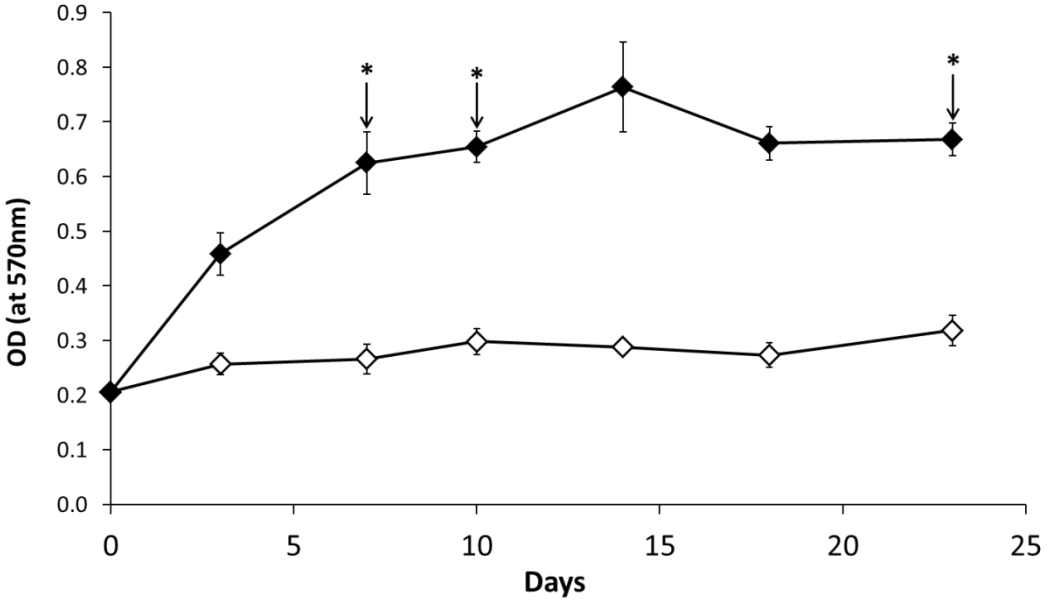

Figure 6-5: MTT viability, expressed as optical density (OD), of 3×10^5 MIN6 cells cultured at 5% oxygen with (closed diamonds) or without (open diamonds) 25% w/w calcium peroxide encapsulated in PDMS disk was determined every 3-4 days for 24 days. Asterisk denotes time points where PMDS-CaO_2 disk was removed for select groups.

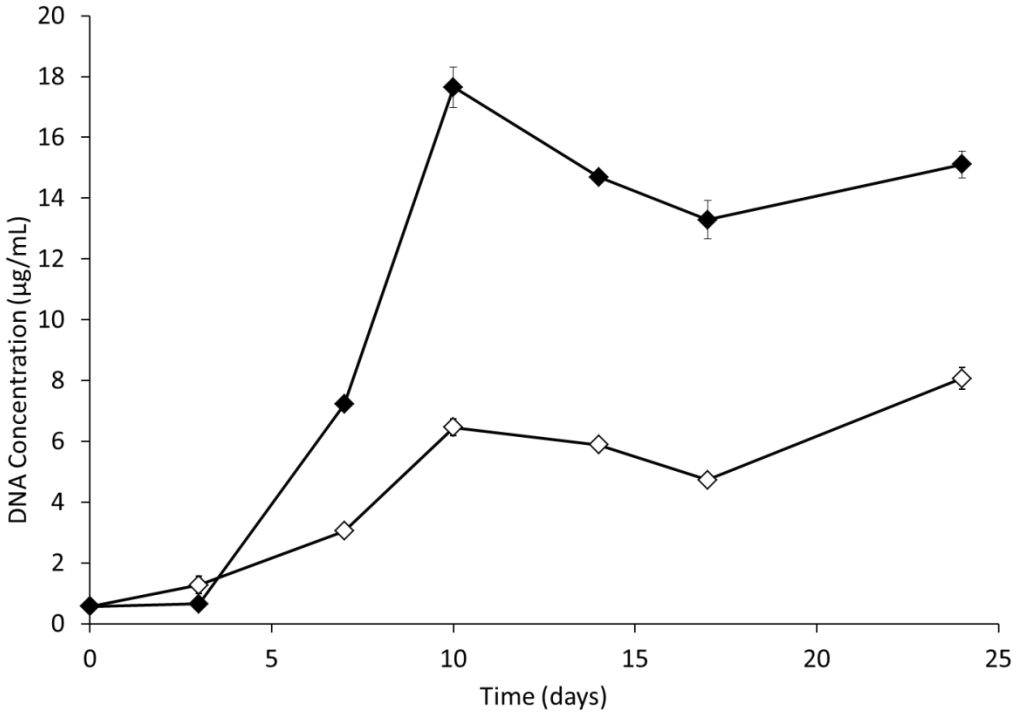

Figure 6-6: DNA quantification of 3×10^5 MIN6 cells cultured at 5% oxygen with (closed diamonds) or without (open diamonds) 25% w/w calcium peroxide encapsulated in PDMS disk was determined every 3-4 days for 24 days.

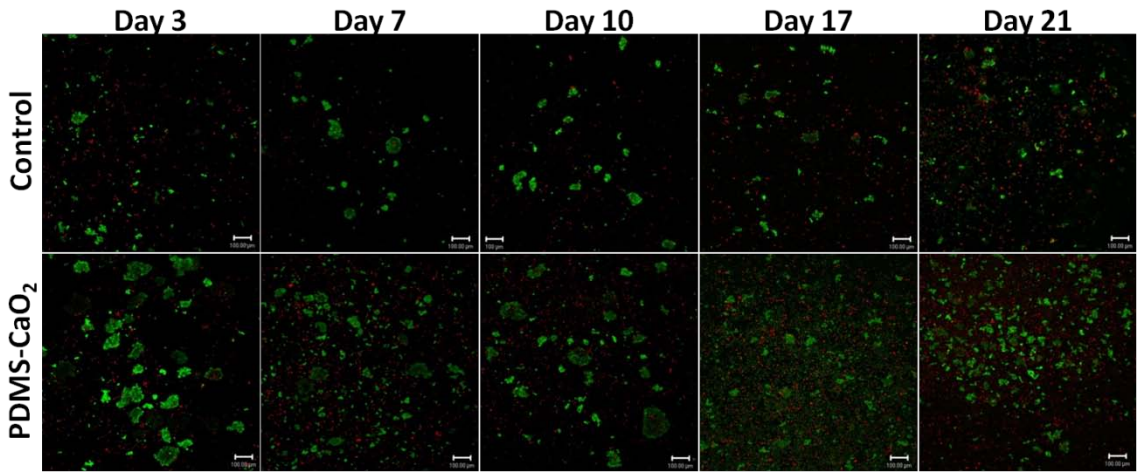

Figure 6-7: Confocal live/dead imaging (live, green, and dead, red) of 3X105 MIN6 cells cultured at 5% oxygen without (top row) or with (bottom row) a 25% w/w calcium peroxide encapsulated in PDMS disk. Imaging was performed at the time points indicated.

6.3.6 VIABILTY AND FUNCTION OF ISLETS AT HYPOXIC CONDITIONS WITH PDMS-CaO_2 DISKS

To evaluate the ability of PDMS-CaO_2 materials to prevent cell death due to hypoxia for islets, rat and human islets were cultured at oxygen tensions similar to the in-vivo environment (5 % oxygen) for three days with or without the oxygen generating material. A single PDMS-CaO_2 disk (1 mm height / 10 mm diameter) was added to the culture dish, while islets were loaded into a cell culture insert. Following 24 to 72 hrs in culture, islet viability was assessed via MTT and Live/Dead confocal imaging, while functionality of the cells was evaluated via glucose stimulated insulin secretion. Islets were also compared to islets cultured under standard incubator oxygen conditions (20 %). As shown in Figure 6-8, rat islets cultured at 5% oxygen without the PDMS-CaO_2 disk exhibited a substantial drop in their metabolic activity, via MTT. The addition of a single PDMS-CaO_2 disk resulted in over a two-fold increase in islet metabolic activity. Islet viability at 5 % oxygen with the PDMS-CaO_2 was statistically identical to control islets

cultured at 20% oxygen (p=0.78 for 24 hrs and p=0.10 for 72 hrs). Live/dead staining and morphological assessment of cells found a greater number of viable cell clusters for groups cultured with PDMS-CaO_2 disks at 5% oxygen, when compared with 5% oxygen controls (see Figure 6-9). The insulin secretions of islets under standard culture at 20% oxygen was compared to that of islets cultured at 5% oxygen with and without a PDMS-CaO2 disk (see Figure 6-10). Islets were cultured for 72 hours and their insulin secretion was determined after 0, 48, and 72 hours in culture via static glucose insulin secretion. Results are expressed as stimulation index (SI), which is the total insulin secreted under stimulated conditions (high glucose) over the total insulin secreted under unstimulated conditions (low glucose). Islets cultured at 5% oxygen lost their insulin responsiveness (SI = 0.5) after 48 hrs (compared to 20% oxygen control p=0.04, compared to 5% oxygen with PDMS-CaO_2 disk p=0.01). Islet cultured at 5% oxygen with a PDMS-CaO_2 disk, however, expressed insulin responsiveness similar to 20% oxygen controls, SI = 2.7 versus SI = 4.1, respectively (p=0.09).

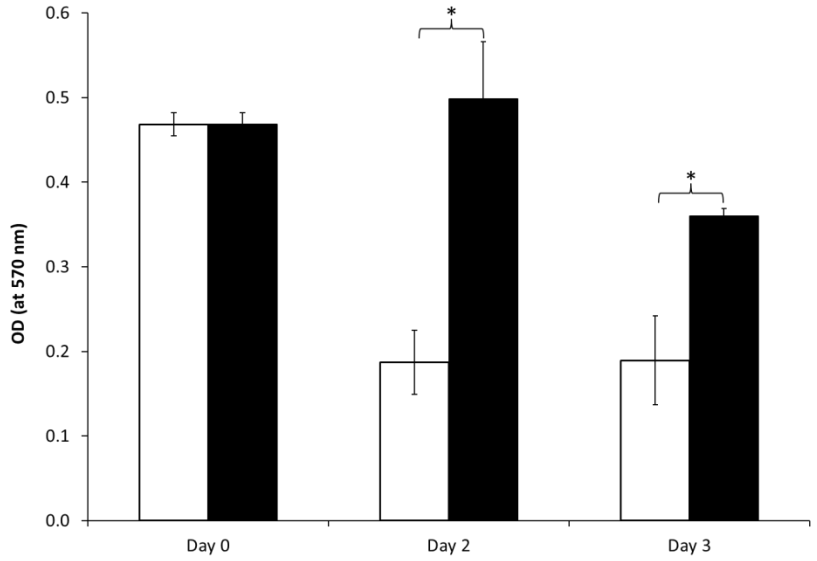

Figure 6-8: MTT viability, expressed as optical density (OD), of 1500 IEQ rat islets cultured at 5% oxygen without (black bars) or with (white bars) 25% w/w calcium peroxide encapsulated in PDMS disk was determined at 0, 2, and 3 days. Asterisk denotes statistical significance between groups ($p<0.05$).

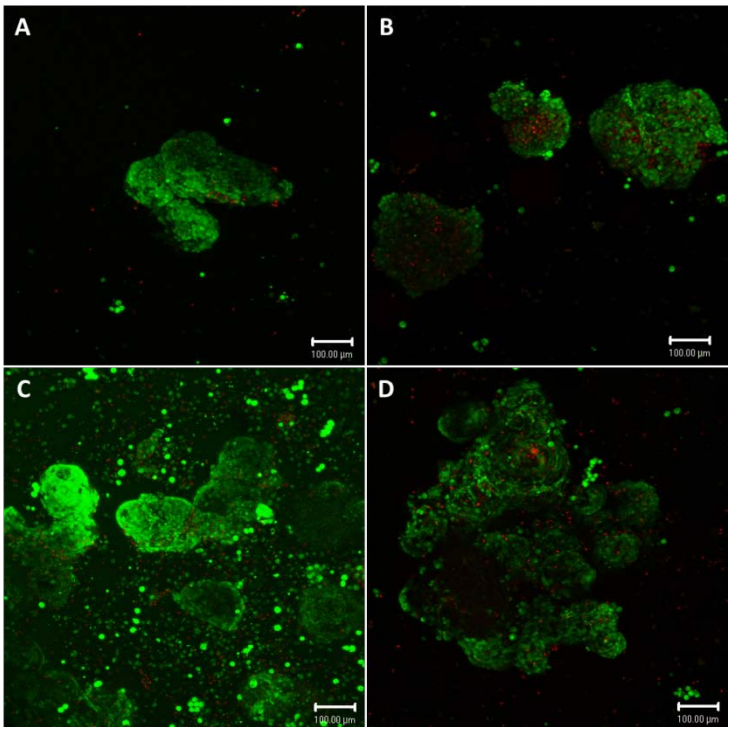

Figure 6-9: Confocal imaging of live cells (green) and dead cells (red) for 1500 IEQ rat islets cultured at 20% oxygen as controls (A) or with a 25% w/w PDMS-CaO_2 Disk (C) or at 5% oxygen as controls (B) or with a 25% w/w PDMS-CaO_2 Disk (D). Assessment was performed after 2 days of culture in indicated conditions.

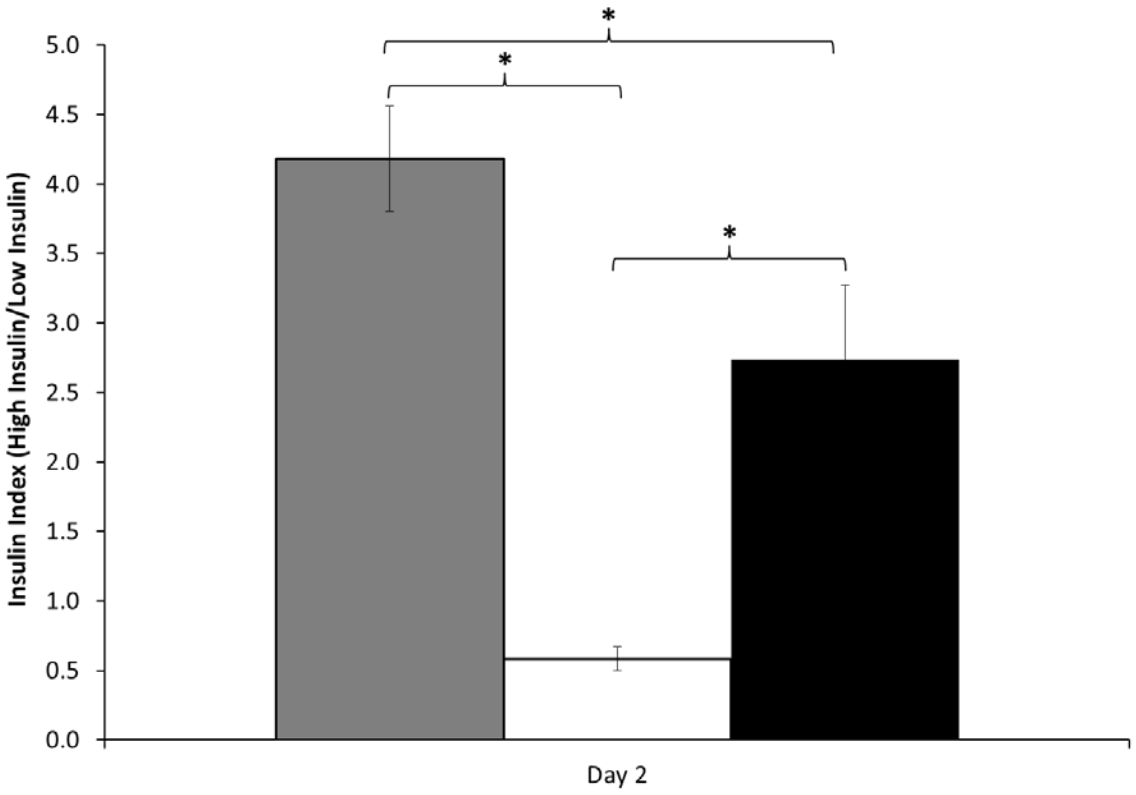

Figure 6-10: Insulin secretion function, assessed via static glucose stimulated insulin release, of 1500 IEQ rat islets cultured at 20% oxygen (grey bar) and at 5% oxygen without (white bar) or with (black bar) a 25% w/w calcium peroxide encapsulated in PDMS disk was determined after 2 days. Values expressed as insulin index, with is insulin secretion during high glucose over insulin secretion during low glucose. Asterisk denotes statistical significance between groups ($p<0.05$).

Similar results were obtained with human islets. In this study, assessment was performed after 72 hrs in culture, but the effect of cell loading was evaluated. As Figure 6-11, the MTT viability of 1500 IEQ and 2500 IEQ human islets cultured at 5% oxygen increased two-fold in the presence of a single PDMS-CaO_2 ($p<0.05$) disk and was statistically identical to 20% oxygen controls. For 100 IEQ, no 5% oxygen treated group was run, because at such low islet loading densities incubation at 5% oxygen does not decrease islet viability significantly. Live/dead staining did not illustrate a difference in the ratio of live/dead cells between groups, but fewer islets were found for the 5% oxygen

control (see Figure 6-12). The insulin secretions of islets after 72 hrs under standard culture at 20% oxygen was compared to that of islets cultured at 5% oxygen with and without a PDMS-CaO2 disk (see Figure 6-13). Control islets cultured at 5% oxygen lost their insulin responsiveness (SI = 0.28), whereas treated islets retained insulin responsiveness (SI = 1.70) ($p<0.05$), albeit it at a significantly lower value than 20% oxygen controls (SI = 6.59) ($p<0.05$).

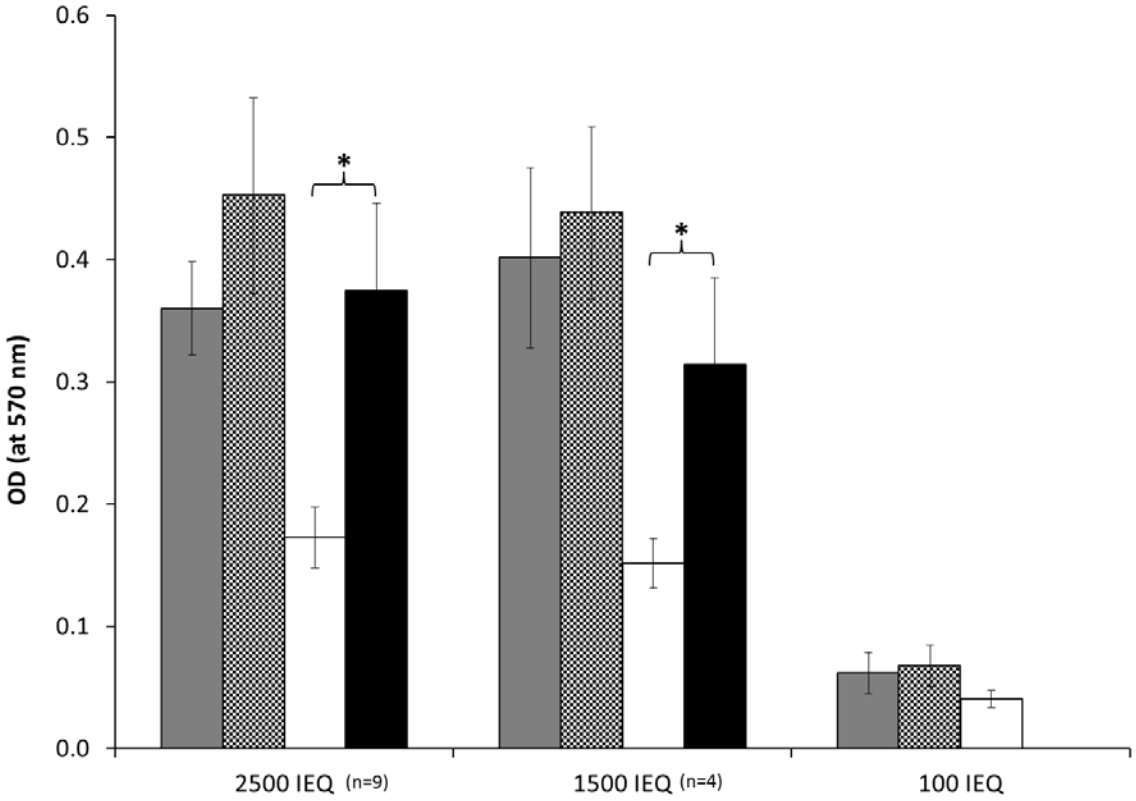

Figure 6-11: MTT viability, expressed as optical density (OD), of 100, 1500, and 2500 IEQ human islets cultured at 5% oxygen without (black bars) or with (white bars) 25% w/w calcium peroxide encapsulated in PDMS disk was determined after 3 days. Similarly for 20% oxygen, controls (grey bars) and PDMS-CaO2 groups (checkered bars) were assessed. Asterisk denotes statistical significance between groups ($p<0.05$).

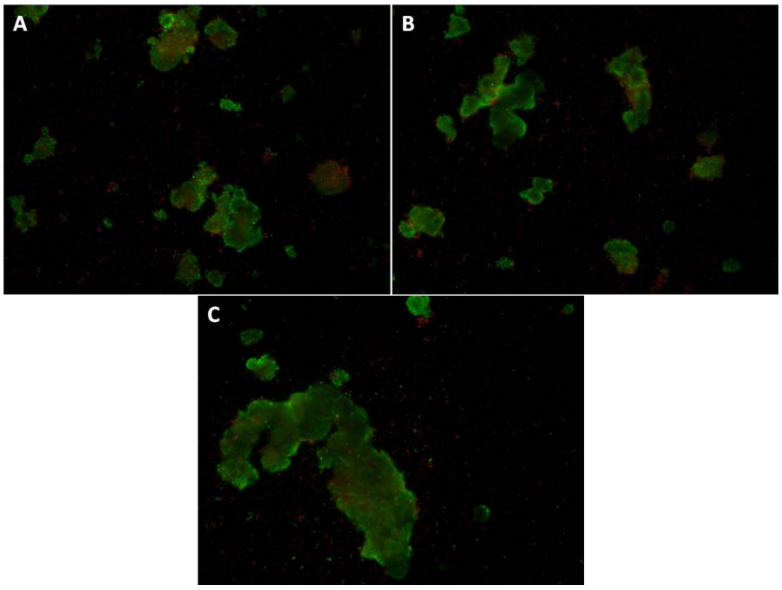

Figure 6-12: Confocal imaging of live cells (green) and dead cells (red) for 1500 IEQ human islets cultured at 20% oxygen as controls (A) or at 5% oxygen without (B) or with a 25% w/w PDMS-CaO2 disk (C). Assessment was performed after 3 days of culture in specified conditions.

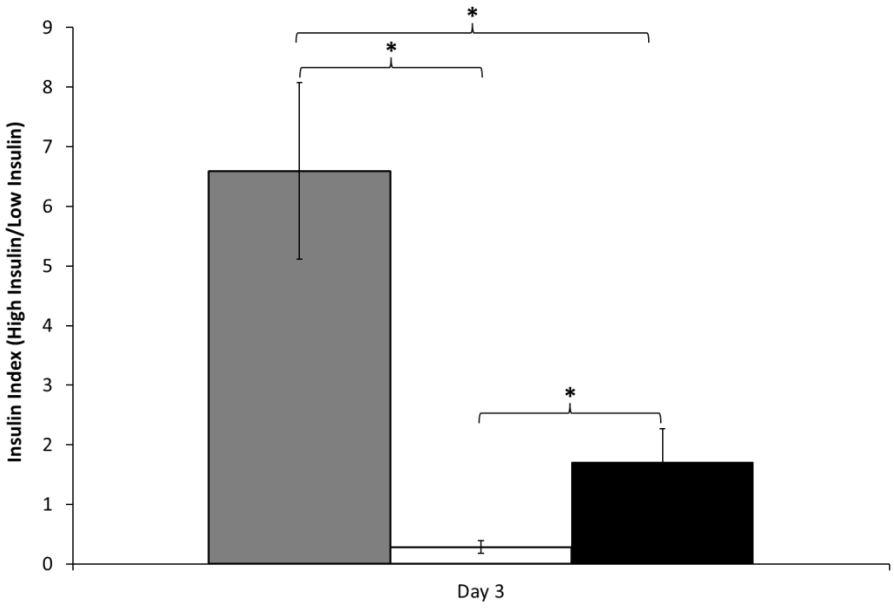

Figure 6-13: Insulin secretion function, assessed via static glucose stimulated insulin release, of 1500 IEQ human islets cultured at 5% oxygen without (white bar) or with (black bar) a 25% w/w calcium peroxide encapsulated in PDMS disk for 3 days, and compared to 20% oxygen controls (grey bar). Values expressed as insulin index, with is insulin secretion during high glucose over insulin secretion during low glucose. Asterisk denotes statistical significance between groups ($p<0.05$).

6.4 DISCUSSION

In this study, we sought to encapsulate calcium peroxide within PDMS disks for use as an oxygen generating biomaterial suitable for sustaining cell viability and function within hypoxic conditions. Without encapsulation, peroxide based compounds, such as calcium peroxide and sodium percarbonate, quickly release oxygen upon coming in contact with water. This results in bursts of oxygen that are too severe for cells and too transient for practical use, as well conversion of the surrounding solution pH into basic conditions. By encapsulating solid peroxide within a biomaterial, we have developed a means to modulate the release of oxygen and minimize harmful by-product formation. The use of a hydrophobic polymer versus a hydrophilic material substantially reduces the reactivity of water with the calcium peroxide by functioning as a diffusion barrier. This was demonstrated in our studies whereby agarose encapsulation provided oxygen for only 5 days compared to over 40 days for PDMS encapsulation. Since PDMS specifically has a low permeability to water, the rate of oxygen release becomes heavily dictated by the rate of water diffusion into the PDMS, which is very low according to its partition coefficient (K_p=0.0258 for water (Zhan et al. 2009) versus K_p=10 for oxygen (Kamiya et al. 1990). Comparatively, encapsulation in PLGA tempers oxygen release to a lesser extent, because the PLGA is progressively degraded by diffusion of water into it. Our method of PDMS encapsulation produced significantly more oxygen (over 20 mmHg compared to ~2 mmHg) and for a longer time than PLGA encapsulation (Oh et al. 2009). Higher concentrations of calcium peroxide (25% w/w) were used for PDMS encapsulation compared to PLGA encapsulation (5% w/w), in order to account for the dampened reactivity of PDMS (as demonstrated in the previous chapter). The geometry and dimensions of the disk, as well as the particle loading density of calcium peroxide,

must be optimized to achieve an optimal release of oxygen. Therefore, we have been able to modulate the temporal release of oxygen from the solid peroxide from minutes to weeks by capitalizing on the variations in the diffusivity, density, and chemical properties of the materials.

While solid peroxide is a promising means to generate a large amount of oxygen through reaction with water, some of the potential byproducts of this reaction pose a threat to cell viability. As part of the decomposition of calcium peroxide to generate oxygen, hydrogen peroxide and hydroxyl radicals are possible by-products. Concentrations of hydrogen peroxide as low as 150 μM may reduce the viability of mouse MIN6 β-cells to 30% (Kimoto et al. 2003). Also, 100 μM to 100 mM of hydrogen peroxide elevated calcium ion release ($[Ca^{2+}]_i$) from rat islets in a dose-dependent manner to levels that are toxic to cells (Tang & J. H. Zhang 2000). Similarly, 5-250 μM hydrogen peroxide caused cell death, as measured by enzyme lactate dehydrogenase (LDH) release assay, of rat islets (Rao et al. 2005). Our experiments demonstrated that there was an initial burst release of hydrogen peroxide from the PDMS-CaO_2 disks in dPBS that decreased to less than 100 μM after the first day. In comparison, the release of hydrogen peroxide from agarose-CaO_2 disks was over ten-fold higher. This shows that PDMS encapsulation not only extends oxygen release, but also diminishes harmful hydrogen peroxide release. Moreover, when the disks were incubated in cell culture media, the production of hydrogen peroxide was less than 30 μM. We hypothesize that this reduction in hydrogen peroxide content when the disks are incubated in culture media versus dPBS is due to the fact that culture media contains numerous compounds that scavenge peroxides. In addition to hydrogen peroxide, free radicals have been shown

to damage the cell membranes and cause cell death of mouse and rat pancreatic islets (Halliwell & Gutteridge 1985; Grankvist et al. 1979). In our studies the levels of hydroxyl radicals released from the PDMS-CaO_2 disks in saline solution and cell culture media was found to be less than 100 nM (estimated <5 nM). This is not surprising since the modified Fenton reaction responsible for hydroxyl radical formation requires reduced iron ions (Fe^{2+}), which are not present in the saline solution. Fe^{2+} ions might be present in cell culture media, but may be neutralized by the added antioxidants. Furthermore, phosphate inhibits hydroxyl formation by lowering dissolved metal concentrations or converting them to more stable complexes (R. Hinchee 1991). If hydroxyl radical production were an issue, islets can be protected from free radical damage by superoxidase dismutase (SOD), catalase, and iron chelators in-vitro and SOD, mannitol, and diethylenetriaminepentaacetic acid (DETAPAC) in-vivo (Halliwell & Gutteridge 1985; Grankvist et al. 1979).

While positive results were obtained in illustrating modulation of oxygen release and minimization of toxic by-products in a novel oxygen generating biomaterial, of particular interest to us was to evaluate its capacity to preserve cell viability and function when cells are exposed to hypoxic conditions. We know from our previous studies on kinetics (the previous chapter) that the rate of oxygen release is dependent on the oxygen concentration of the surroundings. Therefore, we sought to determine the rate of oxygen release in the presence of the cells, which consume oxygen in the environment. The PDMS-CaO_2 disk was incubated with MIN6 cells within a sealed chamber to determine if the amount of oxygen released from the disks was sufficient to meet the oxygen consumption rate of the cells. The results suggested that when confronted with the

oxygen demand from cells, the disks produced almost 5 mmHg per second. Based on the promising results from this short-term incubation of cells in a closed system, the next step was to examine long-term cell culture in a low oxygen open system.

Cell proliferation studies with MIN6 demonstrated that at low oxygen the oxygen generating disks dramatically increased cell numbers compared to controls. On the other hand, the disk had no effect (positive or negative) on cell viability at 20% oxygen, illustrating that the disks are most effective at enhancing cell viability when high cell loading densities leave cells with a shortage of oxygen,. Moreover, total DNA content of the PDMS-CaO_2 groups was significantly greater than the controls after 7 days. Therefore, together, the MTT and DNA results reinforce the idea that supplemental oxygen released from the PDMS-CaO_2 disks promotes proliferation of cells. On day 3, MTT viability of the experimental group was higher than the control, whereas DNA content was similar between the groups. This suggests that the control cells undergo metabolic stress by the low oxygen concentrations, whereas the PDMS-CaO_2 group is shielded from this. Visual inspection of cell morphology over the course of the experiment through live/dead imaging revealed that treated cells tended to form larger cell clusters. We hypothesize that this is due either to aggregation or to the ability of the supplemental oxygen from the disk to maintain larger diameter clusters. Furthermore, when PDMS-CaO_2 disks were removed from treated groups, the cells returned to the same state as controls. This reinforces the theory that the observed enhancements are due solely to oxygen release, and not due to an artifact or initial shielding from hypoxia.

In translating these studies from a primary cell line to islets, we evaluated the capacity of these oxygen generating materials to shield hypoxia induced cell death for

both rat and human islets. For islet experiments, islets were loaded at a high loading density, 1500 IEQ per 10 mm well, to simulate in-vivo conditions of low oxygen availability and confinement. As expected, the viability and functionality of the islets was adversely affected by culturing at such high loading densities and low oxygen tensions. However, incorporation of the PDMS-CaO_2 disks significantly improved islet viability and function. After 48 and 72 hrs, PDMS-CaO_2 disks mitigated rat islet death due to hypoxia by over two-fold, allowing them to maintain similar viability to 20% oxygen controls. Moreover, the disks prevented hypoxia-induced insulin secretion dysfunction, allowing rat islets to maintain similar function to 20% oxygen controls. This can be explained by the supplemental oxygen provided the oxygen generating disks. Due to their innate differences, rat islets and humans islets do not always respond the same way to treatments. Therefore, it was very encouraging that similar positive results were obtained for human islets. By incubating the disks with different loading densities of human islets, we demonstrated again that the disks are most effective at high islet loadings, where oxygen gradients are even more pronounced.

Based on the reactive nature of solid peroxides and research from others developing peroxide based oxygen generators, we were concerned about oxidative stress from reactive by-products. With this in mind, Benjamin et al incorporated catalase into their PLGA-CaO_2 films to degrade any hydrogen peroxide by-products (Lawrence et al. 2009). However, we did not detect significant levels of hydroxyl radical release from our disks. Moreover, considering the low radical scavenging ability of islets, the fact that islets profited from the disks further suggests that there is minimal free radical generation.

Similar performance of the PDMS-CaO_2 disks when incubated with MIN6 cells, rat islets, or human islets demonstrates the applicability of these novel oxygen generators for a wide variety cells. Since they are most beneficial at high cell loading densities, they represent an ideal tool for enhancing oxygenation of cellular-engineered constructs, particularly during the initial engraftment period of implantation. In instances of low oxygen tension, as encountered in transplantation of highly metabolic cells, we anticipate that incorporation of PDMS-CaO_2 disks will generate supplemental oxygen and result in higher cellular viability in-vivo. For example, they might be incorporated to alleviate oxygen deprivation of islets implanted into poorly vascularized sites for extrahepatic transplantation. PDMS is a highly versatile polymer that, as we have shown, can be used for fabrication of scaffolds for tissue engineering or for fabrication of oxygen generating biomaterials. We hypothesize that due to this commonality, the functionality of PDMS-CaO_2 can be incorporated into PDMS scaffolds to create novel oxygen generating scaffolds.

6.5 CONCLUSIONS

In situ oxygen generating material capable of modulated, temporal release of oxygen exceeding 30 days was successfully developed. Encapsulation of solid peroxide within hydrophobic silicone minimizes burst release of oxygen, peroxide exposure, and free radical generation in surrounding milieu. In situ, modulated, and sustainable oxygen generating biomaterials were successfully fabricated using solid calcium peroxide and silicone. Measured hydrogen peroxide, a by-product of calcium peroxide degradation, was below toxic levels for cells after ~2 hrs of incubation. The metabolic activity of MIN6 cells and islets was not impaired by the presence of PDMS-CaO_2 disks at standard

oxygen tensions, and dramatically improved under low oxygen tensions. In addition, the PDMS-CaO_2 disks prevented the loss of insulin functionality of islets cultured at low oxygen tensions, a further testament that the disk is reducing the detrimental effects of hypoxic conditions. These preliminary experiments lay the foundation for the hypothesis that oxygen enhancing materials, encased within biomaterial scaffolds, can provide a beneficial environment to transplanted cells by increased oxygen availability. Current studies are seeking to translate these results in-vivo, where impaired oxygen conditions may further illustrate the potential of this promising biomaterial.

CHAPTER 7. INCORPORATION AND ASSESSMENT OF PDMS ENCAPSULATED CALCIUM PEROXIDE INTO THREE-DIMENSIONAL CONSTRUCTS

7.1 INTRODUCTORY REMARKS

In the development of implantable cellular-based devices, inadequate oxygen delivery represents one of the biggest challenges. This is particularly true for transplantation of islets since the oxygen consumption rates of human islets are up to 10^6 fold higher than for chondrocytes and 10^4 fold higher than for endothelial cells (W. Wang et al. 2005; Motterlini et al. 1998; Heywood et al. 2006). In addition, islets are highly susceptible to functional impairment at moderate oxygen tensions (De Vos et al. 2002; Papas et al. 2007). Therefore, while cell viability may be unaffected, insulin production levels can be reduced by as much as 50% at the threshold between normoxia and hypoxia (Dionne et al. 1993). Combining islets within a macro-scale device for implantation at alternative sites, where access to vasculature may be significantly impaired, further compounds this challenge.

In earlier chapters, we presented the development of a macroporous PDMS scaffold to spatially distribute islets, thereby maximizing mass transport of nutrients to the islets and allowing for vascular infiltration. However, development of an adequate intra-islet vascular network requires 5 to 14 days, by which time the islets may have already suffered severe hypoxia (Metcalfe & Ferguson 2007; Marques et al. 2005; B.S. Harrison et al. 2007; van der Veen et al. 2010). This issue can be addressed by either: prevascularizing the transplant site (Antonello Pileggi et al. 2006); hastening vascularization through the delivery of growth factors; or by the generation of supplemental oxygen. In the two previous chapters, we presented the development of a

novel oxygen generator in the form of calcium peroxide encapsulated in PDMS polymer. We showed that it was capable of producing oxygen for over 40 days with minimal production of hydrogen peroxide and hydroxyl radical by-products. Moreover, it enhanced the viability and function of both rat and human islets cultured at 5 % oxygen under high loading densities. We became intrigued by the possibility of incorporating these oxygen generating capabilities of our PDMS-CaO_2 disk into a three-dimensional construct, particularly our macroporous PDMS scaffold. These preliminary experiments lay the foundation for the hypothesis that oxygen enhancing materials, encased within biomaterial scaffolds, can provide a beneficial environment to transplanted cells by increasing oxygen availability.

Several approaches were undertaken to the PDMS-CaO_2 disks with our macroporous PDMS scaffolds. The simplest method of testing this was by simply placing the PDMS-CaO_2 disk beneath the scaffolds. However, this does not provide for a self-contained unit. When implanted in-vivo, the differences between the two interfaces would create friction and thereby stimulate a negative response. Therefore, our focus was shifted to approaches that would result in a self-contained unit.

Initial studies sought to incorporate a PDMS-CaO_2 disk within a single, three-dimensional scaffold through the use of agarose hydrogel. Agarose gels, mixed with cells, would contain a single PDMS-CaO_2 disk, permitting evaluation of the effects of oxygen generation, in three-dimensions, on the entrapped cells. Furthermore, given that we have demonstrated in Chapter 4 that the use of agarose in this configuration results in hypoxia mediated cell death, this platform should serve as an ideal system for evaluating the benefits of the oxygen generating material.

In another approach, since the oxygen generating disks and macroporous scaffolds are both made of PDMS polymer, we sought to incorporate the calcium peroxide directly into the scaffold during fabrication. However, recall that the PDMS scaffolds are fabricated using the solvent casting particulate leaching technique, whereby salt must leached from the scaffold by incubating them in water for 72 hours. Also recall that oxygen release from the PDMS-CaO_2 disks is activated upon contact with water. Although the final thickness of the scaffolds is twice that of the PDMS-CaO_2 disks, the scaffolds are 90% porous, meaning the scaffold possess only 20% of the PDMS volume present in the disks. Furthermore, due to their high degree of porosity, the scaffolds have a very large surface area, meaning greater reactivity of the calcium peroxide with water may be quite substantial. Therefore, we were uncertain if this method would produce scaffolds capable of sufficient oxygen production.

A final approach was to place a PDMS-CaO_2 disk in the center of the scaffold during fabrication, trapping the disk within the scaffold as it cures. This would not circumvent the leaching step, but by maintaining the original PDMS-CaO_2 disk geometry, we would have predictable oxygen release profiles. In this paper we report the design and fabrication of three dimensional constructs containing PDMS encapsulated calcium peroxide (PDMS-CaO_2). Three constructs were investigated: PDMS scaffold or agarose gel containing a PDMS-CaO_2 disk in the center, or PDMS scaffold containing 25% w/w calcium peroxide throughout its structure. The release of oxygen from the PDMS-CaO_2 constructs was assessed. The effect of the agarose-PDMS-CaO_2 constructs on the viability and function of MIN6 in long-term culture was assessed. The effect of the PDMS scaffold-PDMS-CaO_2 constructs on the viability and function of rat islets in

short-term culture was assessed. Implications of these devices for in-vivo implantation are also discussed.

7.2 MATERIALS AND METHODS

7.2.1 MATERIALS

Calcium peroxide powder was purchased from Sigma-Aldrich (Cat. No. 466271). It has a particle size of -200 mesh and is 75% calcium peroxide with the remainder as calcium hydroxide. Poly(dimethyl siloxane) (PDMS) silicone polymer RTV 615 A+B (room temperature vulcanized) was purchased from GE Silicones. dPBS was purchased from Mediatech and pH balanced to 7.4 using NaOH and HCl. Agarose type VII was purchased from Sigma-Aldrich. Bovine serum albumin (BSA) was purchased from VWR. MTT and MTS cell viability kit was purchased from Promega (Madison, WI). Live/Dead Viability/Cytotoxicity Assay Kit was purchased from Invitrogen. Insulin ELISA was purchased from Mercodia (Winston Salem, NC).

7.2.2 PDMS-CaO_2 DISK AND SCAFFOLD FABRICATION

Two different methods were used to incorporate PDMS-CaO_2 into 90% porous PDMS scaffolds and resulted into two different scaffolds referred to here as: "Scaffolds + PDMS-CaO_2 Disk" and "Scaffolds of PDMS-CaO_2". Both methods require silicone polymer, which in all cases was prepared by mixing 4 parts volume of PDMS monomer with 1 part volume of platinum catalyst.

In addition, the first fabrication method (for scaffold plus PDMS-CaO_2 disk), required the prefabrication of 25% w/w PDMS-CaO_2 disks, which was described earlier in Chapters 5 and 6. Briefly, PDMS-CaO_2 disks were made by mixing 25% w/w of

calcium peroxide powder (Sigma Aldrich) with poly(dimethylsiloxane) (PDMS) silicone polymer (GE Silicones). The calcium peroxide/silicone mixture was loaded into cylindrical molds (10 mm diameter, 1 mm height) and cured after 24 hrs at 40 °C.

For both methods, the scaffold mixture was prepared by thoroughly mixing 90% volume of salt with silicone polymer. In method 1, salt-silicone mixture was loaded into molds (10 mm diameter, 3 mm height) until a 1 mm height was reached. Then, a single 25% w/w PDMS-CaO_2 disk (10 mm diameter, 1 mm height) was pressed on top of the salt-silicone mixture and covered with an additional 1 mm of silicone-salt mixture. In method 2, calcium peroxide was blended into the salt-silicone mixture for a final concentration of 25% w/w. This mixture was then loaded into molds (10 mm diameter, 2 mm thickness) to fill it completely. Both methods then required incubating at 37 °C for 48 hours in order to completely crosslink the silicone. The salt was leached out from the scaffolds by soaking them in deionized water for 72 hours, with water changes every 24 hours.

7.2.3 FINITE ELEMENT ANALYSIS OF PDMS-CaO_2 SCAFFOLDS FOR OXYGEN RELEASE

COMSOL was used to perform finite element analysis on the oxygen release from the PDMS-CaO_2 scaffolds. Models were made for the scaffolds plus PDMS-CaO_2 disk and for the scaffolds of PDMS-CaO_2. Moreover, since the oxygen release from the constructs is dependent on the ambient oxygen concentration, we were interested in modeling oxygen release in the presence of islets loaded on the scaffolds. For these studies, an initial 1500 IEQ loading with oxygen consumption modeled by Monod

kinetics (R_m=-7.2×10^{-2} mol/m^3·s, K_m=5.28×10^{-4} mol/m^3) and with boundary conditions set at 5% oxygen concentration were used.

7.2.4 MEASUREMENT OF OXYGEN PRODUCTION

Constructs were assessed for long-term release of oxygen in dPBS at 37 °C. Oxygen production was monitored within a sealed, titanium chamber in fluorescence amplitude micro oxygen monitoring systems (Instech Laboratories, PA). Oxygen concentration was measured using PreSens (Germany) non-invasive oxygen sensors, which consist of a ruthenium-based spot sensor transmitting fluorescence signals to the computer through optical fiber cables. Blue LED excites the sensor to emit fluorescence, but the fluorescence is quenched when it collides with oxygen molecules. Therefore, the changes in fluorescence can be correlated to oxygen concentration in the solution. These sensors possess a high sensitivity and high signal to noise ratio, and can measure oxygen levels non-invasively without disturbing the culture environment. The chamber itself can hold a total volume of 1 mL. A glass magnetic stir bar is placed at the bottom of the chamber. The oxygen sensor is approximately 1 mm in diameter and is located on the side of the chamber, near the bottom. The system is water jacketed so that the temperature can be controlled at 37 °C. Constructs were tied with suture and suspended within the chamber so that they would remain in the center and not interfere with the stir bar or block the sensor. Logging of oxygen measurements took place every 15 seconds and was commenced immediately before the constructs were placed inside the chamber and the acrylic plug was set in place. The solution was refreshed when the oxygen in the chamber was saturated, which occurred approximately every 3-5 days.

7.2.5 CELL ISOLATION AND CULTURE

MIN6 cells (passages 30-40) were cultured as monolayers in T-flasks and fed every 2-3 days with fresh medium comprised of Dulbecco's modified Eagle's medium (DMEM) supplemented with 10% FBS, 1% penicillin-streptomycin (P/S), and 0.001 % (v/v) β-mercaptoethanol. Rat pancreatic islets were isolated from male Sprague-Dawley (SD) rats using methods described elsewhere (Antonello Pileggi et al. 2006). All procedures were conducted according to the guidelines of the Committee on Care and Use of Laboratory Animals, Institute of Laboratory Animal Resources (National Research Council, Washington DC). Human pancreatic islets of Langerhans were obtained from the NIH/JDRF ICR Consortium or from the Diabetes Research Institute at the University of Miami. Following isolation, islets were cultured in CMRL 1066 (Mediatech) for 48 hrs (rat islets) or MM1 (Mediatech) for 24 hrs following arrival (human islets) in a humidified 37°C, 5% CO_2 / 95% air incubator. CMRL 1066 and MM1 media was supplemented with 10% fetal bovine serum (FBS; Sigma), 1% penicillin-streptomycin (Sigma), and 1% L-glutamine (Sigma).

7.2.6 MIN6 CULTURE WITHIN AGAROSE CONSTRUCTS CONTAINING PDMS-CaO_2 DISKS

We sought to test the feasibility of incorporating PDMS-CaO_2 disks within three-dimensional constructs, independent of the PDMS scaffold. Two cylindrical agarose constructs 10 mm in diameter were fabricated to final dimensions of 2 mm thickness for controls or 3 mm thickness for groups with a PDMS-CaO_2 disk (8 mm diameter, 1 mm thickness) in the center. To create the constructs, mouse insulinoma (MIN6) cells were carefully mixed and uniformly suspended in 2% agarose at 37 °C at a density of 2×10^5,

6×10^6, 10×10^6 cells/mL, pipetted as two consecutive layers into plastic molds, and allowed to gel for 3 mins at room temperature. For constructs containing a PDMS-CaO_2 disk, the disk was sandwiched between the two agarose layers by placing it within the gel after the first layer had been pipetted, but before the second layer was added. Final agarose gels had an initial loading density of 5.0×10^5, 1.5×10^6, and 2.5×10^6 cells per construct and were cultured in 6-well plates with 4 mL of culture media for 3 days at 5% oxygen or 20% oxygen conditions. The agarose-cell constructs were assessed for cell viability via MTT metabolic assay (Promega, WS) and live/dead staining (Invitrogen, CA).

7.2.7 ISLET CULTURE WITHIN PDMS-CaO_2 SCAFFOLDS

Islets used were either of rat, nonhuman primate, or human origin. Islets were seeded onto scaffolds at an islet equivalent (IEQ) density of 1000 IEQ or 1500 IEQ and cultured in 6-well plates for 48, 72, or 96 hours. At the conclusion, whole scaffolds (1000 IEQ or 1500 IEQ) were assessed for MTT viability, while scaffolds were cut into quarters (250 or 375 IEQ) for insulin secretion and live/dead viability assessment. The insulin secretion function of islets was determined by collecting insulin samples from low glucose (40 mg/dL) and high glucose (300 mg/dL) stimuli and quantifying by insulin ELISA assay (ALPCO, NH). The Stimulation Index (SI) of the islets was calculated as insulin secretion during high glucose over the secreted during low glucose.

7.2.8 METABOLIC VIABILITY

Metabolic activity of MIN6 cells or islets was assessed by either MTT assay (Promega). For scaffolds where the PDMS-CaO_2 disks could be removed, samples were

washed once and the PDMS- CaO_2 disks were removed from the scaffold. Following removal, the remaining scaffold was suspended in 250 µL of media within a 48-well non-tissue culture treated plate, and placed in a humidified incubator for one hour to recover from manipulation. 28 µL of MTT dye was added to each well and samples were incubated for one more hour. Afterwards, 185 µL of stop/solubilization solution was added to each well and the plate was stored, wrapped in parafilm, for 24 hours in order to stop metabolism of MTT dye and allow the formazan crystal to be solubilized. A modified version of the same procedure was used for agarose constructs using 300 µL of media, 33.6 µL of MTT dye, and 185 µL of stop/solubilization solution in a 24-well plate. The next day, 120 µL samples from each well were dispensed into a 96-well plate and the absorption at 570 nm was measured using a plate reader. Changes in optical density due to culture media used were compensated for by subtracting media blanks from all wells. In our lab we determined that calcium peroxide reacts with the stop/solubilization solution used in MTT. Therefore, for scaffolds where the PDMS-CaO_2 could not be removed, metabolic assessment was not performed.

7.2.9 LIVE/DEAD VIABILITY

Cell viability was visualized by the LIVE/DEAD Viability/Cytotoxicity Assay Kit (Invitrogen) and imaged through a confocal microscope (Zeiss LSM). Cells were briefly rinsed in HBSS once and then incubated for 45 min in a phosphate buffered saline solution composed of 4 µM calcein AM and 8 µM ethidium homodimer-1 (EthD-1) [reference Kristina Hall]. Afterwards, cells were rinsed a second time in HBSS and placed on a glass slide for visualization via a fluorescence scanning confocal microscope (LSM 510, Zeiss, Germany). Live cells (green) were detected by excitation with light at

494 nm and emission at 517 nm while dead cells (dead) were detected by excitation at 528 nm and emission at 617 nm. Multi-slice images were collected and merged using the projection function on LSM image browser (Zeiss, Germany) software.

7.2.10 INSULIN SECRETION FUNCTION

The scaffolds could not be used whole for insulin secretion assessment since such a large number of islets would generate negative feedback inhibition within the confined space of the assay column. Therefore, at the conclusion of experimental incubation period, the scaffolds were cut into quarter pieces using a scalpel, so that each quarter would contain a fourth of the original loading density. The functional insulin secretion rate of 375 IEQ islets was determined via static glucose-stimulated insulin release (GSIR) assay. Groups were sequentially incubated for one hour intervals in glucose solutions: low glucose (40 mg/dL) high glucose (300 mg/dL), and low glucose again, using a column method, as described in Chapter 4. Briefly, 10mL Poly-Prep columns (Bio-Rad) were placed in Poly-column rack (Bio-Rad), filled with 400 µL of a slurry of Sepharose G-10 (GE Healthcare)/dPBS (10% w/v) and washed with low glucose (2.2 mM) KREB's buffer (26mM sodium bicarbonate, 25mM HEPES, and 0.2% w/v BSA). Islet containing scaffolds were then placed within the columns and an additional 600 µL of bead slurry was added to each column. Columns were then flushed with 4mL of low glucose KREB's solution. Flow in the columns ceased when the liquid level reached the surface of the beads keeping the fluid volume in each column constant. Columns were then incubated for 1 hr for pre-incubation, followed by a 4mL wash with low glucose KREB's, at which the first step of the glucose challenge (Low1) was initiated. After 1 hr, low glucose KREBs was exchanged with high glucose (16.7 mM) KREBs to begin step

two of the challenge (High1). After this hour, high glucose was exchanged with low glucose KREB to begin step three of the challenge (Low2). During each exchange, 1 mL of the respective KREBs solution was added and the 1mL eluate was collected in tubes and stored at – 80 °C for later analysis. Insulin was quantified using the Mercodia Rat or Human Insulin ELISA (Winston Salem, NC), depending on the islet type.

7.2.11 STATISTICAL ANALYSIS

The number of replicates is three, unless indicated otherwise in the figure legends, and results are expressed as mean ± SD. Statistical analysis was performed on all samples using a paired Student's test where differences were considered significant when $p<0.05$.

7.3 RESULTS

7.3.1 OXYGEN GENERATION FROM PDMS-CaO_2 SCAFFOLDS

As shown in previous chapters, oxygen release from calcium peroxide based constructs is highly dependent on construct geometry. Consequently, it was expected that oxygen release from PDMS-CaO_2 would be altered upon incorporation into a scaffold. Oxygen generation from 90% porous PDMS scaffolds (10 mm diameter, 2 mm thickness) containing 25% w/w calcium peroxide was determined within sealed titanium chambers containing dPBS. As shown by the Figure 7-1, the scaffolds produce a sustained and continuous release of oxygen over the course of at least 2 weeks. Upon immediate contact with solution, the scaffolds exhibited a fast release of oxygen for one day. After 2 to 4 days, the rate of oxygen release began to slow down, displaying saturation behavior. Once saturation was reached, the solution was refreshed (as indicated by the asterisks in the figure), and a similar release pattern was observed. This process of refreshing the

solution was repeated approximately every 3-5 days. As shown, the saturation value for oxygen significantly decreased with each consecutive refresh cycle. Conversely, the initial release rate (approximately 12 mmHg/hr) did not change significantly with each refresh cycle.

Another oxygen generating construct used in our studies was the PDMS scaffold containing a PDMS-CaO_2 disk (10 mm diameter, 1 mm thickness) in the center. Comparison of the oxygen release from the PDMS-CaO_2 disk with that from PDMS-CaO_2 scaffolds is shown in Figure 7-2. As illustrated, the incorporation of CaO_2 in PDMS in a macroporous scaffold, as opposed to a solid disk, greatly alters the oxygen generation profiles.

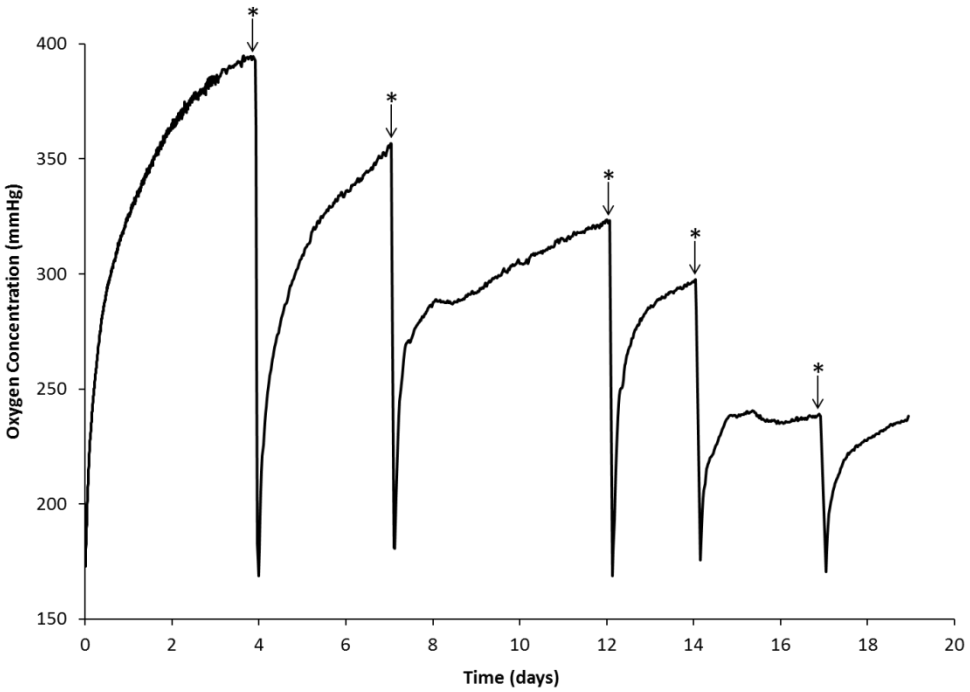

Figure 7-1: Oxygen generation was measured in a sealed titanium chamber for 90% porous PDMS scaffolds containing 25% w/w calcium peroxide with buffer replacements every 4-5 days (indicated by asterisks).

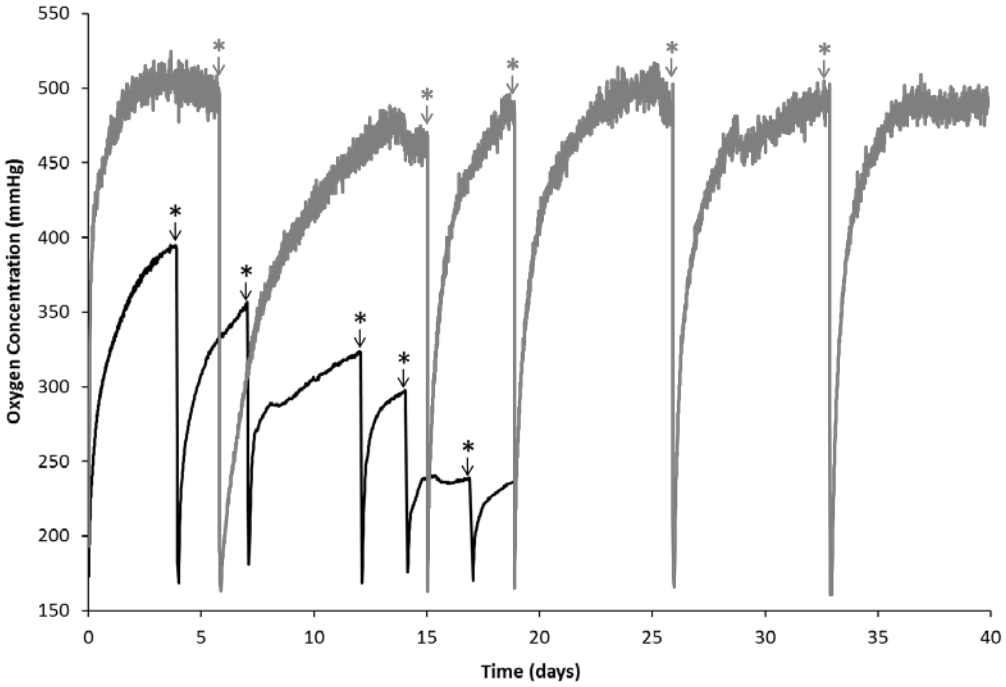

Figure 7-2: Comparative overlay of oxygen generation measured in a sealed titanium chamber for scaffolds plus a 25% w/w PDMS-CaO_2 disk (grey lines) and for 90% porous PDMS scaffolds containing 25% w/w calcium peroxide throughout (black lines) with buffer replacements every 4-7 days (indicated by asterisks).

7.3.2 FINITE ELEMENT ANALYSIS OF PDMS-CaO_2 SCAFFOLDS FOR OXYGEN RELEASE

Figure 7-3 shows the accuracy of COMSOL models for simulating the oxygen release from scaffolds plus PDMS-CaO_2 disk and scaffolds of PDMS-CaO_2. In general, the theoretically predicted values overlapped with the experimentally observed values for the first 2 hours of oxygen release, which were highly linear. After about 2 hrs, the model predicted a continued linear rate of oxygen release, whereas experimentally the oxygen release rate began to slow down. By approximately 9 hrs the model predicted a plateau in the oxygen concentration. By 20 hrs the theoretical and experimental values were similar again, but the oxygen continued to increase for the experimentally observed values. It is important to note that the scaffold, due to being 90% porous and 2 mm thick, has a tenth of the total volume of the disk (10 mm diameter, 1 mm thick), and therefore has a final

total mass of calcium peroxide equivalent to a 5% PDMS-CaO_2 disk. While the 25% w/w PDMS-CaO_2 scaffold releases 300 mmHg of oxygen within the first 20 hrs and continues to release, recall from Chapter 5 that the 5% w/w PDMS-CaO_2 disk only produces 220 mmHg before reaching a plateau after 5 hrs.

In addition, the release of oxygen from these constructs, as well as control scaffolds in the presence of islets loaded on the scaffolds, was modeled with the parameters: an initial 1500 IEQ loading with oxygen consumption modeled by Monod kinetics (R_m=-7.2×10^{-2} mol/m^3·s, K_m=5.28×10^{-4} mol/m^3) and with boundary conditions set at 5% oxygen concentration. The percent of anoxic islets was calculated (only considering the areas occupied by the islets) by dividing the area having oxygen concentrations below the islet K_m by the total area of the scaffolds. Figure 7-4 are two-dimensional models illustrating the predicted oxygen distribution through the scaffold, with areas below K_m represented in black. As shown, at high loading densities and under low oxygen, scaffolds without any oxygen generators, develop a core of low oxygen at the center, with sustainable oxygen levels limited to the periphery. These control scaffolds resulted in 43% of the islets being at viable levels. By incorporating calcium peroxide into the structure of the scaffold, additional oxygen was generation, resulting in 46% of the islets surviving. Finally, by incorporating a solid 25% w/w PDMS-CaO_2 disk into the scaffold, the model predicts that all oxygen limitations are eliminated and 100% of the islets have sufficient oxygen.

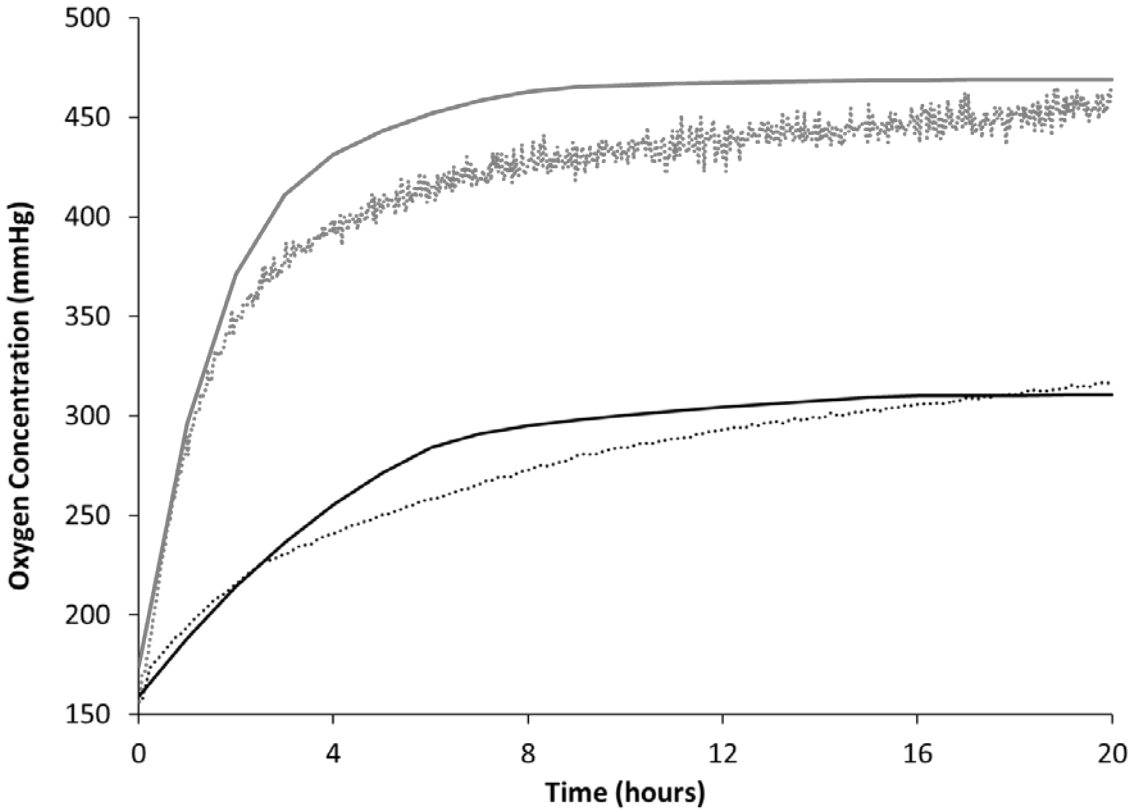

Figure 7-3: Comparison between experimentally observed (dotted lines) and theoretically predicted (solid lines) values for oxygen release, from either scaffolds plus a solid 25% w/w PDMS-CaO_2 disk (grey lines) or for a 90% porous PDMS scaffold containing 25% w/w CaO_2 throughout (black lines).

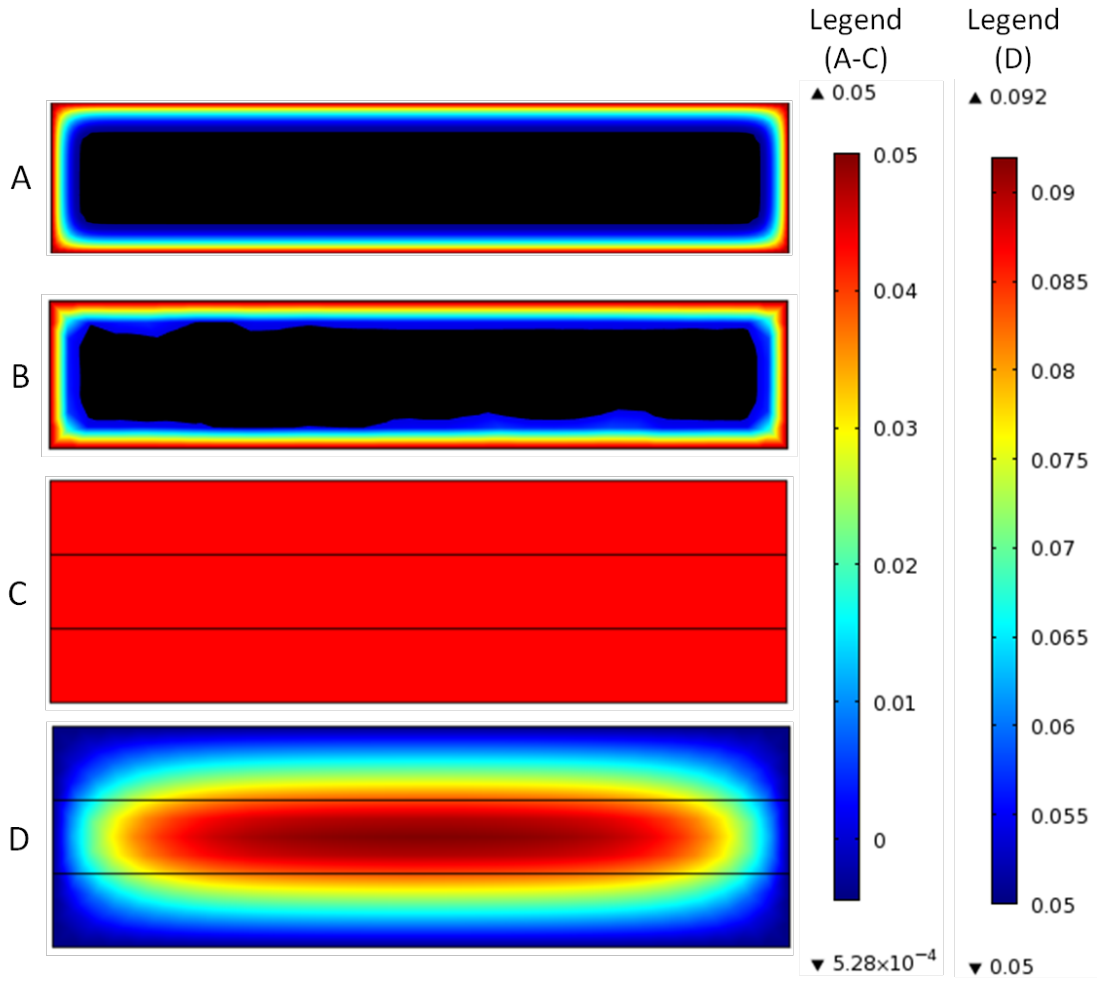

Figure 7-4: Graphic illustrating the distribution of oxygen through scaffolds loaded with 1500 IEQ islets at 5% oxygen, as modeled in COMSOL for: control scaffolds (A), scaffolds of PDMS-CaO_2 (B), and scaffolds plus PDMS-CaO_2 disk (C). Since oxygen levels for scaffolds plus PDMS-CaO_2 disk were greater than 0.05 mol/m^3, an alternative representation shows the full range of oxygen concentrations (D).

7.3.3 PROLIFERATION OF AGAROSE ENCAPSULATED MIN6 CELLS INCUBATED WITH PDMS-CaO_2

To investigate the ability of oxygen generating materials to enhance cell viability, MIN6 cells were loaded within three dimensional constructs fabricated from agarose. An oxygen generating disk was placed in the center of the agarose gel in order to deliver oxygen axially throughout the construct. MIN6 cells of varying cell densities were cultured in agarose constructs with or without a PDMS-CaO_2 disk for 72 hrs at 5% or

20% oxygen. At the conclusion, the constructs were assessed for MTT and live/dead viability. Figure 7-5 shows cell viability of 2.5×10^6 cells in terms of the fold in optical density of each group compared to day 0 controls. After 72 hrs at 20% oxygen, the viability of the cells compared to day zero does not change for either the control group or the group containing PDMS-CaO_2 (fold OD = 0.9 and 1.1, respectively). However, controls cultured at 5% oxygen had their viability halved (fold OD = .53). The viability of the cells at 5% oxygen is significantly improved in the group containing the PDMS-CaO_2 (fold OD = .93), compared to the controls ($p<0.05$), and is statistically similar to groups cultured at 20% oxygen.

The effect of cell density on the utility of PDMS-CaO_2 disks for improving cell viability at 5% and 20% oxygen was evaluated by incubating MIN6 cells within agarose constructs with or without a PDMS-CaO_2 disk at varying cell loadings: 5×10^5, 1.5×10^6, and 2.5×10^6 cells per construct. After 72 hrs, MTT viability was assessed and fold increase of each PDMS-CaO_2 group over its corresponding control was determined. Fold increase was calculated as the OD value for each group treated with the PDMS-CaO_2 disk divided by the OD value of the corresponding control group without the PDMS-CaO_2 disk (for same given cell loading density and oxygen concentration). The fold increase for varying cell densities for groups treated with the PDMS-CaO_2 disk over controls is shown in Figure 7-6. Fold increase values greater than 1.0 indicate that the PDMS-CaO_2 disk has a positive effect on cell viability, whereas values less than 1.0 indicate a detrimental effect. One trend that can be readily observed is that for all cell loading densities, the fold increase of PDMS-CaO_2 groups over controls is higher at 5% oxygen than at 20% oxygen. For relatively low cell loading densities, such as 5×10^5 cells,

the treated groups have lower viability compared to controls (fold less than one) at both 5% and 20% oxygen, exhibiting an inhibition of cell viability when PDMS-CaO_2 disks are present (fold = .57 at 5% oxygen and .20 at 20% oxygen). For 1.5×10^6 cells, the PDMS-CaO_2 disk is detrimental to cell viability at 20% oxygen (fold = .42), but has a neutral effect at 5% oxygen (fold = 1.09). At the highest cell loading, such as 2.5×10^6 cells, the viability of treated groups is greater than controls, at both 5% and 20% oxygen (fold = 1.97 and 1.47, respectively). This shows that there is a general trend at both 5% and 20% oxygen that as cell loading increases, the benefit of PDMS-CaO_2 disk (expressed as the fold increase) increases.

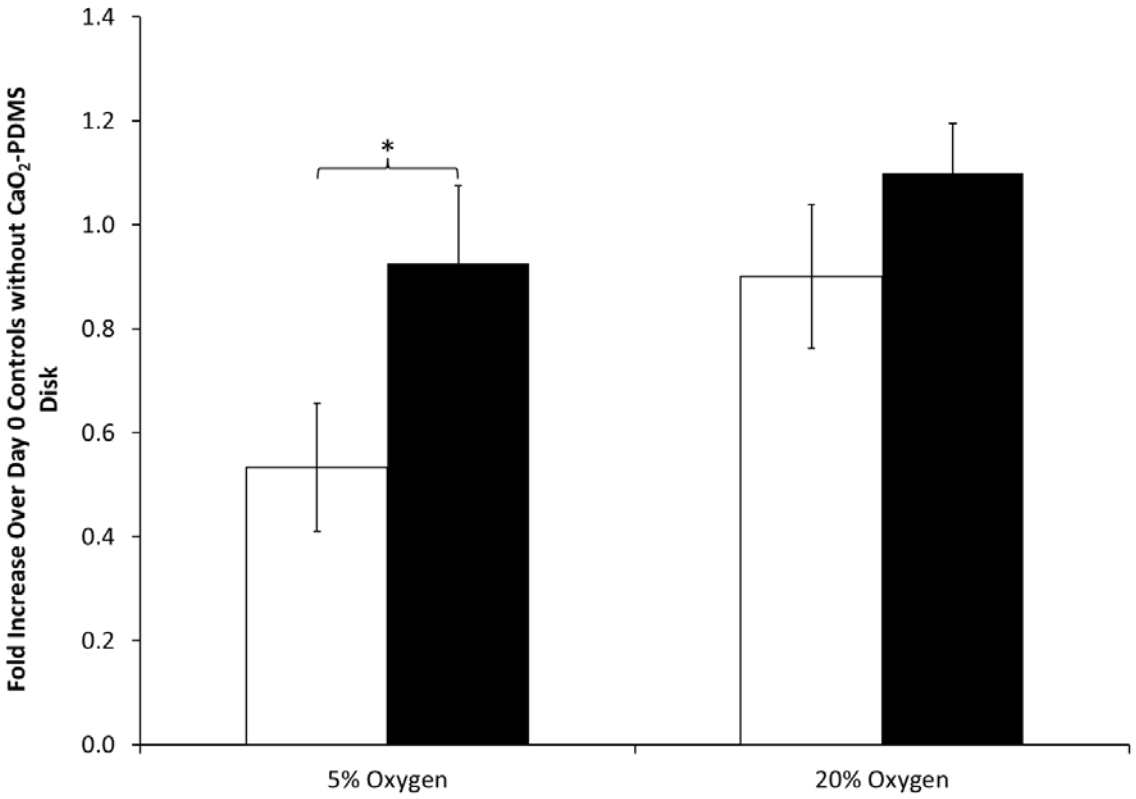

Figure 7-5: MTT viability of 2.5×10^6 MIN6 cells in agarose, without a 25% w/w PDMS-CaO_2 disk (white bars) and with a 25% w/w PDMS-CaO_2 disk (black bars), cultured at 5% and 20% oxygen was determined after 3 days. Asterisks indicate statistical significance between groups ($p<0.05$).

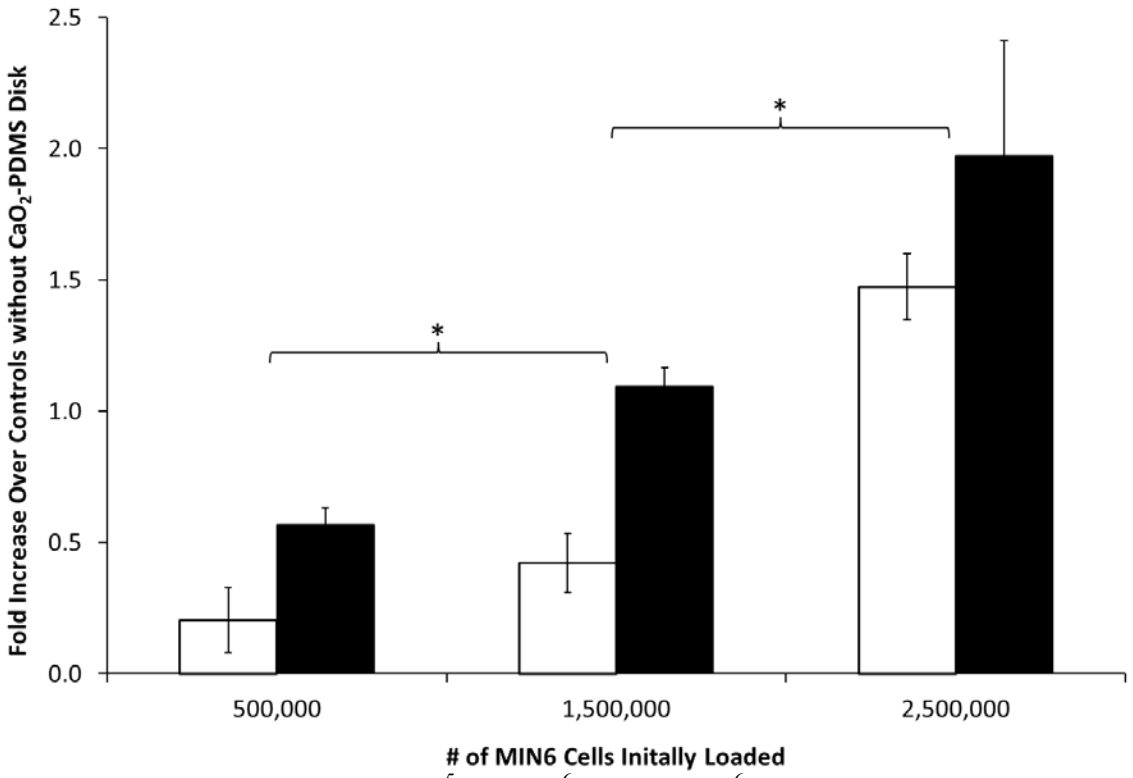

Figure 7-6: MTT viability of 5×10^5, 1.5×10^6, and 2.5×10^6 MIN6 cells in agarose, with or without 25% w/w PDMS-CaO_2 disk, cultured at 20% oxygen (white bars) and 5% oxygen (black bars) was determined after 3 days. Results are expressed as fold increase, which was calculated as the OD value for each group treated with the PDMS-CaO_2 disk divided by the OD value of the corresponding control group without the PDMS-CaO_2 disk (for same given cell loading density and oxygen concentration). Fold increase values greater than one indicate that the PDMS-CaO_2 disk has a positive effect on cell viability, whereas values less than one indicate a detrimental effect. Asterisks indicate statistical significance between groups ($p<0.05$).

Live/dead viability was performed on 2.5×10^6 MIN6 cells in agarose with or without PDMS-CaO_2 disk after 72 hours at 5% or 20% oxygen. In order to map the distribution of live and dead cells, the agarose construct was cut into transversal slices (showing radial distribution) and sagittal slices (showing x-y planar distribution). Figure 7-7 and Figure 7-8 show the live/dead viability of the cells at a transversal (top view) and sagittal (cross-section) view. From transversal images of controls at 5% and 20% oxygen, a rim of live cells can be discerned on the outer edge of the construct, surrounding a core

of dead cells. The same view for PDMS-CaO_2 groups at 5% and 20% oxygen does not exhibit any demarcations. Moreover, PDMS-CaO_2 groups at 5% oxygen illustrate an intermingling of live and dead cells, while at 20% oxygen live cells greatly predominate. Similar results are seen for the sagittal images. Notably, the 5% oxygen controls show hardly any live cells. Also, at 20% oxygen, both control and PDMS-CaO_2 groups demonstrate greater cell viability on the side edges of the construct, while at 5% oxygen the PDMS-CaO_2 group does not.

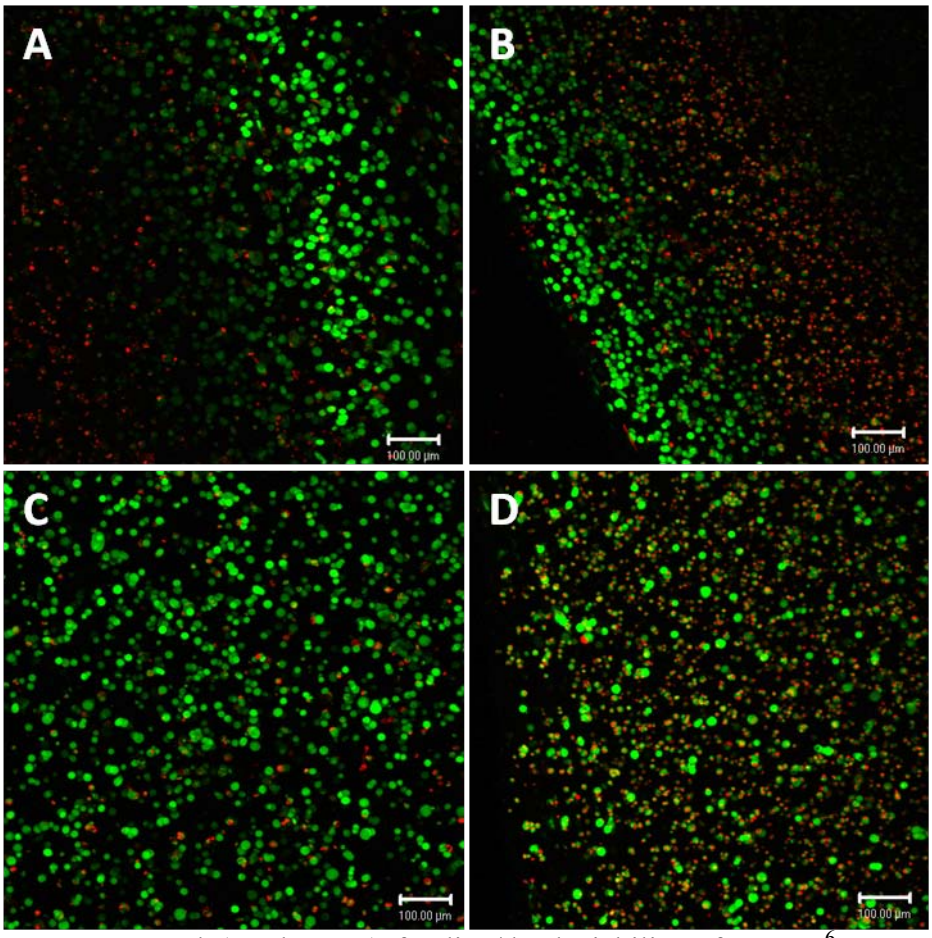

Figure 7-7: Transversal (top-bottom) for live/dead viability of 2.5×10^6 MIN6 cells in agarose, after 72 hrs at 20% oxygen (A,C) without (A) or with a PDMS-CaO_2 disk (C); and at 5% oxygen (C,D) without (C) or with a PDMS-CaO_2 disk (D).

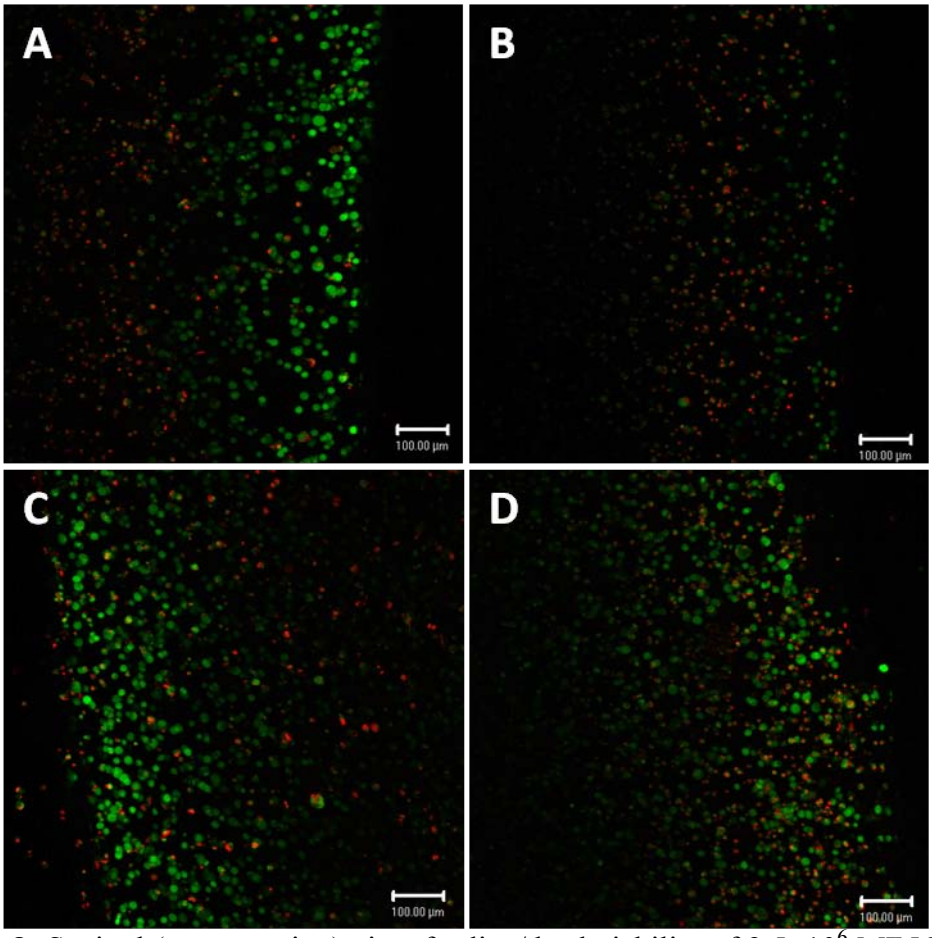

Figure 7-8: Sagittal (cross-section) view for live/dead viability of 2.5×10^6 MIN6 cells in agarose, after 72 hrs at 20% oxygen (A,C) without (A) or with a PDMS-CaO_2 disk (C) and at 5% oxygen (C,D) without (C) or with a PDMS-CaO_2 disk (D).

7.3.4 VIABILITY AND FUNCTION OF ISLETS IN SCAFFOLDS WITH PDMS-CaO_2

To assess the capacity of our oxygen generating materials to enhance islet viability and function in three dimensional scaffolds, islets were seeded onto oxygen generating PDMS scaffolds at high islet loading densities. Rat and human islets were evaluated. Two oxygen generating systems were compared: 1) PDMS scaffold containing a 25% w/w PDMS-CaO_2 disk; and 2) PDMS scaffold composed of 25% w/w CaO_2.

For rat islet studies, 1000 and 1500 IEQ rat islets were seeded onto three different scaffolds: PDMS only scaffold (control); 25% w/w PDMS-CaO_2 scaffold; or PDMS

scaffold plus 25% w/w PDMS-CaO_2 disk, and cultured for 48 hrs at 5% oxygen. Islets were evaluated for live/dead viability, and insulin secretion function. For live/dead viability of 1500 IEQ, a control scaffold at 20% oxygen was assessed for comparison. As Figure 7-9 shows, there are more dead cells in the control scaffold at 5% oxygen than at 20% oxygen. Meanwhile, the PDMS-CaO_2 scaffold appears similar to the 20% oxygen control scaffold, although a greater dispersion of single cells throughout the scaffold is observed. Insulin secretion indices for 1000 IEQ and 1500 IEQ rat islets are shown in Figure 7-10. At 5% oxygen tension, the insulin secretion of islets cultured on control scaffolds was dysfunctional, with an index of 0.68 for 1000 IEQ and an index of 0.80 for 1500 IEQ. Islets cultured on scaffolds made of 25% w/w CaO_2 throughout displayed improved insulin function over controls with functional indices of 1.01 for 1000 IEQ and 1.43 for 1500 IEQ, although not statistically significant due to high error for the 1500 IEQ results. Still higher insulin indices of 1.97 were achieved by culturing islets on scaffolds with a 25% w/w PDMS-CaO_2 disk in the center. Similar improvements were seen by nonhuman primate islets cultured within PDMS scaffolds plus 25% w/w PDMS-CaO_2 disk (data not shown).

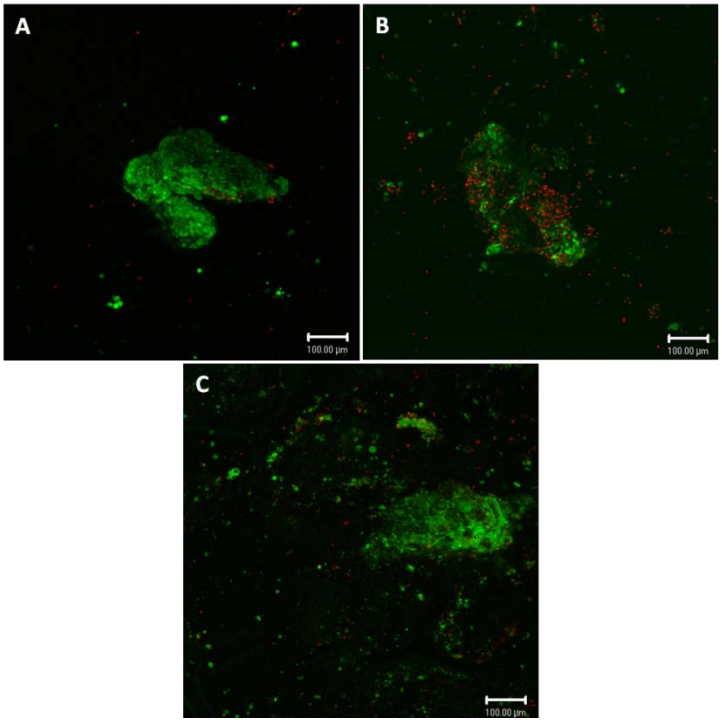

Figure 7-9: Live/dead viability of 1500 IEQ rat islets cultured at 20% oxygen in control scaffolds (A), and at 5% oxygen in control scaffolds (B) or 25% w/w PDMS-CaO_2 scaffolds (C) after 2 days.

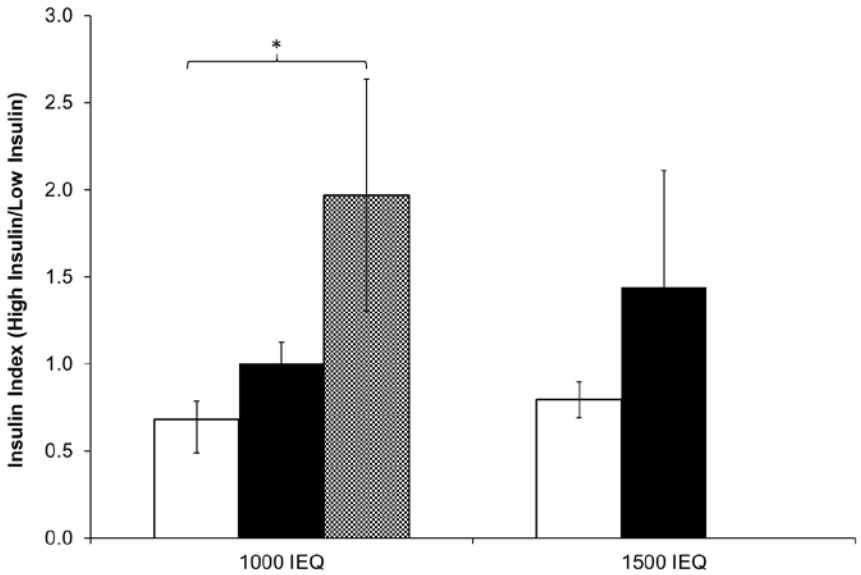

Figure 7-10: Insulin secretion function of 1000 IEQ and 1500 IEQ rat islets cultured at 5% oxygen for 48 hrs was assessed for the groups: control scaffold (white bars), 25% w/w PDMS-CaO_2 scaffold (black bars), and scaffold plus 25% w/w PDMS-CaO_2 (checkered bar). Asterisks indicate statistical significance between groups ($p<0.05$).

Finally, the effect of a PDMS-CaO_2 disk placed beneath the standard macroporous PDMS scaffold was evaluated. In this experiment, 1500 IEQ human islets were cultured on silicone scaffolds with or without a PDMS-CaO_2 disk beneath the scaffold at 5% oxygen for 72 and 96 hrs. Their MTT viability was assessed and expressed as the fold increase over 20% oxygen control scaffolds without a PDMS-CaO_2 disk (see Figure 7-11). With this normalization, a value close to 1.0 indicates that the shift from 20 to 5 % oxygen has no effect on islet viability. Values substantially higher than 1.0 indicate higher viability than 20 % oxygen controls, while values significantly lower than 1.0 indicate a detrimental response. After both 72 and 96 hrs, the MTT viability of islets cultured on control scaffolds at 5% oxygen (fold = 0.83 for 72 hrs and fold = 0.68 for 96 hrs) was lower than control scaffolds at 20% oxygen, indicating hypoxia induced decreases in cell viability. In contrast, scaffolds with a PDMS-CaO_2 disk beneath had similar viability to 20% oxygen control scaffolds (fold = 1.07 for 72 hrs and fold = 0.97 for 96 hrs). This illustrates that the PDMS-CaO_2 disk is capable of mitigating hypoxia induced cell loss within a three-dimensional scaffold.

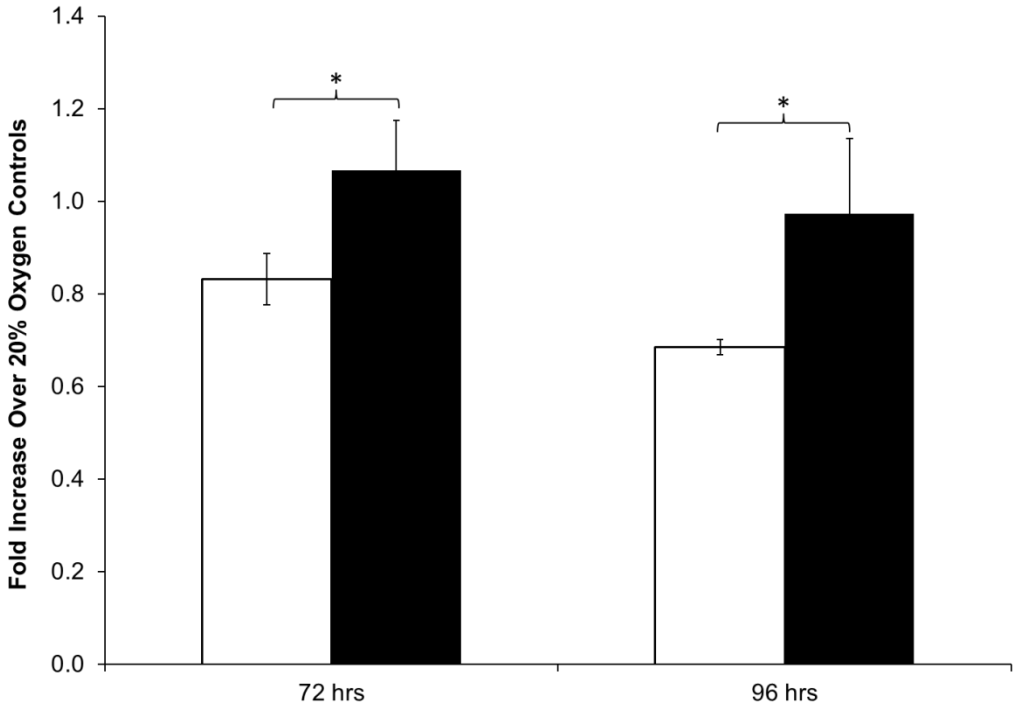

Figure 7-11: MTT viability of 1500 IEQ human islets in a scaffold without a PDMS-CaO_2 disk (white bars) and with a PDMS-CaO_2 disk (black bars), cultured at 5% oxygen was determined after 3 and 4 days and compared to a 20% oxygen scaffold control. Results are expressed as fold increase, which was calculated as the OD value for each group at 5% oxygen divided by the OD value of a control scaffold at 20% oxygen. Fold increase values greater than one indicate that the group, despite being at 5% oxygen, has higher cell viability than 20% oxygen controls. Asterisks indicate statistical significance between groups ($p<0.05$).

7.4 DISCUSSION

In the previous chapters, we had established that modulated oxygen release could be achieved via encapsulation of calcium peroxide within PDMS polymer, into so called PDMS-CaO_2 disks. We demonstrated that these disks could be incubated with cells suffering from low oxygen conditions to increase oxygenation and consequently cell viability. Moreover, positive effects from the disks were also observed for the viability and insulin secretion function of rat and human islets. Encouraged by these results and motivated by the need to develop a method to supplement cell-tissue constructs with

oxygen, we sought to incorporate PDMS-CaO_2 functionality into three-dimensional constructs. Two general methods were employed: (1) a single PDMS-CaO_2 disk was entrapped within agarose gels or PDMS macroporous scaffolds or (2) CaO_2 was embedded into PDMS macroporous scaffolds during their fabrication.

The oxygen releasing potential of 90% porous PDMS scaffolds containing 25% w/w calcium peroxide was determined within a closed chamber. They produced a sustained release of oxygen over the course of at least 2 weeks, which is the time necessary until vascularization in-vivo occurs. Observed saturation behavior is believed to be due to the reversibility of the oxygen releasing kinetics. Initial oxygen release rates did not change appreciably with each refresh cycle because initial rates are primarily driven by the sharp concentration gradient between reactants in the PDMS versus in solution. The fact that the oxygen saturation value decreases over time suggests depletion of the calcium peroxide in the scaffold.

The other oxygen generating construct used in our studies was the PDMS scaffold containing a PDMS-CaO_2 disk in the center. The oxygen release from these PDMS-CaO_2 disks lasted much longer than from PDMS-CaO_2 scaffolds. This can be attributed to the fact that although both constructs contain the same concentration of calcium peroxide (25% w/w), the mass of the scaffolds is one fifth of the disks. Therefore, the scaffolds only contain a fifth of the amount of calcium peroxide that a 25% w/w disk contains, and are equivalent in terms of total mass loading to a 5% w/w PDMS-CaO_2 disk. Theoretical models predicted similar initial oxygen release rates to experimentally observed values and then quickly plateaued. Experimentally, the scaffolds continued to release oxygen for four more days, surpassing the amounts predicted by the model and the amounts released

from a 5% w/w PDMS-CaO_2 disk. We suspect that the reason for this increased oxygen release is due to the fact the scaffolds have a greater surface area exposed to water, which leads to faster reactivity.

We evaluated the ability of PDMS-CaO_2 to function effectively as an oxygen generator within a three-dimensional construct by embedding a PDMS-CaO_2 disk within the center of an agarose gel containing MIN6 cells. MTT viability results showed that, regardless of initial cell loading densities, the viability of groups with PDMS-CaO_2 relative to controls groups was consistently higher at 5% oxygen than at 20% oxygen. This may be attributed to the additional oxygen released from PDMS-CaO_2 disks, raising the 5% oxygen conditions to be more similar to 20% oxygen. For relatively low cell loading densities, such as 5×10^5 cells, the PDMS-CaO_2 disks inhibited cell viability, whereas for high cell loadings, such as 2.5×10^6 cells, the PDMS-CaO_2 disks improved cell viability relative to controls without the disk. This can be explained by the fact that lower cell loading densities leads to a lower total rate of oxygen consumption, which coupled with oxygen release from the PDMS-CaO_2 disks, results in a surplus of oxygen. Conversely, at higher cell loading densities without the PDMS-CaO_2 disk, an oxygen deficit may result. These findings suggest that too much oxygen can be detrimental to cells. Therefore, we must exercise caution when using the PDMS-CaO_2 disk, taking into consideration the cell loading densities and initial oxygen conditions of their planned use. Live/dead viability the control groups without the PDMS-CaO_2 disks revealed that live cells were limited to a thin rim on the outer edge of the construct, while the core predominantly had dead cells. This is not surprising considering that cells on the outer edge of the construct should be more viable since they are in direct contact with exterior

oxygen tensions. Meanwhile, cells in the center only receive oxygen that has managed to diffuse through half of the construct and must compete with oxygen consumption from cells all around them. In published studies using continuous cell lines, this remodeling pattern, high concentration of viable cells on the periphery of the structure, is highly commented (C Stabler et al. 2001). On the other, the PDMS-CaO_2 groups had a uniform distribution of predominantly live cells at 20% oxygen and an intermingling of live and dead cells at 5% oxygen, indicating a divergent pattern in cellular remodeling. In this group, the PDMS-CaO_2 disk alleviates central hypoxia by providing an additional source of oxygen originating in the center of the construct, where it is most needed.

To assess the capacity of our oxygen generating materials to enhance islet viability and function in three dimensional scaffolds, islets were seeded onto oxygen generating PDMS scaffolds at high islet loading densities and investigated experimentally as well as modeled. The models developed suggested that scaffolds with a CaO_2 disk would provide more oxygen release than scaffolds with CaO_2throughout. This is to be expected since scaffolds with the disk contain more total calcium peroxide, and consequently more oxygen releasing potential. Our experimental results appear to support these models, where insulin secretion function of rat islets was significantly improved by incorporation of a PDMS-CaO_2 disk into scaffolds, while CaO_2 incorporation throughout the scaffold resulted in only modest improvements. In addition, human islets studies, while performed using PDMS-CaO_2 disk under the macroporous scaffold and not within the scaffold itself, further support the hypothesis that these materials result in substantial increases in the oxygen profiles within these three-dimensional scaffolds.

7.5 CONCLUSIONS

PDMS encapsulated calcium peroxide was successfully incorporated into three–dimensional constructs while still retaining oxygen generating potential. PDMS-CaO_2 disks incorporated into agarose constructs enhanced the viability of MIN6 cells at high cell loading densities and low oxygen tensions. Therefore, the benefits of the disk are attributed to its release of oxygen. 25% w/w PDMS-CaO_2 scaffolds were observed to produce oxygen for at least two weeks despite being 90% porous and having undergone salt leaching in water for three days. Moreover, a 25% w/w PDMS-CaO_2 disk within the PDMS macroporous scaffold prevented hypoxia induced dysfunction of insulin secretion, when cultured under low oxygen availability. Calcium peroxide distributed throughout the macroporous scaffold resulted in only modest improvements in insulin secretion. Furthermore, loss of human islet cell viability under hypoxia was completely prevented through the use of a single PDMS-CaO_2 disk near the macroporous scaffold. These studies demonstrate the versatility of the disks to be implemented into a variety of three-dimensional constructs, as well as illustrate the need to systematically evaluate the oxygen generating potential of a given prototype. Given the need for methods to enhance oxygenation of not only transplanted islets, but of various other tissue engineered constructs as well, the implications of this study for scaffold design are highly promising.

CHAPTER 8. CONCLUSIONS AND RECOMMENDATIONS FOR FUTURE WORK

8.1 SUMMARY AND CONCLUDING REMARKS

Glucose is the vital currency of energy in the body, and when its accessibility is jeopardized as in patients with Diabetes mellitus, the body is severely compromised. Treatment of diabetes through exogenous insulin supplementation, either by manual injections or an insulin pump, is unable to provide tight, physiological control of blood glucose levels, leading to complications such as diabetic retinopathy, nephropathy, and neuropathy. Cell-based treatments, such as clinical islet transplantation, where β-cell function is restored through the transplantation of allogeneic pancreatic islets would provide optimal regulation, long-term treatment, and significant reduction in detrimental side effects. Current clinical trials of islet transplantation into the portal vein of the liver have resulted in patients with superior control in blood glucose levels, high C-peptide levels, and insulin independence for several years (A. M. Shapiro et al. 2006), but the hepatic site is implicated as the cause for islet dysfunction and destruction by exposing islets to mechanical stress, inflammatory response, toxins, and immune attack (Mattsson et al. 2004; Moberg et al. 2002; U. Johansson et al. 2003; H. Johansson et al. 2005; Z. Yang et al. 2004; van der Windt et al. 2007; Bennet et al. 2000). Selection of an alternative site for islet cell transplantation that minimizes these factors would provide a superior environment for the islets, leading to reduced islet loss and improved function, but this necessitates the design of a biomaterial support for the islets in order to provide adequate mechanical protection and spatial distribution. Moreover, due to the high metabolic demand of islets, methods of improving oxygenation at the transplant site and

permitting vascular infiltration into the biomaterial are essential to transplant success. Therefore, there is a strong need to develop alternative sites and devices for islet cell transplantation that would provide mechanical protection to the islets, while providing a minimally invasive implantation and the safety of retrievability.

The central hypothesis of this dissertation was that a highly porous scaffold, fabricated from biocompatible and biostable materials, would enhance islet engraftment and function within an alternative transplant site, by providing mechanical protection, spatial distribution, and intra-device vascularization. In addition, by utilizing the biomaterial as a means to supplement oxygen short-term, as well as a platform for the introduction of cells that accelerate vascularization for the long term, a superior bioartificial pancreas device, requiring only a reasonable number of islets and scalable to humans, would be produced. Initial studies were focused on the development of a biomaterial scaffold that is capable of mechanically protecting the islets and spatially distributing them, while also allowing for intra-device vascularization. Next, the oxygen generating potential of novel encapsulated solid peroxide was evaluated. Then, the scaffolds and oxygen generator were evaluated for their effect in promoting islet survival and function.

8.1.1 MACROPROUS PDMS SCAFFOLDS FOR ISLET TRANSPLANTATION

Macroporous PDMS scaffolds were designed with optimal porosity (90%) and pore size (250 to 425 μm) for balance between mechanical stability and particle retention. Our results showed that the highest porosities investigated resulted in scaffolds with weakened mechanical structure leading to collapse of pores and lower final porosities. Scaffold pore size was primarily determined by particulate diameter, and influenced

heavily the retention of loaded particles used as islet simulants. Smallest pore sizes (150 to 250 μm) were the most effective for trapping small particles (~50 μm), but did not allow large particles (150 μm and 200 μm) to enter the scaffold. On the other hand, largest pore sizes (425 to 600 μm) allowed large particles to enter and embed themselves, but provided only a minimal barrier for small particles. Due to the high variability of islet diameters depending on species and islet isolation procedures, we selected a median pore size to compromise retention between small and large islets.

PDMS scaffolds exhibited minimal levels of endotoxin, and biocompatibility studies revealed scaffolds had a high degree of biostability and biocompatibility, with fibronectin coated scaffolds promoting positive remodeling. Surface modification by adsorption of proteins, encouraged the adhesion and proliferation of MIN6 and human mesenchymal stem cells. Islets cultured on the scaffold at normal oxygen tension retained viability and insulin secretion function comparable to two-dimensional controls. However, culture of islets on scaffolds at low oxygen tension resulted in higher viability and insulin secretion function compared to two-dimensional controls and alternative three-dimensional agarose gels. Finally, islet-loaded scaffolds transplanted into the omentum of syngeneic rats successfully reversed diabetes in slightly shorter time than controls. Explanted grafts showed retention of islets expressing high levels of insulin and infiltration of blood vessels into the scaffold.

8.1.2 PDMS ENCAPSULATED CALCIUM PEROXIDE FOR OXYGEN RELEASE

We designed and developed PDMS encapsulated calcium peroxide for oxygen release. The kinetics of oxygen release from calcium peroxide powder was determined. Finite element analysis modeled for encapsulated calcium peroxide can be used as an

accurate predictor of oxygen release in the design of oxygen releasing materials. Encapsulation of calcium peroxide in a hydrophilic versus a hydrophobic polymer was shown to modulate the release of oxygen and harmful hydrogen peroxide byproduct. Oxygen releasing disks increased the proliferation of MIN6 cells cultured in two-dimensions and three-dimensional agarose constructs at 5% oxygen compared to controls. Moreover, the disks improved the viability and insulin secretion function of islets cultured at high loading densities and low oxygen tension. Finally, PDMS encapsulated calcium peroxide was incorporated into three dimensional constructs. They were demonstrated to release oxygen for two weeks as well as improve islet viability and insulin secretion function at low oxygen tensions.

8.2 RECOMMENDATIONS FOR FUTURE WORK

The overall goal of this dissertation was to develop an oxygen generating, macroporous scaffold for extrahepatic islet transplantation in order to treat type 1 diabetes mellitus (T1DM). The research presented here met the objectives of designing an implantable, retrievable scaffold that mechanically protects, spatially distributes, and allows vascular infiltration in order to treat diabetes. Moreover, this work demonstrates that scaffolds can be successfully modified to generate supplemental oxygen for at least two weeks without impairing function. Nonetheless, there remains a great deal for improvement, particularly by exploiting the scaffold as a platform for other strategies.

High retention of islets within the scaffold is critical to transplant success, making it one of the most important aspects in scaffold design. To prevent the loss of small islets through the scaffold, we added fibrin glue to the outside after loading. However, we envision that fibrin glue might not be needed for this purpose if scaffolds were fabricated

with multimodal pore sizes. For example, the top half of the scaffold could be composed of large pores (425 to 600 μm) to allow large islets to enter, whereas the bottom half could be composed of small pores (150 to 250 μm) to retain even the smallest islets. Also, the islets might be entrapped more efficiently and distributed more evenly within the scaffold if alternative methods of seeding could be developed and explored.

Another critical factor implicated in the limited success of islet transplantation that we did not touch upon is the loss of vascular connections and disruption of cell-matrix contacts that occur during islets isolations (Antonello Pileggi et al. 2006; Lai et al. 2005; Balamurugan et al. 2006). Basement membrane proteins, such as collagen IV, laminin, and fibronectin are responsible for engaging integrins on the surface of islets to mediate adhesion, providing structural support, and activating intracellular chemical signaling pathways (Hamamoto et al. 2003; Jiang et al. 2002; Kaido et al. 2004). Our scaffolds only had a minimal coating of fibronectin on their surface and consequently really only served as a structural framework. Islets cultured on scaffolds containing extracellular matrix components have exhibited improved survival in-vitro (Lucas-Clerc et al. 1993) and in-vivo (Daoud et al. 2010; Salvay et al. 2008). Therefore, we anticipate that "bioactivation" of the scaffold by greater incorporation of extracellular matrix components would result in healthier islets.

We also anticipate that the macroporous, PDMS scaffold will serve a dual purpose as not only a carrier for islets, protecting them from mechanical stresses and maintaining them spatially distributed, but also as a future platform for delivery of molecules or co-culture of cells. We have demonstrated with oxygen release from PDMS encapsulated calcium peroxide scaffolds that the scaffolds can be doped for slow, long-

term release of molecules. Of particular interest is the targeted delivery of immunosuppressive drugs, such as dexamethasone, which are necessary for transplantation of allogeneic islets. By delivering the drugs via the scaffold, instead of intravenously, you would not only achieve a slower release, but also minimize drug exposure to other tissues in the body. Alternatively, antioxidants, such as catalase, ascorbic acid, or ceria, could be embedded directly in the scaffold to act upon any free radicals generated from the calcium peroxide decomposition or secondary reactions. This would minimize exposure of islets to free radicals, which would be highly beneficial given the innate, low free radical scavenging ability of islets. Potentially, as demonstrated by the culture of MIN6 cells and human mesenchymal stem cells, scaffolds can serve as a co-culture system by having adherent cell lines proliferate on the scaffold surface prior to islet loading. Co-culture of mesenchymal stem cells in particular may have a positive effect on islet viability and function, stimulating angiogenesis, or immunomodulating the environment. Thus, the scaffold provides a micro niche environment for localized activity.

The finite element model developed here can be used to roughly predict the oxygen release from PDMS encapsulated calcium peroxide disks for varying concentrations of calcium peroxide and different construct geometries. To simplify analysis of such a complex system, assumptions were made on the chemical reactivity of calcium peroxide and the interactions of molecules embedded in PDMS. We only considered the direct conversion of calcium peroxide into oxygen. However, in reality the process may involve a hydrogen peroxide intermediate. Moreover, multiple side reactions may occur, each one affecting the other. In addition, as discussed earlier in Chapter 5, the

transport of water and water soluble molecules into PDMS is poorly understood. More accurate models could be developed if there were a greater understanding of calcium peroxide reactivity and aqueous-PDMS interactions. However, this would be more in the scope of recommendations for future work in chemical engineering.

REFERENCES

Abdi, R. et al., 2008. Immunomodulation by mesenchymal stem cells: a potential therapeutic strategy for type 1 diabetes. *Diabetes*, 57(7), pp.1759-1767.

Amory, B., Mourmeaux, J.L. & Remacle, C., 1988. In vitro cytodifferentiation of perinatal rat islet cells within a tridimensional matrix of collagen. *In Vitro Cellular Developmental Biology Journal of the Tissue Culture Association*, 24(2), pp.91-99.

Anon, 1993. The effect of intensive treatment of diabetes on the development and progression of long-term complications in insulin-dependent diabetes mellitus. The Diabetes Control and Complications Trial Research Group. *N Engl J Med*, 329(14), pp.977-86.

Ao, Z. et al., 1993. Survival and function of purified islets in the omental pouch site of outbred dogs. *Transplantation*, 56(3), pp.524-9.

Aoki, T. et al., 2005. Intrasplenic transplantation of encapsulated genetically engineered mouse insulinoma cells reverses streptozotocin-induced diabetes in rats. *Cell Transplantation*, 14(6), pp.411-21.

Armani, D., Liu, C. & Aluru, N., 1999. Re-configurable fluid circuits by PDMS elastomer micromachining. In *Twelfth IEEE International Conference on Micro Electro Mechanical Systems, 1999. MEMS'99.* IEEE, p. 222–227.

Atlas, R.M., 1977. Stimulated petroleum biodegradation. *CRC Critical Reviews in Microbiology*, 5(4), pp.371-386.

Aucoin, L. et al., 2002. Interactions of corneal epithelial cells and surfaces modified with cell adhesion peptide combinations. *J Biomater Sci Polym Ed*, 13(4), pp.447-462.

Aung, T. et al., 1995. Comparison of various gels for immobilization of islets in bioartificial pancreas using a mesh-reinforced polyvinyl alcohol hydrogel tube. *Transplantation Proceedings*, 27(1), pp.619-21.

Baker, A.M. & Hatton, W., 1987. Calcium peroxide as a seed coating material for padi rice. *Plant and Soil*, 99(2-3), pp.357-363.

Balamurugan, A.N. et al., 2006. Prospective and challenges of islet transplantation for the therapy of autoimmune diabetes. *Pancreas*, 32(3), pp.231-43.

Barrie, J.A. & Machin, D., 1969. The sorption and diffusion of water in silicone rubbers: Part I. Unfilled rubbers. *Journal of Macromolecular Science, Part B*, 3(4), pp.645-672.

Beattie, G.M. et al., 2002. A novel approach to increase human islet cell mass while preserving beta-cell function. *Diabetes*, 51(12), pp.3435-3439.

Behravesh, E. et al., 1999. Synthetic biodegradable polymers for orthopaedic applications. *Clinical Orthopaedics and Related Research*, 367(367 Suppl), p.S118-S129.

Bennet, W. et al., 1999. Incompatibility between human blood and isolated islets of Langerhans: a finding with implications for clinical intraportal islet transplantation? *Diabetes*, 48(10), pp.1907-14.

Bennet, W. et al., 2000. Damage to porcine islets of langerhans after exposure to human blood in vitro, or after intraportal transplantation to cynomologus monkeys: protective effects of sCR1 and heparin. *Transplantation*, 69(5), pp.711-719.

Berman, D.M. et al., 2010. Mesenchymal stem cells enhance allogeneic islet engraftment in nonhuman primates. *Diabetes*, 59(10), pp.2558-68.

Bloch, K. et al., 2006. Immobilized microalgal cells as an oxygen supply system for encapsulated pancreatic islets: a feasibility study. *Artif Organs*, 30(9), pp.715-718.

Blomeier, H. et al., 2006. Polymer scaffolds as synthetic microenvironments for extrahepatic islet transplantation. *Transplantation*, 82(4), pp.452-459.

Bocca, N. et al., 2008. Soft corticosteroids for local immunosuppression: exploring the possibility for the use of loteprednol etabonate for islet transplantation. *Die Pharmazie*, 63(3), pp.226-32.

Brendel, M D et al., Improved functional survival of human islets of Langerhans in three-dimensional matrix culture. *Cell Transplantation*, 3(5), pp.427-35.

Brezonik, P.L., 1994. *Chemical Kinetics and Process Dynamics in Aquatic Systems*, Lewis.

Brown, X.Q., Ookawa, K. & Wong, J.Y., 2005. Evaluation of polydimethylsiloxane scaffolds with physiologically-relevant elastic moduli: interplay of substrate mechanics and surface chemistry effects on vascular smooth muscle cell response. *Biomaterials*, 26(16), pp.3123-3129.

Bucholz, R.W., Carlton, A. & Holmes, R.E., 1987. Hydroxyapatite and tricalcium phosphate bone graft substitutes. *Orthop Clin North Am*, 18(2), pp.323-334.

Buchwald, Peter, 2009. FEM-based oxygen consumption and cell viability models for avascular pancreatic islets. *Theoretical Biology and Medical Modelling*, 6, p.5.

Buchwald, Peter et al., 2009. Quantitative assessment of islet cell products: estimating the accuracy of the existing protocol and accounting for islet size distribution. *Cell Transplantation*, 18(10), pp.1223-35.

Calafiore, R., 1998. Actual perspectives in biohybrid artificial pancreas for the therapy of type 1, insulin-dependent diabetes mellitus. *Diabetes Metab Rev*, 14(4), pp.315-324.

Calafiore, R. et al., 1992. Intravascular transplantation of microencapsulated islets in diabetic dogs. *Transplant Proc*, 24(3), pp.935-936.

Calafiore, R. et al., 2006. Microencapsulated pancreatic islet allografts into nonimmunosuppressed patients with type 1 diabetes: first two cases. *Diabetes Care*, 29(1), pp.137-138.

Caplan, A.I., 2009. Why are MSCs therapeutic? New data: new insight. *J Pathol*, 217(2), pp.318-324.

Cassidy, D.P. & Irvine, R.L., 1999. Use of calcium peroxide to provide oxygen for contaminant biodegradation in a saturated soil. *Journal of Hazardous Materials*, pp.25-39.

CDC's Division of Diabetes Translation Division of Health Interview Statistics, N.C. for C.D.P. and H.P. and the N.C. for H.S. ed., 2006. Annual Number (in Thousands) of New Cases of Diagnosed Diabetes Among Adults Aged 18-79 Years, United States, 1980–2005.

Chaikof, E.L., 1999. Engineering and material considerations in islet cell transplantation. *Annual Review of Biomedical Engineering*, 1, pp.103-27.

Chaudhry, Q.A., Hanke, M. & Morgenstern, R., 2009. Simulation of transport of lipophilic compounds in complex cell geometry. *Metabolism Clinical And Experimental*, pp.3-7.

Chemicals, S., IXPER Calcium Peroxide.

Chen, Ge et al., 2001. The mechanism and applicability of in situ oxidation of trichloroethylene with Fenton' s reagent. *Journal of Hazardous Materials*, 87(1-3), pp.171-186.

Chen, Guoping et al., 2005. Culturing of skin fibroblasts in a thin PLGA-collagen hybrid mesh. *Biomaterials*, 26(15), pp.2559-66.

Chen, X. et al., 2007. The epididymal fat pad as a transplant site for minimal islet mass. *Transplantation*, 84(1), pp.122-125.

Chevalier, L.R. & Mccann, C.D., 2008. Feasibility of calcium peroxide as an oxygen releasing compound in treatment walls. *International Journal of Environment and Waste Management*, 2(3), pp.245-256.

Cohn, C.A., Simon, S.R. & Schoonen, M.A.A., 2008. Comparison of fluorescence-based techniques for the quantification of particle-induced hydroxyl radicals. *Particle and Fibre Toxicology*, 5(1), p.2.

Colton, C K & Avgoustiniatos, E.S., 1991. Bioengineering in development of the hybrid artificial pancreas. *Journal of Biomechanical Engineering*, 113(2), pp.152-170.

COMSOL, 2010a. Comsol Chemical Reaction Engineering Module 4.0a.

COMSOL, 2010b. Comsol Multiphysics 4.0a.

Cox, M.E., 1986. Oxygen diffusion in poly (dimethyl siloxane) using fluorescence quenching . I . Measurement technique and analysis. *Engineering Sciences*, 24, pp.621-636.

Cuthbertson, R.A. & Mandel, T.E., 1986. A comparison of portal versus systemic venous drainage in murine foetal pancreatic islet transplantation. *The Australian Journal of Experimental Biology and Medical Science*, 64 (Pt 2), pp.175-84.

Daoud, J.T. et al., 2010. Long-term in vitro human pancreatic islet culture using three-dimensional microfabricated scaffolds. *Biomaterials*, 32(6), pp.1536-1542.

De Vos, P., Hamel, a F. & Tatarkiewicz, K., 2002. Considerations for successful transplantation of encapsulated pancreatic islets. *Diabetologia*, 45(2), pp.159-73.

De Vos, P. et al., 1997. Efficacy of a prevascularized expanded polytetrafluoroethylene solid support system as a transplantation site for pancreatic islets. *Transplantation*, 63(6), pp.824-30.

Deng, C. et al., 2007. Biological properties of the chitosan-gelatin sponge wound dressing☆. *Carbohydrate Polymers*, 69(3), pp.583-589.

Devarapalli, M., Lawrence, B.J. & Madihally, S.V., 2009. Modeling nutrient consumptions in large flow-through bioreactors for tissue engineering. *Biotechnology and Bioengineering*, 103(5), pp.1003-15.

Di Colo, G., 1992. Controlled drug release from implantable matrices based on hydrophobia polymers☆. *Biomaterials*, 13(12), pp.850-856.

Dionne, K.E., Colton, C K & Yarmush, M.L., 1993. Effect of hypoxia on insulin secretion by isolated rat and canine islets of Langerhans. *Diabetes*, 42(1), pp.12-21.

Dong, J. et al., 2001. In vivo evaluation of a novel porous hydroxyapatite to sustain osteogenesis of transplanted bone marrow-derived osteoblastic cells. *J Biomed Mater Res*, 57(2), pp.208-216.

Dufour, J.M. et al., 2005. Development of an ectopic site for islet transplantation, using biodegradable scaffolds. *Tissue Engineering*, 11(9-10), p.1323–1331.

Ellis, M.J. & Chaudhuri, J.B., 2006. Poly(lactic-co-glycolic acid) hollow fibre membranes for use as a tissue engineering scaffold. *Biotechnol Bioeng*, 96(1), pp.177-187.

Ely, D.L. et al., 1991. Androgen receptor and the testes influence hypertension in a hybrid rat model. *Hypertension*, 17(6 Pt 2), pp.1104-1110.

Embury, J. et al., 2001. Proteins linked to a protein transduction domain efficiently transduce pancreatic islets. *Diabetes*, 50(8), pp.1706-1713.

Falorni, A. et al., 1996. Culture maintenance of isolated adult porcine pancreatic islets in three-dimensional gel matrices: morphologic and functional results. *Pancreas*, 12(3), pp.221-229.

Favre, E. et al., 1994. Sorption, diffusion and vapor permeation of various penetrants through dense poly(dimethylsiloxane) membranes: a transport analysis. *Journal of Membrane Science*, 92(2), pp.169-184.

Folkman, J. & Hochberg, M., 1973. Self-regulation of growth in three dimensions. *The Journal of Experimental Medicine*, 138(4), pp.745-53.

Fraker, Chris et al., Novel method of islet potency assessment by gluocse stimulated insulin release.

Gao, Y. et al., 2006. Characterization and osteoblast-like cell compatibility of porous scaffolds: bovine hydroxyapatite and novel hydroxyapatite artificial bone. *J Mater Sci Mater Med*, 17(9), pp.815-823.

George, S., 2001. Transport phenomena through polymeric systems. *Progress in Polymer Science*, 26(6), pp.985-1017.

Ghosh, S. et al., 2007. The double porogen approach as a new technique for the fabrication of interconnected poly(L-lactic acid) and starch based biodegradable scaffolds. *Journal of Materials Science: Materials in Medicine*, 18(2), pp.185-93.

Grankvist, K., Marklund, S. & Täljedal, I.B., 1979. Influence of trace metals on alloxan cytotoxicity in pancreatic islets. *FEBS letters*, 105(1), pp.15-8.

Greenberg, A.E., 1995. *Standard Methods for the Examination of Water and Wastewater* A. D. Eaton et al., eds., American Public Health Association.

Guan, J. et al., 1998. Glucose turnover and insulin sensitivity in rats with pancreatic islet transplants. *Diabetes*, 47(7), pp.1020-6.

Hall, K., Gattas-Asfura, K. & Stabler, Cl, 2011. Microencapsulation of islets within alginate/poly(ethylene glycol) gels cross-linked via Staudinger ligation. *Acta Biomaterialia*, 7, pp.614-624.

Halliwell, B. & Gutteridge, J.M., 1985. The importance of free radicals and catalytic metal ions in human diseases. *Mol Aspects Med*, 8(2), pp.89-193.

Hamamoto, Y. et al., 2003. Beneficial effect of pretreatment of islets with fibronectin on glucose tolerance after islet transplantation. *Hormone and Metabolic Research*, 35(8), pp.460-5.

Hanh, D.N., Rajbhandari, B.K. & Annachhatre, A.P., 2005. Bioremediation of sediments from intensive aquaculture shrimp farms by using calcium peroxide as slow oxygen release agent. *Environmental Technology*, 26(5), pp.581-9.

Harris, L.D., Kim, B.S. & Mooney, D J, 1998. Open pore biodegradable matrices formed with gas foaming. *J Biomed Mater Res*, 42(3), pp.396-402.

Harrison, B.S. et al., 2007. Oxygen producing biomaterials for tissue regeneration. *Biomaterials*, 28(31), pp.4628-4634.

Hayashi, T., 1994. Biodegradable polymer for biomedical use. *Prog. Polymer Science*, 19, pp.663-702.

Heise, U., Osborn, J.F. & Duwe, F., 1990. Hydroxyapatite ceramic as a bone substitute. *Int Orthop*, 14(3), pp.329-338.

Herman, B. et al., 1988. Irreversible injury in anoxic hepatocytes precipitated by an abrupt increase in plasma membrane permeability. *Faseb J*, 2(2), pp.146-151.

Hesse, U.J. et al., 1986. Comparison of splenic and renal subcapsular islet autografting in dogs. *Transplantation*, 41(2), pp.271-4.

Heywood, H.K., Bader, D.L. & Lee, D.A., 2006. Rate of oxygen consumption by isolated articular chondrocytes is sensitive to medium glucose concentration. *J Cell Physiol*, 206(2), pp.402-410.

Hillborg, H. et al., 2000. Crosslinked polydimethylsiloxane exposed to oxygen plasma studied by neutron reflectometry and other surface specific techniques. *Polymer*, 41, pp.6851-6863.

Hinchee, R., 1991. Use of hydrogen peroxide as an oxygen source for in situ biodegradation Part I. Field studies. *Journal of Hazardous Materials*, 27(3), pp.287-299.

Hinchee, R.E. & Olfenbuttel, R.F., 1991. *In Situ Bioreclamation/On Site Bioreclamation* First., Butterworth-Heinemann.

Hodgins, D. et al., 2007. Biocompatible materials developments for new medical implants. *Med Device Technol*, 18(6), pp.30,32-35.

Hogg, N., 1999. The kinetics of S-transnitrosation--a reversible second-order reaction. *Analytical Biochemistry*, 272(2), pp.257-62.

Hou, Q.P. & Bae, Y.H., 1999. Biohybrid artificial pancreas based on macrocapsule device. *Adv Drug Deliv Rev*, 35(2-3), pp.271-287.

Howard, D. et al., 2008. Tissue engineering : strategies , stem cells and scaffolds. *Society*, pp.66-72.

Hsiong, S.X. & Mooney, D J, 2006. Regeneration of vascularized bone. *Periodontology 2000*, 41, pp.109-122.

Hussey, A.J. et al., 2009. Seeding of pancreatic islets into prevascularized tissue engineering chambers. *Tissue engineering. Part A*, 15(12), pp.3823-33.

Inoue, H. et al., 2008. Bioimaging assessment and effect of skin wound healing using bone-marrow-derived mesenchymal stromal cells with the artificial dermis in diabetic rats. *J Biomed Opt*, 13(6), p.64036.

Iwata, H. et al., 1994. Feasibility of agarose microbeads with xenogeneic islets as a bioartificial pancreas. *J Biomed Mater Res*, 28(9), pp.1003-1011.

Jewrajka, S.K. et al., 2007. Novel biostable and biocompatible amphiphilic membranes. *Journal of Biomedical Materials Research Part A*.

Jiang, F.-X., Naselli, G. & Harrison, L.C., 2002. Distinct distribution of laminin and its integrin receptors in the pancreas. *The Journal of Histochemistry and Cytochemistry: Official Journal of the Histochemistry Society*, 50(12), pp.1625-32.

Jo, S. et al., 2001. Synthesis and characterization of oligo(poly(ethylene glycol) fumarate) macromer. *Macromolecules*, 34(9), pp.2839-2844.

Johansson, H. et al., 2005. Tissue factor produced by the endocrine cells of the islets of langerhans is associated with a negative outcome of clinical islet transplantation. *Diabetes*, 54, pp.1755-1762.

Johansson, U. et al., 2003. Inflammatory mediators expressed in human islets of Langerhans: implications for islet transplantation. *Biochem Biophys Res Commun*, 308, pp.474-479.

Jordan, R.B., 2007. *Reaction Mechanisms of Inorganic and Organometallic Systems* Third., Oxford University Press.

Juang, J.H. et al., 1995. Outcome of subcutaneous islet transplantation improved by a polymer device. *Transplantation Proceedings*, 27(6), pp.3215-6.

Jungermann, K. & Kietzmann, T., 2000. Oxygen: modulator of metabolic zonation and disease of the liver. *Hepatology*, 31(2), pp.255-260.

Kaido, T. et al., 2004. Regulation of human beta-cell adhesion, motility, and insulin secretion by collagen IV and its receptor alpha1beta1. *The Journal of Biological Chemistry*, 279(51), pp.53762-9.

Kamiya, Y. et al., 1990. Sorption and partial molar volume of gases in poly (dimethyl siloxane). *Journal of Polymer Science Part B: Polymer Physics*, 28(8), pp.1297-1308.

Kaneto, H. et al., 1999. Beneficial effects of antioxidants in diabetes: possible protection of pancreatic beta-cells against glucose toxicity. *Diabetes*, 48(12), pp.2398-2406.

Karunakaran, R. & Kennedy, J.P., 2007. Synthesis , characterization , and crosslinking of copolymers. *Polymer*, pp.4284-4290.

Kaufman, D.B. et al., 1990. Purified canine islet autografts. Functional outcome as influenced by islet number and implantation site. *Transplantation*, 50(3), pp.385-91.

Kellouche, S. et al., 2007. Tissue engineering for full-thickness burns: a dermal substitute from bench to bedside. *Biochemical and Biophysical Research Communications*, 363(3), pp.472-8.

Khor, H.L. et al., 2003. Preliminary study of a polycaprolactone membrane utilized as epidermal substrate. *Journal of Materials Science: Materials in Medicine*, 14(2), pp.113-120.

Khorasani, M.T. & Mirzadeh, H., 2004. Laser surface modification of silicone rubber to reduce platelet adhesion in vitro. *J Biomater Sci Polym Ed*, 15(1), pp.59-72.

Kim, H.W., Knowles, J.C. & Kim, H.E., 2005. Hydroxyapatite porous scaffold engineered with biological polymer hybrid coating for antibiotic Vancomycin release. *J Mater Sci Mater Med*, 16(3), pp.189-195.

Kimoto, K. et al., 2003. Gliclazide protects pancreatic beta-cells from damage by hydrogen peroxide. *Biochem Biophys Res Commun*, 303(1), pp.112-119.

Kin, T., Korbutt, Gregory S & Rajotte, Ray V, 2003. Survival and metabolic function of syngeneic rat islet grafts transplanted in the omental pouch. *American Journal of Transplantation*, 3(3), pp.281-5.

Kobayashi, N., 2008. Bioartificial pancreas for the treatment of diabetes. *Cell Transplant*, 17(1-2), pp.11-17.

Koopman, D.C. & Lee, H.H., 1992. Second-order reversible reactions and diffusion in a slab-like medium—II. Further analysis and general results. *Chemical Engineering Science*, 47(15-16), pp.3989-3998.

Krampera, M. et al., 2003. Bone marrow mesenchymal stem cells inhibit the response of naive and memory antigen-specific T cells to their cognate peptide. *Blood*, 101(9), pp.3722-3729.

Kuntz, E. & Kuntz, H.-D., 2005. *Hepatology, Principles and Practice* 2nd ed., Germany: Springer.

Lacy, P.E. et al., 1991. Maintenance of normoglycemia in diabetic mice by subcutaneous xenografts of encapsulated islets. *Science (New York, N.Y.)*, 254(5039), pp.1782-4.

Lai, Y. et al., 2005. Vascular endothelial growth factor increases functional beta-cell mass by improvement of angiogenesis of isolated human and murine pancreatic islets. *Transplantation*, 79(11), pp.1530-6.

Lavabre, D. et al., 1993. Reversible, mixed first-and second-order and autocatalytic reactions as particular cases of a single kinetic rate law. *The Journal of Physical Chemistry*, 97(20), p.5321–5326.

Lawrence, B.J., Devarapalli, M. & Madihally, S.V., 2009. Flow dynamics in bioreactors containing tissue engineering scaffolds. *Biotechnology and Bioengineering*, 102(3), pp.935-47.

Lee, S.B. et al., 2005. Study of gelatin-containing artificial skin V: fabrication of gelatin scaffolds using a salt-leaching method. *Biomaterials*, 26(14), pp.1961-8.

Leng, J. et al., 2006. Microevaporators for kinetic exploration of phase diagrams. *Physical Review Letters*, 96(8), pp.1-4.

Levine, R., 2009. CSTR design for reversible reactions. *Chemical Engineering*, 116(9), pp.46-49.

Li, B., Chen, J. & Wang, J.H.-C., 2006. RGD peptide-conjugated poly(dimethylsiloxane) promotes adhesion, proliferation, and collagen secretion of human fibroblasts. *Journal of Biomedical Materials Research Part A*, 79(4), pp.989-98.

Liao, W. et al., 2009. Therapeutic effect of human umbilical cord multipotent mesenchymal stromal cells in a rat model of stroke. *Transplantation*, 87(3), pp.350-359.

Liu, H. et al., 2004. A study on a chitosan-gelatin-hyaluronic acid scaffold as artificial skin in vitro and its tissue engineering applications. *Journal of Biomaterials science. Polymer edition*, 15(1), pp.25-40.

Lo, H. et al., 1996. Poly(L-lactic acid) foams with cell seeding and controlled-release capacity. *Journal of Biomedical Materials Research*, 30(4), pp.475-484.

Lo, H., Ponticiello, M.S. & Leong, K.W., 1995. Fabrication of controlled release biodegradable foams by phase separation. *Tissue Engineering*, 1(1), pp.15-28.

Low, S.P. et al., 2006. Evaluation of mammalian cell adhesion on surface-modified porous silicon. *Biomaterials*, 27(26), pp.4538-4546.

Lucas-Clerc, C. et al., 1993. Long-term culture of human pancreatic islets in an extracellular matrix: morphological and metabolic effects. *Molecular and Cellular Endocrinology*, 94(1), pp.9-20.

Maitra, B. et al., 2004. Human mesenchymal stem cells support unrelated donor hematopoietic stem cells and suppress T-cell activation. *Bone Marrow Transplant*, 33(6), pp.597-604.

Marques, A.P., Reis, R.L. & Hunt, J.A., 2005. An in vivo study of the host response to starch-based polymers and composites subcutaneously implanted in rats. *Macromol Biosci*, 5(8), pp.775-785.

Martin, Darren J et al., 2000. Polydimethylsiloxane / polyether-mixed macrodiol-based polyurethane elastomers : biostability. *Biomaterials*, 21.

Martinek, J. et al., 2008. A novel approach to simulate Hodgkin-Huxley-like excitation with COMSOL Multiphysics. *Artificial Organs*, 32(8), pp.614-9.

Mastrogiacomo, M. et al., 2005. Tissue engineering of bone: search for a better scaffold. *Orthod Craniofac Res*, 8(4), pp.277-284.

Mata, A., Fleischman, A.J. & Roy, S., 2005. Characterization of polydimethylsiloxane (PDMS) properties for biomedical micro/nanosystems. *Biomedical Microdevices*, 7(4), p.281–293.

Mattsson, G. et al., 2004. Evidence of functional impairment of syngeneically transplanted mouse pancreatic islets retrieved from the liver. *Diabetes*, 53, pp.948-954.

McDonald, J.C. et al., 2000. Fabrication of microfluidic systems in poly(dimethylsiloxane). *Electrophoresis*, 21(1), pp.27-40.

Meagher, N.E. & Rorabacher, D.B., 1994. Mathematical treatment for very rapid second-order reversible kinetics as measured by stopped-flow spectrophotometry with corrections for the cell concentration gradient. *The Journal of Physical Chemistry*, 98(48), pp.12590-12593.

Meghana, K., Sanjeev, G. & Ramesh, B., 2007. Curcumin prevents streptozotocin-induced islet damage by scavenging free radicals: a prophylactic and protective role. *Eur J Pharmacol*, 577(1-3), pp.183-191.

Merkel, T. et al., 2000. Gas sorption, diffusion, and permeation in poly (dimethylsiloxane). *Journal of Polymer Science Part B: Polymer Physics*, 38(3), p.415–434.

Metcalfe, A.D. & Ferguson, M.W.J., 2007. Tissue engineering of replacement skin: the crossroads of biomaterials, wound healing, embryonic development, stem cells and regeneration. *Journal of the Royal Society, Interface / the Royal Society*, 4(14), pp.413-37.

Mikos, A G et al., 1993. Preparation of poly(glycolic acid) bonded fiber structures for cell attachment and transplantation. *Journal of Biomedical Materials Research*, 27(2), pp.183-189.

Mikos, A G et al., 1993. Laminated three-dimensional biodegradable foams for use in tissue engineering. *Biomaterials*, 14(5), pp.323-330.

Miller, C., 1995. Oxidation behavior of aqueous contaminants in the presence of hydrogen peroxide and filter media. *Journal of Hazardous Materials*, 41(1), pp.105-116.

Moberg, L. et al., 2002. Productions of tissue factor by pancreatic islet cells as a trigger of detrimental thrombotic reactions in clinical islet transplantation. *Lancet*, 360, pp.2039-2045.

Moioli, E.K. et al., 2008. Synergistic actions of hematopoietic and mesenchymal stem/progenitor cells in vascularizing bioengineered tissues. *PLoS ONE*, 3(12), p.e3922.

Montesano, R. et al., 1983. Collagen matrix promotes reorganization of pancreatic endocrine cell monolayers into islet-like organoids. *The Journal of Cell Biology*, 97(3), pp.935-939.

Mooney, D J et al., 1996. Novel approach to fabricate porous sponges of poly(D,L-lactic-co-glycolic acid) without the use of organic solvents. *Biomaterials*, 17(14), pp.1417-1422.

Morarescu, D., West-Mays, J.A. & Sheardown, H.D., 2010. Effect of delivery of MMP inhibitors from PDMS as a model IOL material on PCO markers. *Biomaterials*, 31(8), pp.2399-407.

Motterlini, R. et al., 1998. Depression of endothelial and smooth muscle cell oxygen consumption by endotoxin. *Am J Physiol*, 275(3 Pt 2), pp.H776-82.

Murakami, T., 1998. Dynamics of polymeric solid surfaces treated with oxygen plasma: effect of aging media after plasma treatment. *Journal of Colloid and Interface Science*, 202(1), pp.37-44.

Murphy, W.L. et al., 2002. Salt fusion: an approach to improve pore interconnectivity within tissue engineering scaffolds. *Tissue Engineering*, 8(1), pp.43-52.

Nagano, T., 2009. Bioimaging probes for reactive oxygen species and reactive nitrogen species. *Journal of Clinical Biochemistry and Nutrition*, 45(2), p.111.

Nagano, T., 2003. Development of novel fluorescence probes that can reliably detect reactive oxygen species and distinguish specific species *. *Biochemistry*, 278(5), pp.3170 -3175.

Nishikawa, M. et al., 2008. Stable immobilization of rat hepatocytes as hemispheroids onto collagen-conjugated poly-dimethylsiloxane (PDMS) surfaces: Importance of direct oxygenation through PDMS for both formation and function. *Biotechnology and Bioengineering*, 99(6), p.1472–1481.

Norman, J.J. & Desai, T.A., 2005. Control of cellular organization in three dimensions using a microfabricated polydimethylsiloxane-collagen composite tissue scaffold. *Tissue Engineering*, 11(3-4), pp.378-386.

Northup, A. & Cassidy, D., 2008. Calcium peroxide (CaO2) for use in modified Fenton chemistry. *Journal of Hazardous Materials*, 152, pp.1164-1170.

Nunes, C.R. et al., 1997. Long-term ingrowth and apposition of porous hydroxylapatite implants. *J Biomed Mater Res*, 36(4), pp.560-563.

Oh, S.H., Kang, S.G. & Lee, J.H., 2006. Degradation behavior of hydrophilized PLGA scaffolds prepared by melt-molding particulate-leaching method: comparison with control hydrophobic one. *J Mater Sci Mater Med*, 17(2), pp.131-137.

Oh, S.H. et al., 2009. Oxygen generating scaffolds for enhancing engineered tissue survival. *Biomaterials*, 30(5), pp.757-762.

Ohgawara, H. et al., 1998. Membrane immunoisolation of a diffusion chamber for bioartificial pancreas. *Artif Organs*, 22(9), pp.788-94.

Ohgawara, H. et al., 1991. Survival and B-cell function of neonatal pig pancreatic islet-like cell clusters in an extracellular matrix. *Pancreas*, 6(6), pp.625-630.

Otsu, K. et al., 2009. Concentration dependent inhibition of angiogenesis by mesenchymal stem cells. *Blood*, 113(18), pp.4197-205.

Papas, K.K. et al., 2007. A stirred microchamber for oxygen consumption rate measurements with pancreatic islets. *Biotechnology and Bioengineering*, 98(5), p.1071–1082.

Paraskevas, S. et al., 2000. Cell loss in isolated human islets occurs by apoptosis. *Pancreas*, 20(3), pp.270-276.

Perez-Basterrechea, M. et al., 2008. Plasma–fibroblast gel as scaffold for islet transplantation. *Tissue Engineering Part A*, 15(3), p.569–577.

Peterson, S.L. et al., 2004. Poly(dimethylsiloxane) thin films as biocompatible coatings for microfluidic devices: cell culture and flow studies with glial cells. *Journal of Biomedical Materials Research. Part A*, 72(1), pp.10-8.

Pierre, J. & Oddou, C., 2007. Engineered bone culture in a perfusion bioreactor: a 2D computational study of stationary mass and momentum transport. *Computer Methods in Biomechanics and Biomedical Engineering*, 10(6), pp.429-38.

Pileggi, Antonello et al., 2006. Reversal of diabetes by pancreatic islet transplantation into a subcutaneous, neovascularized device. *Transplantation*, 81(9), pp.1318-24.

Pollok, J.M., Ibarra, C. & Vacanti, J.P., 1997. Immunoisolation of xenogeneic islets using a living tissue engineered cartilage barrier. *Transplantation Proceedings*, 29(4), pp.2131-3.

Rafael, E. et al., 2008. Intramuscular autotransplantation of pancreatic islets in a 7-year-old child: a 2-year follow-up. *American Journal of Transplantation*, 8(2), pp.458-62.

Randall, G.C. & Doyle, P.S., 2005. Permeation-driven flow in poly(dimethylsiloxane) microfluidic devices. *Proceedings of the National Academy of Sciences of the United States of America*, 102(31), pp.10813-8.

Ranjitprakash, A. et al., 2006. Small volume PCR in PDMS biochips with integrated fluid control and vapour barrier. *Sensors and Actuators B: Chemical*, 113(1), pp.398-409.

Rao, P. et al., 2005. Protective effect of a radical scavenger, MCI-186 on islet cell damages induced by oxidative stress. *Transplantation Proceedings*, 37(8), pp.3457-8.

Ratner, B.D. & Bryant, S.J., 2004. Biomaterials: where we have been and where we are going. *Annual Review of Biomedical Engineering*, 6(1), pp.41-75.

Ratner, B.D. et al., 2004. *Biomaterials Science, Second Edition: An Introduction to Materials in Medicine* Second., Academic Press.

Ravikumar, J.X. & Gurol, M.D., 1994. Chemical oxidation of chlorinated organics by hydrogen peroxide in the presence of sand. *Environmental Science & Technology*, 28(3), pp.394-400.

Robertson, R Paul, 2002. Intrahepatically transplanted islets--strangers in a strange land. *Journal of Clinical Endocrinology & Metabolism*, 87(12), pp.5416-5417.

Robertson, R Paul, 2004. Islet transplantation as a treatment for diabetes - a work in progress. *The New England Journal of Medicine*, 350(7), pp.694-705.

Romero, A. et al., 2009. In situ oxidation remediation technologies: kinetic of hydrogen peroxide decomposition on soil organic matter. *Journal of Hazardous Materials*, 170(2-3), pp.627-632.

Roth, J. et al., 2008. Surface functionalization of silicone rubber for permanent adhesion improvement. *Langmuir*, 24(21), pp.12603-12611.

Ryzhik, I.M., Jeffrey, A. & Zwillinger, D., 2007. *Table of Integrals, Series and Products*, Academic Press.

Sachlos, E., Czernuszka, J.T. & Road, P., 2003. Making tissue engineering scaffolds work. Review on the application of solid freeform fabrication technology to the production of tissue engineering scaffolds. *Tissue Engineering*, 5, pp.29-40.

Sakurai, T. et al., 2004. The efficient prevascularization induced by fibroblast growth factor 2 with a collagen-coated device improves the cell survival of a bioartificial pancreas. *Pancreas*, 28(3), pp.e70-9.

Salvay, D.M. et al., 2008. Extracellular matrix protein-coated scaffolds promote the reversal of diabetes after extrahepatic islet transplantation. *Transplantation*, 85(10), pp.1456-1464.

Schmidtke, T., White, D. & Woolard, C., 1999. Oxygen release kinetics from solid phase oxygen in Arctic Alaska. *Methods*, pp.157-165.

Schumb, W.C., Satterfield, C.N. & Wentworth, R.L., 1955. *Hydrogen Peroxide, (American Chemical Society. Monograph Series)*, Reinhold Pub. Corp.

Semenza, G.L., 1999. Regulation of mammalian O2 homeostasis by hypoxia-inducible factor 1. *Annual Review of Cell and Developmental Biology*, 15, pp.551-578.

Shapiro, A.M. et al., 2006. International trial of the Edmonton protocol for islet transplantation. *New England Journal of Medicine*, 355(13), pp.1318-1330.

Shiku, H. et al., 2006. Oxygen permeability of surface-modified poly(dimethylsiloxane) characterized by scanning electrochemical microscopy. *Chemistry Letters*, 35(2), p.234–235.

Silva, A.I. et al., 2006. An overview on the development of a bio-artificial pancreas as a treatment of insulin-dependent diabetes mellitus. *Medicinal Research Reviews*, 26(2), p.181–222.

Silva, A. & Mateus, M, 2009. Development of a polysulfone hollow fiber vascular bio-artificial pancreas device for in vitro studies. *Journal of Biotechnology*, 139(3), p.236–249.

Simmons, A. et al., 2004. Long-term in vivo biostability of poly (dimethylsiloxane)/poly (hexamethylene oxide) mixed macrodiol-based polyurethane elastomers. *Biomaterials*, 25(20), p.4887–4900.

Simmons, A. et al., 2008. Biostability and biological performance of a PDMS-based polyurethane for controlled drug release. *Biomaterials*, 29(20), p.2987–2995.

Simovic, S. & Prestidge, C.A., 2007. Nanoparticle layers controlling drug release from emulsions. *European Journal of Pharmaceutics and Biopharmaceutics*, 67(1), pp.39-47.

Speier, S. et al., 2008. Noninvasive in vivo imaging of pancreatic islet cell biology. *Nature Medicine*, 14(5), pp.574-8.

Stabler, C et al., 2001. The effects of alginate composition on encapsulated betaTC3 cells. *Biomaterials*, 22(11), pp.1301-10.

Storrs, R. et al., 2001. Preclinical development of the Islet Sheet. *Annals of the New York Academy of Sciences*, 944, pp.252-266.

Sun, A.M., 1988. Microencapsulation of pancreatic islet cells: a bioartificial endocrine pancreas. *Methods in Enzymology*, 137, pp.575-80.

Tang, J. & Zhang, J.H., 2000. Mechanisms of [Ca2+]i elevation by H2O2 in islets of rats. *Life Sciences*, 68(4), pp.475-81.

Teixeira, S., Ferraz, M.P. & Monteiro, F.J., 2007. Biocompatibility of highly macroporous ceramic scaffolds: cell adhesion and morphology studies. *Journal of Materials Science: Materials in Medicine*.

Temenoff, J.S., Steinbis, E.S. & Mikos, Antonios G, 2003. Effect of drying history on swelling properties and cell attachment to oligo(poly(ethylene glycol) fumarate) hydrogels for guided tissue regeneration applications. *Journal of Biomaterials science. Polymer Edition*, 14(9), pp.989-1004.

Tiedge, M. et al., 1997. Relation between antioxidant enzyme gene expression and antioxidative defense status of insulin-producing cells. *Diabetes*, 46(11), pp.1733-1742.

Toworfe, G.K. et al., 2004. Fibronectin adsorption on surface-activated poly (dimethylsiloxane) and its effect on cellular function. *Journal of Biomedical Materials Research Part A*, 71(3), p.449–461.

Toworfe, G. et al., 2006. Nucleation and growth of calcium phosphate on amine-, carboxyl-and hydroxyl-silane self-assembled monolayers. *Biomaterials*, 27(4), p.631–642.

Trivedi, N. et al., 2000. Improved vascularization of planar membrane diffusion devices following continuous infusion of vascular endothelial growth factor. *Cell Transplantation*, 9(1), pp.115-124.

Tse, W.T. et al., 2003. Suppression of allogeneic T-cell proliferation by human marrow stromal cells: implications in transplantation. *Transplantation*, 75(3), pp.389-397.

Vacík, J. et al., 2008. Cultivation of human keratinocytes without feeder cells on polymer carriers containing ethoxyethyl methacrylate: in vitro study. *Journal of Materials Science: Materials in Medicine*, 19(2), pp.883-8.

van der Veen, V.C. et al., 2010. Biological background of dermal substitutes. *Burns: Journal of the International Society for Burn Injuries*, 36(3), pp.305-21.

van der Windt, D.J. et al., 2007. Rapid loss of intraportally transplanted islets: an overview of pathophysiology and preventive strategies. *Xenotransplantation*, 14(4), pp.288-297.

Verneuil, E., Buguin, A. & Silberzan, P., 2004. Permeation-induced flows: Consequences for silicone-based microfluidics. *Europhysics Letters (EPL)*, 68(3), pp.412-418.

Vollmer, A.P. et al., 2005. Development of an integrated microfluidic platform for dynamic oxygen sensing and delivery in a flowing medium. *Lab on a Chip*, pp.1059-1066.

Waite, A.J., Bonner, J.S. & Autenrieth, R., 1999. Kinetics and stoichiometry of oxygen release from solid peroxides. *Environmental Engineering Science*, 16(3), p.187–199.

Walling, C., 1975. Fenton's reagent revisited. *Accounts of Chemical Research*, 8(4), pp.125-131.

Wang, R.N. & Rosenberg, L, 1999. Maintenance of beta-cell function and survival following islet isolation requires re-establishment of the islet – matrix relationship. *Journal of Endocrinology*, pp.181-190.

Wang, T.-W. et al., 2006. The effect of gelatin-chondroitin sulfate-hyaluronic acid skin substitute on wound healing in SCID mice. *Biomaterials*, 27(33), pp.5689-5697.

Wang, W. et al., 2005. Increased oxygen consumption rates in response to high glucose detected by a novel oxygen biosensor system in non-human primate and human islets. *Journal of Endocrinology*, 185(3), pp.445-455.

Warnock, G.L. et al., 1990. Critical mass of islets that function after implantation in a large mammalian. *Hormone and Metabolic Research. Supplement Series*, 25, pp.156-61.

Warnock, G.L. & Rajotte, R V, 1992. Pancreatic Islet Cell Transplantation: A new era in transplantation. *Canadian Family Physician*, 38, pp.1655-60.

Watson, J.M., 1996. The behaviour of water in poly(dimethylsiloxane). *Journal of Membrane Science*, 110(1), pp.47-57.

Watson, J.M. & Payne, P.A., 1990. A study of organic compound pervaporation through silicone rubber. *Journal of Membrane Science*, 49(2), pp.171-205.

Watts, R.J. et al., 1999. Hydrogen peroxide decomposition in model subsurface systems. *Journal of Hazardous Materials*, pp.229-243.

Watts, R.J. & Teel, A.L., 2005. Chemistry of modified fenton's reagent (catalyzed H2O2 propagations–CHP) for in situ soil and groundwater remediation. *Journal of Environmental Engineering*, (April), pp.612-622.

Watts, R.J., Udell, M.D. & Monsen, R.M., 2009. Use of iron minerals in optimizing the peroxide treatment of contaminated soils. *Water Environment Research*, 65(7), pp.839-844.

Weber, C.J. et al., 1978. Tissue culture preservation and intramuscular transplantation of pancreatic islets. *Surgery*, 84(1), pp.166-74.

Whang, K. et al., 1995. A novel method to fabricate bioabsorbable scaffolds. *Polymer*, 36(4), pp.837-842.

White, S.A. et al., 2001. Pancreas resection and islet autotransplantation for end-stage chronic pancreatitis. *Annals of Surgery*, 233(3), pp.423-31.

White, S.A. et al., 2000. The risks of total pancreatectomy and splenic islet autotransplantation. *Cell Transplantation*, 9(1), pp.19-24.

Witkowski, P. et al., 2009. Islet grafting and imaging in a bioengineered intramuscular space. *Biomaterials*, 88(9), pp.1065-1074.

Woerly, S., 2000. Restorative surgery of the central nervous system by means of tissue engineering using NeuroGel implants. *Neurosurgical Review*, 23(2), pp.59-77; discussion 78-79.

Wu, H et al., 1999. In situ electrochemical oxygen generation with an immunoisolation device. *Annals of the New York Academy of Sciences*, 875, pp.105-125.

Yang, H. et al., 1994. Comparative studies of in vitro and in vivo function of three different shaped bioartificial pancreases made of agarose hydrogel. *Biomaterials*, 15(2), pp.113-120.

Yang, Z. et al., 2004. Inflammation blockade improves pancreatic islet function. *Transplant Proceedings*, 36, pp.2864-2865.

Yasunami, Y., Lacy, P.E. & Finke, E.H., 1983. A new site for islet transplantation - a peritoneal-omental pouch. *Transplantation*, 36(2), pp.181-2.

Yeargers, E.K., Shonkwiler, R.W. & Herod, J.V., 1996. *An Introduction to the Mathematics of Biology: With Computer Algebra Models*, Springer.

Zanzotto, A. et al., 2004. Membrane-aerated microbioreactor for high-throughput bioprocessing. *Biotechnology and Bioengineering*, 87(2), pp.243-54.

Zeng, J. et al., 2005. Photo-Induced Solid-State Crosslinking of Electrospun Poly(vinyl alcohol) Fibers. *Macromolecular Rapid Communications*, 26(19), pp.1557-1562.

Zhan, X. et al., 2009. Pervaporation properties of PDMS membranes cured With different cross-linking reagents for ethanol concentration from aqueous solutions. *Chinese Journal of Polymer Science*, 27(04), p.533.